Author’s response

List of relevant change.

Following reviewer’s recommendations and comments, change in the manuscript are listed:

- In section 5, parts related to the description of parameterizations are now reported in a dedicated section 6.
- In section 5, the section 5.6 note on the impact of vertical movement on ice microphysic.
- Appendices A in the former version of the manuscript becomes Appendices C
- Part of the texts that discuses about total concentrations integrated beyond 15µm in section 5.3 is reported in Appendices A
- Appendices B contains Figures on the impact of vertical velocity on ice microphysics
- Tables that summarize differences of ice microphysical properties in the conclusion is now reported in Appendices D.

Appendices E is added, since some recent personal works suggest that PSD parameterizations should consider that NWP ice microphysical parameterizations assumes that ice hydrometeors are spheres.

Answers to the first Referee R1.

We want to thank Dr. Baumgardner to review our study and making comments that allow to improve our manuscript.

Legend of styles

- **Reviewer comment**
- Author’s answer
- (R1#i): flag to relate the change in the new manuscript (see author’s comment)
- *“Change in the manuscript”*

1) In the introduction and conclusions the authors emphasize the importance of dynamics on the cloud properties, then there is a very brief analysis of vertical velocity but after that section, no further effort is made to link microphysical properties to vertical velocity. In addition, given that updrafts are usually associated with hydrometeor growth and downdrafts with cloud decay, lumping all the results together regardless of vertical velocity direction will mask possibly important trends. The analysis has to include stratification by updraft and downdraft.

The topic of stratification of our results as function of vertical velocity (updraft and downdraft) comes back often in the comment by reviewer R1. We reply here to all the comments linked to this topic.

Before presenting our results, the variability of the parameters as function of vertical movement and their intensity have been studied. However, no real tendencies have been identified that would allow to present our results also as function of updraft and downdraft.

Hence, parameterization or stratification of microphysical properties in MCS as function of vertical velocity (up and down) is not possible (with our in-situ dataset). However, in a first order, our study investigates variability of bulk microphysical properties of the icy part of MCS as function of temperature ranges and Z ranges (i.e. MCS reflectivity zones). If, no clear tendencies have been found as function of vertical velocities, we decide to investigate the probability to observe a vertical movement as function of Z (or MCS reflectivity zones). This work is discussed in section 3.2 with data from RASTA only; which contains much more data than in-situ measurement (more than a million of points versus about 53000 points for in-situ measurement). Then, the conclusion of this section is that the probability to observe vertical movement (updraft or downdraft) tend to increase with MCS reflectivity zones (or Z at constant altitude).

Line 27 page 5: Why are you using absolute values?

and

Line 1 page 6: This does not seem reasonable to me to use absolute values as there is a very large difference between updrafts or downdrafts when it comes to storm dynamics and precipitation development.

and

Line 20 page 6: Somewhere it needs to be emphasized the significance of the updraft versus downdraft zones as they relate to the microphysical properties.

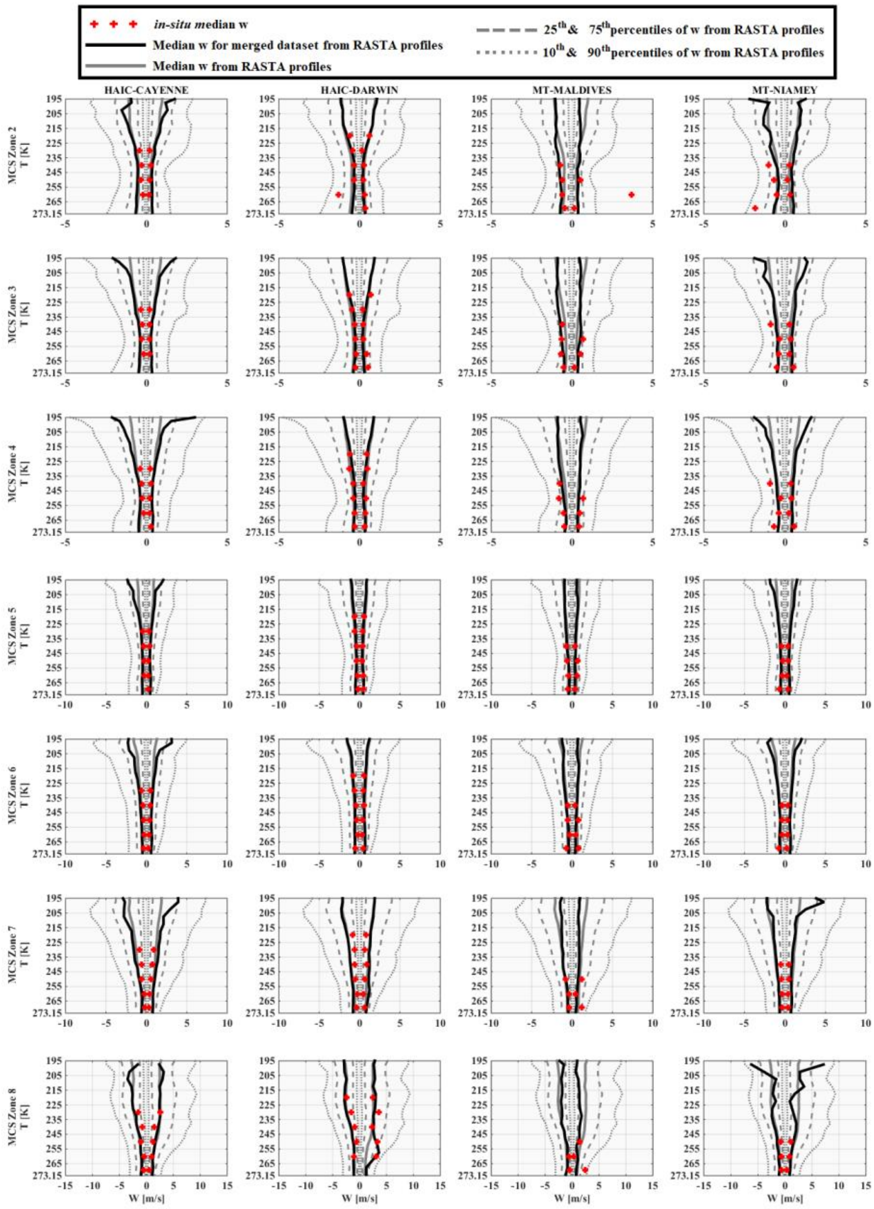

Figure R 1: from the top line to the bottom line vertical velocities for MCSRZ 2 to MCSRZ 8.

Figure R 1 shows median updraft and downdraft in each MCS reflectivity zones (MCSRZ 2 to MCSRZ 8 from the top line to the bottom line respectively) and for each airborne campaign (Cayenne, Darwin, Maldives Island and Niamey, from left column to right column respectively). Black lines represent median updraft and downdraft for each respective airborne campaigns, while grey lines are median (solid line), 25th and 75th percentiles (dashed lines) and 10th and 90th percentiles (dotted lines) for the merged dataset. Black lines and grey lines are calculated using RASTA vertical profiles. The red stars are median downdraft and updraft when taken only vertical movement measured by the aircraft (in-situ measurement).

We can see that median updraft and median downdraft for each airborne campaigns from in-situ and RASTA measurement agree well with median updraft and downdraft for the merged dataset in each MCSRZ. Also, we can observe a symmetry between updraft and downdraft in all MCS reflectivity zones for each campaigns, meaning that at a given altitude, absolute magnitude of downdraft is about the magnitude of updraft for median, 25th, 75th,10th and 90th calculated percentiles.

The decision of taking a threshold of 1m/s for updraft and downdraft, is motivated by the fact that we have to take into account the measurement uncertainty (less than 0.5m/s). Moreover, knowing that variance of vertical turbulences are about 1.5 m^2/s^2 (Large Eddy Simulations at 50 m resolution; personal communication with Dr. R. Didier). We take roughly a value of 1m/s to be the threshold to detect vertical movement, such $-1m/s < w < 1m/s$ there is no noticeable vertical movement neither upward nor downward. Hence, investigating the probability to observe vertical movement with an absolute magnitude larger than 1m/s seems reasonable to determine which MCS reflectivity zones have a higher probability to be linked to a convective area.

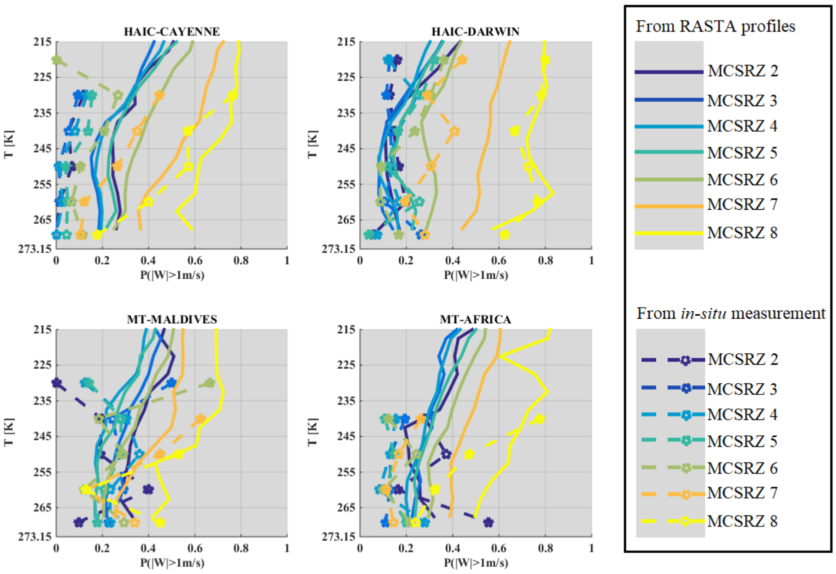

Figure R 2 : Probability to observe vertical velocity with absolute magnitude larger than 1m/s in each MCS reflectivity zone (MCSRZ; color scale) for measurement from the radar Doppler RASTA in solid lines and in dashed lines with stars marker for in-situ measurement.

Figure R 2, is similar to Figure 3 in our reviewed study. It shows probability to observe vertical movement with magnitude larger than 1m/s in each MCS reflectivity zones (solid lines). Solid lines in Figure R 2 are probabilities calculated from RASTA measurement and dashed lines with stars are probabilities calculated with w measured at the flight level. Both type of probabilities are different in each MCS zones and probabilities made with in-situ measurement are smaller than these calculated with RASTA retrievals; except in MCS reflectivity zones 8 in Darwin where they are similar. From there, we know from the point of view of vertical velocity that the in-situ dataset is not similar to the dataset from RASTA retrievals: different probability to observe vertical velocity with magnitude larger than 1m/s (updraft and downdraft).

Impact of vertical velocity on Median relative differences:

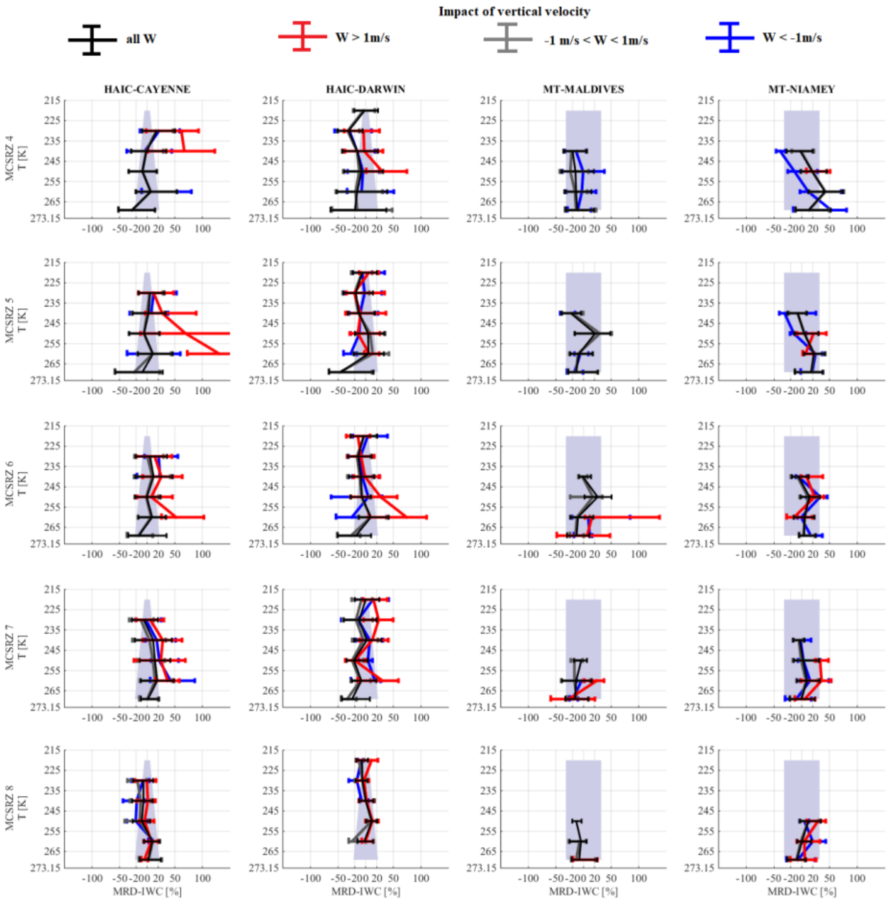

Figure R 3 : Median relative difference of IWC (MRD-IWC) with regards to median IWC calculated for the merged dataset in each MCS reflectivity zone (Figure 5-a). Results are sorted as function of MCSRZ 4 (top line) to MCSRZ 8 bottom line. Blue lines represent MRD-IWC for vertical velocity smaller than -1m/s. Grey lines represent MRD-IWC for vertical velocity larger than -1m/s and smaller than 1m/s. Red lines represent MRD-IWC for vertical velocity larger 1m/s. The black lines represent MRD-IWC when there is no distinction as function of vertical velocity (same as in Figure 5-b, c, d, e).

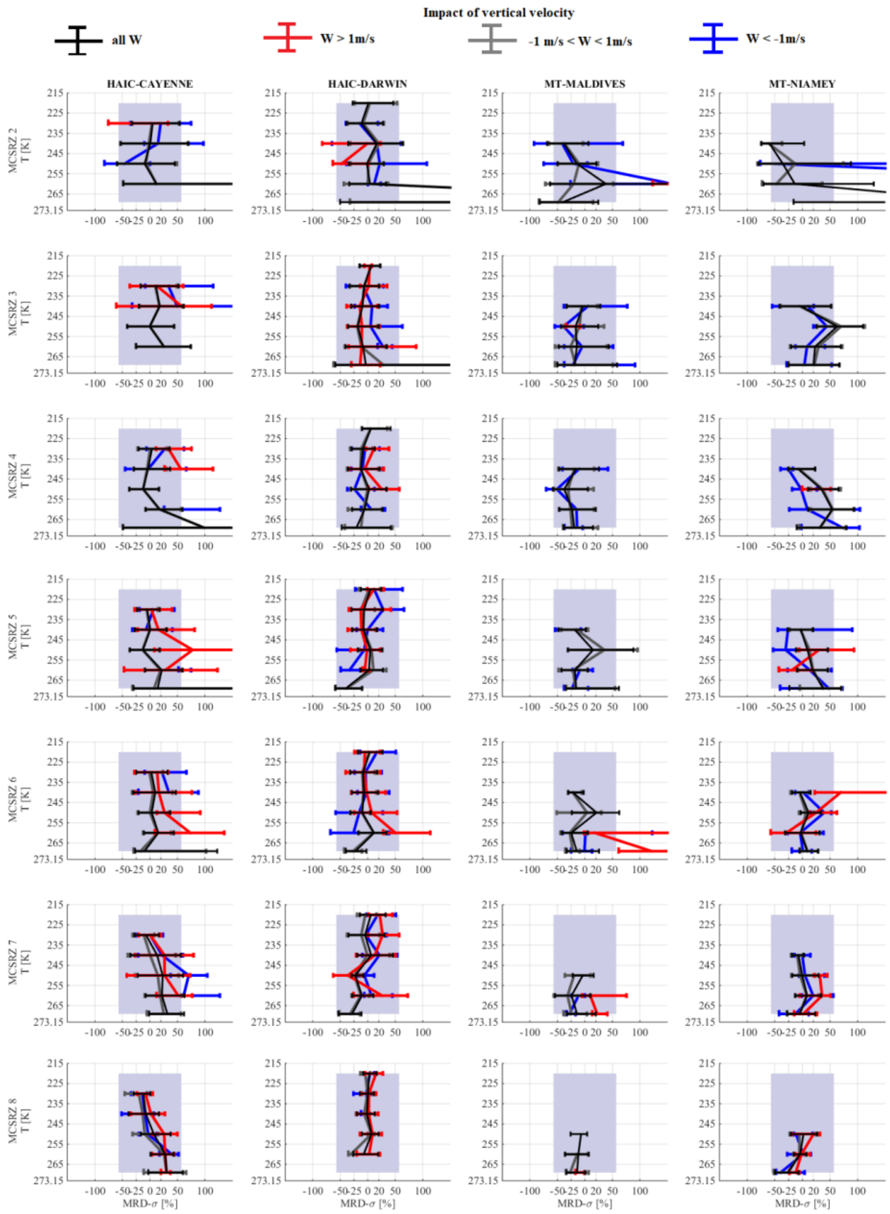

Figure R 4 : Median relative difference of extinction (MRD-σ) with regards to median extinction calculated for the merged dataset in each MCS reflectivity zone (Figure 6-a). Results are sorted as function of MCSRZ 2 (top line) to MCSRZ 8 bottom line. Blue lines represent MRD- σ for vertical velocity smaller than -1m/s. Grey lines represent MRD- σ for vertical velocity larger than -1m/s and smaller than 1m/s. Red lines represent MRD- σ for vertical velocity larger 1m/s. The black lines represent MRD- σ when there is no distinction as function of vertical velocity (same as in Figure 6-b, c, d, e).

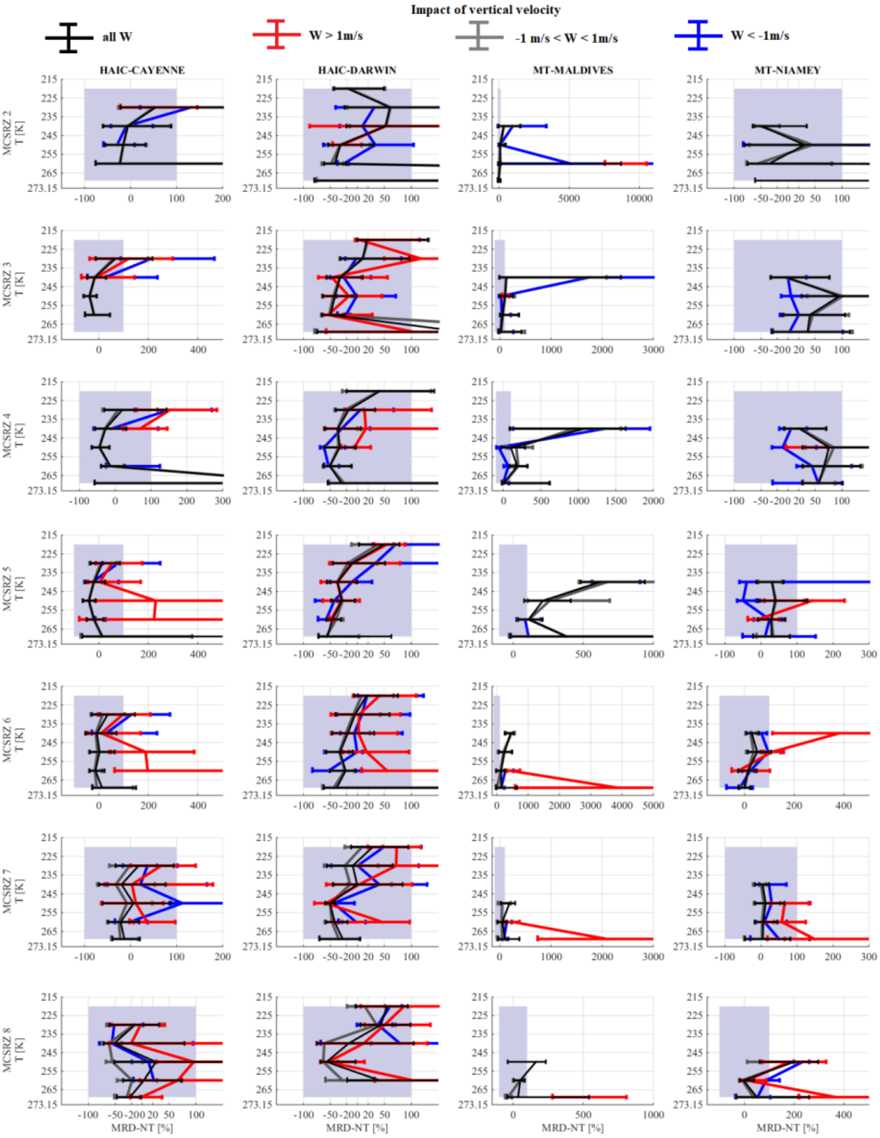

Figure R 5 : Median relative difference of total concentration of hydrometeors (MRD-NT) with regards to median total concentrations calculated for the merged dataset in each MCS reflectivity zone (Figure 8-a). Results are sorted as function of MCSRZ 2 (top line) to MCSRZ 8 bottom line. Blue lines represent MRD-NT for vertical velocity smaller than -1m/s. Grey lines represent MRD-NT for vertical velocity larger than -1m/s and smaller than 1m/s. Red lines represent MRD-NT for vertical velocity larger 1m/s. The black lines represent MRD-NT when there is no distinction as function of vertical velocity (same as in Figure 8-b, c, d, e).

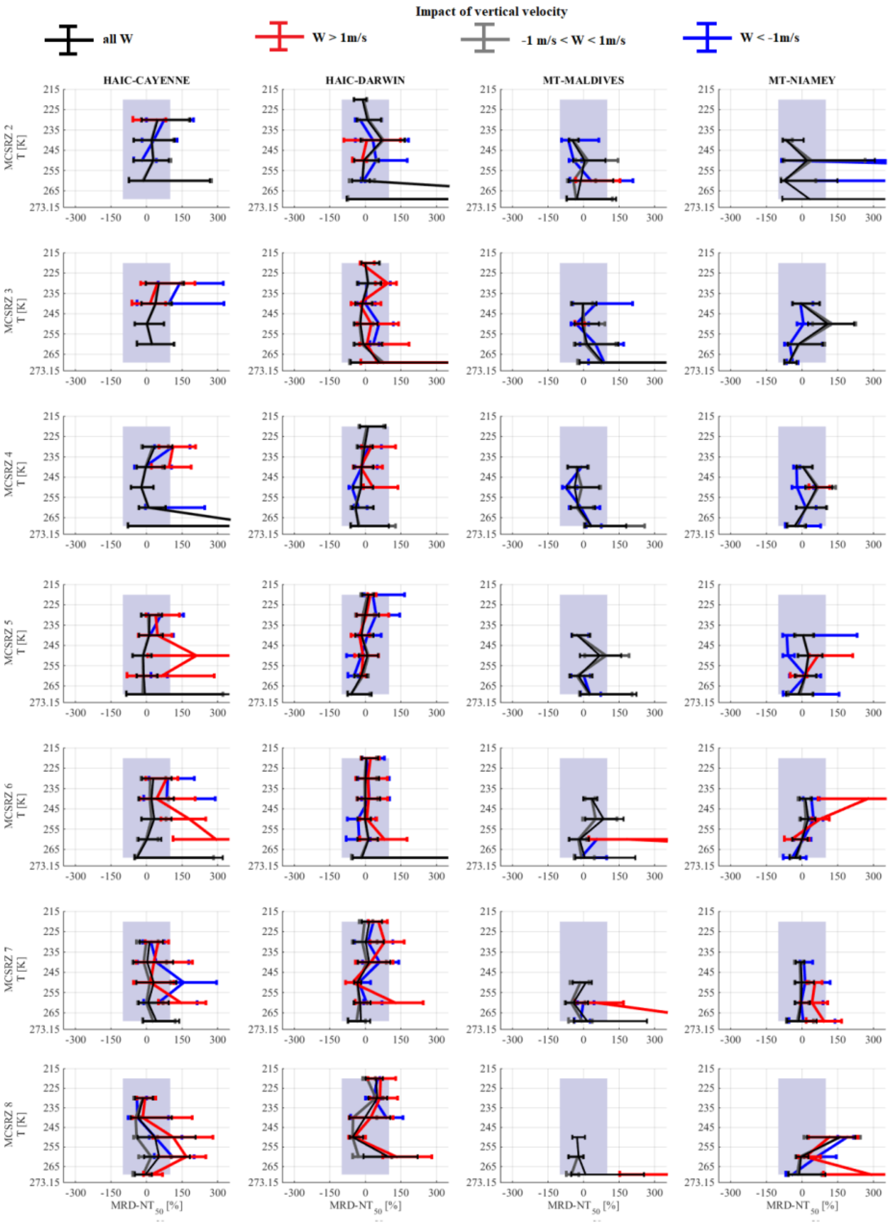

Figure R 6 : Median relative difference of concentration of hydrometeors summed over Dmax for Dmax larger than 50µm (MRD-NT_{50}) with regards to median total concentrations calculated for the merged dataset in each MCS reflectivity zone (Figure 9-a). Results are sorted as function of MCSRZ 2 (top line) to MCSRZ 8 bottom line. Blue lines represent MRD-NT_{50} for vertical velocity smaller than -1m/s. Grey lines represent MRD-NT_{50} for vertical velocity larger than -1m/s and smaller than 1m/s. Red lines represent

MRD-NT$_{50}$ for vertical velocity larger 1m/s. The black lines represent MRD-NT$_{50}$ when there is no distinction as function of vertical velocity (same as in Figure 9-b, c, d, e).

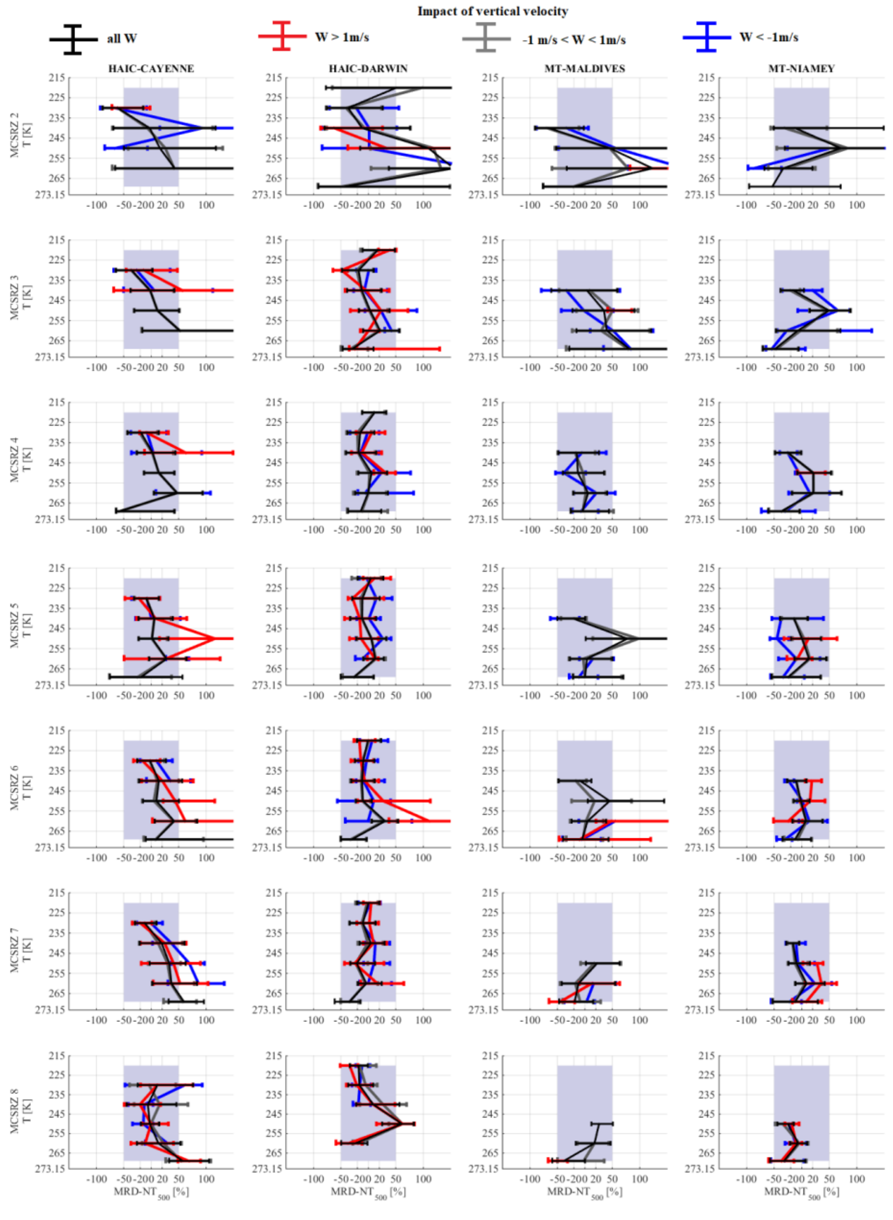

Figure R 7 : Median relative difference of concentration of hydrometeors summed over Dmax for Dmax larger than 500µm (MRD-NT$_{500}$) with regards to median total concentrations calculated for the merged

dataset in each MCS reflectivity zone (Figure 10-a). Results are sorted as function of MCSRZ 2 (top line) to MCSRZ 8 bottom line. Blue lines represent MRD-NT$_{500}$ for vertical velocity smaller than -1m/s. Grey lines represent MRD-NT$_{500}$ for vertical velocity larger than -1m/s and smaller than 1m/s. Red lines represent MRD-NT$_{500}$ for vertical velocity larger 1m/s. The black lines represent MRD-NT$_{500}$ when there is no distinction as function of vertical velocity (same as in Figure 10-b, c, d, e).

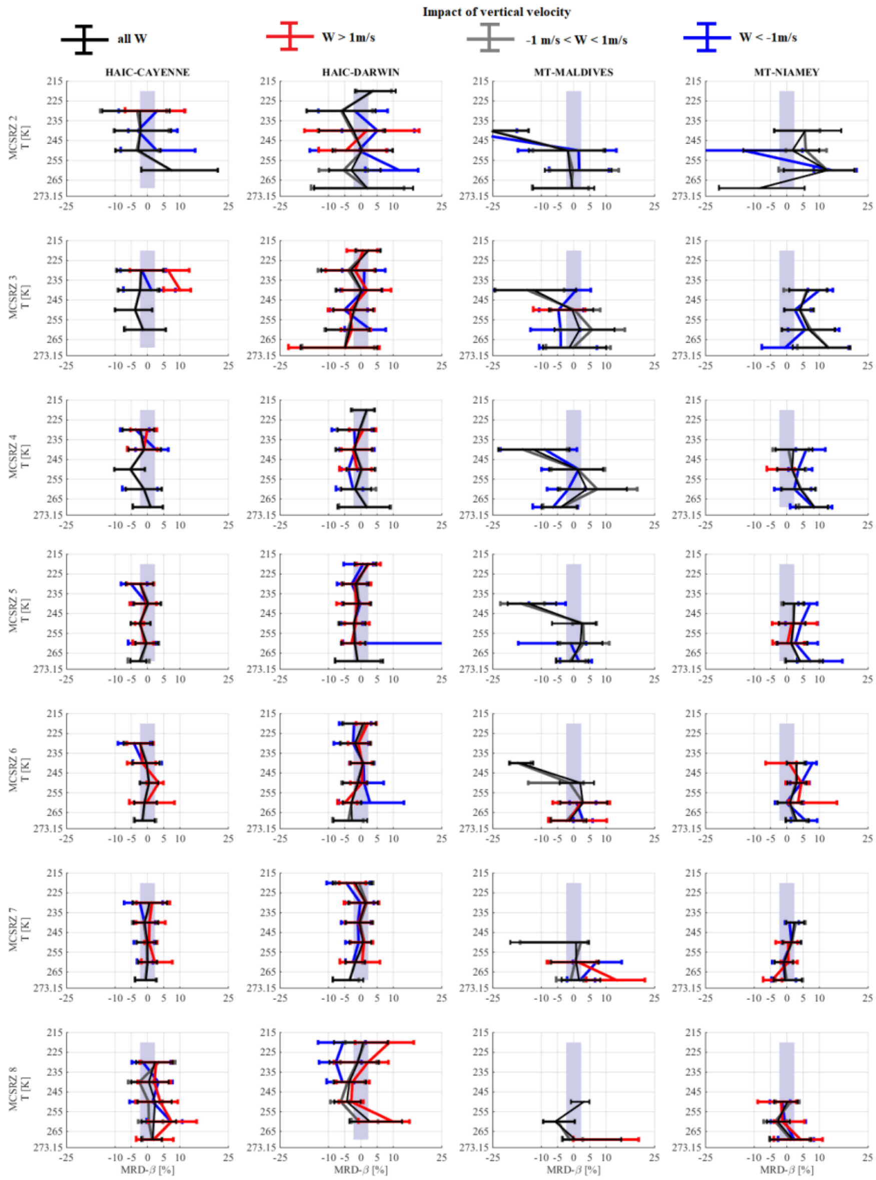

Figure R 8 : Median relative difference of the exponent of mass-size relationship β (MRD-β) with regards to median β calculated for the merged dataset in each MCS reflectivity zone (Figure 11-a). Results are sorted as function of MCSRZ 2 (top line) to MCSRZ 8 bottom line. Blue lines represent MRD-β for vertical velocity smaller than -1m/s. Grey lines represent MRD-β for vertical velocity larger than -1m/s and smaller than 1m/s. Red lines represent MRD-β for vertical velocity larger 1m/s. The black lines represent MRD-β when there is no distinction as function of vertical velocity (same as in Figure 11-b, c, d, e).

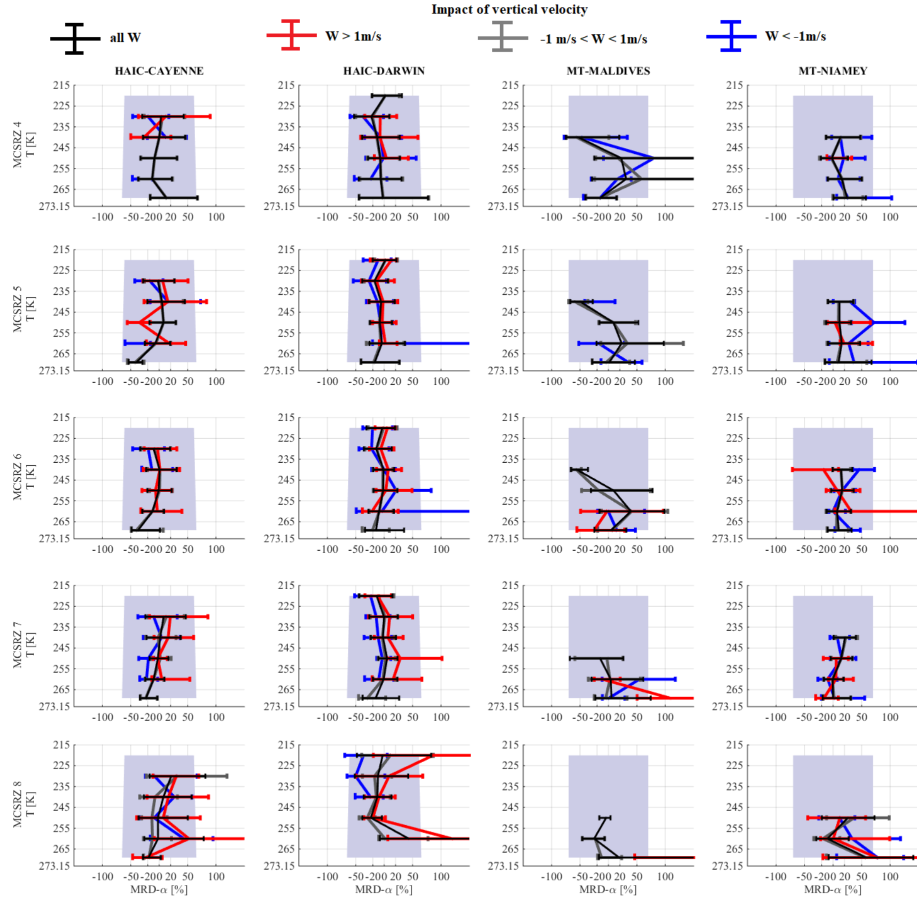

Figure R 9 : Median relative difference of the pre-factor of mass-size relationship α (MRD-α) with regards to median α calculated for the merged dataset in each MCS reflectivity zone (Figure 12-a). Results are sorted as function of MCSRZ 4 (top line) to MCSRZ 8 bottom line. Blue lines represent MRD-α for vertical velocity smaller than -1m/s. Grey lines represent MRD-α for vertical velocity larger than -1m/s and smaller than 1m/s. Red lines represent MRD-α for vertical velocity larger 1m/s. The black lines represent MRD-α when there is no distinction as function of vertical velocity (same as in Figure 12-b, c, d, e).

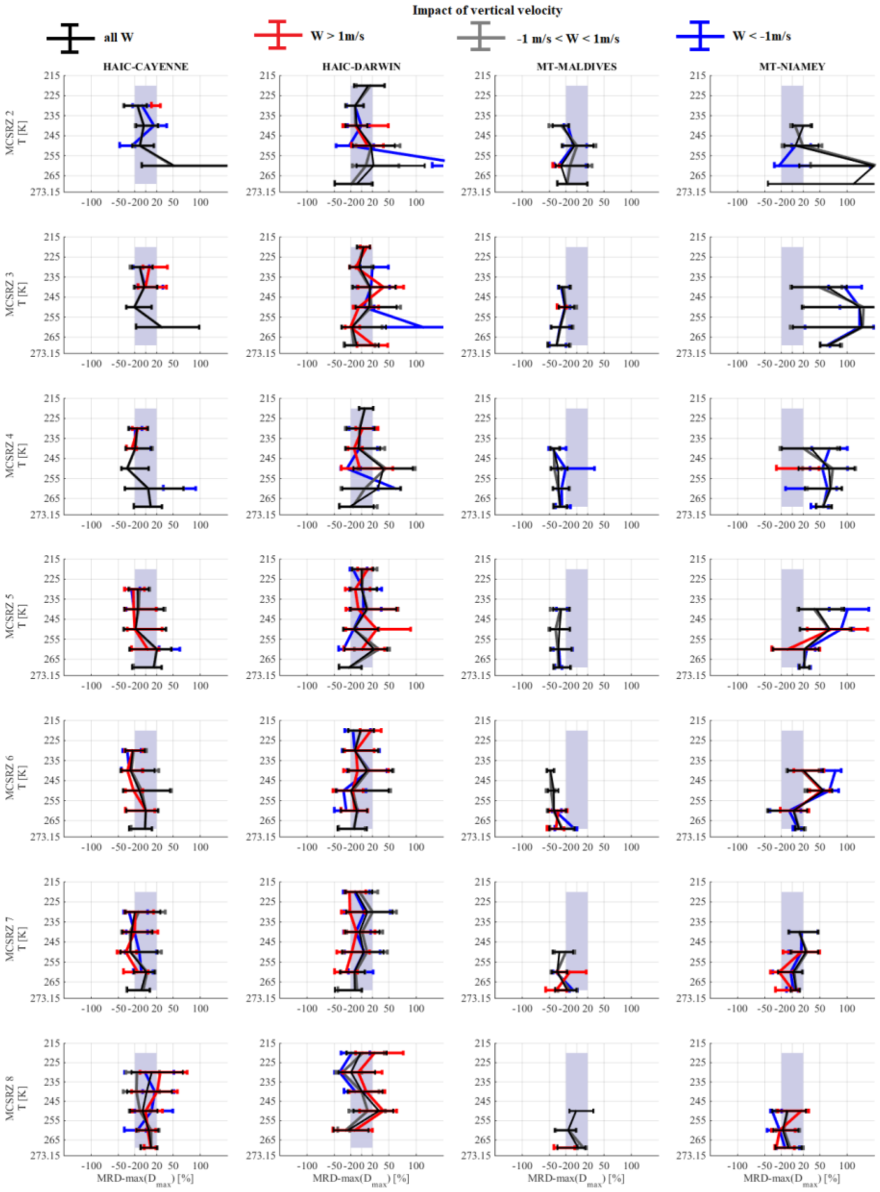

Figure R 10 : Median relative difference of size of larger hydrometeors in PSD (MRD-max(D_{max})) with regards to median max(D_{max}) calculated for the merged dataset in each MCS reflectivity zone (Figure 13-a). Results are sorted as function of MCSRZ 2 (top line) to MCSRZ 8 bottom line. Blue lines represent MRD-max(D_{max}) for vertical velocity smaller than -1m/s. Grey lines represent MRD-max(D_{max}) for vertical velocity larger than -1m/s and smaller than 1m/s. Red lines represent MRD-max(D_{max}) for vertical velocity

larger 1m/s. The black lines represent MRD-max(D_{max}) when there is no distinction as function of vertical velocity (same as in Figure 13-b, c, d, e).

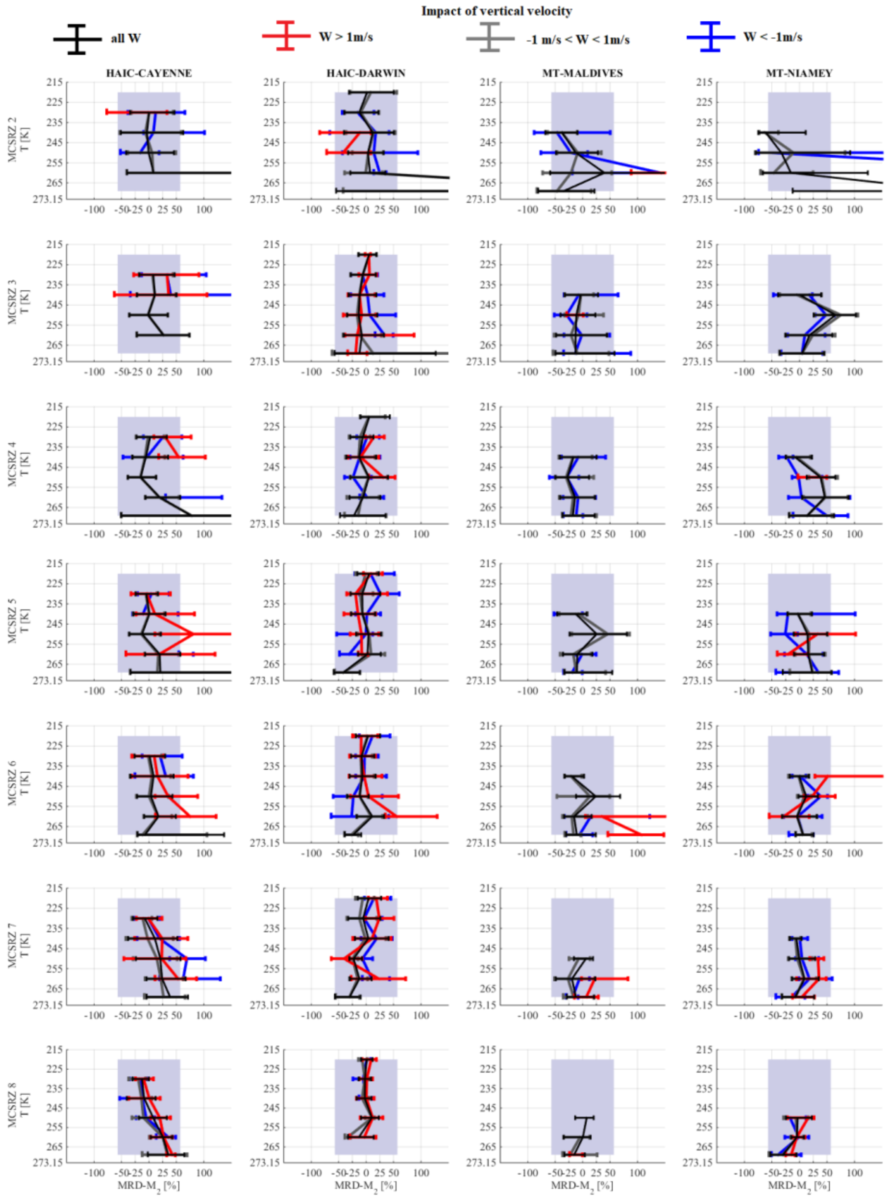

Figure R 11: Median relative difference of second moment of PSD M_2 (MRD-M_2) with regards to median M_2 calculated for the merged dataset in each MCS reflectivity zone (Figure 14-a). Results are sorted as function of MCSRZ 2 (top line) to MCSRZ 8 bottom line. Blue lines represent MRD-M_2 for vertical velocity smaller than -1m/s. Grey lines represent MRD-M_2 for vertical velocity larger than -1m/s and smaller than 1m/s. Red lines represent MRD-M_2 for vertical velocity larger 1m/s. The black lines represent MRD-M_2 when there is no distinction as function of vertical velocity (same as in Figure 14-b, c, d, e).

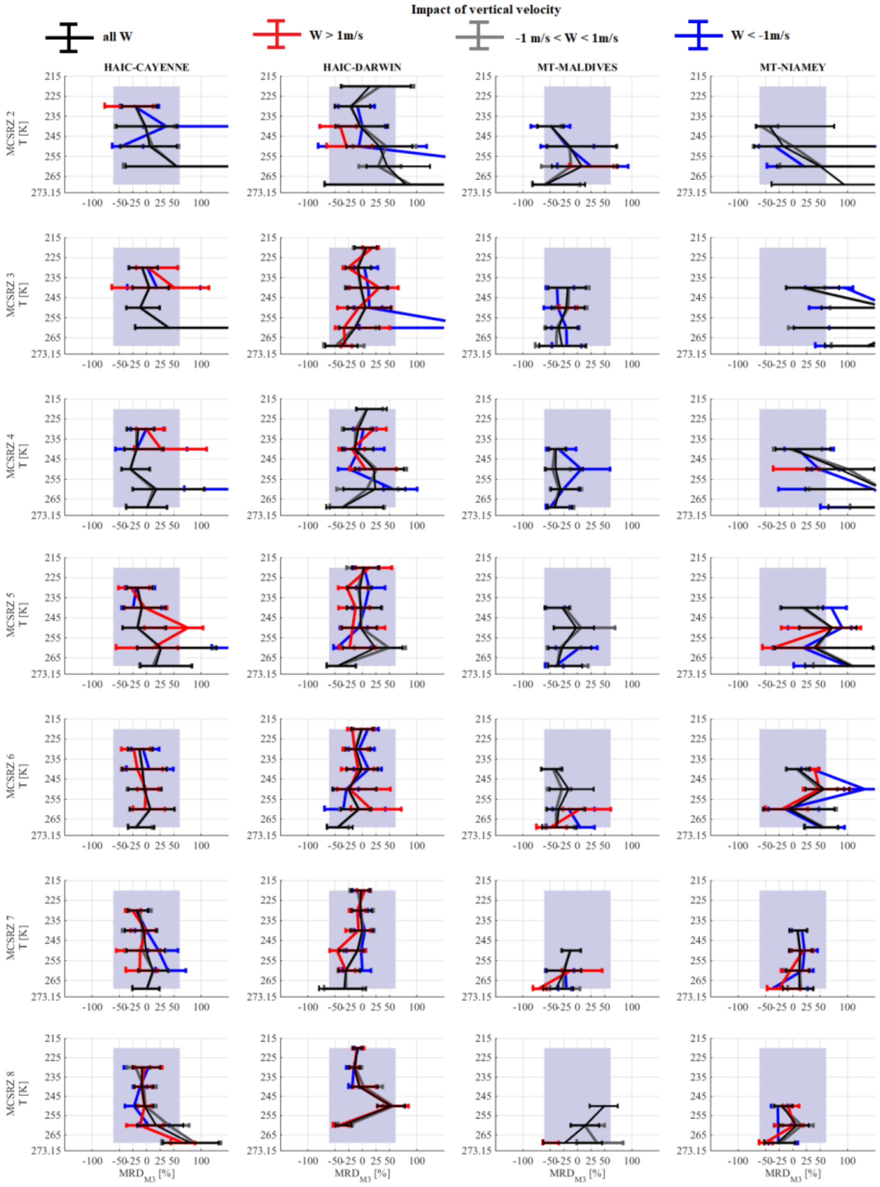

Figure R 12: Median relative difference of third moment of PSD M_3 (MRD-M_3) with regards to median M_3 calculated for the merged dataset in each MCS reflectivity zone (Figure 14-a). Results are sorted as function of MCSRZ 2 (top line) to MCSRZ 8 bottom line. Blue lines represent MRD-M_3 for vertical velocity smaller than -1m/s. Grey lines represent MRD-M_3 for vertical velocity larger than -1m/s and smaller than 1m/s. Red lines represent MRD-M_3 for vertical velocity larger 1m/s. The black lines represent MRD-M_3 when there is no distinction as function of vertical velocity (same as in Figure 15-b, c, d, e).

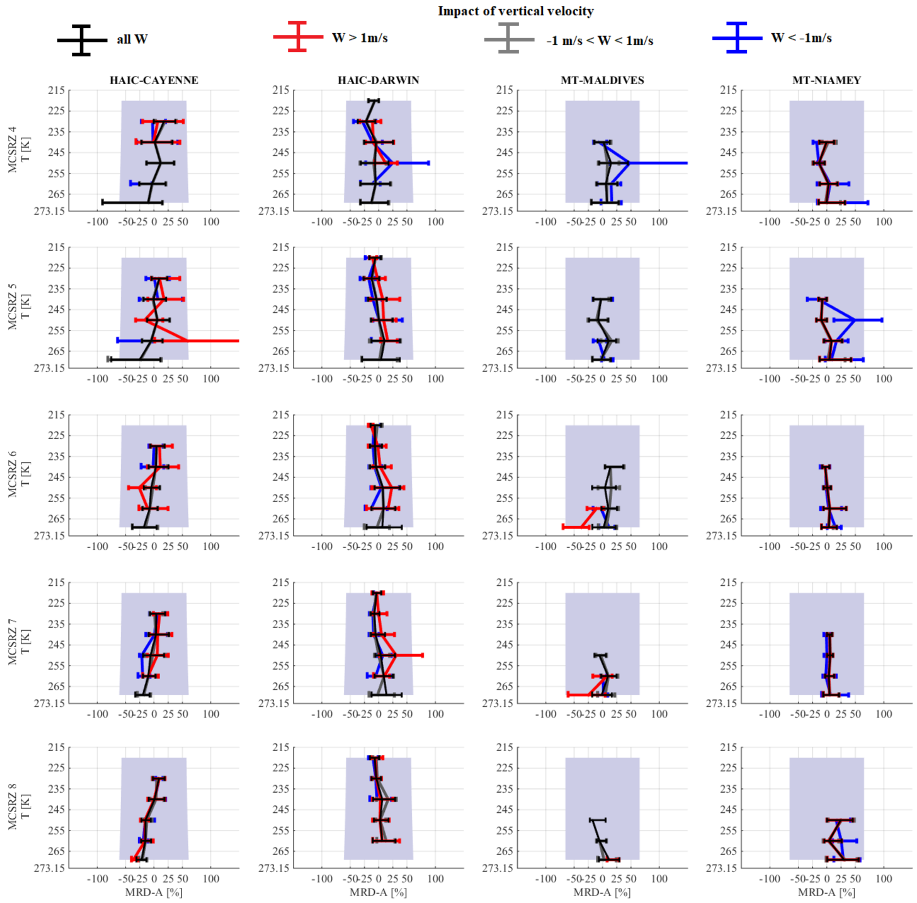

Figure R 13 : Median relative difference of the ratio A(=IWC/M2; MRD-A) with regards to median A calculated for the merged dataset in each MCS reflectivity zone (Figure 16-a). Results are sorted as function of MCSRZ 4 (top line) to MCSRZ 8 bottom line. Blue lines represent MRD-A for vertical velocity smaller than -1m/s. Grey lines represent MRD-A for vertical velocity larger than -1m/s and smaller than 1m/s. Red lines represent MRD-A for vertical velocity larger 1m/s. The black lines represent MRD-A when there is no distinction as function of vertical velocity (same as in Figure 16-b, c, d, e).

Figure R 3 to Figure R 13 show the median relative difference of the studied parameters X (MRD-X; X being used to replace IWC, σ, NT, NT50, NT500, β, α, max(Dmax), M2, M3 and A=IWC/M2) with regards to the median of the X parameter in each MCS reflectivity zones. These figures shows 4 types of MRD-X: (i) MRD-X when w <-1m/s (downdraft: w<0m/s; blue lines), (ii) MRD-X when -1m/s < w < 1m/s (w≈0m/s; grey lines), (iii) MRD-X when w>1m/s (updraft: w>0m/s; red lines) and (iv) MRD-X when w is not considered (black lines; merged dataset).

Firstly, we can notice that MRD-X for w≈0m/s (grey lines) are similar to MRD-X for the merged dataset (black line), showing that impact of downdraft and updraft have nearly no impact on the median tendencies calculated for each microphysical parameters presented in our study. Secondly, there are few differences between MRD-X for downdraft and MRD-X for the merged dataset (black line). However, these differences are not significant compared to uncertainties of each microphysical parameters (U(X)/X; grey bands).

Concerning the impact of updraft on microphysical parameters (red lines), there are some noticeable differences, where MRD-X for updraft are larger than MRD-X for the merged dataset and larger than U(X)/X. It appears that updraft tends to impact mainly concentrations of small hydrometeors and IWC for some type of MCS and some MCS reflectivity zones. So for NT (Figure R5), we observe larger NT for updraft in MCS observed over Cayenne, Maldives and Niamey. For Cayenne, it appears in MCS reflectivity zone 5 and 6 for temperatures between 245K and 265 K with NT 2 to 3 times larger than NT for merged dataset. For MCS over Maldives, median NT are 5 times to 20 times larger than NT when there is no noticeable vertical movement in MCS reflectivity zones 6, 7 and 8. Finally for MCS over Niamey, we observe larger NT in updraft than NT for the merged dataset in MCS reflectivity zones 6 for T around 240 K and in MCS reflectivity zones 8 above the bright band. We have similar conclusions for NT_{50} (Figure R6), except that ratio between NT_{50} in updraft and NT_{50} when no updraft is smaller than the ratio between NT in updraft and NT when no updraft.

IWC are impacted by updraft only for MCS over Cayenne, in MCS reflectivity zone 4, 5, 6 and 7. IWC in updraft tend to be larger about +50% than IWC when no updraft, except in MCS reflectivity zones where IWC are about 2 times larger in updraft than IWC when no updraft.

This investigation on the impact of updraft and downdraft on ice microphysics, shows that updraft may have an impact on concentrations of small hydrometeors and IWC. However, updraft does not impact all type of MCS in the same way. So, there is a need to performed deeper investigations on updraft impact.

Despites some noticeable impact of updraft on ice microphysic for our dataset, there is not significant (recurrence trough all types of MCS or as function of T or Z) results to assess them for the merged dataset. So we cannot add a stratification of our results as function of updraft and downdraft, as for the parameterizations provided in our study.

Page 2 line 27 (R1#1).

"*Investigations on the impact of vertical velocity has been performed asides, however no significant tendencies were found to allow us to present our results as function of vertical velocity.*"

Page 2 line 36 (R1#2).

"*The third section presents the analysis of radar reflectivity factors (Z) which provides the ranges of Z to perform the intercomparison between the four types of MCS. Moreover, for each range of Z a statistical analysis of vertical velocity is presented to bind the vertical dynamic of MCS and ice microphysical properties. The section 4 present the methodology of intercomparison used in this study. And section 5, present the inter-comparison of the microphysical parameters as function of Z and T. The end of this section is dedicated to present shortly the results of the investigations performed about the impact of vertical velocity. The sixth section, provide the* *parameterization of visible extinction and the parameterization of ice hydrometeors distributions. The last section adds the discussion and conclusion.*"

We propose to re-write the sub-section 3.2 (R1#3)

"

3.2 Retrieved vertical velocity in MCS reflectivity zones

This section investigates links between retrieved vertical velocity and MCS reflectivity zones. We assume that Vz (V_d) = w_{ret} + Vt, where Vt is the terminal velocity of hydrometeors (Delanoë et al., 2007, 2014) and w_{ret} the vertical wind speed. In a first order, our study investigates variability of bulk microphysical properties of the icy part of MCS as function of temperature range and Z range (i.e. MCS reflectivity zones). As no clear tendencies have been found as function of vertical velocities, we decide to investigate the probability to observe significant vertical movement in each range of Z (or MCS reflectivity zones). In other words, we investigate if there is any relationship between MCS reflectivity zones and vertical dynamic of MCS. We assume that convective part of MCS are associated with pronounced updraft and downdraft and that stratiform part of MCS have non-pronounced vertical velocity (w≈0m.s-1) (see Figure 16 from Houze 2004).

Figure 3 shows median updraft ($w_{ret}>0$) and downdraft ($w_{ret}<0$) in each MCS reflectivity zones (MCSRZ 2 to MCSRZ 8 from the top line to the bottom line respectively) and for each airborne campaign (Cayenne, Darwin, Maldives Island and Niamey, from left column to right column respectively). Black lines represent median updraft and downdraft for each respective airborne campaigns, while grey lines are median (solid line), 25^{th} and 75^{th} percentiles (dashed lines) and 10^{th} and 90^{th} percentiles (dotted lines) for the merged dataset. Black lines and grey lines are calculated using RASTA vertical profiles. The red stars are median downdraft and updraft when we use only vertical velocity measured by the aircraft (w; in-situ measurement).

We can observe a symmetry between updraft and downdraft in all MCS reflectivity zones for each campaigns, meaning that at a given altitude, absolute magnitude of downdraft is about the magnitude of updraft for median, 25^{th}, 75^{th}, 10^{th} and 90^{th} calculated percentiles. For RASTA measurement, we can see that median updraft ($w_{ret}>0m.s^{-1}$) and median downdraft ($w_{ret}<0m.s^{-1}$) for each airborne campaigns agree well with median updraft and downdraft for the merged dataset in all MCS reflectivity zones. Except for Maldives observations where median w_{ret} are smaller for T < 255K. Also, median in-situ w tend to be a bit smaller than median w_{ret}, except for updraft in Maldives above the bright band; $w≈2.5m.s^{-1}$ versus wret $≈1m.s^{-1}$.

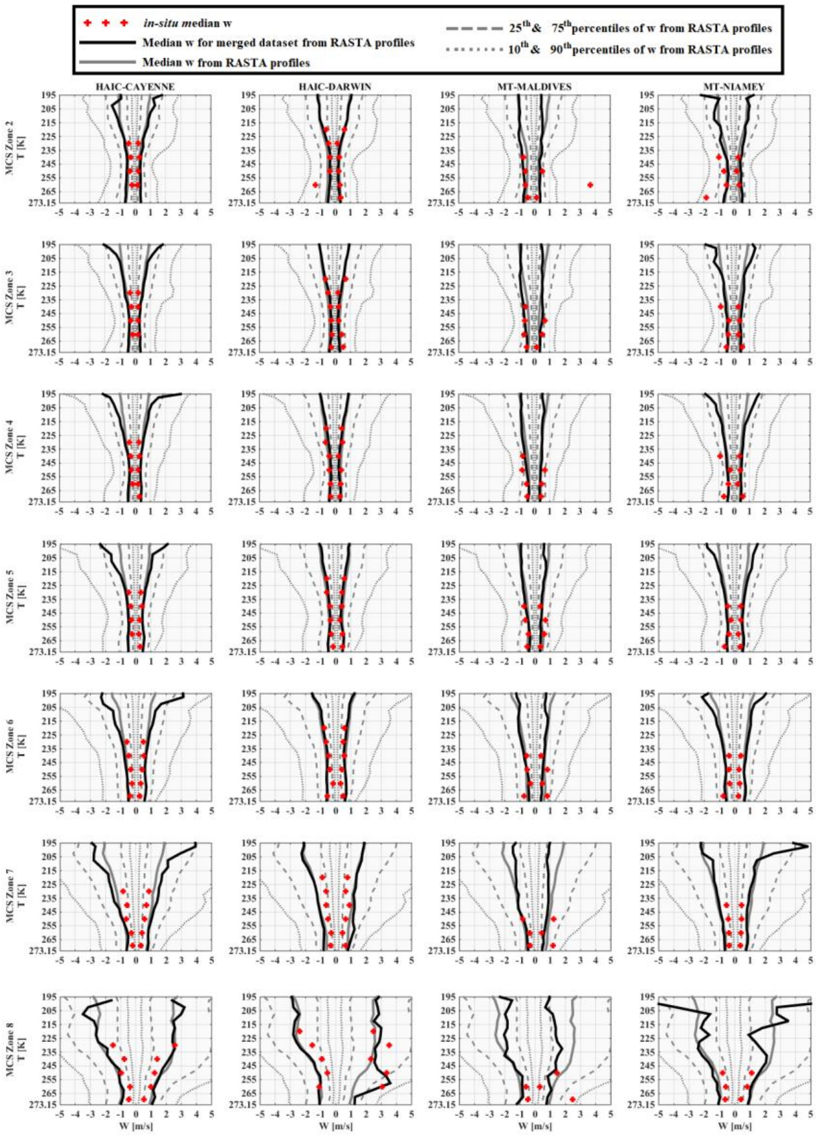

Figure 3: from the top line to the bottom line vertical velocities for MCS reflectivity zone 2 to MCS reflectivity zone 8.

In general the updraft and downdraft wind speeds increase with altitude and MCS reflectivity zones, where magnitudes of vertical velocity (negative and positive) are highest for MCS reflectivity zones 8. For all 4 datasets vertical wind speeds of MCS reflectivity zones 2-6 are smaller than 1m.s^{-1}.

To complete our study on vertical dynamic that could exist in each MCS reflectivity zones, we study the probability to observe vertical movement. We use a threshold for vertical velocity to distinguish between discernible vertical movement and nearly not.

We take roughly a value of 1m/s to be the threshold to detect vertical movement, such -1m/s < w < 1m/s there is no noticeable vertical movement neither upward nor downward. The decision of taking a threshold of 1m/s for updraft and downdraft, is motivated by the fact that we have to take into account the measurement uncertainty (less than 0.25-0.5m.s-1). Moreover, knowing that variance of vertical turbulences are about 1.5 m^2/s^2 (Large Eddy Simulations at 50 m resolution; Strauss et al., 2019). The fact that median w_{ret} for the merged dataset in MCS reflectivity zones 2 to 6 are smaller than 1m.s-1 consolidate our decision to take a threshold of $1m.s^{-1}$.

Then, knowing T and Z, a probability to observe $| w_{ret} | \geq 1m\ s^{-1}$ is calculated as a function of MCS reflectivity zones and temperature. Colored solid lines in Figure 4 are probabilities calculated from RASTA measurement and dashed lines with stars are probabilities calculated with vertical velocity measured at the aircraft level (in-situ measurement). Both type of probabilities are different in each MCS zones and probabilities made with in-situ measurement are smaller than these calculated with RASTA retrievals; except in MCS reflectivity zones 8 in Darwin where they are similar. Hence, we know from the point of view of vertical velocity that the in-situ dataset is not representative to the observations from RASTA retrievals: different probability to observe vertical velocity with magnitude larger than 1m/s (updraft and downdraft).

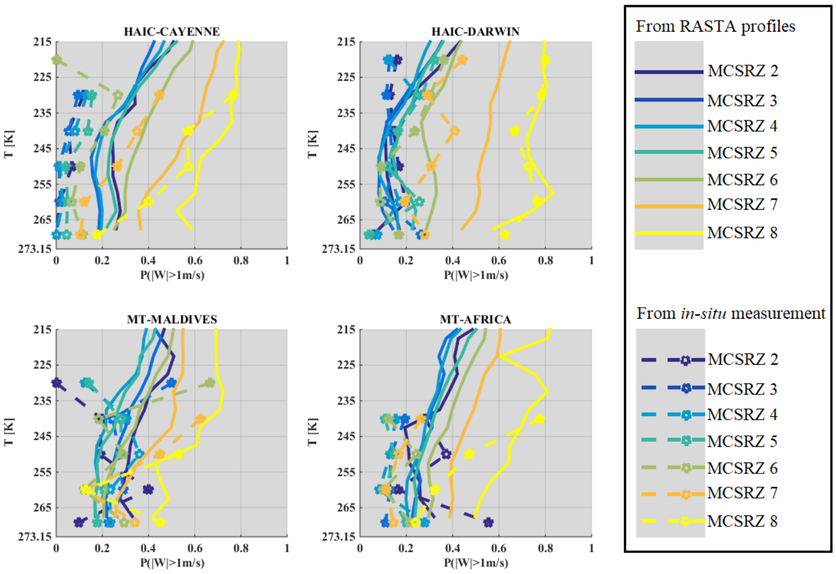

Figure 4: Probability to observe vertical velocity with absolute magnitude larger than 1m/s in each MCS reflectivity zone (MCSRZ; color scale) for measurement from the radar Doppler RASTA in solid lines and in dashed lines with stars marker for in-situ measurement.

In Figure 4 we show that probabilities to observe | w_{ret} | ≥ 1m s^{-1} are highest for MCS reflectivity zones 8 then 7 and 6, meaning that these MCS reflectivity zones tend to be more impacted by vertical movement (convective areas of MCS), than it is the case for other MCS reflectivity zones. Also, these probabilities generally increase with altitude for all airborne campaigns. Which meet the conclusions from Figure 3. Generally, in MCS reflectivity zones 5, 4, 3, and 2, the probabilities P(|w_{ret} ≥1|) as a function of T are close to each other with a decreasing trend as reflectivity decreases, except for the Maldives campaign. Statistically, MCS reflectivity zones 8 and 7 represent for all 4 datasets the most convective part of observed MCS and the lower reflectivity zones the stratiform part with significantly lower vertical wind speeds.

As a conclusion, at a constant altitude largest Z tend to be related with largest probabilities to observe vertical movement (downward or upward). In other words, MCS reflectivity zones 7 and 8 are good candidates to represent observations in the convective area of MCS or closer to the most convective part of MCS."

We add a sub-section in the end of section 5 (note that a new version of section 5 is written to satisfy comment of reviewer R2; see answer to reviewer 2) specific on the topic of impact of vertical velocity on ice microphysic (R1#4).

"

5.6 note on the impact of vertical movement on ice microphysic

This section discussed about the investigation performed about the impact of vertical velocity on the ice microphysical parameters presented earlier in this section 5. We separated the merged dataset in three sub-datasets such: i) w <-1m/s , (ii) -1m/s < w < 1m/s and (iii) w>1m/s. Then, median relative difference for the three conditions and for each parameters presented in this section 5 were calculated and compared to the median relative difference when no distinction is performed as function of vertical velocity. Firstly, we noticed that MRD-X for the merged dataset and MRD-X for the second condition (i.e. 1m/s < w < 1m/s) are similar (MRD-X: X being used to replace IWC, σ, NT, NT_{50}, NT_{500}, β, α, max(Dmax)). Secondly, differences of MRD-X in updraft and in downdraft with regards to MRD-X for merged dataset and no vertical movement are visible. But most of the times these differences are not enough pronounced compared to measurement uncertainties (U(X)/X).

Appendices B shows the Figures that shows when updraft have an impact on ice microphysic parameters for a given range of temperature and MCS reflectivity zones. So, Figure B1 shows MRD-IWC, Figure B2 shows MRD-NT and Figure B3 shows MRD-NT50. For the others parameters impact of updraft are uncommon.

It appears that updraft tends to impact mainly concentrations of small hydrometeors and IWC for some type of MCS and some MCS reflectivity zones. So for NT (Figure B2), we observe larger NT for updraft in MCS observed over Cayenne, Maldives and Niamey. For Cayenne, it appears in MCS reflectivity zone 5 and 6 for temperatures between 245K and 265 K with NT 2 to 3 times larger than NT for merged dataset. For MCS over Maldives, median NT are 5 times to 20 times larger than NT when there is no noticeable vertical movement in MCS reflectivity zones 6, 7 and 8. Finally for MCS over Niamey, we observe larger NT in updraft than NT for the merged dataset in MCS reflectivity zones 6 for T around 240 K and in MCS reflectivity zones 8 above the bright band. We have similar conclusions for NT_{50} (Figure B3), except that ratios between NT_{50} in updraft and NT_{50} when no updraft is smaller than the ratio between NT in updraft and NT when no updraft.

IWC are impacted by updraft, only for MCS over Cayenne, in MCS reflectivity zone 4, 5, 6 and 7. IWC in updraft tend to be larger about +50% than IWC when no updraft, except in MCS reflectivity zones where IWC are about 2 times larger in updraft than IWC when no updraft.

This investigation on the impact of updraft and downdraft on ice microphysics, shows that updraft may have an impact on concentrations of small hydrometeors and IWC. However, updraft does not impact all type of MCS in the same way. So, there will need to perform deeper investigations on updraft impact.

Despites some noticeable impact of updraft on ice microphysic for our dataset, there is no significant (recurrence trough all types of MCS or as function of T or Z) results to assess them for the merged dataset. So, the parameterization provided in the next section are not functions of vertical velocity. "

2) The discussion in several places talks about the importance of crystal shape, simulations using oblate spheroids, aggregation and the various mass-diameter relationships that depend on particle habit; however, even though in all four projects the 2D-S is used, an OAP with 10 µm resolution, there are no images shown or used in this analysis. This is a large omission of the most valuable piece of information that is available in this data set and would address a number of the questions that are raised hypothetically.

It is not an omission, shape of hydrometeors is not the topic of this study. We study bulk ice microphysical properties, and mass-size relationship in a way to focus on more general tendencies.

But to study variability of mass-size relationship, we use images of 2D-S and PIP to do our statistics and calculate the surface-size and perimeter-size relationships as it is describes in Fontaine et al., (2014) and Leroy et al., (2016). This, to deduce the exponent of mass-size relationship Beta and then study the variability of crystals shape through it (see Fontaine et al., (2014) and Leroy et al., (2016)). As this study is focused on bulk parameters; parameters summed over the size of hydrometeors. We study, the variability of shapes of hydrometeors through the variability of Beta in the 4 datasets. Moreover, the datasets contains some millions of images, our thought is that showing randomly some images even taken at each level and as function of radar reflectivity would have no statistical meaning for our study and would make the paper less clear as it contains already a lot of figures. However, this study is not scientifically exhaustive concerning the datasets we are using and future publications could be dedicated to images only.

Others reviewer's comments in supplement.

Line 8 page 2: Instead of relative terms like "large" and "small", please list the actual size ranges for reference further in the study.

We propose to rephrase this section (R1#5).

"*A number of studies (Gayet et al., (2012); Lawson et al., (2010) and Stith et al., (2014)), demonstrate the presence of different type of ice hydrometeors in evolving MCS. In the active convective area, ~~large~~ super cooled droplets larger than 500µm until 3mm, were observed near -4°C and rimed ice hydrometeors about the same size below -11°C. Also at -47°C ~~large~~ rimed particles about 2-3mm from updraft regions coexisting with ~~small~~ ice crystals about 100µm (pristine ice) were encountered. Near the convective zone of MCS (i.e fresh anvil) presence of pristine ice (about 100µm), aggregates of hexagonal plates (about 500µm to 1mm) and capped columns (about*

500µm) has been reported (Lawson et al., 2010). In aged anvils, columns (~100µm), plates (~100µm), and small aggregates (about 200µm) are observed near -43°C while large aggregates about 2mm and more are found at lower altitudes (-36°C). Also in the cirrus part of MCS bullet-rosettes about 500µm and less (more common for in situ cirrus (Lawson et al., 2010)) and chain-like aggregates from 100µm to about 1mm are found (aggregates of small rimed droplets caused by electric fields: Gayet et al., 2012; Stith et al., 2014)."

Line 24 page 3: The term "barycentre" is not one that is commonly used in this context, and considering you use Dmax in one case, and radius in the other, I think a very brief clarification would be useful here.

As the processing of OAP for our dataset is presented and described in Leroy et al., 2016. We use the same definition of Dmax given in Leroy et al., 2016 (end of page 3): "The definition used in this study also varies from the others above in that Dmax is the largest length through the center of the particle image". This definition comes with a detailed figure, the Figure 1 in Leroy et al., 2016 (see below).

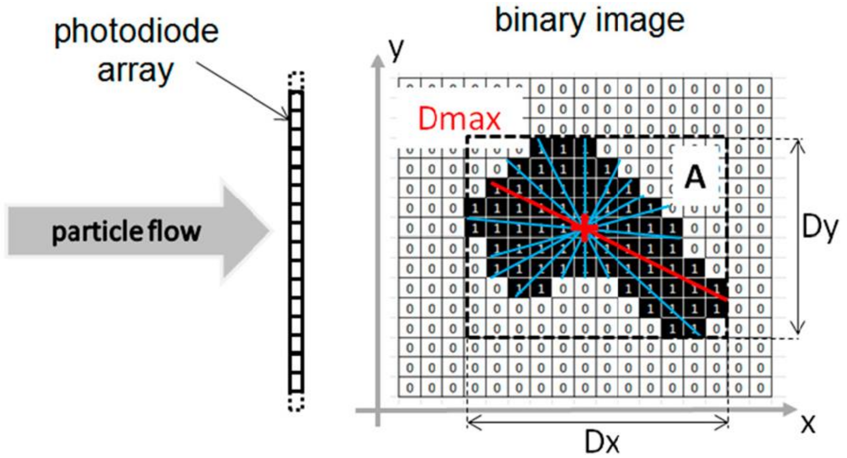

FIG. 1. Definition of particle dimensions that are extracted from OAP binary images. Blue lines illustrate some possible diameters passing through the center of the image, whereas the red line highlights the longest one, which is defined in this study as the maximum dimension.

We suggest to rephrase this section as (R1#6):

"*Both OAP probes record black and white images of hydrometeors with a resolution of 10µm and 100µm (2D-S and PIP, respectively). They are used to derived the size of hydrometeors (Dmax [cm] in this study), their projected surface (S [cm2]), their concentrations as a function of their size (N(Dmax) [#/L/µm]). The sizes of hydrometeors span from 10 µm to 1.28 cm with Dmax calculated as a function of the projected surface of hydrometeors (taking the maximum of radius passing through its barycentre; see Figure 1 in Leroy et al., 2016).*"

Line 26 page 3: How is IWC derived from the OAPs, i.e. what ice density or what mass-diameter relationship is used?

<u>And</u>

Line 27 page 3: This is quite confusing. What do simulations of the reflectivity factor have to do with retrieving IWC from the IKP-2?

First of all, IWC are not retrieved from OAP only by taking a mass-size relationship from former studies, nowhere in this paper there is a mention of such methodology.

In fact, there is two type of IWC used in this study. For both HAIC-HIWC campaigns, IWC was measured directly with the IKP-2 probes. It measures Total water content and then deduce IWC knowing relative humidity. For Megha-Tropiques we use simulations of radar reflectivity factors using PSD, and aspect ratio calculated with OAP (Fontaine et al., 2014 & 217) to retrieve IWC. The accuracy of the method to retrieve IWC from Z has been evaluated and tested in Fontaine et al., (2017).

We propose to rephrase this section (R1#7):

"*During both HAIC-HIWC campaigns, the IKP-2 probe was used to measure total condensed water, composed exclusively of ice water content (IWC [g m-3]) and water vapour, then IWC were deduced using in-situ measurement of relative humidity. However, IWCs< 0.1g m-3 are not considered in this study, due to IKP-2 uncertainties particularly important for low IWC measurements (see Strapp et al. 2016a). For both Megha-Tropiques campaigns, IWC was retrieved using simulations of the reflectivity factor Z, thereby using the approximation of ice oblate spheroids (Fontaine et al., 2017; Fontaine et al., 2014). Results about accuracy of IWC retrieved from this method with regards to IKP-2 measurement are discussed in Fontaine et al., (2017).*"

Line 6 page 4: In the introduction and abstract 215K is listed as the minimum T

Indeed, more clarification are needed concerning the temperature range of the dataset.

We propose to rephrase the sentence line 35 page 2 "The statistical analysis includes more than 55844 data points of 5 s measurement duration in the temperature range from 215K to 273.15K." By (R1#8):

"*Our statistical analysis is performed on cloud radar Doppler measurement and in-situ measurement. Cloud radar measurements include more than one million of data points of radar reflectivity factors and retrieved vertical velocities spanning from 170K to 273.15K (Temperature profiles from RASTA are calculating using re-analysis of ECMWF). And in-situ measurements include 55844 data points of 5 s duration in the temperature range from 215K to 273.15K.*"

Line 2 page 5: Where do you discuss how ice is differentiated from liquid?

Indeed, few unclear words mention it at line 24 page 12. We propose to add some explanation at the end of section 2 (R1#9).

"*Moreover, investigations have been performed to detect supercooled water using Rosemount icing detector (Baumgardner and Rodi 1989; Claffey et al. 1995; Cober et al. 2001) and Cloud Droplet Probe measurement.*

Few cases of super cooled water were detected and remove from the dataset (Leroy et al., 2016). Hence, the dataset used in this study is using exclusively data collected where only ice particles were measured. "

Line 12 page 8: This section is very confusing on many levels. First of all, it is not at all clear where the IKP measurements are. The text says "Figure 5" but there are 5 panels of Fig. 5.

IKP measurement of HAIC_HIWC and retrieved IWC of Megha-Tropiques are merged, then statistic (calculus of median, 25^{th} and 75^{th} percentile) as function of temperature and MCS reflectivity zones are performed on this merged dataset. Which is done for all other microphysical parameters used in this study.

We propose to rephrase the beginning of this section (R1#10).

"*This section discuss about IWC measured during HAIC-HIWC project and the IWC retrieved for the Megha-Tropiques project. IWC from the four dataset were merged to calculate the main statistic (merged dataset). Figure 5 shows median IWC for the merged dataset as a function of T and as function of MCS reflectivity zones (colored lines). Solely …"*

Secondly, the IWC is apparently being derived from the Z using T-matrix simulations but this is making a huge assumption about the habits of the ice crystals and seems to ignore the possibility of mixed phase.

We use IWC retrieved from radar reflectivity factors only for the Megha-Tropiques project. There is no retrieved IWC in mixed phase condition. More details on this methodology can be find in Fontaine et al., (2014 and 2017).

To the end of the added paragraph noticed for the comment line 2 page 5, we propose to add (R1#11)

"*Also, retrieval of IWC for the Megha-Tropiques project were not performed in mixed phase conditions (more details in Fontaine et al., (2014) and (2017)).*"

It seems that uncertainty is only being based on uncertainty in OAP measurements but the uncertainty in derived IWC simulations is certainly much larger than the uncertainty in the OAP derived IWC.

There is uncertainty specific to measurement from IKP-2 probes available only for HAIC-HIWC project that vary as function of T. And uncertainty specific to the retrieval method used for the Megha-Tropiques project. This method is described in two publications Fontaine et al., (2014) and (2017). Here, we using the uncertainty with regards to measurement of IKP estimated in Fontaine et al., (2017).

Thirdly, this figure should be presented as two figures, 5a as one and 5b-e as another. Not only is it too cluttered but it is very difficult to see the details in the individual panels.

New figures are made (see revised manuscript), taking into account this comment and the comment of the second reviewer using colour blind-friendly colour schemes.

Line 26 page 8: I cannot understand what is being described here, i.e. what is the uncertainty from the IKP and what is the uncertainty from the T-matrix simulations. Please clarify.

As IKP-2 was used only for HAIC-HIWC its uncertainty is only plotted on Figure 5-b) and Figure 5-c), this uncertainty vary as function of T and is showed by the grey band in Figure 5-b) and Figure 5-c). The uncertainty of retrieved IWC is only shown on Figure 5-d) and Figure 5-e), as IWC for Megha-Tropiques are retrieved from the method described in Fontaine et al., (2014) and (2017). Note that Figure 5-b, c, d, e) wil become Figure 6-a, b, c, d) in the new manuscript.

We propose to rephrase the under lighted text with (R1#12)

"*Figure 6 shows MRD-IWC for the four different campaigns. It is necessary that we recall that median IWC as function of T and MCS reflectivity zones are calculated using a merged dataset where there are IWC from direct measurement and retrieved IWC from Z and PSD (Fontaine et al., 2017). Then, there is two different uncertainties to consider to evaluate the MRD-IWC in each campaigns. Firstly, for Darwin and Cayenne campaigns the IWC were measured with IKP-2 probe (direct measurement) with an uncertainty on measured IWC increasing with temperature (~5% at 220K and ~20% at 273.15 K; Strapp et al., 2016). Secondly, for Niamey and Maldives IWC were retrieved using the method described by Fontaine et al., (2017) (indirect measurement) with an uncertainty with regards to the IKP estimated by about ±32%. Hence, in Figure 6-a) and Figure 6-b) the grey band area show the uncertainty of the IKP-2 probe that was used for Cayenne and Darwin campaigns. While in Figure 6-c) and Figure 6-d) the grey band area describe the uncertainty on the retrieval method for IWC that was used for datasets of Niamey and Maldives.*

Note that confidence in direct bulk IWC measurements from the IKP-2 is significantly higher than in indirect IWC calculations from the retrieval method (Fontaine et al., 2017)."

Line 16 page 9: These dashed lines are the same, at least on this figure, cannot differentiate dashed from dod-dashed.

A new figure 5 is performed. Median IWC for merged dataset (black solid line), and for each campaigns are removed (other black dashed and dotted lines with markers). Then, the curve for the Heymsfield et al., (2009) is now plotted with a black solid line.

Line 5 page 10: Are these in T bins of 10C?

Yes, statistics are performed on 10°C bins.

Line 16 page 10: This is an important point to be addressed, how important are the < 100 um particles?

The contribution of particles smaller than 100µm on the visible extinction is about 2% (median) in the range T [235K; 273.15K] and 10 % in the range T [215K; 225K]. Statistic calculated aver all the merged dataset (see figure R14 below).

We propose to rephrase the sentence with this comment (R1#13).

"*Note, that if we took uncertainties for particles smaller than 100µm (with (U(D))/D=±50% and (U(N))/N=±100%) the uncertainty on the calculation of σ would increase to ± 122%. The reason why we do not take into account uncertainty of smaller particle is due to that these particles contribute little to the visible extinction (2% in the range [235K; 273.15] and 10% in the range [215K; 225K].*"

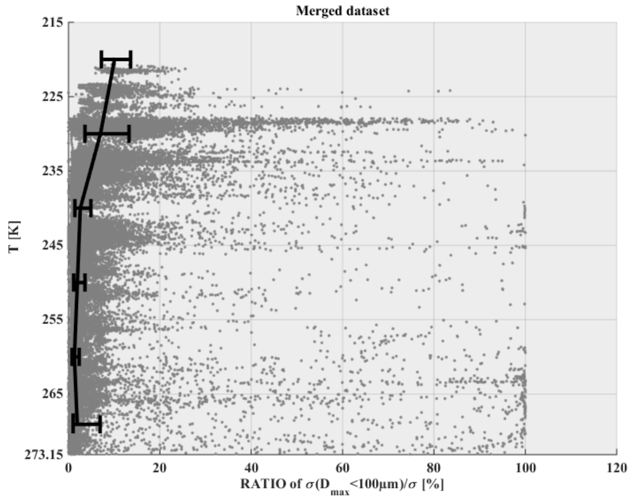

Figure R 14: on x axis ratio of visible extinction calculated with particles smaller than 100µm over the visible extinction over all the spectrum of size of ice hydrometeors. On y axis the temperature. Black solid line represent median ratio. Statistic performed over the merged dataset.

Line 21 page 10: Why are there two lines?

Be careful, there is only one grey dashed line that become a black solid line in the new figure.

Line 24 page 12: This means few were detected or few removed? What about the radar data?

See answer for the comment at line 20 page 6. This sentence is deleted in the new version of the manuscript as the topic is addressed earlier.

Line 10 page 14: On what is this assumption based?

I cannot remember why, this sentence appears here, or retrieve the context of this assumptions exactly. This sentence is deleted in the new manuscript.

Line 20 page 14: This is possibly a result of sample sets that have Dmax>500 um. Where is this documented, i.e. data points at each T level at each Dmax condition?

And

Line 22 page 14: Exactly my point, what are the sample size of these conditions?

For each parameters presented in this study, either for the merged dataset or the campaigns individually (for calculation of MRD-X), the calculation are performed with the same conditions. The samples in each conditions (T bins and Z bins) have the same size for all parameters. Indeed, data points are selected if they meet the temperature and radar reflectivity criteria, but also the total concentration has to be positive (for Dmax >50µm); mixed phased conditions being excluded. So, the size of the samples (i.e. same number of data points) for NT, NT_{50}, NT_{500}, IWC, visible extinction, mass-size relationship coefficient, and max(Dmax) are the same. So, if for a point there is no measurement of particle larger than 500µm NT_{500} is equal to 0 L^{-1} which bring the MRD-NT_{500} to -100% for this point.

So sample size has no impact on the comparison of MRD-NT, MRD NT_{50} and MRD-NT_{500}, as it is the same for all of them.

We propose to add a comment to the end of section 4 (R1#14).

"*For each parameters presented in this study, either for the merged dataset or the campaigns individually (for calculation of MRD-X), the calculation are performed with the same conditions. The samples in each conditions (T bins and Z bins; Z bins vary as function of altitude, i.e. MCS reflectivity zones) have the same size for all parameters. Indeed, data points are selected if they meet the temperature and radar reflectivity criteria, but also the total concentration has to be positive (for Dmax >50µm); mixed phased conditions being excluded. So, the size of the samples (i.e. number of data points in each ranges of T and of Z) for NT, NT_{50}, NT_{500}, IWC, visible extinction, mass-size relationship coefficient, and max(D_{max}) are equal.*"

Line 4 page 15: Any aerosol measurements of any type on these flights? CN? PCASP?

For sure there is no measurement of aerosol concentration of any types for the Megha-Tropiques campaigns. So, there is no general results that could be produced for this study.

Line 19 page 16: Why CWC instead of IWC?

Pure Writing mistakes.

Line 18 page 17: Why speculate? With the OAPs, especially the 2D-S you have that information.

Yes we have this information, here through the exponent Beta of the mass-size relationship. The perimeter-size relationship and surface size relationship that allow to calculate the exponent β of the mass-size relationship, are calculated using the images from the 2D-S and the PIP. Somewhere, β describe globally the variability of the shapes of hydrometeors.

We propose to add these two sentences line 30 page 15 (R1#15).

"*These two relationships are calculated using Images from 2D-S and PIP. Hence, β is a proxy parameter that describe the global (all over the size range of hydrometeors from 50µm to 1.2cm) variability of the shape of the recorded hydrometeors during the sampling process (Leroy et al., 2014; Fontaine et al., 2014)*"

However, this section do not describe correctly the message that we wanted to give. So we propose to rephrase the part of the section 5.4 from the line 4 page 16 until the line 21 page 17 (R1#16).

"*In order to estimate the uncertainty on the calculation of β (grey band in Figure 14 (a), (b), (c), and (d), results from (Leroy et al., 2016) have been utilized, with U(β)/β=±2.3%. However, if we have calculated the uncertainty* *on retrieved β from the uncertainty on the measurement of the size and concentration of hydrometeors from OAP images, the uncertainty would have been by about 44%. In general, MRD-β in MCS reflectivity zones 8 and 7 tend to be in the range of U(β)/β assuming that β are similar for all observed MCS in the four campaigns for the conditions described by MCS reflectivity zones 7 and 8.*

However, in MCS reflectivity zones 2 to 6 MRD-β are more scattered around U(β)/β with sometimes larger MRD-β than uncertainty of β. Especially for MCS over Maldives and Niamey. Over Maldives at higher altitudes β tend to be smaller compared to the median β calculated for the merged dataset. While, MCS over Niamey tend to have β larger than median β calculated for the merged dataset.

Overall, the predictability of β coefficients as a function of T and MCS reflectivity zone remains challenging. We are aware of the fact that the power-law approximation has certain limits, trying to impose one single β to an entire crystal population composed of smaller (dominated by pristine ice) and larger crystals (more aggregation, also riming).

For HAIC-HIWC data, coefficients α are retrieved, while matching measured IWC from IKP-2 with calculated IWC thereby integrating PSD times m(D) power law relationship. For Maldives and Niamey datasets, coefficients α are retrieved from T-matrix simulations of the reflectivity factor (Fontaine et al., 2017).

For both situation, α calculation is solely constrained by the fact that the mass of ice crystals remains smaller or equal than the mass of an ice sphere with the same diameter D_{max}:

$$\alpha = \frac{IWC}{\sum_{15}^{12845} N(D_{max}) \cdot D_{max}^{\beta} \cdot \Delta D_{max}} \quad | \quad \alpha \cdot D_{max}^{\beta} \leq 0.917 \cdot \frac{\pi}{6} \cdot D_{max}^{3} \quad \left[g\ cm^{-\beta}\right]. \qquad (6)$$

For the uncertainty calculation of α we take the maximum value of β which is 3:

$$\frac{U(\alpha)}{\alpha} = \sqrt{\left(\frac{U(IWC)}{IWC}\right)^2 + 3 \cdot \left(\frac{U(D)}{D}\right)^2 \left(\frac{U(N)}{N}\right)^2} \qquad (7)$$

Figure 15 shows median α coefficients as a function of T and MCS reflectivity zone. As has been already stated in previous studies, α is strongly linked to the variability of β (Fontaine et al., 2014; Heymsfield et al., 2010). Figure 15 compared to Figure 13 confirms that results for α have similar trends as those discussed for β. α vary from 5.10^{-4} (in MCS reflectivity zone 2) to ≈2.10^{-2} (in MCS reflectivity zone 8). In general, α increases as a function of T for a given MCS reflectivity zone and also increases as a function of MCS reflectivity zone (and associated IWC) for a given T level. As already stated for the median exponent β in Figure 13, median α in MCS reflectivity zones 4, 5, 6, 7 and 8 are more or less overlapping. ~~*Median α in MCS reflectivity zones 2 and 3 are shown for completeness reasons, however with less confidence as they are related to IWC generally smaller than 0.1g m^{-3}.*~~

From Figure 16(a) and Figure 16(b) we can note that even with a good accuracy of the measured IWC (from IKP-2; U(IWC)/IWC ≈ ±5% for the typical IWC values observed in HAIC-HIWC at 210K), the uncertainty of α, is rather large which is mainly due to uncertainties in OAP size and concentration measurements. Taking into account the large uncertainty on the retrieved α, we find that MRD-α for all 4 tropical datasets for MCS reflectivity zones 4, 5, 6, 7, and 8 are smaller than U(α)/α. For data from Niamey (Figure 16 (d)), α tend to be larger than median α for the tropical dataset (MRD-α not centered on 0, but shifted to positive values).

In previous sections, this study documented similar IWC values and visible extinction coefficients for a given range of Z and T and a clear increase of IWC and visible extinction coefficient from MCS reflectivity zones 4 to 8. The increase of α and β with MCS reflectivity zones is not as much clearly visible, whereas at least α seems to increase with temperature in different MCS reflectivity zones). And we cannot ignore that α and β tend to be larger in MCS reflectivity zone 8 than in MCS reflectivity zone 4, especially at higher altitude. But, the increase of IWC and visible extinction with MCS reflectivity zone Z is not linked to an increase of the mass-size coefficients. This conclusion takes into account the variability of the mass-size coefficients shown by 25 and 75 percentiles. Moreover, ice hydrometeors habits describe with β in MCS reflectivity zone 4, 5 and 6 are different in MCS over Maldives and MCS over Niamey compared to MCS over Darwin and Cayenne (smaller β over Maldives and larger β over Niamey).

As visible extinction (hence projected surface) and IWC are similar for the same range of T and Z in all types of MCS, but the shapes of crystals might be different from one to another MCS location. Our assumptions is that the ratio of projected surface vs IWC is similar. In other words the density of ice per surface unity (or by pixels of projected surface) is similar as function of T and Z in all types of MCS even if there might be a possibility that the habit or the shape can be different (pure oceanic MCS vs pure continental MCS). Note that these assumptions are established for IWC larger than 0.1g.m^{-3}."

Line 14 page 18: How are aggregates being defined?

Ice crystals aggregates are an agglomerate of pristine ice, the growth process of aggregates is leading by sedimentation of ice crystals (see Westbrook et al., 2004). But all the physic of aggregation process is still not well known; i.e. sticking coefficient for example.

We propose to rephrase this sentence (R1#17).

"*In this section, it is shown that in the stratiform part of MCS, largest hydrometeors are larger in MCSs over Niamey than in other types of MCS, and tend to be smaller in MCS over Maldives Islands. Mainly, large crystals (Dmax > 1mm) are agglomerates of pristine ice crystals, for which the growth process is leaded by aggregations (by sedimentation) instead of vapour diffusion. Some large pristine ice were found in the dataset (especially over Maldives see Figure 1 in Fontaine et al., 2014) but usually their size do not exceed 3 to 4 mm. So our observations of max(D_{max}) suggest that aggregation efficiency is different from one MCS type to another.*"

Line 18 page 18: What is this analysis telling us that the IWC and visibility don't? The 2nd moment is visibility and the 3rd moment the IWC.

It might be true for the liquid hydrometeors, but theoretically there is no reason for ice hydrometeors that it is always true. This is why second Moment is discussed separately.

For the visibility we have:

$$\sigma = 2 \int_0^\infty N(D_{max}) \cdot e_s \cdot {D_{max}}^{f_s} \cdot dD_{max} = 2 \cdot S_T$$

Where fs is the fractal dimension of the surface-size relationship that vary between 1 and 2 (see Mitchell 1996).

While for the second Moment we have:

$$M_2 = \int_0^\infty N(D_{max}) \cdot {D_{max}}^2 \cdot dD_{max}$$

However, when plotting σ versus M2 we can see that these two quantities are proportional. Indeed, Figure R15 tells us that there is a ratio between M_2 and S_T. The computation of this ratio $R_{M2-\sigma}$ is 0.72 (0.66, 0.68, 0.72, 0.75 and 0.78 for 10th, 25th, 50th, 75th and 90th percentiles) such:

$$R_{M2-\sigma} \cdot \sigma = \frac{\pi}{4} M_2$$

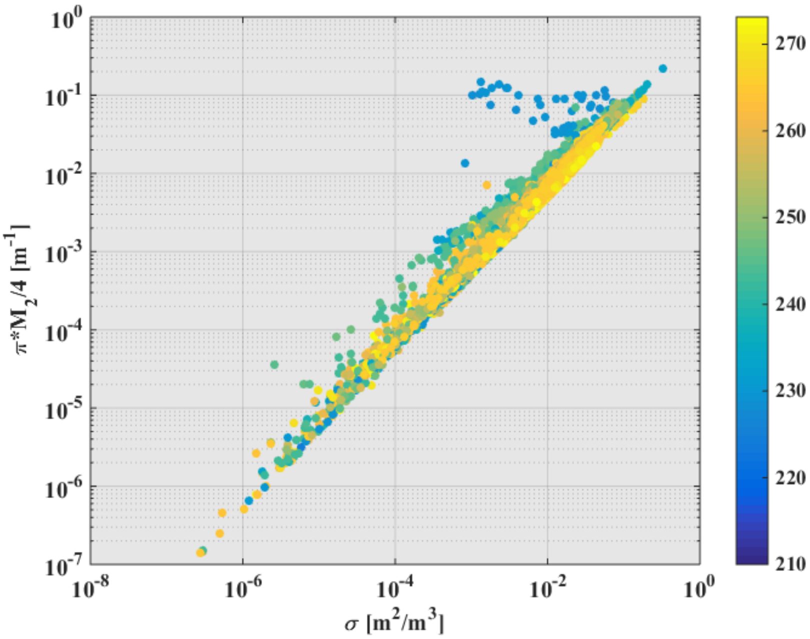

Figure R 15: on y-axis second moment of PSD (M_2) as function of visible extinction of ice hydrometeors on x-axis. Data points are colored as function of in-situ Temperature in Kelvin.

Similar demonstrations can be done for the relationship between the third moment of PSD M_3 and the IWC.

For the IWC we have:

$$IWC = \int_0^\infty N(D_{max}) \cdot \alpha \cdot {D_{max}}^\beta \cdot dD_{max}$$

Where α and β are the coefficient of the mass-size relationship. For mass-size relationship β is rarely equal to 3 (except maybe for individual frozen droplets). And recent studies suggest that β (and α) could even vary as function of D_{max} (Erfani and Mitchell 2016; Coutris et al., 2017).

For the third Moment we have:

$$M_3 = \int_0^\infty N(D_{max}) \cdot D_{max}{}^3 \cdot dD_{max}$$

Figure R16, show that there is a trend of proportionality between IWC and the third Moment. But the spread is definitely too large to assume that third moment is equal to IWC or proportional to it.

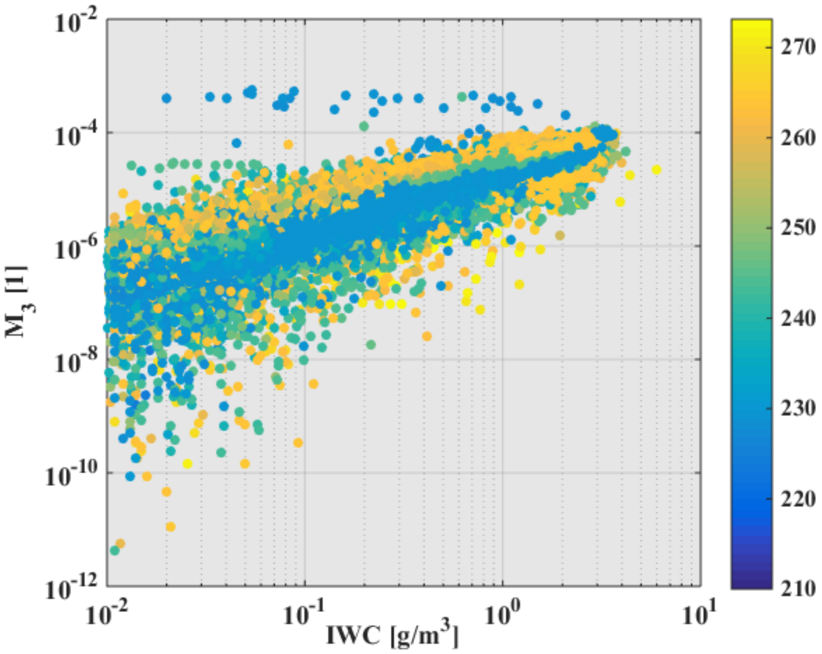

Figure R 16: on y-axis third moment of PSD (M_3) as function of IWC on x-axis. Data points are colored as function of in-situ Temperature in Kelvin.

Line 36 page 23: How does this differ from "Effective Radius"? This is really just the area weighted diameter

Yes, but as this study provide an update of a former parameterization, we prefer to keep the same notation used in this former study (Field et al., 2007). Also, it can be find different definition of effective radius that are not exactly similar to the ratio of the third Moment and the second moment (see Delanoë et al., 2007; Heymsfield et al., 2002).

Answers to the second Referee R2.

We want to thank Dr. Frey to review our study and making comments that allow to improve our manuscript.

Legend of styles

- **Reviewer comment**
- Author’s answer
- (R2#i): flag to relate the change in the new manuscript (see author’s comment)
- *“Change in the manuscript”*

Major comments

Meteorological conditions:
You mention and compare data from four different field campaigns. However, you only very briefly mention the differences in conditions of these campaigns. I think it would be useful to know more about what distinguishes the data sets (see comment above). Like major differences in meteorological or dynamical conditions, land/sea convection or orographical effects, monsoon or other special season, development stages of the MCS during the aircraft observations (developing, mature, decaying), microphysical characteristics as particle shapes which you would get from the optical array probes, or any other conditions that could lead to specific characteristics of the respective datasets.

This study aims to document some of ice microphysical properties (not all) in MCS as function of Z and T. It uses a merged dataset of in-situ measurement performed in 4 MCS over 4 different locations. Main tendencies (median calculation) are calculated as function for this merged dataset. However, it is a will that we take only into account as function of Z and T, as this results could be used in future studies using CloudSat radar reflectivity profiles or the future EarthCare mission’s data. In this conditions only T, Z and the locations of the data will be known. This is why, we study the impact of the locations of MCS globally, and not as function of others conditions. We agree that further investigations could be provided taking into account meteorological conditions and dynamics, as life cycle of MCS (developing, mature, and decaying) could also be taken into consideration. This kinds of studies would need more information than these provided by our dataset, to me more accurate and the use of passive remote sensing from geostationary satellites would be helpful for this. This is why we think it is beyond of the topic of this study. It would make it more complex to understand.
However, we can provide add some information. The datasets include MCS from West African monsoon that developed over the continent, MCS linked to the ITCZ over the Indian Ocean during the wet MJO phase and the dry MJO phase (small isolated convective systems), MCS developed over land/ocean/cost during the North Australian monsoon and MCS developed over land/ocean/cost during the wet season over the north of south America. Also, MCS were sampled in there mature stage.

We propose to add some comments in the beginning of section 2 (R2#1):

“*This study uses a data set where MCSs were observed in four different locations in the tropics and related to two different projects:*

1. *Megha-Tropiques in Niamey, during July and August 2010: observation of continental MCS formed over the region of Niamey (Niger) during the West African Monsoon (Drigeard et al., 2015; Fontaine et al., 2014; Roca et al., 2015). These MCS developed over the continent. 7665 points of 5 seconds.*
2. *Megha-Tropiques in Maldives, during November and December 2011: observation of oceanic MCS developed over the southern part of the Maldives and related to the ITCZ (Inter Tropical Convergence Zone) in the Indian Ocean. (Fontaine et al., 2014; Martini et al., 2015; Roca et al., 2015). It includes MCS developed during the wet phase of MJO and two event with isolated convective systems developed during the dry phase of MJO. 3347 points of 5 seconds.*

3. *HAIC-HIWC in Darwin, from January to March 2014: observations of MCS formed over Darwin and the North-East cost of Australia during the North Australian Monsoon (Leroy et al., 2016; Protat et al., 2016; Strapp et al. 2016; Leroy et al. 2017, Fontaine et al. 2017). During this campaigns, MCS developed over the land, the ocean, and near the cost. 23265 points of 5 seconds.*
4. *HAIC-HIWC in Cayenne during May 2015: observations of MCS developed over the French Guyana during the peak of its raining season (Yost et al., 2018). Same as for Darwin, MCS developed over the land, the ocean, and near the cost. 21567 points of 5 seconds.*

Note that observations were performed in mature MCS."

Naming convention:

The merged data set from the four campaigns is sometimes named differently in the manuscript and figures (tropical, global, global tropical...). Please keep it to one name! I would suggest not to use 'global' as it only contains tropical campaigns. As it is not clear whether different locations in the tropics have a significant influence on the data, I would suggest simply using 'merged' (or 'combined') data set, that makes it clear that not data from all over the tropics are used (as might be possible in satellite data studies for example).

The comment is taken into account, and a new naming convention will be used for the "tropical dataset" such "*merged dataset*".

Radar reflectivity zones:

How were the thresholds for the 8 zones chosen? How do you motivate the thresholds? Is it possible to interpret each zone in respect to a certain MCS development stage, or do they distinguish in some other MCS characteristic?

In some cases it seems that particularly the lower classes do not really differ from each other (e.g. page 6, line 2/3 or page 25, line 32/33). What is the reason to keep separate zones and not combining them into one?

The description of how were chosen the limits of the 8 MCS reflectivity zones is given in the manuscript page 5 line 5 to line 13.

The motivation to choose limits of MCS reflectivity zones regarding the percentiles given in Figure 1 and Table A1 holds in two facts. First, the variability of Z vary along the altitude. We can observe in Figure 1 that Z extend from about -20dBZ to 18 dBZ at 260K while it spread out from -10dBZ to 10 dBZ at 200K. So, this has to be considered if we want to sort our dataset as function of T and Z. So the limit of the Z range cannot be the same for each altitude has meeting ice hydrometeors linked to 15 dBZ or linked to -20dBZ at 200K is quiet impossible. The second fact holds on result on a former study (Cetrone and Houze 2009) which shows that distributions of Z as function of altitude are not the same in convective and stratiform part of MCS. This former study was performed with the 13GHz radar profiler on board TRMM satellite (Tropical Rainfall Measuring Mission), which is more sensitive to the precipitating particles (large drops and large ice crystals). The radar used in our study is more sensitive to smaller size of hydrometeors, then it is more adapted to the properties of ice crystals presented in our study.

We do not think that only MCS reflectivity zones can give information about the stage of the MCS in its life cycle (i.e. Formation, maturation, decaying), analyse of geostationary satellites would be more helpful for this topic (Fiolleau and Roca 2013). But, studying the distribution of MCS reflectivity zones as function of life cycle of MCS and brightness temperature and/or visible reflectance would be interesting for a future study.

MCS reflectivity zone has to be seen as a recalling of Z, but it add the information of the place of the Z among the distribution of Z in MCS (not for all of clouds).

Yes, it seems that the dynamic in lower MCS reflectivity zones is similar (i.e. 2, 3, 4 and 5), that could be put in a same class. But these class do not have the same range of IWC, visible extinction etc…

So put all the lower class of MCS zones together would bring less accurate profiles of the microphysic parameters.

We propose to re-write a part of the section 3.1 (from line 3 page 4 to the end of the section; R2#2):

"*Figure 1 shows that distributions of Z are not totally similar for all 4 airborne campaigns. MCS can expend over hundreds or thousands square kilometres, where size and repartition of their convective and stratiform areas can vary from one MCS to another. So the same sampling strategy in two different MCS would provide two different mean or median profiles of ice microphysics properties as function of T. But two different sampling strategy in the same MCS would have the same results. The idea of this study is to compare the properties of ice hydrometeors* *for different tropical MCS locations, thereby rendering comparable different MCS systems (as a function of temperature), through the analysis of the frequency distribution of profiles of Z dividing all MCS into eight zones. This strategy aims to reduce the impact of the different flight patterns and objectives for sampling MCS during each airborne campaigns used in this study.*

Note that Z at 94 GHz is linked to the ice water content (Fontaine et al., 2014; Protat et al., 2016), but also to the size distribution of ice hydrometeors, respective crystal sizes, and mean diameter (Delanoë et al., 2014).

Our motivation to choose the limits of Z ranges on what the statistic of ice hydrometeors properties holds in two facts. First, Figure 1 shows that the variability of Z at a given T is large and this variability of Z vary along the altitude. We can observe in Figure 1 that Z extend from about -20dBZ to 18 dBZ at 260K while it spread out from -10dBZ to 10 dBZ at 200K. So, this has to be considered if we want to sort our dataset as function of T and Z. So the limit of the Z range cannot be the same for each altitude has meeting ice hydrometeors linked to 15 dBZ or linked to -20dBZ at 200K is quiet impossible. The second fact holds on result on a former study. Indeed, Cetrone and Houze, (2009) used the profiling radar of TRMM satellite ((Tropical Rainfall Measuring Mission; Huffman et al., 2007) to demonstrate with frequency distributions of radar reflectivity Z as a function of height that higher Z occur more often in convective echoes of MCS (in West African Monsoon, Maritime Continent and Bay of Bengal) than in their stratiform echoes. This former study was performed with the 13GHz radar profiler on board TRMM satellite, which is more sensitive to the precipitating particles (large drops and large ice crystals). The radar used in our study is more sensitive to smaller size of hydrometeors, then it is more adapted to sort the properties of ice crystals presented in our study. Hence, this study presents ice microphysical properties in MCS as a function of temperature layers and also as a function of zones of reflectivity Z. In order to fix the limits of a limited number of Z levels, this study takes the percentiles of all merged campaigns datasets shown by the solid lines (all data) in Figure 1. This defines Z ranges as a function of height. Hereafter, these ranges will be called MCS reflectivity zones and numbered 1 to 8:

- *MCS reflectivity zone 1:* $Z < Z^{1th}$
- *MCS reflectivity zone 2 :* $Z \in [Z(T)^{1th}\,; Z(T)^{10th}[$
- *MCS reflectivity zone 3 :* $Z \in [Z(T)^{10th}; Z(T)^{30th}[$
- *MCS reflectivity zone 4 :* $Z \in [Z(T)^{30th}; Z(T)^{50th}[$
- *MCS reflectivity zone 5 :* $Z \in [Z(T)^{50th}; Z(T)^{70th}[$
- *MCS reflectivity zone 6 :* $Z \in [Z(T)^{70th}; Z(T)^{90th}[$
- *MCS reflectivity zone 7 :* $Z \in [Z(T)^{90th}; Z(T)^{99th}[$
- *MCS reflectivity zone 8 :* $Z \geq Z(T)^{99th}$

”

And add these comments in the conclusion line 35 page 25 (R2#3):
“*We do not think that alone, MCS reflectivity zones can give information about the stage of a MCS in its life cycle (i.e. Formation, maturation, decaying). The analysis of geostationary satellites data would be more suited for this topic (Fiolleau and Roca 2013). But, studying the distribution of MCS reflectivity zones as function of life cycle of MCS and brightness temperature and/or visible reflectance could be a future investigation.*
However, this study demonstrates…”

Paper length:

At the beginning of section 5 you introduce the general outline of Figures 5, 6, and 8 - 16, which I found a very good idea to keep the description of each figure short.
However, Section 5 still is too long! I would suggest to closely check from which figures/subsections you draw major conclusions and move those that only bear minor conclusions into a supplement and mention the investigation of the respective parameter in 1-2 sentences in the main manuscript. This will keep the manuscript more focused and the reader's attention. I will give some suggestions below, but you might want to identify other sections that could be moved yourself.
We propose to rewrite the section 5. First we take into account the comment about total concentrations, and remove the part talking about NT to put it in an appendices. But we keep the part concerning the mass-size coefficient. Secondly, we removed the part of the section 5 dedicated to the two parameterization, to do a section only dedicated to this topic. Note that figures have been remade due to reviewer 1 comments.
(R2#4)
"

5 In-situ Observations in tropical MCS: HAIC-HIWC and Megha-Tropiques projects

5.1 Ice water content

This section discuss about IWC measured during HAIC-HIWC project and the IWC retrieved for the Megha-Tropiques project. IWC from the four dataset were merged to calculate the main statistic (merged dataset). Figure 5 shows median IWC for the merged dataset as a function of T and as function of MCS reflectivity zones (colored lines). Solely, the graphical representation is limited to medians of IWC for MCS reflectivity zones 4 to 8. Indeed, IWC in MCS reflectivity zones 2 and 3 are linked to IWC smaller than 0.1 g m^{-3}, where IWC data are subject to less confidence. Globally, 30% of the data observed in 4 tropical MCS have an IWC lower than 0.1g m^{-3}, and the lower limit of MCS reflectivity zone 4 is defined with the 30th percentiles of Z. The figure reveals an IWC increases with increasing MCS reflectivity zone for a given range of temperature. IWC median values differ clearly as a function of the MCS reflectivity zone, and this for the entire range of temperatures, with only a few exceptions above the freezing level (T $\in$ [265 K; 273 K[), between MCS reflectivity zones 4 and 5, and MCS reflectivity zones 7 and 8, respectively, with small overlap in IWC ranges. In MCS reflectivity zones 4 to 7, median IWC increase with increasing T between 215 K and 260 K (where IWC has its maximum) and then slightly decrease as T further increases towards 273K. In MCS reflectivity zone 8 IWC behaves rather similar with a maximum IWC already reached at 250 K.

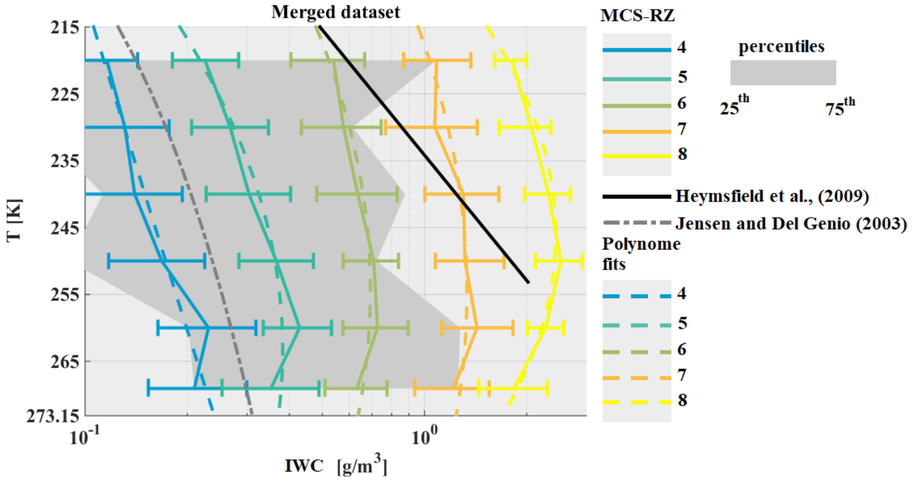

Figure 5: Median of IWC in [g/m^3] on x-axis, as a function of temperature in [K] on y-axis for different MCS reflectivity zones. Results for the merged dataset including both MT and both HAIC-HIWC datasets. The grey band represents 25th and 75th percentiles of merged dataset. Extremity of error bar show 25th and 75th percentiles of IWC in each MCS-RZ.

Figure 6 shows MRD-IWC for the four different campaigns. It is necessary that we recall that median IWC as function of T and MCS reflectivity zones are calculated using a merged dataset where there are IWC from direct measurement and retrieved IWC (Fontaine et al., 2017). Then, there is two different uncertainties (grey bands) to consider to evaluate the MRD-IWC in each campaigns. Firstly, for Darwin and Cayenne campaigns the IWC were measured with IKP-2 probe (direct measurement) with an uncertainty on measured IWC increasing with temperature (~5% at 220K and ~20% at 273.15 K; Strapp et al., 2016). Secondly, for Niamey and Maldives IWC were retrieved using the method described by Fontaine et al., (2017) (indirect measurement) with an uncertainty with regards to the IKP estimated by about ±32%. Hence, in Figure 6-a) and Figure 6-b) the grey band area show the uncertainty of the IKP-2 probe that was used for Cayenne and Darwin campaigns. While in Figure 6-c) and Figure 6-d) the grey band area describe the uncertainty on the retrieval method for IWC that was used for Niamey and Maldives.

Note that confidence in direct bulk IWC measurements from the IKP-2 is significantly higher than in indirect IWC calculations from the retrieval method (Fontaine et al., 2017).

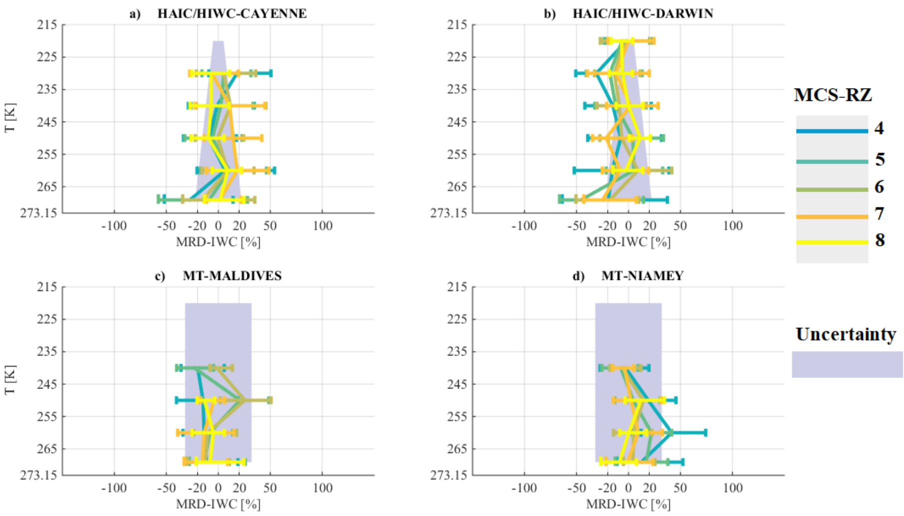

Figure 6: Median relative difference (MRD) of IWC during a) HAIC-HIWC in Cayenne, b) HAIC-HIWC in Darwin, c) Megha-Tropiques Maldives Islands and d) Megha-Tropiques in Niamey, with respect to median of IWC for the Tropical dataset on x-axis as a function of temperature in [K] on y-axis. The grey bands represent the uncertainties of the IWC measurement in b) and c), and the median deviation between measurement and the IWC retrieval method (Fontaine et al. 2016) in d) and e). Lines are colored as a function of the MCS reflectivity zones where in-situ measurement were performed, dashed colored lines are corresponding to the polynomial fit. Extremity of error bar show 25th and 75th percentiles of IWC relative error in each MCS reflectivity zone.

In addition, Figure 6(a), (b), (c), and (d) show MRD-IWC for all MCS reflectivity zones as a function of T. For all 4 tropical MCS, MRD-IWC in MCS reflectivity zones 4 to 8 are distributed around 0 and are in general less than

30-40% (25th to 75th percentiles). Measured IWC in MCS reflectivity zone 8 are in particular good agreement with the median IWC for all 4 tropical datasets, except maybe for high altitude MT-Niamey data. Uncertainty U(IWC)/IWC for IKP-2 measurements (Darwin and Cayenne) especially at high altitude (about 5%) is smaller than the expected deviation MRD-IWC. For mid and lower altitudes, MRD-IWC for Darwin and Cayenne particularly for zones 5 and 8 are of the order of corresponding U(IWC)/IWC. Concerning, MCS over Niamey and the Maldives Island, MRD-IWC (25th to 75th percentiles) in general do not exceed corresponding U(IWC)/IWC.

For comparison purposes with former studies, two IWC-T relationships from literature are added in Figure 5(a). Jensen and Del Genio (2003) suggested an IWC-T relationship in order to account for the limited sensitivity of the precipitation radar aboard the TRMM satellite, not allowing for small ice crystals at the top of convective clouds' anvils to be observed. They used radar reflectivity factors of a 35GHz radar based on Manus Island (North-East of Australia; 2.058°S, 147.425°E), thereby calculating IWC from an IWC-Z relationship (IWC=0.5(0.5.*$Z^{0.36}$*); Jensen et al., 2002). The resulting IWC-T relationship given by Jensen and Del Genio (2003) is reported by a dashed-dotted grey line, which fits between 75th percentiles of merged median IWC of MCS reflectivity zone 4 and 25th percentile of MCS reflectivity zones 5. We recall that IWC, as a function of T, in MCS reflectivity zones 4 and 5 are related to Z between 30th-50th and 50th-70th percentiles, respectively. We may notice that the IWC-T relationship from Jensen and Del Genio (2003) is different and smaller than the median IWC (4 tropical campaigns). Hence, IWC-T relationship from Jensen and Del Genio (2003) is more adapted to stratiform part of MCS where convective movement occurs less often.*

Moreover, Heymsfield et al., (2009) established an IWC-T relationship based on 7 fields campaigns (black line in Figure 5. They focused their study on maritime updrafts in tropical atmosphere for a temperature range T ∈ [213.15K; 253.15K]. Their suggested IWC tend to be in the range of IWC of MCS reflectivity zones 6- 8 with IWC increasing with T. We already showed in section 3.2 that MCS reflectivity zones 7 and 8 have higher probabilities to be convective (updraft regions with higher magnitudes of vertical velocity), as compared to other MCS reflectivity zones. Therefore, Heymsfield et al., (2009) IWC parametrizations for maritime updrafts are not inconsistent with data from this study.

Overall, this section demonstrates that variation of IWC with the temperature is similar in all type of MCSs for corresponding ranges of radar reflectivity factors. Hence, we assume that IWC-Z-T relationships developed in Protat et al., (2016) is usable for all types of MCS in the Tropics, at least for IWC larger than 0.1g m^{-3}.

5.2 Visible extinction

Figure 7 shows visible extinction coefficients (σ) calculated from OAP 2D images (approximation of large particles; Van de Hulst, 1981):

$$\sigma = 2 \cdot \sum_{15\mu m}^{12845\mu m} N(D_{max}) \cdot S(D_{max}) \cdot \Delta D_{max} \quad [m^{-1}] \qquad (1)$$

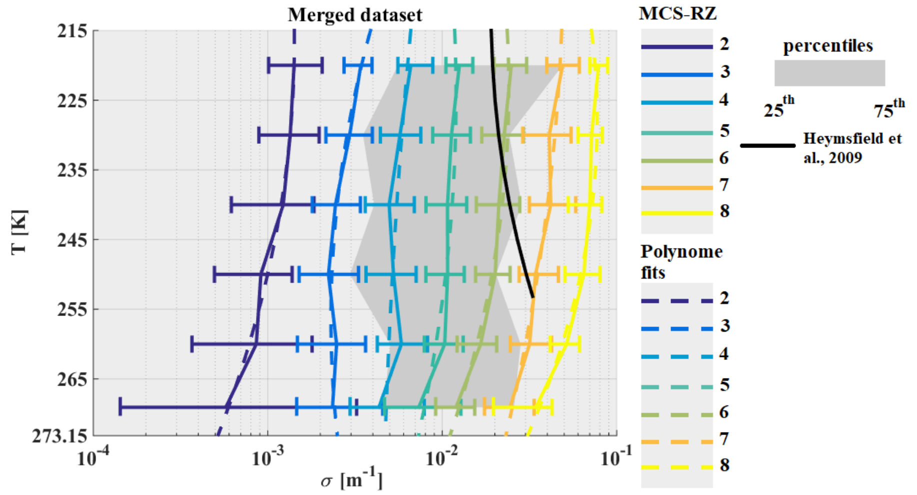

Figure 7: Same as Figure 5 but for visible extinction σ given on x-axis in m⁻¹.

In Figure 7, median σ (4 tropical campaigns) increase with MCS reflectivity zone as expected, and also increase with altitude (decrease with T), with larger gradients for T ∈ [245; 273.15] than for T ∈ [215K; 245K].

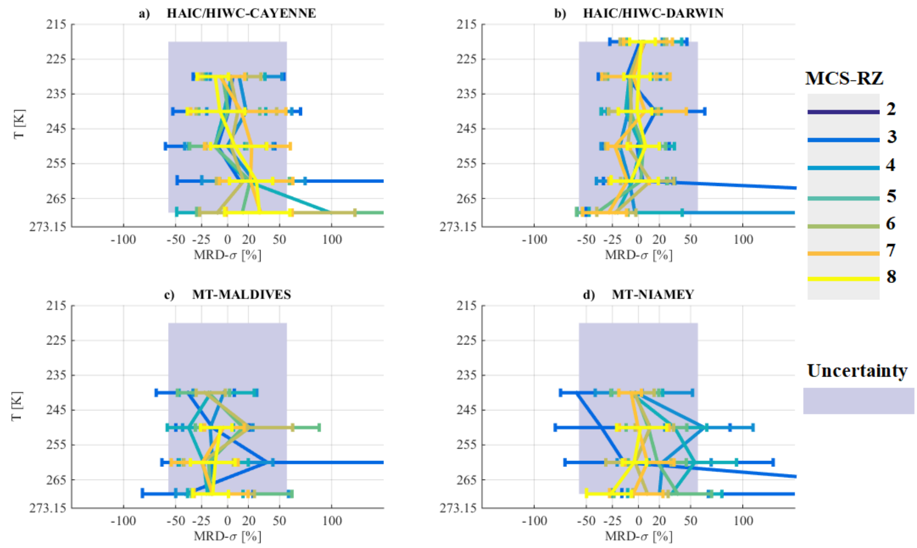

Figure 8: Same as Figure 6 but for visible extinction MRD-σ.

The uncertainty (U(σ)/σ) (grey band in Figure 8(a) to Figure 8(d) is calculated as follows:

$$\frac{U(\sigma)}{\sigma} = \sqrt{2 \cdot \frac{U(D)}{D}^2 + \frac{U(N)}{N}^2} = \pm 57\% \qquad (2)$$

With $\frac{U(D)}{D} = \pm 20\%$, taking into account the uncertainty in the calculation of the size of hydrometeors and $\frac{U(N)}{N} = \pm 50\%$ for the uncertainty on the calculation of the concentration of hydrometeors from optical array probes (Baumgardner et al., 2017). Above uncertainties are those for particles larger than 100 µm. Note, that if we took uncertainties for particles smaller than 100µm ($with\ \frac{U(D)}{D} = \pm 50\%\ and\ \frac{U(N)}{N} = \pm 100\%$) the uncertainty on the calculation of σ would increase to ± 122%. The reason why we do not take into account uncertainty of smaller particle it is because these particles contribute little to the visible extinction (2% in the range [235K; 273.15] and 10% in the range [215K; 225K]."

For all 4 types of tropical MCS, MRD-σ shown in Figure 8(a), 8(b), 8(c), and Figure 8(d) are in general smaller or equal to $\pm\frac{U(\sigma)}{\sigma}$. Hence, visible extinction in tropical MCS tend to be similar for all types of MCS observed in the same range of T and MCS reflectivity zone. Also MRD-σ trends are very comparable to above discussed MRD-IWC trends.

Furthermore, a σ–T relationship from Heymsfield et al. (2009) (black line) is added in Figure 7, which is calculated, as a function of T, as the sum of the total area of particles larger than 50µm plus the total area of particles smaller than 50µm multiplied with a factor of 2 in order to satisfy Eq. (1) and to compare with results of this study. We conclude that σ–T estimation presented in Heymsfield et al. (2009) for maritime convective clouds is rather comparable to median σ calculations (merged dataset) in MCS reflectivity zones 6 to 7 corresponding to higher reflectivity zones, and thus statistically to zones with some remaining convective strength.

5.3 Concentration of ice hydrometeors

Subsequently are presented observed total concentrations for the merged datasets integrating particle sizes beyond 55µm ($N_T(D_{max} > 55\mu m)$; hereafter $N_{T,55}$):

$$N_T(D_{max} > 50\mu m) = \sum_{Dmax=55}^{Dmax=12845} N(D_{max}) \cdot \Delta D_{max} \qquad [L^{-1}] \qquad (3)$$

Median of $N_{T,55}$ as a function of T and MCS reflectivity zones are shown in Figure 9 as well as MRD-$N_{T,55}$ for the 4 tropical MCS locations in Figure 10 (a), 10(b), 10(c), and 10(d). We observe an increase of median $N_{T,55}$ with altitude for all MCS reflectivity zones. Also $N_{T,55}$ increases with MCS reflectivity zones for a given T, with highest $N_{T,55}$ in MCS reflectivity zone 8. The range of variability for $N_{T,55}$ reveals significant overlap of 25th and 75th percentiles of neighboring MCS reflectivity zones.

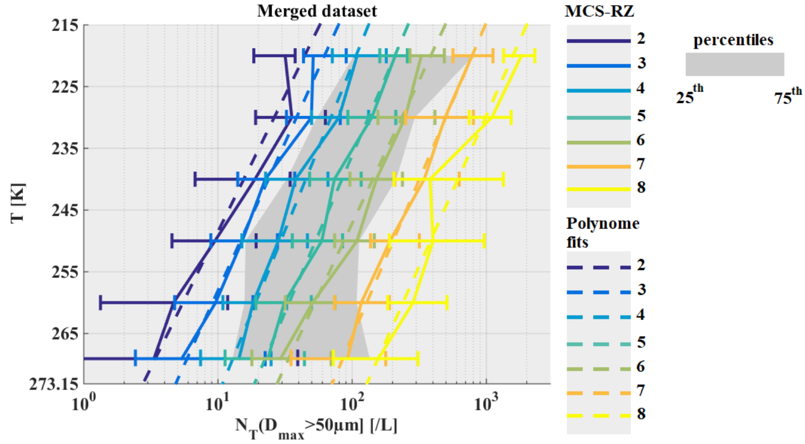

Figure 9: Same as Figure 5, but for total concentrations integrated beyond D_{max}=55µm in [L^{-1}].

Figure 10 show MRD-NT55 where measurement uncertainty on concentrations are assumed ±100% (Baumgardner et al., 2017). MRD- $N_{T,55}$ in 4 different tropical MCS locations, particularly for higher MCS reflectivity zones are of the order and even larger (75th percentile MRD-$N_{T,55}$) than the measurement uncertainty. Even if the limit of concentrations of ice hydrometeors are not well defined between neighboring MCS reflectivity zones (Figure 9). These concentrations tend to be similar for a given range of T and Z for the four different MCS locations.

A similar investigation is performed for total concentrations integrating beyond 15 µm (NT). Since major conclusion are similar to these given for NT55, figures for NT are shown in Appendices A. Globally, median of $N_{T,55}$ for the tropical dataset are smaller by about one order of magnitude with respect to the median of N_T for the same MCS reflectivity zone. And NT over Maldives tend to be larger than median NT for the merged dataset.

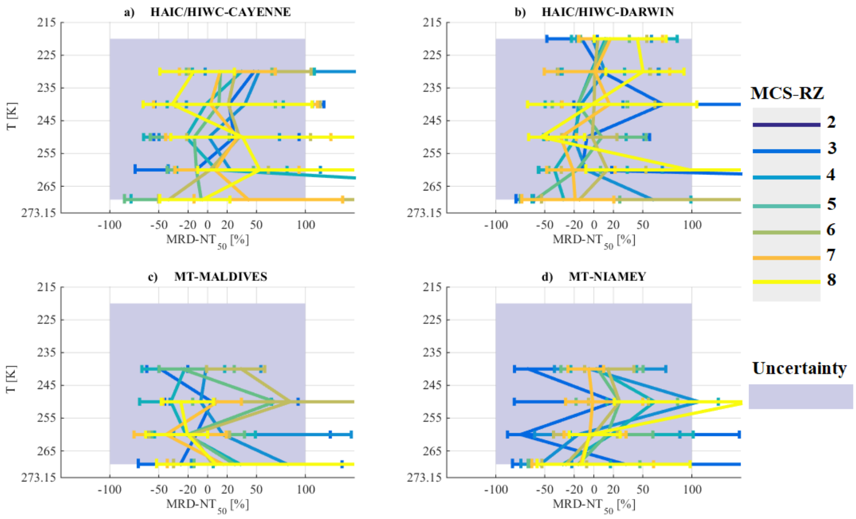

Figure 10: Same as Figure 6, but for MRD-NT$_{50}$.

Finally, Figure 11 shows concentrations of hydrometeors when number PSD are integrated only beyond 500µm (hereafter $N_{T,500}$; eq. (4)), where the uncertainty on their measurement is estimated as about ±50% for hydrometeors larger than 100µm (Baumgardner et al., 2017).

$$N_T(D_{max} > 500\mu m) = \sum_{Dmax=505}^{Dmax=12845} N(D_{max}) \cdot \Delta D_{max} \qquad [L^{-1}] \tag{4}$$

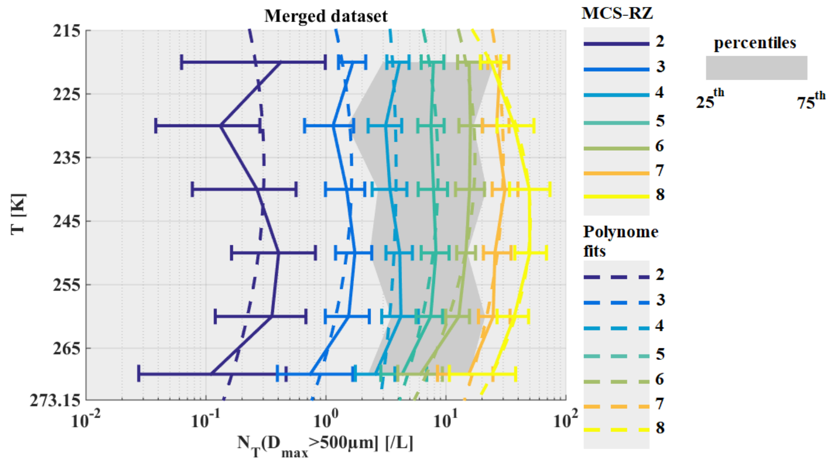

Figure 11: Same as Figure 5, but for concentrations of hydrometeors integrated beyond D_{max} =500µm in [L^{-1}].

In Figure 11 median $N_{T,500}$ are presented as a function of T and MCS reflectivity zone. The curves of median $N_{T,500}$ are different from curves of median N_T and $N_{T,55}$. Indeed, particularly for higher MCS reflectivity zones and in lower altitude levels (T ∈ [250K; 273.15K]), $N_{T,500}$ tends to increase with altitude, reaches a maximum value around T ∈ [235K; 250K], and then rather decreases for T ∈ [215K; 235K]. The range of variability for $N_{T,500}$ reveals a rather small overlap, if any, of 25^th and 75^th percentiles of neighboring MCS reflectivity zones 8, 7, and may be 6, mainly at coldest T ∈ [215K; 225K]. No overlap for MCS reflectivity zones 2-5 and concentration of ice hydrometeors beyond 500µm are rather constant from 215K to 265K for observations in MCS reflectivity zones 3 to 5. ~~We can assume that sedimentation does not significantly impact hydrometeors of sizes below 500 µm, but should impact larger hydrometeors.~~

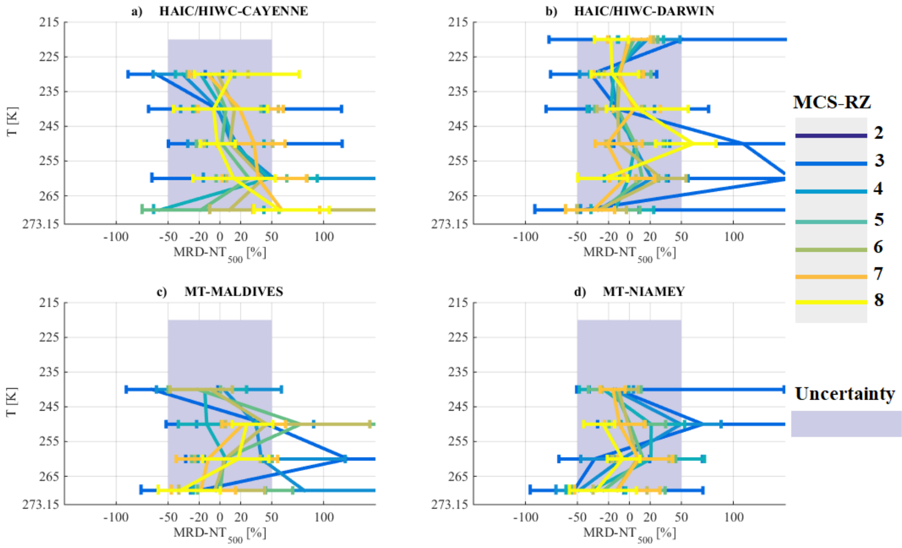

Figure 12: Same as Figure 6, but for MRD-NT$_{500}$.

Figure 12 (a), 12(b), 12(c), and 12(d) reveal that MRD-$N_{T,500}$ in higher MCS reflectivity zones are considerably smaller or roughly equal to the measurement uncertainty for large hydrometeors. Some smaller exceptions are noticeable where MRD-$N_{T,500}$ are larger than the measurement uncertainty for very low altitudes at T ∈ [265K; 273.15K[, namely Cayenne in MCS reflectivity zones 7 and 8, and Darwin in MCS reflectivity zone 8. Note, that in general MRD-$N_{T,500}$ have smaller 75^th percentiles (from Figure 10 (b), 10(c), 10(d), and 10(e)) compared to respective MRD-$N_{T,55}$ and MRD-N_T, showing that variability in each MCS reflectivity zone for hydrometeors larger than 500µm is smaller than the variability of concentrations which include smaller ($N_{T,55}$) and smallest (N_T) hydrometeors. This finding is clearly related to the uncertainty estimation given by (Baumgardner et al., 2017)) that small hydrometeors (D_{max}< 100µm) have a larger estimated uncertainty of 100% (due to shattering, very small sample volume), compared to the uncertainty of only 50% for larger hydrometeors (D_{max}>100µm). Hence, it is not surprising that variability around a median value is larger for N_T and $N_{T,55}$ than for $N_{T,500}$. It is important to resume here that not just MRD-$N_{T,500}$ is smaller than the uncertainty of 50%, but also that MRD-$N_{T,500}$ is tremendously smaller than MRD-$N_{T,55}$ and MRD-N_T. Even though we have to keep in mind that we'll never have *sufficient statistics in flight data, due to sampling bias of flight trajectories and variability of microphysics from one system to another. Indeed, Leroy et al., (2017) demonstrated that median mass diameter MMD_{eq} generally decrease with T and increasing IWC for the dataset of HAIC-HIWC over Darwin. However, for two flights performed in the same MCS, Leroy et al., (2017) showed that high IWC were linked to large MMD_{eq}, where MMD_{eq} tends to increase with IWC. This demonstrates that comparable high IWC can be observed for two different microphysical conditions (short-lived typical oceanic MCS versus long lasting tropical storm in one and the same dataset).*

We show that total concentrations starting from 15µm can be different between MCS locations as a function of T and Z, especially in oceanic MCS over Maldives Islands in the decaying part of these MCSs where measured concentrations can reach 10 times the median concentrations observed globally for merged tropical dataset. Also MCS over Niamey show larger concentrations near the convective part of MCS. However, concentrations of ice hydrometeors beyond 55µm tend to be more similar as function of T and Z, even if the limits between each MCS reflectivity zones are not well defined.

Between 4 MCS locations, differences of aerosol loads and available ice nuclei might exist. Despite those possible differences, ice crystal formation mechanisms may be primarily controlled by dynamics, thermodynamics and particularly by secondary ice production rather than primary nucleation; (Field et al., 2016; Phillips et al., 2018; Yano and Phillips, 2011) that regulate the concentrations of hydrometeors beyond ~55µm making these concentrations quiet rather similar for different MCS locations.

5.4 Coefficients of mass-size relationship

The relationship between mass and size of ice crystals is complex. Usually in field experiments the mass of individual crystals is not measured, instead bulk IWC is measured which is the integrated mass of an ice crystal population per sample volume to be linked to PSDs of ice hydrometeors. Yet IWC is not always measured or with low accuracy. Due to the complex shape of ice hydrometeors, various assumptions allow to estimate the mass of ice crystals for a given size. Indeed, many habits of ice crystals can be observed in clouds, primarily as a function of temperature and ice saturation (Magono and Lee, 1966; Pruppacher et al., 1998). Also hydrometeors of different habits can be observed at the same time (Bailey and Hallett, 2009). Locatelli and Hobbs (1974) and Mitchell (1996) suggested mass-size relationships represented as power laws with $m = \alpha \cdot D^{\beta}$ for different precipitating crystal habits. Coefficients α and β vary as a function of the ice crystals habit. Further studies performed calculations of mean mass-size relationships (also using power law approximations) retrieved from simultaneous measurements of particle images combined with bulk ice water content measurements (Brown and Francis, 1995; Cotton et al., 2013; Heymsfield et al., 2010). Schmitt and Heymsfield (2010), Fontaine et al (2014), Leroy et al. (2016) showed that mass-size relationship coefficients α and β vary as a function of temperature. In the latter studies, coefficient β is calculated from OAP images, and then α is retrieved either also from processed images or constrained with integral measured IWC or radar reflectivity factor Z. Recently, Coutris et al (2017) retrieved masses of hydrometeors by an inverse method using direct measurement of PSD and IWC. In this latter study, the mass of ice crystals is retrieved without any assumption on the type of function linking mass and size of ice hydrometeors.

This study uses the power law assumption to constrain the mass of ice hydrometeors. Thereby, the β exponent of the mass-size power law relationship is calculated (eq. 7) as presented in Leroy et al (2016) for hydrometeors defined by D_{max} dimension:

$$\beta = 1.71 \cdot f_s - 0.62 \cdot f_p \tag{5}$$

Here f_p is the exponent of the perimeter-size power law relationship (Duroure et al. 1994) with $P(D_{max}) = e_p \cdot D_{max}^{fp}$ $[cm]$ and f_s is the exponent of the 2D image area-size relationship (Mitchell, 1996) with $S(D_{max}) = e_s \cdot D_{max}^{fs}$ $[cm^2]$. These two relationships are calculated using Images from 2D-S and PIP. Hence, β is a proxy parameter that describe the global (all over the size range of hydrometeors from 50µm to 1.2cm) variability of the shape of the recorded hydrometeors during the sampling process. Figure 13 shows the variability of β as a function of temperature and MCS reflectivity zones for the merged dataset. For a given MCS reflectivity zone, β increases with increasing temperature. Also for a given temperature, β increases with MCS reflectivity zone, although MCS reflectivity zones 4, 5, 6, 7, and 8 share a range of common values for β, making it more uncertain to predict with a good accuracy using a parametrization as function of IWC and T.

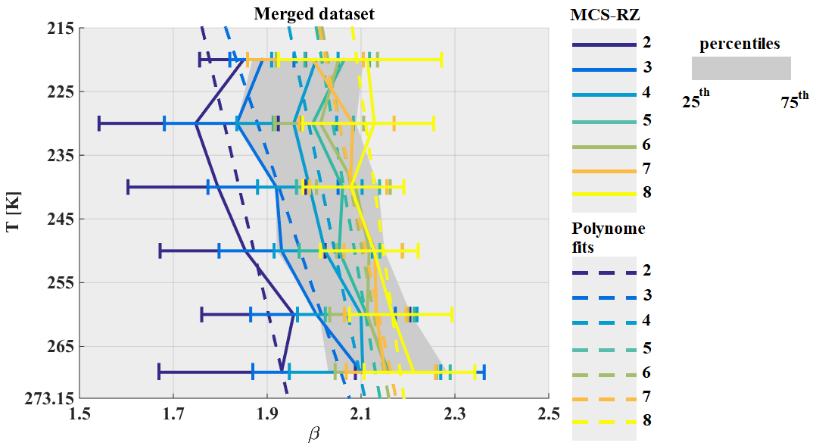

Figure 13: As Figure 5, but for exponent β of mass-size relationships for used ice hydrometeor size definition D_{max}.

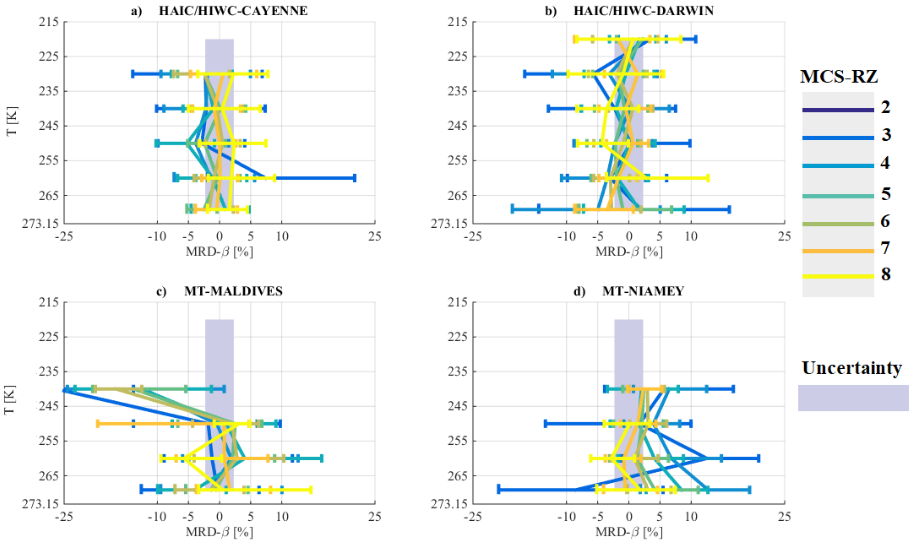

Figure 14: As Figure 6, but for exponent MRD-β.

In order to estimate the uncertainty on the calculation of β (grey band in Figure 14 (a), (b), (c), and (d), results from (Leroy et al., 2016) have been utilized, with U(β)/β=±2.3%. However, if we have calculated the uncertainty on retrieved β from the uncertainty on the measurement of the size and concentration of hydrometeors from OAP images, the uncertainty would have been by about 44%. In general, MRD-β in MCS reflectivity zones 8 and 7 tend to be in the range of U(β)/β assuming that β are similar for all observed MCS in the four campaigns for the conditions described by MCS reflectivity zones 7 and 8.

However, in MCS reflectivity zones 2 to 6 MRD-β are more scattered around U(β)/β with sometimes larger MRD than uncertainty of β. Especially for MCS over Maldives and Niamey. Over Maldives at higher altitudes β tend to be smaller compared to the median β calculated for the merged dataset. While, MCS over Niamey tend to have β larger than median β calculated for the merged dataset.

Overall, the predictability of β coefficients as a function of T and MCS reflectivity zone remains challenging. We are aware of the fact that the power-law approximation has certain limits, trying to impose one single β to an entire crystal population composed of smaller (dominated by pristine ice) and larger crystals (more aggregation, also riming).

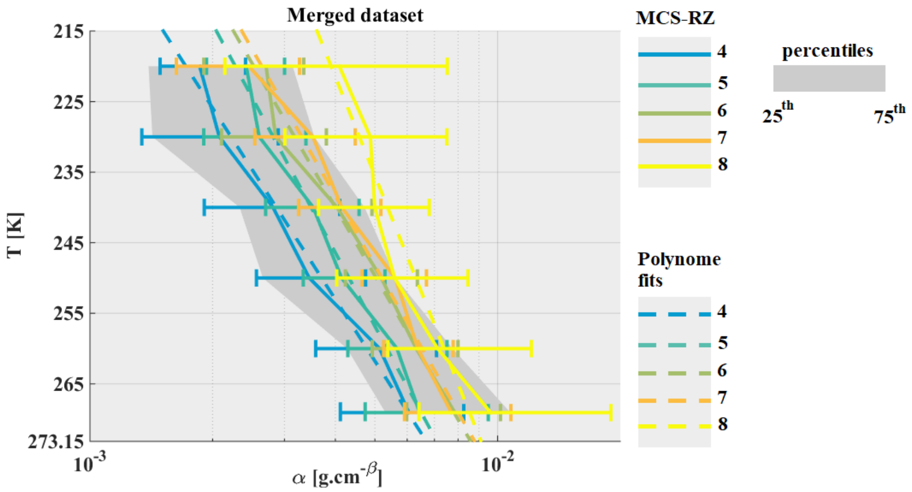

Figure 15: Same as Figure 5, but for α of mass-size relationships for used ice hydrometeor size definition D_{max}.

For HAIC-HIWC data, coefficients α are retrieved, while matching measured IWC from IKP-2 with calculated IWC thereby integrating PSD times m(D) power law relationship. For MT data, coefficients α are retrieved from T-matrix simulations of the reflectivity factor (Fontaine et al., 2017). α calculation is solely constrained by the fact that the mass of ice crystals remains smaller or equal than the mass of an ice sphere with the same diameter D_{max}:

$$\alpha = \frac{IWC}{\sum_{15}^{12845} N(D_{max}) \cdot D_{max}^{\beta} \cdot \Delta D_{max}} \quad | \quad \alpha \cdot D_{max}^{\beta} \leq 0.917 \cdot \frac{\pi}{6} \cdot D_{max}^{3} \quad [g\ cm^{-\beta}]. \qquad (6)$$

For the uncertainty calculation of α we take the maximum value of β which is 3:

$$\frac{U(\alpha)}{\alpha} = \sqrt{\left(\frac{U(IWC)}{IWC}\right)^2 + 3 \cdot \left(\frac{U(D)}{D}\right)^2 \left(\frac{U(N)}{N}\right)^2} \qquad (7)$$

Figure 15 shows median α coefficients as a function of T and MCS reflectivity zone. As has been already stated in previous studies, α is strongly linked to the variability of β (Fontaine et al., 2014; Heymsfield et al., 2010). Figure 15 compared to Figure 13 confirms that results for α have similar trends as those discussed for β. α vary from 5.10^{-4} (in MCS reflectivity zone 2) to ≈2.10^{-2} (in MCS reflectivity zone 8). In general, α increases as a function of T for a given MCS reflectivity zone and also increases as a function of MCS reflectivity zone (and associated IWC) for a given T level. As already stated for the median exponent β in Figure 13, median α in MCS reflectivity zones 4, 5, 6, 7 and 8 are more or less overlapping. ~~Median α in MCS reflectivity zones 2 and 3 are shown for completeness reasons, however with less confidence as they are related to IWC generally smaller than 0.1g m⁻³.~~

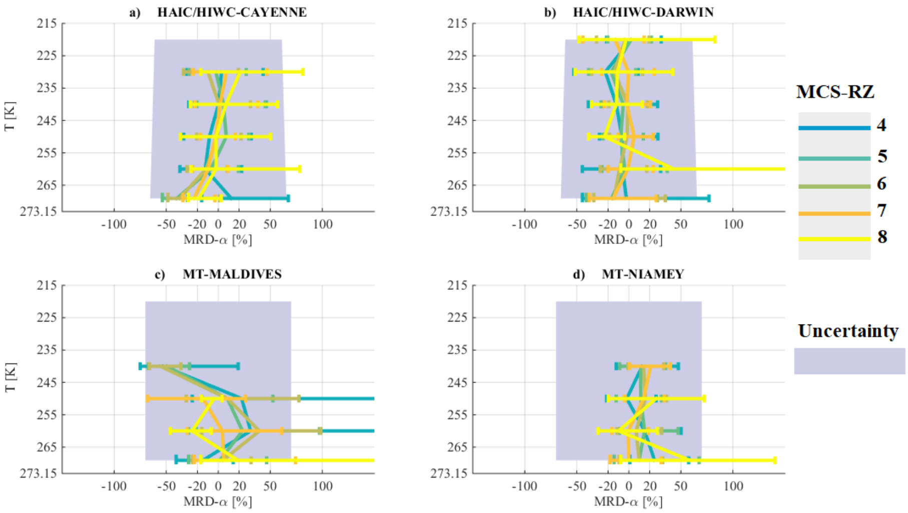

Figure 16: As Figure 6, but for exponent MRD-α.

From Figure 16(a) and Figure 16(b) we can note that even with a good accuracy of the measured IWC (from IKP-2; U(IWC)/IWC ≈ ±5% for the typical IWC values observed in HAIC-HIWC at 210K), the uncertainty of α, is rather large which is mainly due to uncertainties in OAP size and concentration measurements. Taking into account the large uncertainty on the retrieved α, we find that MRD-α for all 4 tropical datasets for MCS reflectivity zones 4, 5, 6, 7, and 8 are smaller than U(α)/α. For data from Niamey (Figure 16 (d)), α tend to be larger than median α for the tropical dataset (MRD-α not centered on 0, but shifted to positive values).

In previous sections, this study documented similar IWC values and visible extinction coefficients for a given range of Z and T and a clear increase of IWC and visible extinction coefficient from MCS reflectivity zones 4 to 8. The increase of α and β with MCS reflectivity zones is not as much clearly visible, whereas at least α seems to increase with temperature in different MCS reflectivity zones). And we cannot ignore that α and β tend to be larger in MCS reflectivity zone 8 than in MCS reflectivity zone 4, especially at higher altitude. But, the increase of IWC and visible extinction with MCS reflectivity zone Z is not linked to an increase of the mass-size coefficients. This conclusion takes into account the variability of the mass-size coefficients shown by 25 and 75 percentiles. Moreover, shapes of ice hydrometeors in MCS reflectivity zone 4, 5 and 6 are different in MCS over Maldives and MCS over Niamey compared to MCS over Darwin and Cayenne (smaller β over Maldives and larger β over Niamey).

As visible extinction (hence projected surface) and IWC are similar for the same range of T and Z in all types of MCS, but the shapes of crystals might be different from one to another MCS location. Our assumptions is that the ratio of projected surface vs IWC is similar. In other words the density of ice per surface unity (or by pixels of projected surface) is similar as function of T and Z in all types of MCS even if there might be a possibility that the habit or the shape can be different (pure oceanic MCS vs pure continental MCS). Note that these assumptions is establish for IWC larger than 0.1g.m^{-3}

5.5 Largest ice hydrometeors

Figure 17 investigates the variability of the size of the largest ice hydrometeors in the PSD (hereafter max(D_{max}) as defined in Fontaine et al (2017)). Figure 17 reveals globally for all MCS reflectivity zones that the median of max(D_{max}) increases with T, with larger hydrometeors at cloud base compared to cloud top, particularly in the stratiform cloud part, where PSD are mainly impacted by a combination of aggregation and sedimentation. At higher levels for T ∊ [215K; 245K[largest median of max(D_{max}) are observed in the most convective MCS reflectivity zone 8, followed by zones 7, 6, and 5, where sedimentation becomes more and more active. Below the 250K level, largest max(D_{max}) can be observed in MCS reflectivity zones 6 and 7 (still significant sedimentation source from above), followed by 5 (increasing depletion of large crystals) and 8 (more convective or at least transition zone from convective to stratiform cloud part). Smallest max(D_{max}) are observed in MCS reflectivity zones 2 and 3.

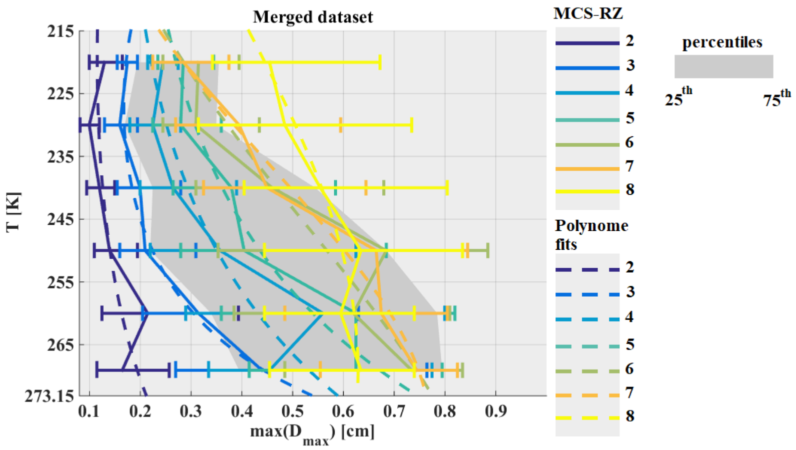

Figure 17: As Figure 5, but for maximum size of hydrometeors max(D_{max}) in PSD in [cm].

MRD-max(D_{max}) shown in Figure 18(a), 18(b), 18(c), and 18(d) are a bit larger than the measurement uncertainty estimated with ±20% ((Baumgardner et al., 2017). Cayenne, Darwin, and Niamey data are centered around the median max(D_{max}) of the 4 tropical datasets in MCS reflectivity zone 8 for all type of MCSs, in MCSs reflectivity zone 7 in MCS over Darwin, Cayenne and Niamey. MCSs over Cayenne et Darwin tend to have similar max(D_{max}) in other MCS reflectivity zones. Maldives dataset shows mainly negative MRD-max(D_{max}) values, indicating that max(D_{max}) for the Maldives Island data are generally smaller than those of the other three tropical datasets. Also MCS over Niamey show larger max(D_{max}) in MCS reflectivity zones 2 to 4, illustrating that snow aggregates can reach larger sizes during the West African monsoon than in other MCS locations.

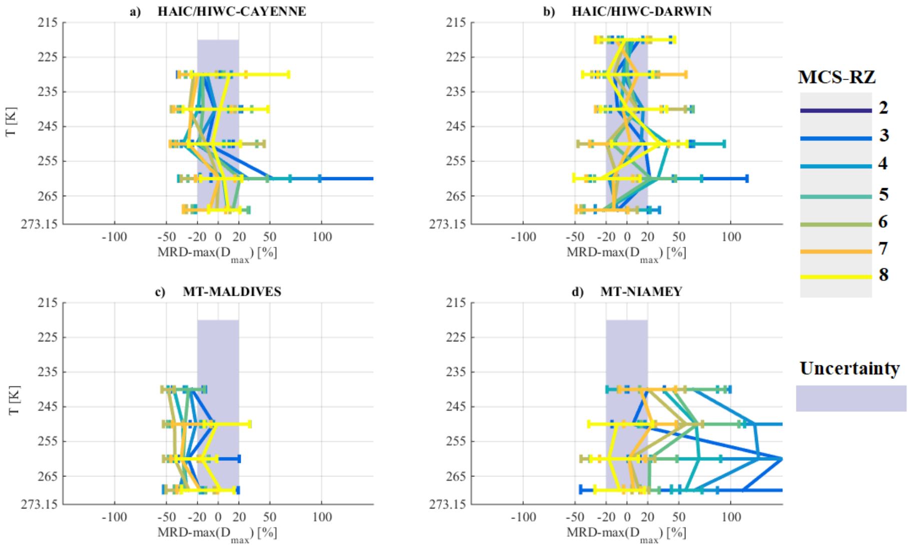

Figure 18: As Figure 6, but for maximum size of hydrometeors max(D_{max})

In this section, it is shown that in the stratiform part of MCS, largest hydrometeors are larger in MCSs over Niamey than in other types of MCS, and tend to be smaller in MCS over Maldives Islands. Mainly, large crystals (Dmax > 1mm) are agglomerates of pristine ice crystals, for which the growth process is leaded by aggregations (by sedimentation) instead of vapour diffusion. Some large pristine ice were found in the dataset (especially over Maldives see Figure 1 in Fontaine et al., 2014) but usually their size do not exceed 3 to 4 mm. Hence, aggregation efficiency is different from one MCS type of MCS to another, this could explain the differences of mass-size coefficient β, as it is calculated on the slope in a log-log scale of mean perimeter and mean surface as a function of median diameter in each size bin. Because, large hydrometeors have a non-negligible impact on the slope (i.e. fp and fs, see Eq. (5)).

5.6 note on the impact of vertical movement on ice microphysic

This section discussed about the investigation performed about the impact of vertical velocity on the ice microphysical parameters presented earlier in this section 5. We separated the merged dataset in three sub-datasets such: i) w <-1m/s , (ii) -1m/s < w < 1m/s and (iii) w>1m/s. Then, median relative difference for the three conditions and for each parameters presented in this section 5 were calculated and compared to the median relative difference when no distinction is performed as function of vertical velocity. Firstly, we noticed that MRD-X for the merged dataset and MRD-X for the second condition (i.e. 1m/s < w < 1m/s) are similar (MRD-X: X being used to replace IWC, σ, NT, NT_{50}, NT_{500}, β, α, max(Dmax)). Secondly, differences of MRD-X in updraft and in downdraft with regards to MRD-X for merged dataset and no vertical movement are visible. But most of the times these differences are not enough pronounced compared to measurement uncertainties (U(X)/X).

Appendices B shows the Figures that shows when updraft have an impact on ice microphysic parameters for a given range of temperature and MCS reflectivity zones. So, Figure B1 shows MRD-IWC, Figure B2 shows MRD-NT and Figure B3 shows MRD-NT50. For the others parameters impact of updraft are uncommon.

It appears that updraft tends to impact mainly concentrations of small hydrometeors and IWC for some type of MCS and some MCS reflectivity zones. So for NT (Figure B2), we observe larger NT for updraft in MCS observed over Cayenne, Maldives and Niamey. For Cayenne, it appears in MCS reflectivity zone 5 and 6 for temperatures between 245K and 265 K with NT 2 to 3 times larger than NT for merged dataset. For MCS over Maldives, median NT are 5 times to 20 times larger than NT when there is no noticeable vertical movement in MCS reflectivity zones 6, 7 and 8. Finally for MCS over Niamey, we observe larger NT in updraft than NT for the merged dataset in MCS reflectivity zones 6 for T around 240 K and in MCS reflectivity zones 8 above the bright band. We have similar conclusions for NT_{50} *(Figure B3), except that ratios between* NT_{50} *in updraft and* NT_{50} *when no updraft is smaller than the ratio between NT in updraft and NT when no updraft.*

IWC are impacted by updraft, only for MCS over Cayenne, in MCS reflectivity zone 4, 5, 6 and 7. IWC in updraft tend to be larger about +50% than IWC when no updraft, except in MCS reflectivity zones where IWC are about 2 times larger in updraft than IWC when no updraft.

This investigation on the impact of updraft and downdraft on ice microphysics, shows that updraft may have an impact on concentrations of small hydrometeors and IWC. However, updraft does not impact all type of MCS in the same way. So, there will need to perform deeper investigations on updraft impact.

Despites some noticeable impact of updraft on ice microphysic for our dataset, there is no significant (recurrence trough all types of MCS or as function of T or Z) results to assess them for the merged dataset. So, the parameterization provided in the next section are not functions of vertical velocity.

6. Parameterizations as function of IWC and T

6.1 visible extinction

Since we concluded from Figure 7 and Figure 8 that visible extinction σ and IWC in tropical MCS tend to be similar for all MCS locations in the same range of T and for corresponding MCS reflectivity zones 4 to 8. Moreover Figure 19 shows that there is a linear relationship between log(σ) and log(IWC). Moreover it seems that log(σ) decrease with temperature increasing at constant log(IWC). Then, we performed a surface fitting using input coefficients log(IWC) and T to fit log(sigma) to deduce a parametrization of σ (Eq. (8)) as a function of IWC and T for deep convective cloud data (merged dataset) of this study limiting data to IWC > 0.1g m^{-3}*:*

$$\sigma = exp(-0.0194587 \cdot T + 0.9134019 \cdot ln(IWC) + 1.2423609) \qquad [m^{-1}] \qquad (8)$$

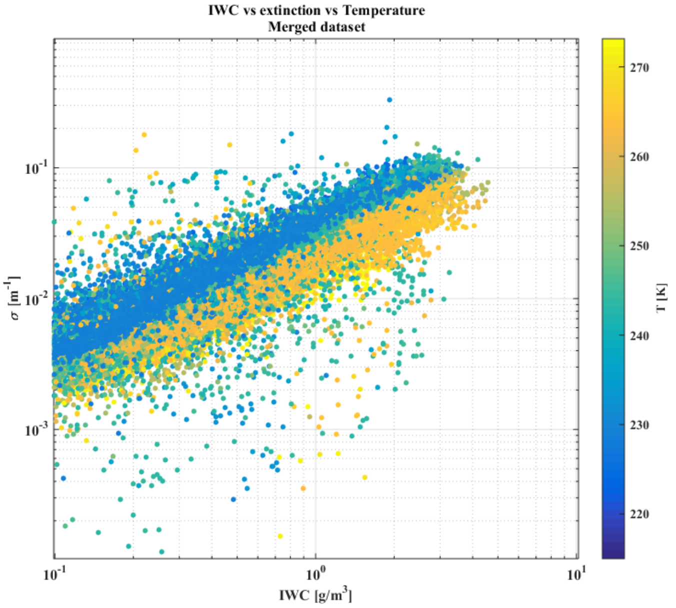

Figure 19: visible extinction in [m-1] on y-axis as function of IWC in [kg.m-3] on x axis and as function of T in [K] with color scale. Scatter plot using the merged dataset (4 campaigns).

An evaluation of this parametrization is presented in Figure 20, where black lines in Figure 20-a) to Figure 20-d) represent median relative errors of σ (with 25^{th} and 75^{th} percentiles represented by whiskers) for the merged dataset predicted with Eq. (8) with respect to retrieved σ from OAP images from Eq. (2). In addition, median relative errors of σ for individual MCS datasets over Darwin, Cayenne, Maldives Islands, and Niamey with respect to σ calculations (Eq. (8)) are shown in Figure 20(a), Figure 20(b), Figure 20 (c), and Figure 20(d), respectively. The uncertainty $\pm \frac{U(\sigma)}{\sigma}$ is given with the grey band. All relative errors (25^{th} - 75^{th} percentiles) tend to be smaller than $\pm \frac{U(\sigma)}{\sigma}$, with median relative errors that are smaller than ±25% of σ uncertainty calculated from Eq. (2). In general, Eq. (8) seems to produce smallest relative errors of σ for Niamey and Darwin datasets (especially for IWC<2g m^{-3}).

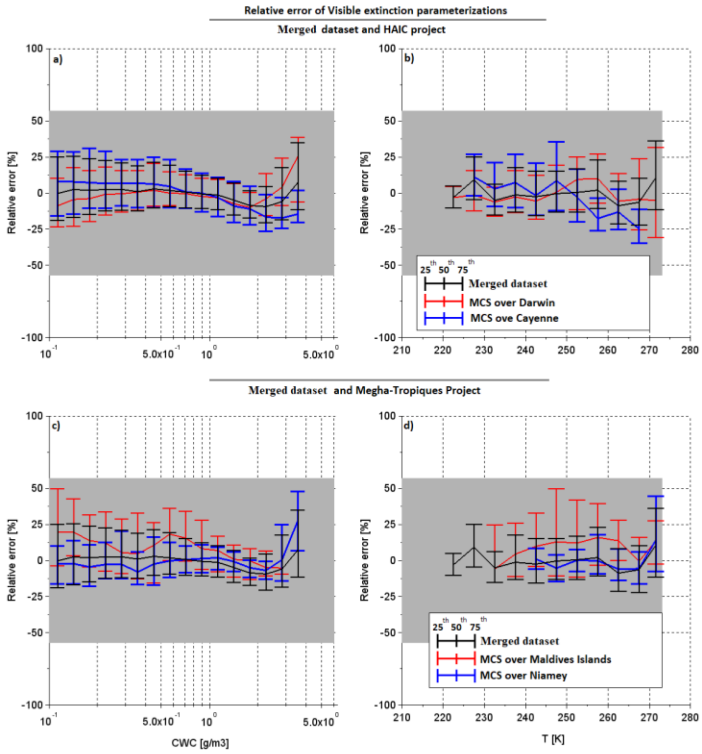

Figure 20: Relative errors of predicted visible extinction Eq. (3) with respect to measured visible extinction for a), b), c), and d. Relative errors as a function of IWC in a) and c) and as a function of T in b) and d). Black lines in 4 sub figures represent the relative errors when calculated for the entire tropical dataset. In a) and b) red lines show median relative error for MCS over Darwin, and blue line for MCS over Cayenne. In c) and d) red line represent median relative errors for MCS over Maldives Islands and blue lines for MCS over Niamey. Bottom of error bar shows 25th percentiles of relative errors and 75th percentiles are given by top of error bar.

~~To sum up, visible extinction calculated from equation (1) showed similar behavior for all four types of tropical MCS. Indeed, for the same range of temperature and radar reflectivity factors we find very comparable visible extinction in all 4 MCS locations, thereby taking into account the measurement uncertainty. Similar results as for the visible extinction has been documented in a previous section for IWC. From those two results, we can assume that in MCS zones where IWC is larger than 0.1g m^{-3} hydrometeor populations are similar in shape and density. This is why the development of a parameterization of the visible extinction as a function of temperature and IWC (beyond 0.1g m^{-3}) has been presented (see equation (3)).~~ Noteworthy, optically thick clouds are responsible of large errors in retrieved cloud water path and condensed water concentration profiles retrieved from satellite imageries (Smith, 2014; Yost et al., 2010). Parameterizations, such as presented here, could help to improve retrieval methods on cloud water path but more investigations on the benefit of such parameterizations are needed, which is beyond the scope of this study.

6.2 Parameterization of ice hydrometeors distributions

6.2.1 Observations of PSD moment

Moments of PSD are convenient for numerical weather prediction to model microphysics of hydrometeor populations, since knowing the PSD n^{th} order moment allows to roughly describe cloud processes and their hydrometeors properties. Commonly, PSD of ice hydrometeors are modeled with Gamma distributions (Heymsfield et al., 2013; McFarquhar et al., 2007). The calculation of the n^{th} order moment is defined in Eq. (9) for PSD obtained from size distribution measurements of hydrometeors, for example with OAP (optical array probes):

$$M_n = \sum_{D_{max}=55\mu m}^{D_{max}=1,2cm} N(D_{max}) \cdot D_{max}^n \cdot \Delta D_{max} \qquad [m^{n-3}] \tag{9}$$

The uncertainty of the n^{th} (n=2 and 3 in our study) moment is:

$$\frac{U(M_n)}{M_n} = \sqrt{n \cdot \frac{U(D)}{D}^2 + \frac{U(N)}{N}^2} \tag{10}$$

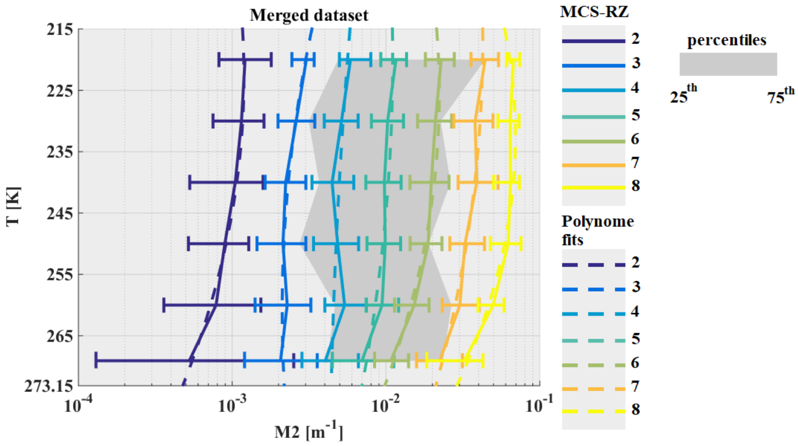

Figure 21: Same as Figure 5, but for M_2 per meter.

Figure 21 shows median second moment M_2 as a function of T for all MCS reflectivity zones for the merged global tropical dataset. Median M_2 slightly decrease with temperature for all individual MCS reflectivity zones, and distinctly increase with MCS reflectivity zone for a given T. The range of variability of median M_2 shows mainly negligible overlap, if any, of 25th and 75th percentiles of neighboring MCS reflectivity zones with the exception between MCS reflectivity zones 8 and 7 at low altitude (T ∈[265; 273.15[).

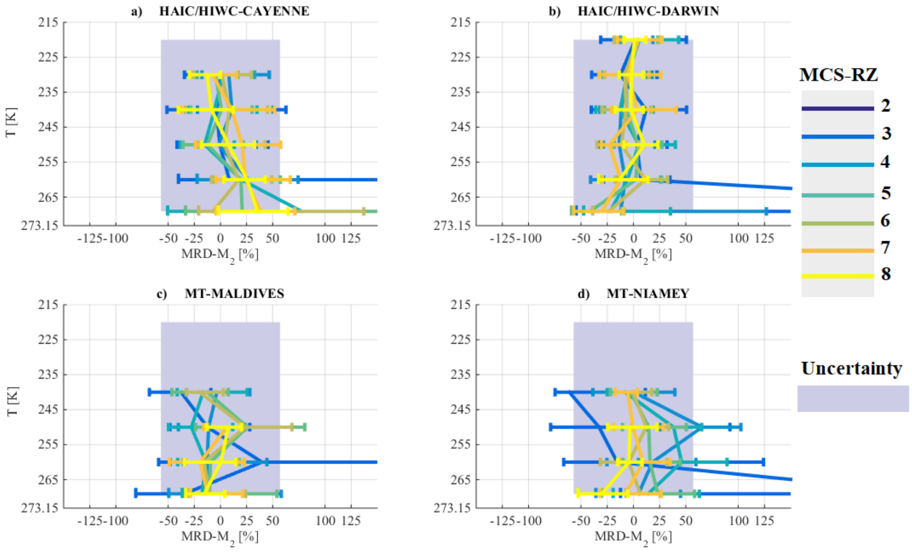

Figure 22: Same as Figure 6, but for MRD-M₂.

All 4 tropical MCS (Figure 22 (a), (b), (c), and (d)) show good agreement with the medians of M_2 in MCS reflectivity zones 3 to 8, with MRD-M_2 significantly smaller than $U(M_2)/M_2$. Few minor exceptions can be found for MCS over Cayenne (Figure 22 (b)) and Darwin (Figure 22 (c)) in the temperature range [265K; 273.15[. Also MCS over Niamey (Figure 22 (e)) show a larger MRD-M_2 in MCS reflectivity zones 2 and 3 for $T \in$ [265K; 273.15K[and $T \in$ [245K; 255K[, respectively.

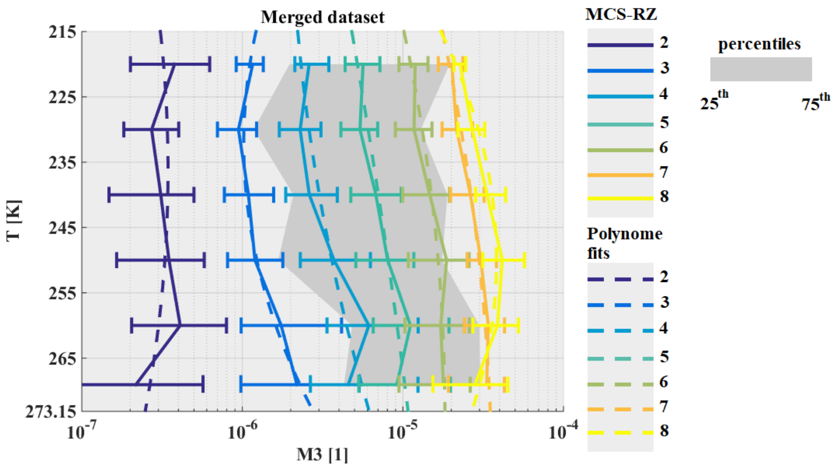

Figure 23: Same as Figure 5, but for the M_3 for unity dimension.

Figure 23 presents median third moment M_3 for global tropical dataset as a function of T and for different MCS reflectivity zones. Median M_3 in highest MCS reflectivity zones 8, 7, and to some extent zone 6 resemble the corresponding curves of median IWC (Figure 5), with a maximum value for median M_3 for $T \in [245K; 260K[$. We also obtain a clear increase in median M_3 with MCS reflectivity zone from 2 to 8. The range of variability for M_3 reveals no overlap of 25th and 75th percentiles of neighboring MCS reflectivity zones 2-7, solely zone 7 overlaps with zone 8 for all temperatures. Third moment of MCS over Cayenne, Darwin and Maldives Islands in MCS reflectivity zones 2 to 8, shows MRD-M_3 smaller than $U(M_3)/M_3$, with few minor exceptions basically in the range of $T \in [265K; 273.15K[$. MCS over Niamey tend to have MRD-M_3 that are sometimes larger than $U(M_3)/M_3$. Indeed, M_3 for MCS over Niamey tend to be larger in MCS reflectivity zones 5 and 2 in the range of $T \in [265K; 273.15K[$, and in MCS reflectivity zone 4 for T larger than 255K as well as in MCS reflectivity zone 3 for T larger than 245K.

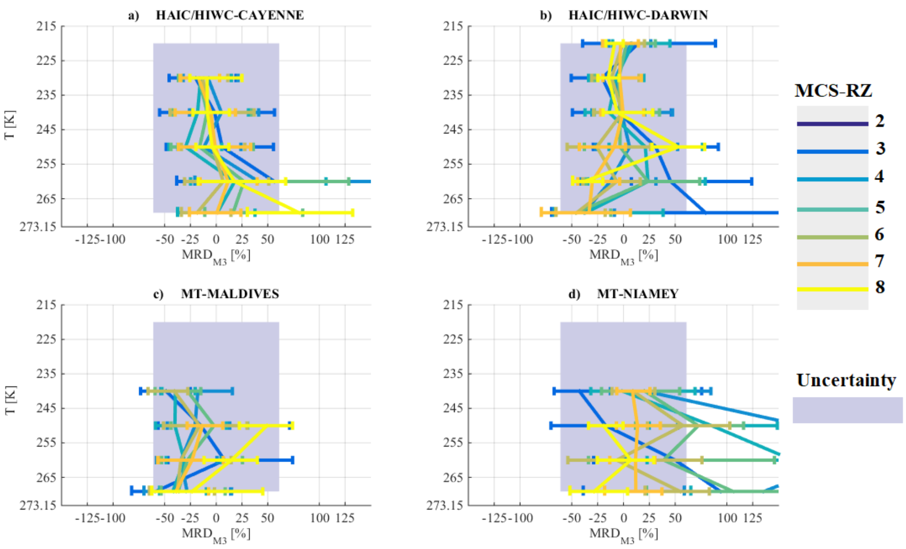

Figure 24: Same as Figure 6, but for the M_3.

Overall, this section illustrates that second and third moments of PSD are similar as a function of T and Z for all MCS locations of the underlying dataset. However, there are exceptions in MCS reflectivity zones 2, 3 and 4 in MCS over Niamey where larger third moments are calculated compared to those deduced for the merged global tropical dataset. Despite those exceptions, the next section explores the possibility to parameterize the second and third PSD moments as a function of IWC and temperature.

6.2.2 Parameterizations of M_2 and M_3

This section presents parametrizations to predict the 2nd and 3rd moment of the PSD for the merged dataset as a function of T and IWC (for this section IWC in the equation are in [kg m^{-3}]), including IWC data larger than 0.1g

m^{-3}. Indeed some moments can be directly linked to bulk properties of hydrometeor populations. For example, moment M_0 for ice and liquid hydrometeors is equal to the total number concentration (N_T), moments M_2 and M_3 for liquid particles are proportional to visible extinction and liquid water content. However, for ice hydrometeors the physical interpretation of moments M_2 and M_3 is less obvious since ice hydrometeors are not spherical particles. The results for α and β coefficients of the $m(D_{max})$ relationship presented in section 5.3, illustrate that β varies between 1.5 and 2.3. This means that IWC is proportional to PSD moments between $M_{1.5}$ and $M_{2.3}$. Also uncertainties on the retrieved β coefficients do not allow to assess the variability of β as a function of IWC and T. Former studies performed in different cloud environments report mean values of β around 2. For example, Leroy et al., (2016) found β=2.15 for HAIC-HIWC in Darwin, Cotton et al., (2013) suggested β=2.0, Heymsfield et al., (2010) suggested β=2.1, and Brown and Francis (1995) established β=1.9. We are also aware of the fact that findings of β also depend on the utilized size parameter (D_{max}, D_{eq}, etc…) of 2D images. Hence, we apply β=2 as an approximation, also proposed by Field et al., (2007), to link the second moment of hydrometeor PSD with IWC (Eq. 11). Subsequently the ratio IWC/M_2 is calculated and denoted A.

$$M_2 = \frac{IWC}{A} \qquad [m^{-1}] \tag{11}$$

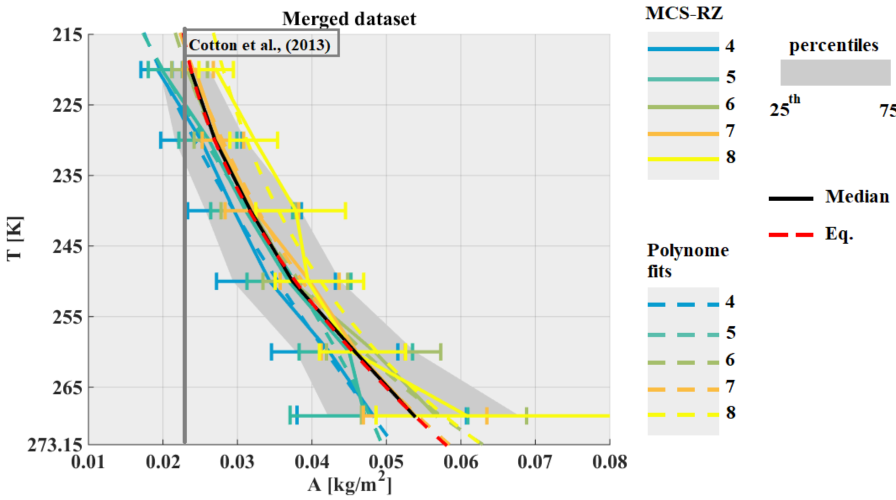

Figure 25: Same as Figure 5, but for the ratio A= IWC/M_2 in [kg m^{-2}].

Figure 25 shows retrieved median coefficients A for the global tropical dataset as a function of MCS reflectivity zone and T. Note that A is calculated in SI units (note that in Eq. (11) IWC is in kg m^{-3}). The black solid line gives the median of A as a function of T, thereby merging all MCS reflectivity zones for the merged dataset with IWC > 0.1g m^{-3}. The grey band gives corresponding 25th and 75th percentiles of that median A. In addition, are calculated median A for all individual MCS reflectivity zones (on Figure 25) are solely illustrated median A for zones 4 to 8) for the global tropical dataset as a function of T. In general, median A calculated for individual MCS reflectivity zones 5, 6 and 7 are very similar to the median A when merging all MCS reflectivity zones (black solid line), whereas median A calculated for MCS reflectivity zone 4 tends to have smaller A values and median A calculated *for MCS reflectivity zone 8 have larger median A values than the overall median A (all MCS reflectivity zones merged) for comparable temperatures.*

However, when taking into account the variability in median A calculated for individual MCS reflectivity zones and associated 25th and 75th percentiles we can state that median A generally increases with T, however it is not possible to assess that A increases with MCS reflectivity zones or IWC. As a comparison, we include the value of the pre-factor α (in SI unity) from Cotton et al. (2013) mass-size relationship (β=2.0, as is for second moment M_2, and α=0.0257). Clearly, α=0.0257 is not suited for deep convective systems as it represents ice crystals for T $\in$[215K; 225K[.

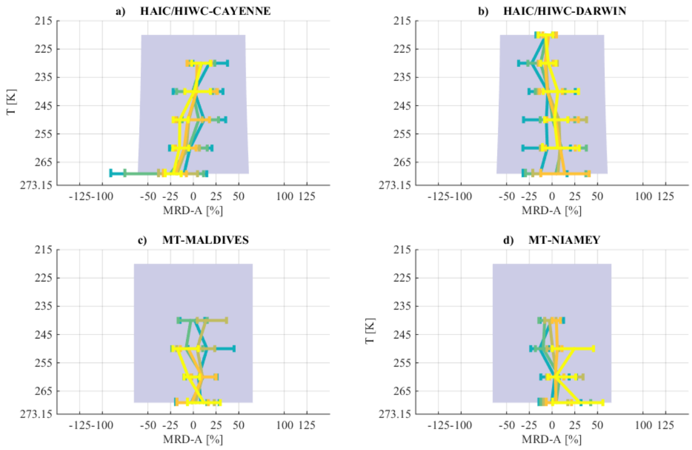

Figure 26: Same as Figure 6, but for the ratio MRD-A.

Figure 26 (a), 26(b), 26(c), and 26(d) illustrate that MRD-A are significantly smaller than U(A)/A, (same uncertainty than α: $U(\alpha)/\alpha$ = U(A)/A and median MRD results centered around 0%). Comparing results of A (Figure 26) with results presented for α (Figure 15, section 5.4) it is obvious in terms of variability and MRD in each type of MCS that A is better adapted to parametrize the PSD 2nd moment as a function of T. Eq. (12) then fits the median of ratio A for the global tropical dataset (red dashed line, all MCS reflectivity zones merged), as a function of T in deep convective systems for IWC larger 0.1g m^{-3}:

$$A(T) = 0.0000075 \cdot T^2 - 0.0030598 \cdot T + 0.3334963 \qquad [kg.m^{-2}] \tag{12}$$

Hence, Field et al., (2007) proposed to retrieve the third moment M_3 as function of M_2 and T. These equations are recalled here with (in our case n=3):

$$M_n = M_2^{F(n)} \cdot D(n) \cdot exp(E(n) \cdot T_c) \tag{13}$$

T_C denotes temperature in °C and D(n), E(n) and F(n) are given by:

$$D(n) = exp(13.6 - 7.76 \cdot n + 0.479 \cdot n^2) \tag{14}$$

$$E(n) = -0.0361 + 0.0151 \cdot n + 0.00149 \cdot n^2 \tag{15}$$

$$F(n) = 0.807 + 0.00581 \cdot n + 0.0457 \cdot n^2 \tag{16}$$

Figure 27 provides median relative errors (whiskers represent 25th and 75th percentiles) of parametrized moments M_2 (Figure 27 (a) and Figure 27 (b)) and M_3 (Figure 27 (c) and Figure 27 (d)) compared to respective moments calculated directly (Eq. (9) from PSD measurements (merged dataset). These relative errors are shown as a function of IWC (Figure 27(a) and Figure 27(c)) and as a function of T (Figure 27(b) and Figure 27(d)). Firstly, the red line shows median relative error of M_2 retrieved from Eq. (11) compared to M_2 derived from measured PSD (Eq. 10). In addition the grey band illustrates the uncertainty $U(M_2)/M_2$. Figure 27 (a) illustrates that below 2g m^{-3}, the median of this relative error is close to 0% with 25th and 75th percentiles significantly smaller than $U(M_2)/M_2$. However, for largest IWC beyond 2g m^{-3}, median relative errors are getting large (40% for 4g m^{-3} and 75% for 4.5g m^{-3}) and need to be corrected in order to reduce the bias between predicted M_2 and observed M_2. This is why Eq. (11) is modified with an expression shown in Eq. (17) in order to improve prediction of M_2 compared to measured M_2 (Eq. (10)) for highest IWC:

$$M_2 = \frac{IWC}{A(T)} \cdot exp\big(0.005853 \cdot exp(1025 \cdot IWC)\big) \qquad [m^{-1}] \tag{17}$$

The effect of the expression added in Eq. (17) is illustrated by the blue line in Figure 27 (a) and Figure 27 (b), where median relative error of predicted M_2 are now closer to 0% also for large IWC. ~~Still, Eq. (12+17) seems to underestimate measured M_2 by about 15% for IWC of 4.5g m^{-3} instead of 75% overestimation before correction.~~ Note that in Figure 27 (b), median relative errors of the two above parametrizations (red and blue solid line) of M_2 are superposed as a function of T with a median relative error close to 0%. This means that the second part of equation (17) does not introduce any significant bias as a function of T, since the occurrence of IWC > 2g m^{-3} is smaller than 1% for the merged dataset.

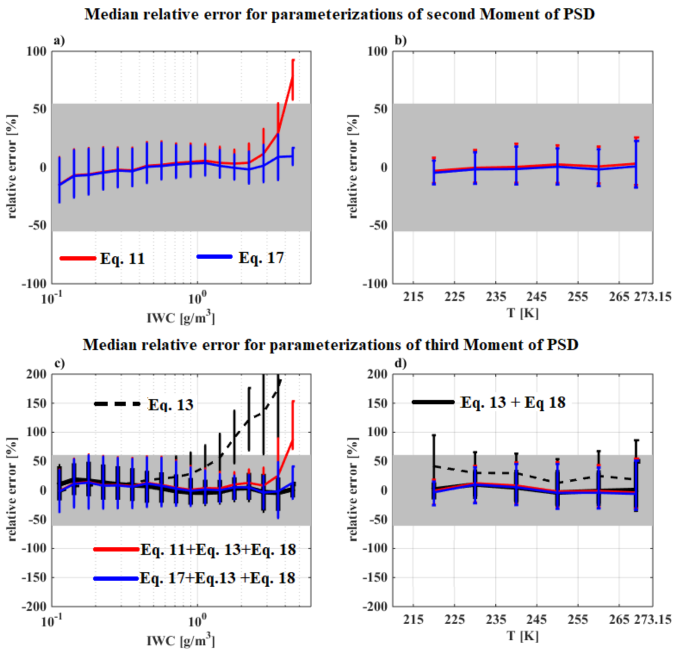

Figure 27: Relative error of parametrized M_2 and M_3 for merged dataset as a function of IWC in a) and c), and as a function of T in b) and d). Solid lines give median relative error and whiskers denote 25th and 75th percentiles of relative error. Grey bands shows measurement uncertainties for M_2 (55%; a) and b)) and M_3 (61%; c) and d)), respectively.

In Figure 27 (c) and Figure 27 (d)) are shown median relative error for parameterizations of the third moment, where the median relative error for all parameterization are calculated as function of measured M_3. First, we discuss the median relative error for parametrization of 3rd moment M_3 according to Field et al., (2007) (Eq. (13); black dashed lines) using the measured M_2. Then, we can see that the parameterization of Field et al., (2007) overestimate M_3 for IWC larger than 1g m-3 and that overestimation of M_3 increase with IWC. Moreover, this overestimation of M_3 tend to decrease a bit as function of T.

To reduce this significant median relative error on measured M_3, particularly for large IWC in deep convective cloud systems, we provide a M_3 correction function for Eq. (13) as function of T and IWC:

$$M_3 = [-5.605 - 1.059 \cdot log(IWC) + 0.009536 \cdot T - 0.0418 \cdot log(IWC)^2 + 0.0007889 \cdot log(IWC) \cdot T] \cdot M_2^{F(3)} \cdot D(3) \cdot exp(E(3) \cdot T_c) \quad (18)$$

Then, three series of median relative error of M_3 where M_3 are computed with Eq. (19). First, Eq. (19) is used with measured M_2 (black solid lines) to show the efficiency of the correction applied as function of IWC and T and described in Eq. (19). Then, Eq. (19) is applied to M_2 calculated using Eq. (11) where there is no correction as function of IWC to calculate M_2 (red solid lines). We can observe that M3 are overestimated for IWC larger than 3g.m-3, and that there is no bias as function of T with median relative error close to 0%. Finally, Eq. (19) is used *to compute M3 from M2 calculated with Eq. (17) when impact of large IWC is taken into account. We can see median relative error close to 0% for the third example of parameterization (i.e. Eq. (17) and Eq. (18)) with no bias as function of IWC and T.*

An identical investigation on median relative errors in the prediction of 2nd and 3rd moment as presented in Figure 27 has been investigated for individual MCS locations (figures not shown). For all type of tropical MCS, we observe that M_2 from Eq. (17) and M_3 from Eq. (18) tend to have smaller to equal median relative errors compared to the relative uncertainties $U(M_2)/M_2$ and $U(M_3)/M_3$, respectively. Beyond this general statement there are two noticeable observations. The first observation is that median relative errors of M_3 from Eq. (18) calculated either with M_2 from measurements (Eq. (9)) of from parametrized M_2 from Eq. (17) for MCS over Maldives Islands are close to $U(M_3)/M_3$ with 75th percentiles reaching 100% for IWC in the [0.3; 0.6] g m^{-3}. The second observation is that for MCS over Niamey, M_3 from Eq. (18) with M_2 from Eq. (9) or from Eq. (17) tend to overestimate respective moments calculated directly from PSD measurements by about 30 or 50%, respectively, in the area of higher IWC ([2; 3] g m^{-3}).

This section aims to produce parameterizations of the second and third moments of ice hydrometeor size distributions, which can be useful for the calculation of hydrometeor size distributions in numerical weather prediction using gamma distributions, but also (see the next section) for calculating rescaled ice hydrometeors size distributions (Field et al., 2007).

6.2.3 Rescaling of measured ice hydrometeors size distributions

From bulk properties as mixing ratio and total concentration in numerical weather prediction (NWP), ice hydrometeors size distributions (or PSD) properties can be derived from moment parameterization allowing simplified prediction of cloud microphysical processes such as precipitation. Usually, ice hydrometeors size distributions for hydrometeors are modeled by gamma distributions. Since the method of gamma distributions is relatively well documented, we focus this study on another type of PSD parameterization, which studies 'rescaled PSD' dealing with a 'mean diameter' defined by the ratio of the third moment over the second moment.

In this section, we propose an update for the method proposed by Field et al., (2007) for deep convective cloud systems and IWC larger than 0.1g m^{-3}. For the entire dataset of this study we therefore apply the above method utilizing Eq. (19) and Eq. (20) to calculate function $\Phi_{2,3}(x)$ and x for individual measured PSD :

$$\Phi_{2,3}(x) = N(D_{max}) \cdot \frac{M_3^3}{M_2^4} \tag{19}$$

With x being the characteristic size:

$$x = D_{max} \cdot \frac{M_2}{M_3} = \frac{D_{max}}{L_{2,3}} \tag{20}$$

$\Phi_{2,3}(x)$ and x are dimensionless functions. Moreover, Field et al., (2007) deduced from their dataset, $\Phi_{2,3}(x)$ depending on cloud location; i.e. tropical troposphere or mid-latitude troposphere (here we focus on the equation established for the tropics):

$$Tropics: \Phi_{2,3}(x) = 152 \cdot exp(-12.4 \cdot x) + 3.28 \cdot x^{-0.78} \cdot exp(-1.94 \cdot x) \tag{21}$$

Hence, the variability of PSD in clouds, is not given by $\Phi_{2,3}(x)$ but by the variability of the 2nd and 3rd moments that allow retrieving functions x and $\Phi_{2,3}(x)$. Then, knowing x, $\Phi_{2,3}(x)$, M_2, and M_3 concentrations of ice hydrometeors can be parameterized such:

$$D_{max} = x \cdot \frac{M_3}{M_2} \tag{22}$$

and

$$N(D_{max}) = \Phi_{2,3}(x) \cdot \frac{M_2^4}{M_3^3} \tag{23}$$

Figure 28 shows the probability distribution function (PDF) of observed rescaled PSD in tropical MCS as a function of the x parameter. Thick black line represents $\Phi_{2,3}(x)$ from Field et al., (2007), thin dashed grey line represents median of $\Phi_{2,3}(x)$ for a given range of x, with whiskers showing 25th and 75th percentiles of $\Phi_{2,3}(x)$. The figure illustrates that Eq. (21) from Field et al., (2007) represents rather well $\Phi_{2,3}(x)$ as a function of x in highest PDF region (dark red area) and fits well the median plot for $x \in [0.3; 6]$. However, Field et al., (2007) performed their study for diameter larger than 100µm while this study calculates rescaled PSD for D_{max} larger than 15µm for the underlying dataset. Thus, Eq. (21) does not fit median $\Phi_{2,3}(x)$ for x smaller than 0.3. Also for x > 6, Eq. (21) decreases too fast compared to the median of $\Phi_{2,3}(x)$ calculated for the global tropical dataset of this study, although Field et al., (2007) considered ice hydrometeors up to 2cm, whilst this study extrapolates PSD until 1.2845cm only. A likely assumption to explain the differences for large x > 6 might be that the merged tropical dataset of this study may have measured PSD with largest hydrometeors at a far higher frequency than this was the case for the dataset of Field et al., (2007).

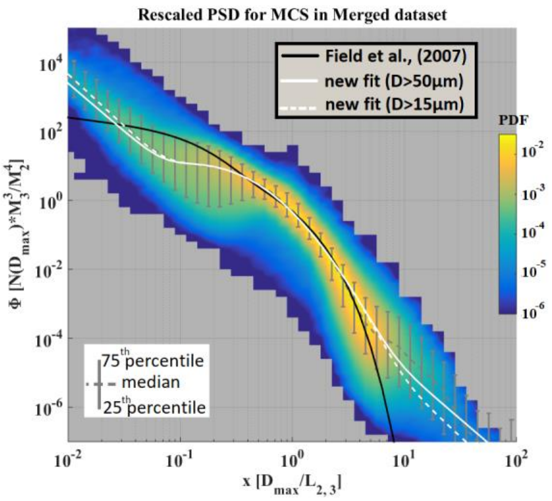

Figure 28: Probability distribution function of rescaled PSD ($\Phi_{2,3}$) on y axis as a function of hydrometeor characteristics size (x) on x axis, for the Global tropical datasets. Black lines show fitted functions from Field et al., (2007), grey dotted lines show median rescaled PSD with error bar from 25th and 75th percentiles of

rescaled PSD. Solid white line presents the new fitted function for the global tropical dataset for PSD beyond 55µm and dashed white line shows fitted function for PSD beyond 15µm (Eq. 25).

White lines (dashed and solid) show new fitted $\Phi_{2,3}(x)$ for the global tropical dataset of this study. The white dashed and solid lines can be represented by the following equation and aim to fit the median ($\Phi_{2,3}(x)$) of Figure 28 as a function of x:

$$Tropics: \Phi_{2,3}(x) = [exp(a_1) \cdot x^{a_2}] + \left[b_1 \cdot exp\left(-\frac{(ln(x) - b_2)^2}{b_3^2}\right)\right] \quad (24)$$

Where b1 = 9.484, b2 = -1.895 and b3 = 1.083. Note that dashed and solid white lines use different sets of coefficients a_1 and a_2 (Table 1). For white dashed line, a_1 and a_2 are calculated for D_{max} beyond 15µm, whereas for white solid line, a_1 and a_2 are calculated for D_{max} beyond 55µm. We can notice that the function for $D_{max} \geq$ 15µm produces higher $\Phi_{2,3}(x)$ as compared to the function fitted for $D_{max} \geq$55µm. In order to explain this difference, we recall that for MCSs over the Maldives Island concentrations of hydrometeors with $D_{max}\leq$55µm are higher compared to 3 other tropical MCS locations, which could affect the fitted coefficients a_1 and a_2 in the two different versions of $\Phi_{2,3}(x)$ calculations for the global tropical dataset. Another difference in small particle measurements could be a pure technical difference in small particle measurements (including shattering/out-of-focus/small sample volume artefacts) between 2D-S probe (this study) and 2D-C probe (Field et al. (2007) study).

Table 1 : Coefficients a1 and a2 for Eq. (25).

	a_1	a_2
Tropics: D_{max} >15µm	*-5.4114*	*-3.0026*
Tropics: D_{max} > 55µm	*-5.0032*	*-2.7822*

"

<u>Discussion of results:</u>

The discussion would benefit from relating your results to results of former studies, do your findings agree/disagree with what others have found? If your results are completely new, than it should be pointed out more clearly! Also, please point out more clearly what your parameterisations are useful for and how the scientific community benefits from your work.

In section 5.1, we compare our results to IWC-T relationship calculated for clouds in the tropics : "*For comparison purposes with former studies, two IWC-T relationships from literature are added in Figure 5(a). Jensen and Del Genio (2003) suggested an IWC-T relationship in order to account for the limited sensitivity of the precipitation radar aboard the TRMM satellite, not allowing for small ice crystals at the top of convective clouds' anvils to be observed. They used radar reflectivity factors of a 35GHz radar based on Manus Island (North-East of Australia; 2.058°S, 147.425°E), thereby calculating IWC from an IWC-Z relationship (IWC=0.5*(0.5.Z0.36); Jensen et al., 2002). The resulting IWC-T relationship given by Jensen and Del Genio (2003) is reported by a dashed-dotted grey line, which fits between 75th percentiles of tropical median IWC of MCS reflectivity zone 4 and 25th percentile of MCS reflectivity zones 5. We recall that IWC, as a function of T, in MCS reflectivity zones 4 and 5 are related to Z between 30th-50th and 50th-70th percentiles, respectively. We may notice that the IWC-T relationship from Jensen and Del Genio (2003) is different and smaller than the median IWC (4 tropical campaigns).*
Moreover, (Heymsfield et al., 2009) established an IWC-T relationship based on 7 fields campaigns (dashed grey line in Figure 5(a). They focused their study on maritime updrafts in tropical atmosphere for a temperature range T ∊ [213.15K; 253.15K]. Their suggested IWC tend to be in the range of IWC of MCS reflectivity zones 6- 8 with IWC increasing with T. We already showed in section 3.2 that MCS reflectivity zones 7 and 8 have higher probabilities to be convective (updraft regions with higher magnitudes of vertical velocity), as compared to other MCS reflectivity zones. Therefore, (Heymsfield et al., 2009) IWC parametrizations for maritime updrafts are not inconsistent with data from this study."

In section 5.2, we compare our results from visible extinction-T relationships from Heymsfield et al., (2009): "*Furthermore, a σ–T relationship from Heymsfield et al. (2009) (grey dashed line) is added in Figure 6 (a), which is calculated, as a function of T, as the sum of the total area of particles larger than 50µm plus the total area of particles smaller than 50µm multiplied with a factor of 2 in order to satisfy Eq. (1) and to compare with results of this study. We conclude that σ–T estimation presented in Heymsfield et al. (2009) for maritime convective clouds is rather comparable to median MRD-σ calculations (4 tropical campaigns) in MCS reflectivity zones 6 to 7 corresponding to higher reflectivity zones, and thus statistically to zones with some remaining convective strength.*"

Page 18 line 9, we propose to add references who founds similar results (R2#5).
"*It confirms conclusions from Frey et al., (2011) and Cetrone and Houze (2009), who suggest that there are larger ice hydrometeors in MCS over continent than MCS over maritime regions.*"

Also, we performed an update and a comparison of parameterization of 2nd Moment and 3rd Moment of PSD and the parameterization of ice hydrometeors size distribution as function of IWC and T performed by Field et al., 2007 for tropical convective clouds. This parameterization was used in the microphysical scheme based on (Wilson and Ballard, 1999) used in the configuration of the Met Office Global Atmosphere version 6.1 (Walters et al., 2017). Which was the version of the Unified Model used operationally by the Met Office for global weather and climate prediction. More precisely, the ice-snow concentrations was computed with the moment parametrization developed by (Field et al., 2007) and the mass-diameter relationship from Cotton et al., (2013).

We propose to add the following comment in the conclusion section at the page 28 line 8 of the original version of the manuscript (R2#6):
"*To conclude on the parameterization of ice hydrometeors distribution. We performed an update of the computation of PSD as function of IWC and T performed by Field et al., 2007 for tropical convective clouds (see Eq. (11), Eq. (17) and Eq. (18)). This parameterization was used in the microphysical scheme based on (Wilson and Ballard, 1999) used in the configuration of the Met Office Global Atmosphere version 6.1 (Walters et al., 2017). Which was the version of the Unified Model used operationally by the Met Office for global weather and climate prediction. More precisely, the ice-snow concentrations was computed with the moment parameterization developed by (Field et al., 2007) and the mass-diameter relationship from Cotton et al., (2013). Here, we suggest to use the new parameterization developed in our study for ice-snow concentrations when IWC are larger than 0.1 g.m^{-3}. Otherwise, we suggest to keep either the original version of Field et al., (2007) parameterization with the Cotton et al., (2013) mass size relationship or the original version of Field et al., (2007) parameterization with A as function of temperature which would be a fit of the 25th percentile of A in MCS reflectivity zone 4 (see Table C12 in Appendices C).*"

Moreover, we propose to add a comment on how to use the MCS reflectivity zones after the former comment (R2#7).
"*We showed that IWC tend to be similar as function of temperature and MCS reflectivity zone, suggesting that IWC-Z-T relationship developed by Protat et al., (2016) would be available for IWC larger than 0.1g.m-3 in tropical MCS. In other words there is a confident relationship between IWC, Z and T in tropical MCS. Then, for the evaluation of NWP, we suggest to define the MCS reflectivity zones using the 25th percentiles of IWC as the lower limit of each MCS reflectivity zones (see Table C2 in Appendices C). Hence, for each MCS reflectivity zone visible extinction, hydrometeors concentrations (NT_{50}, NT_{500}, M_2 and M_3), reflectivity factors at 94GHz and vertical velocities from NWP can be compared with the findings of this study (see Table in Appendices C). This methodology should help to identify where NWP fails to represent the links between different parameters and IWC. Indeed, study the spatiotemporal variability of IWC in MCS is a complex topic. It needs a time reference and a space reference. For MCS, the time reference can be its life cycle, but there are MCS that have a more complex life cycle than others (merging of MCS, a new growing stage after a decaying stage). Concerning the space reference, there is a common view which is to observe the MCS from its most active area; its convective part. There are two difficulties to take into account here. First, there are very few direct measurement of cloud microphysic in the very convective area of MCS. Second, MCS can be the aggregation of many convective cells that can be well or not well organized (Houze 2004). Moreover, we saw that large IWC tend to be more associated to vertical movement than lower IWC, but it is not always true.*
This is why we propose to test NWP using the statistic performed in this study, by testing the different conditions of others microphysical parameters observed with a given IWC and temperature."

Specific comments

page 2, line 4-5: "An accurate estimation of the spatiotemporal distribution of the Ice Water Content (IWC) is a key 5 parameter for evaluating and improving numerical weather prediction (Stephens et al., 2002)." Does this statement make sense in the light of your manuscript where you use IWC as input for your parameterisation and not obtain it as output?

It is right that IWC in our study is used as an input. In fact, we use it at a key parameter, that will test if the others parameters are in agreement with the range that they are observed knowing IWC and the temperature. See the text added in the end of the former comment.

page 3, line 2: better say: This study uses a data set where MCSs were observed in four different locations in the tropics and related to two different projects:
Done.

page 3, line 19: IKP-2 - please introduce abbreviation.
Change are made in the manuscript such (R2#8):
"*performed with the isokinetic evaporator probe (hereafter IKP-2 probe)***"**

page 3, line 22: Are you really giving D_max in cm?
Yes, shape properties of ice crystals are calculated in cgs unit, such mass-size relationship, surface-size relationship and perimeter size relationship. Also note that in section 5.5 largest size of hydrometeors are given in cm.

page 3, line 31: Please introduce the radar reflectivity factor Z as it is an important parameter in your study and reader less familiar with radar measurements might not properly know it.

The definition is introduce at page 2 line 28: "*The latter will be accomplished by a composite analyses of microphysical properties and simultaneously measured radar reflectivity factor (Z).*"!

page 3, line 35: "The processing holds particularly for both data sets of the HAIC-HIWC project. "
I don't quite understand what you want to say with this sentence? Please rephrase.
(R2#9)
"*Detailed description of data processing is documented in Leroy et al. (2016 and 2017), Protat et al. (2016), Strapp et al. (2016b), and Davison et al. (2016). These references give a processing description for both datasets of the HAIC-HIWC project. But, Megha-Tropiques datasets (Fontaine et al. (2014)) were reprocessed in order to undergo exactly the same version of processing tools for comparison reasons in this study.***"**

page 4, line 2/3: mean profiles of Z:
Did you perform some kind of weighting when combining the data sets from the four campaigns for the number of data points that go into the mean? If not the results/means will be shifted towards the HAIC-HIWC campaigns, which have significantly more data points. This should be discussed.
We do not use mean profiles, but percentiles profiles. However, percentiles calculation from radar data takes into account more data from cloud radar profiles than for the in-situ data. There are less in-situ measurement for MT project than for cloud radar profiles measurement, because the PIP probe was not working in the second half of the two campaigns of MT project. However, the cloud radar worked perfectly over all the MT-project. The percentiles of Z are calculated for a merged dataset that include 11 flights for MT over Niamey, 11 flights for MT over Maldives, 19 flights for HAIC-HIWC over Darwin and 17 flights for HAIC-HIWC over Cayenne.

We propose to add line 41 page 3 (R2#10):
"*The percentiles of Z are calculated for a merged dataset that include 11 flights for MT over Niamey, 11 flights for MT over Maldives, 19 flights for HAIC-HIWC over Darwin and 17 flights for HAIC-HIWC over Cayenne. Percentiles are not calculated as function of the number of profiles but by temperature ranges of 5K where only points with Z larger than -30dBZ are taken into account*."

page 5, line 26: The usage of ECMWF reanalysis temperatures: Due to the much coarser resolution of the ECMWF data (compared to aircraft point measurements), what implications does it have on the uncertainties of your results?

First, profiles are measured as function of their altitude. Then, using reanalysis of ECMWF and knowing the flight altitude and its temperature of the aircraft, the cloud radar profiles temperature is computed. Hence, ECMWF temperature profiles are adjusted for each profiles measured by RASTA by the in-situ measurement of the temperature. So uncertainty of ECMWF reanalysis, affect the statistics on Z profiles as function of the temperature, but it does not affect the statistic on the in-situ measurement.

page 7, line 20f: U(X)/X - Is this parameter denoted by the grey shading in the subfigures b-e? Then mention it here as well.
(R2#11)
"*In order to take into account the uncertainties in all type of measurements, uncertainties (hereafter noted U(X)/X) represented by grey bands on Figure showing MRD-X) for each parameter X were taken from Baumgardner et al. (2017)*"

page 11, line 1-5: You are concluding that "... _ in tropical MCS tend to be similar for all MCS locations in the same range of T and for corresponding MCS reflectivity zones, ..." but your parametrisation is only a function of T and IWC, but not dependent on reflectivity zone? How does that fit? In that respect I was missing a figure showing measured values alongside the parametrisation (not only the relative errors as in Fig. 7). It could also help to explain more how you arrive at this parameterisation.
In section, 5.1 we pointed out that there could be a unique IWC-Z-T relationships (given by Protat et., 2016) for tropical MCS for IWC larger than 0.1g.m-3. So performing a parameterization as function of IWC and T is similar to perform a parameterization as function of reflectivity zones (i.e. Z(T)). A parameterization as function of IWC and T is more convenient than a parameterization as function of Z and T. In the first case, it can be used by model and observations. While in the second case it can only being used with observations, since simulations of radar reflectivity factors at 94 GHz are not accurate for NWP.

When plotting visible extinction versus IWC and T there is a linear relationship between log(σ) and log(IWC). Moreover it seems that log(σ) decrease with temperature increasing at constant log(IWC). Then, we performed a surface fitting using input coefficients log(IWC) and T to fit log(sigma).

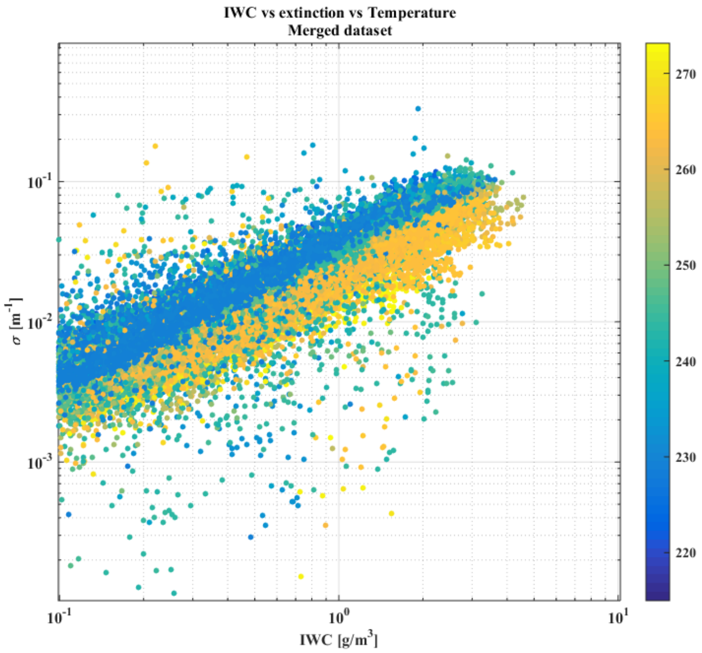

Figure 19: visible extinction in [m-1] on y-axis as function of IWC in [kg.m-3] on x axis and as function of T in [K] with color scale. Scatter plot using the merged dataset (4 campaigns).

We add the previous figure in the section concerned by parameterization of visible extinction (R2#12; see also answer to the major comment about length of section5).

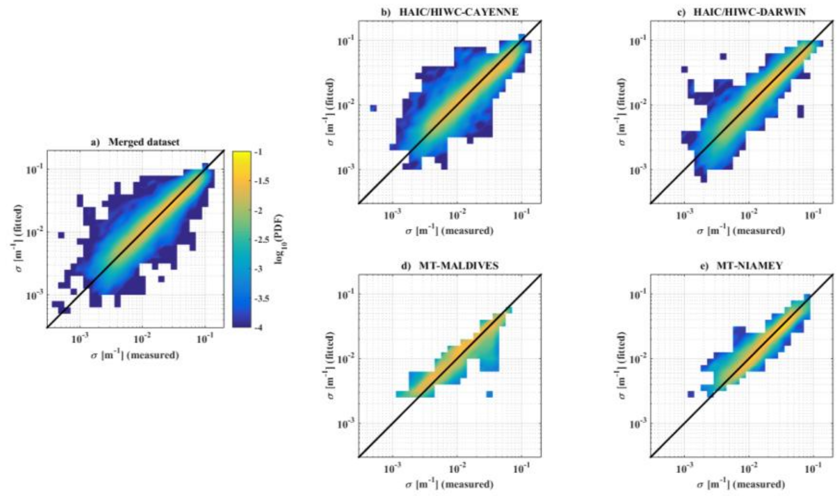

Figure R2: Visible extinction calculated from equation (8) on y-axis as a function of measured visible extinction on x-axis. a) for the merged dataset, b) for the Cayenne campaign, c) for the Darwin campaign, d) for the Maldives campaign and e) for the campaign over Niamey. Probability distribution function (PDF) are given by the color scale. Black line represent the function x=y.

Figure R2 show that visible extinction computed with equation (3; in the original versions of the manuscript) versus measured visible extinction are mainly distributed around the black curve y=x.

Some change have been made for the section concerning the parameterization of visible extinction (R2#12).

"***6.1 visible extinction***

Since we concluded from Figure 7 and Figure 8 that visible extinction σ and IWC in tropical MCS tend to be similar for all MCS locations in the same range of T and for corresponding MCS reflectivity zones 4 to 8. Moreover Figure 19 shows that there is a linear relationship between log(σ) and log(IWC). And log(σ) decrease with temperature increasing at constant log(IWC). Then, we performed a surface fitting using input coefficients log(IWC) and T to fit log(sigma) to deduce a parametrization of σ (Eq. (8)) as a function of IWC and T for deep convective cloud data (merged dataset) of this study limiting data to IWC > 0.1g m^{-3}:

$$\sigma = exp(-0.0194587 \cdot T + 0.9134019 \cdot ln(IWC) + 1.2423609) \qquad [m^{-1}] \qquad (8)$$
"

page 12, line 22: "... identical image data processing to remove shattering artefacts..." which method exactly do you use? This might be quite important for the resulting data. For example, when you use the interarrival time method from Field et al., 2006, using the same time threshold for all data sets might lead to errors. The best threshold might even vary from one flight to the next in the same campaign (at least in my experience, see e.g. Frey et al., 2011, where interarrival times have been adapted for each single flight). Thus, using only one threshold for all four campaigns might lead to removal of 'good' images in one case and incomplete removal of 'bad' images in another case.

As it is not the first publication using part of this dataset, and that processing applied to this is exactly the same as in Leroy et al. (2016 and 2017) we give the reference if the reader wants more details; in the manuscript page 3 line 34:

"*Accurate description of data processing is documented in Leroy et al. (2016 and 2017), Protat et al. (2016), Strapp et al. (2016b), and Davison et al. (2016).*"

Indeed, Field et al., (2006) was used to remove shattering. Except, that the cut off time threshold computed using Gaussian function to fit inter-arrival time of natural particle and Gaussian function to fit inter-arrival time of shattered particles, were calculated every second; both for PIP and 2D-S probe.

More details in Leroy et al., (2016): "*In addition, a fraction of cloud particles inevitably hit the probe's housing during sampling and may break up into multiple fragments that are recorded by the probe (Field et al. 2003; Korolev and Isaac 2005; Heymsfield 2007). During the HAIC/H1IWC field campaign, the frequency of such events was reduced by using specially designed probe leading edge tips to minimize shattering. However, the remaining images related to splashing/shattering events had to be removed as effectively as possible; otherwise, PSD measurements and their derived microphysical properties would be subject to errors. Most of the images related to a shattering/splashing event were removed by a careful analysis of (i) the ratio between the particle's area and its sizes in the x and y directions and (ii) the interarrival times between neighboring particles. The interarrival time technique is commonly used and has been described and tested by Field et al. (2006), Baker et al. (2009), Lawson (2011), and Korolev and Field (2015). In this study, the image processing rejected particles presumed to be associated with shattering if their interarrival times were lower than a cutoff value that was calculated once per second.*"!

page 12/13, Section 5.3 until page 13, line 20: Since the conclusions from Figure 8 and 9 are similar, and due to the uncertainties related to the small particles, I think Fig. 8 and the corresponding text would be a good candidate to move to a supplement and only briefly mention here. See main comment about the length of the manuscript above.

We agree, and put figure 8 (in the old manuscript) on total concentration in the appendices A (R2#13).

"

Appendices A

Figure A1 shows median total concentration (N_T) as a function of T and MCS reflectivity zone (N_T) for the merged datasets where concentrations of ice hydrometeors are integrating beyond 15µm:

$$N_T = \sum_{Dmax=15}^{Dmax=12845} N(D_{max}) \cdot \Delta D_{max} \qquad [L^{-1}] \qquad (A1)$$

Median N_T systematically increase with MCS reflectivity zone and altitude, however with significant overlap of 25^{th} and 75^{th} percentiles of neighboring MCS reflectivity zones. Measurement uncertainty on concentrations given for small hydrometeors is about ±100% (Baumgardner et al., 2017).

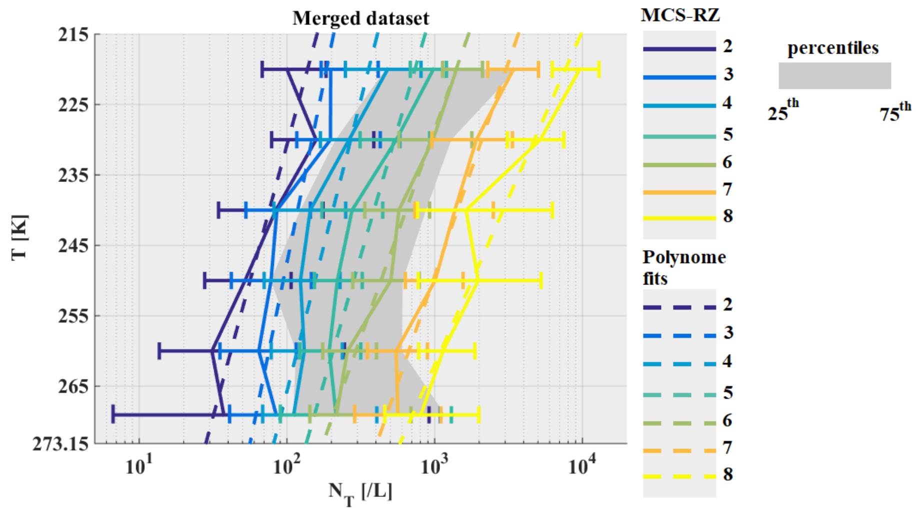

Figure A1: Same as Figure 5, but for concentrations of hydrometeors integrated beyond D_{max} =15µm in [L^{-1}].

Figure A2 (a), Figure A2 (b), Figure A2 (c), and Figure A2 (d) show MRD-N_T of MCS in the different tropical locations. For MCS over Darwin and Cayenne, in all MCS reflectivity zones MRD-N_T are smaller than the measurement uncertainty, whereas for Niamey data this is the case only in MCS reflectivity zones 2, 5, 6 and 7. MCS over Maldives Islands yield significantly larger MRD-N_T than the measurement uncertainty, and those are primarily positive. Hence, MCS over Maldives Islands have larger concentrations of hydrometeors for a same range of T and Z, than the three other types of tropical MCS. However, these larger concentrations observed do not concern zones where highest concentrations of hydrometeors were observed. For example, in MCS reflectivity zone 4 where MRD-N_T is reaching 1000%, N_T for the Maldives dataset are approximately 1000 L^{-1}, which is similar to N_T observed in MCS reflectivity zones 7 and 8 for the same range of $T \in$ [235K; 245K[for the merged dataset. We recall that identical image data processing to remove shattering artefacts and to correct for out of focus images (Field et al., 2003; Korolev and Isaac, 2005; Leroy et al., 2016) have been applied for all 4 tropical datasets. Also the presence of super cooled droplets has been investigated (RICE, CDP probe), and few periods with super cooled water content have been removed for this study. Moreover, we show in section 5.5 that MCSs over Maldives Islands tend to have smaller max(D_{max}) especially in MCS reflectivity zones 4, 5, 6 and 7 compared to the other MCS locations and that concentrations beyond 500µm in Maldives Islands observations are in the same range as the other types of MCS.

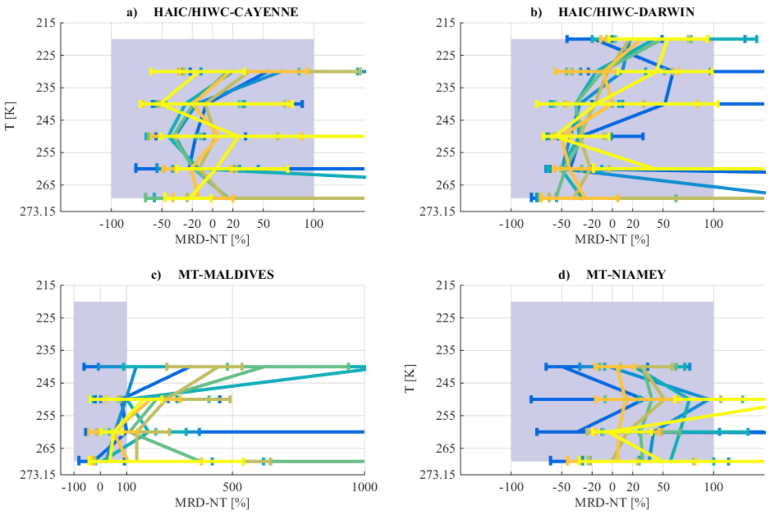

Figure A2: Same as Figure 6, but for MRD-NT.

"

page 14, line 30: "in the decaying parts"
I think here is the first time where you mention these MCS to be decaying. Is it true for the whole of the Maldives measurements, or only for parts of the measurements with the small particles (or only for specific Z)? This relates to my main comment about the meteorological differences between the MCSs in the different campaigns.
No this is a misunderstanding we are talking about the decaying part of MCS, contrary to the active part of the MCS (convective area).
We propose to rephrase this sentence (R2#14):
"*We observe that total concentrations starting from 15µm can be different between MCS locations as a function of T and Z, especially in oceanic MCS over Maldives Islands in the more stratiform part of these MCSs where measured concentrations can reach 10 times the median concentrations observed globally for merged tropical dataset.*"

page 15, line 29/30: What are ep and es?
They are respectively the pre-factor of the perimeter-size relationship and the pre-factor of the surface-size relationship; power-law relationship. However, they have no interest in our study. They are here, to write correctly the equations.

page 16, line 10: "merged with subsequently sampled rather small local convective systems"
Since you focus your study on MCS, can these rather small convective systems still be classified as MCS? Otherwise, should they not be removed from the data set?
MCS over Maldives in the second period of the campaigns were weaker because of the dry phase of the MJO. However, the dataset over Maldives is quiet small (compared to others) and these data are still related to convective systems. So we decided to keep these data.
But this part has been rewritten and this the discussion linked to this comment deleted. Has we are no longer agree that it is due to a lack of statistic (it would be the same for all parameters). We simply agree that shape of hydrometeors are different in these condition for the Maldives (see new section 5, in the major comment section).

page 15-17/Section 5.4:
Maybe this section could also go into the supplement (no major conclusion drawn)? and only briefly mention in main manuscript.

This section study the shape of ice hydrometeors (β) coefficient and somewhere their density (α). Tendencies and results given in this section might interest scientist community working on mass-size relationship. We keep it, but some change have been made (see new section 5 in the major comment section).

page 17/18, section 5.5:
Also this section could be moved to a supplement?
Length of section 5 have been reduced, we want this part stay in the main part of the manuscript. As the section 5.4 before, it shows that ice hydrometeors can be different in some of their properties. Even if they are similar considering their IWC or visible extinction.

page 18, line 22: "Commonly, number PSD of ice hydrometeors are modeled with Gamma distributions."
Maybe give one or two example references.
We propose to add these two references (R2#15):

Heymsfield, A. J., Schmitt, C. and Bansemer, A.: Ice Cloud Particle Size Distributions and Pressure-Dependent Terminal Velocities from In Situ Observations at Temperatures from 0° to −86°C, J. Atmos. Sci., 70(12), 4123–4154, doi:10.1175/JAS-D-12-0124.1, 2013.

McFarquhar, G. M., Timlin, M. S., Rauber, R. M., Jewett, B. F., Grim, J. A. and Jorgensen, D. P.: Vertical Variability of Cloud Hydrometeors in the Stratiform Region of Mesoscale Convective Systems and Bow Echoes, Monthly Weather Review, 135(10), 3405–3428, doi:10.1175/MWR3444.1, 2007.

page 22, line 22: How would M3 derived from parameterised M2 according to Eq. (18+13) look lie? Why don't you show this as well? Above you make an improvement to theM2 parameterisation, so why do you use the presumably worse parameterisation for deriving M3 here now? Which would also presumably lead to a worse M3 retrieval?
This part is modified, to make it easier to understand. Relative errors are plotted separately for the 2nd moment and for the third moment. There, is no change for the 2nd Moment except that a new function (18; now 17) has been calculated for IWC in [$kg.m^{-3}$] (NWP units).
Then, we show only the relative error for M3 derived with M2 using equation (14; now 13); the original parameterization of Field et al., (2007). As for equation (18; now 17) we computed a new equation (19; now 18) where IWP is in [$kg.m^{-3}$].
In this new version of manuscript, we show relative error for three other computation of the third moment. First, when the equation (19; now 18) is applied with measured M2, to show efficiency of the equation (19; now 18). Then, when the equation (19; now 18) is applied to M2 derived from the equation (12; now11) when there is no correction for the calculation of M2 as function of IWC. It show that equation (19; now 18) fails to compute M3 for large IWC if M2 are not calculated correctly with equation (18; now 17). Finally, when the equation (19; now 18) is used with M2 calculated with equation (18; now 17), it show the efficiency of the new parameterization of M2 and M3 developed in our study.
The new version is written after the new section 5 (in section 6.2.2) in the major comment section.

page 23, line 14/15: "blue solid lines represent median relative error when estimated M3 is calculated from parametrized M2 from Eq. (18+13) and Eq. (19)."
This is not, what the legend in Figure 17 says?
See new version, this has been changed.

page 23, lines 19-27: Maybe show the figures in a supplement?
We agree to show the figures in the reviewer answer. However, the new version of the manuscript has already a lot of figures and 3 more Appendices.

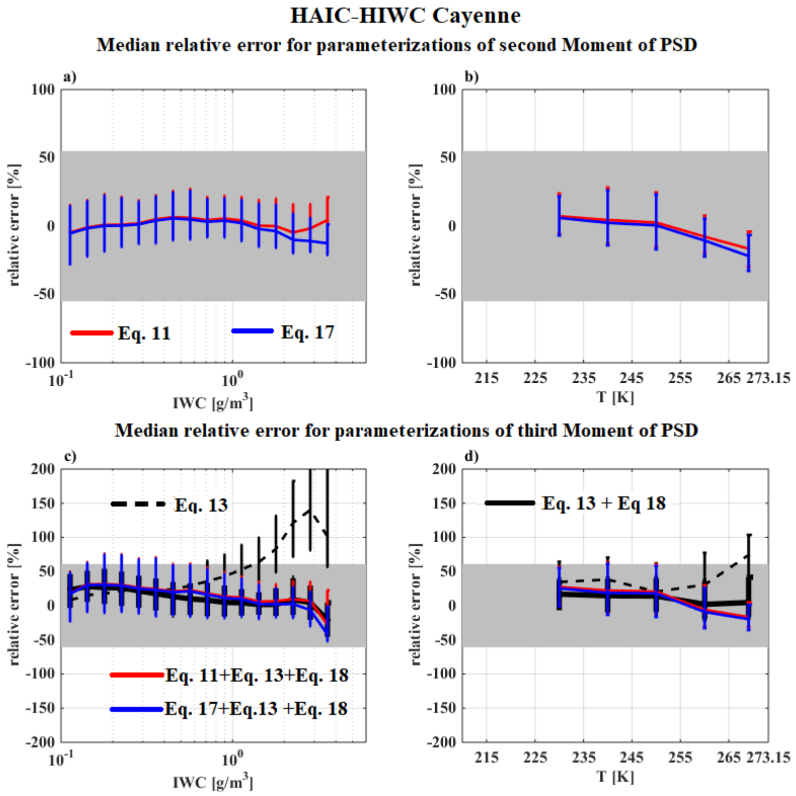

Figure R 3: ***Relative error of parametrized M_2 and M_3 for MCS over Cayenne as a function of IWC in a) and c), and as a function of T in b) and d). Solid lines give median relative error and whiskers denote 25th and 75th percentiles of relative error. Grey bands shows measurement uncertainties for M_2 (55%; a) and b)) and M_3 (61%; c) and d)), respectively***

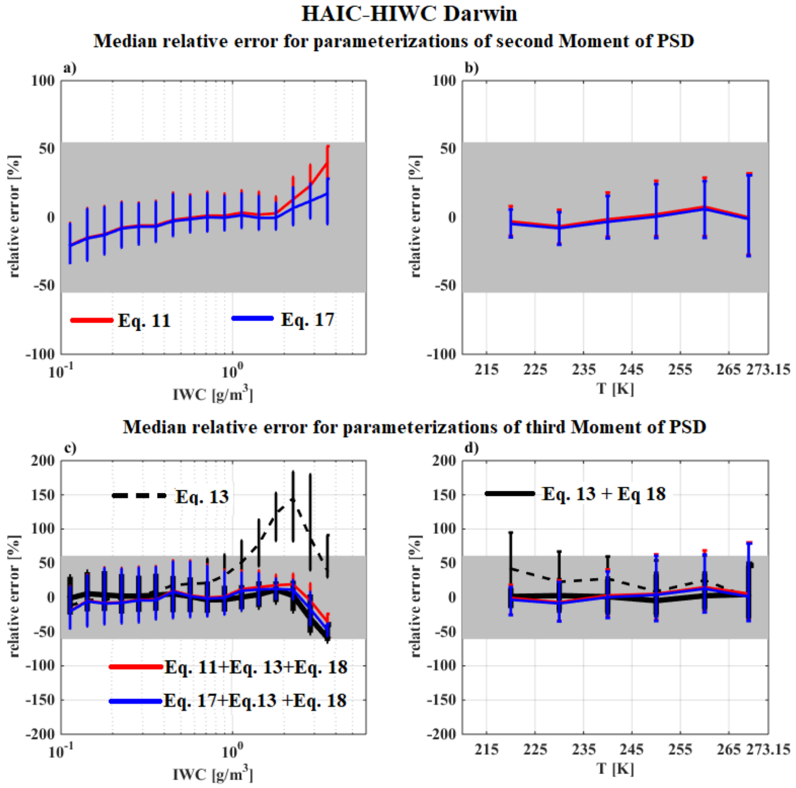

Figure R4: ***Relative error of parametrized M_2 and M_3 for MCS over Darwin as a function of IWC in a) and c), and as a function of T in b) and d). Solid lines give median relative error and whiskers denote 25th and 75th percentiles of relative error. Grey bands shows measurement uncertainties for M_2 (55%; a) and b)) and M_3 (61%; c) and d)), respectively***

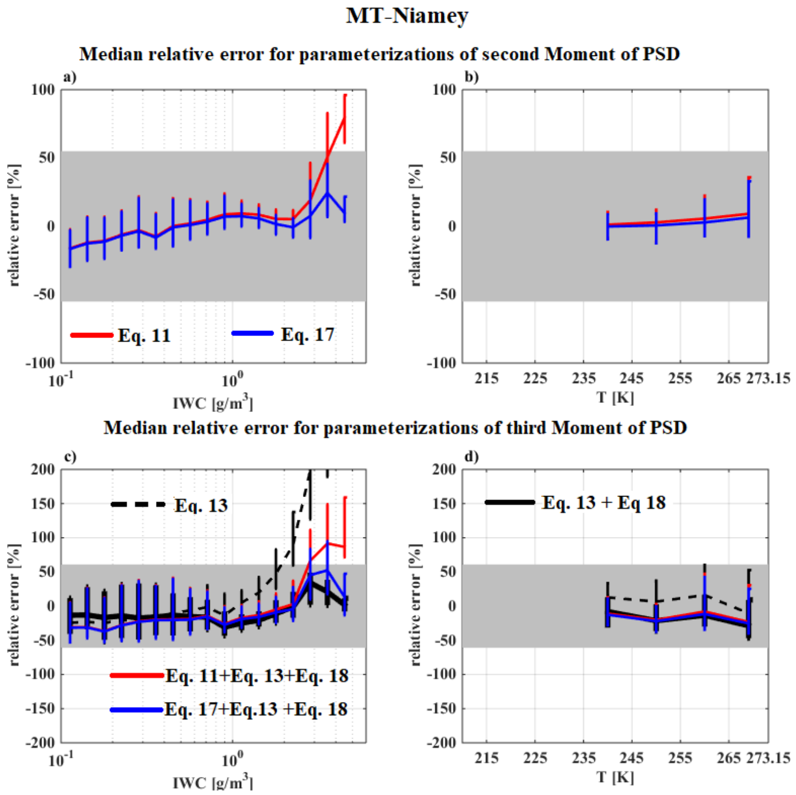

Figure R5: ***Relative error of parametrized M_2 and M_3 for MCS over Niamey as a function of IWC in a) and c), and as a function of T in b) and d). Solid lines give median relative error and whiskers denote 25th and 75th percentiles of relative error. Grey bands shows measurement uncertainties for M_2 (55%; a) and b)) and M_3 (61%; c) and d)), respectively***

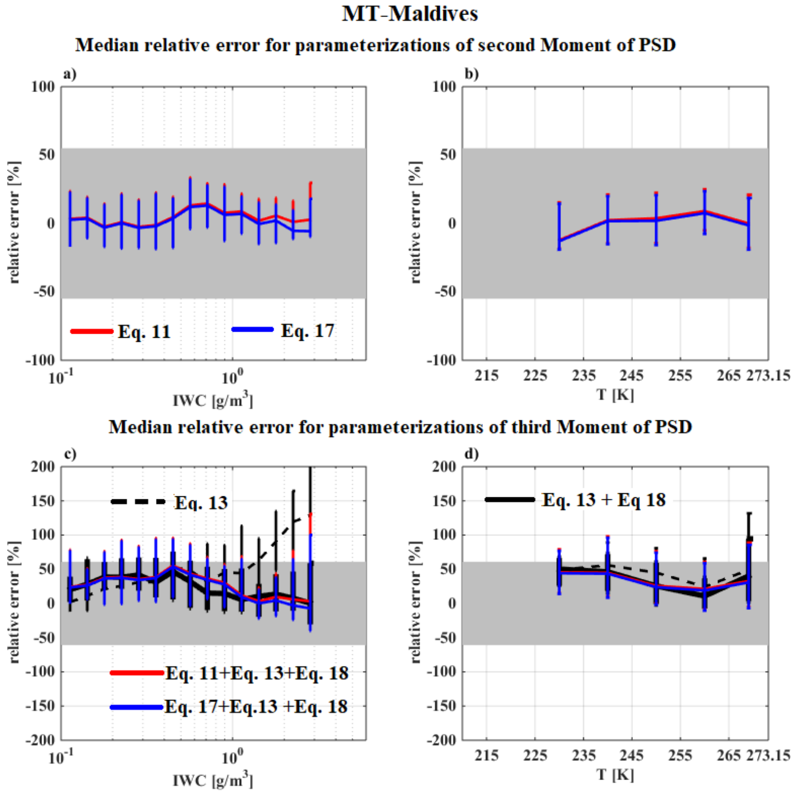

Figure R6: ***Relative error of parametrized M_2 and M_3 for MCS over Maldives as a function of IWC in a) and c), and as a function of T in b) and d). Solid lines give median relative error and whiskers denote 25th and 75th percentiles of relative error. Grey bands shows measurement uncertainties for M_2 (55%; a) and b)) and M_3 (61%; c) and d)), respectively***

page 24, line 20: "extrapolates PSD" - I think you mean measured PSD (I strongly suggest to never extrapolate any PSD!). Please rephrase!

This sentence need more informations (R2#16)

", whilst this study extrapolates PSD until 1.2845cm only (reconstruction of partial images to calculate particle size according to Korolev and Sussman 2000)."

page 25, line 32/33: Is there a difference between zones 1-5 or would it actually suffice to combine them into one reflectivity zone? (related to my main comment on radar reflectivity zones)

It seems that there is no difference in dynamic, they have all low probabilities of vertical movement. Then, low probabilities to be associated with convective zones. That is why we assume they are all more related to the stratiform part of MCS. However, they have different range of IWC, Z, total concentrations, and visible extinction. Moreover, there is no confident measurement of IWC in MCS reflectivity zone 2 and 3. So, we prefer to give our results as they are with the 8 MCS zones. And future investigations could improve our view of the difference in each MCS reflectivity zones.

page 26, lines 14-20: Would it be possible to make a more general point here: Possibly that aggregation process efficiency is higher for convection over land than over islands and higher over islands close to large land masses than over islands in the middle of an ocean? Are there other studies you could relate to? Or is it the convective system size (larger in Niamey...)?

Unfortunately, the impact of the size of MCS has not been investigated yet.
(R2#17)
"*aggregation process efficiency is higher for convection over land than over islands and higher over islands close to large land masses than over islands in the middle of an ocean. It seems to confirm the results of Frey et al., (2011) and Cetrone and Houze (2009).*"

<u>Technical corrections</u>
page 2, line 34: "predictions fails" - predictions fail
page 3, line 18: an 'and' missing: "..., and the cloud radar RASTA..."
page 4, line 14: Should be 4, not 5 airborne campaigns.
page 7, line 11, and page 8 line1: "(Figures 5, 6, 8, 9, 10, 11, 12, 13, 14, 15 and 16)" better (Figures 5, 6, and 8 - 16)
page 8, line 17: "Globally"- do you mean 'generally'?
page 10, line 14: start with lower case 'with' after equation.
page 18, line 15: "different from one MCS type of MCS to another" remove 'of MCS'.
page 26, line 5: "for individual the MCS locations)," remove 'the' and ')'.7

Figures and Tables
Figure 1: This plot is very busy. Maybe it would be easier to read if you split the figure into four subfigures (one for each campaign) with the black lines for the merged data set in each of the subfigures?
We think it is necessary and more interesting to see all the percentiles profiles of the merged dataset and the four campaigns. It allows to compares them to each other's. Also the goal of this figure is to show the limit of the MCS reflectivity zones.

Figure 2: Colours: Generally, it is advised to choose colourblind-friendly colour schemes, and the rainbow scheme is unfortunately not one of those (among other shortcomings of this colour table, see e.g. the open letter to the scientific community here: https://www.climate-lab-book.ac.uk/2014/end-of-the-rainbow/). In subfigure b, I find it hard to distinguish between MCS zone 2 and 3, thus a different colouring would help here, too.
The axis labels (numbers) are too small, please enlarge.
Done, see new figures in the new section 5 and 6, in the answer of the major comment concerning length of section 5.

Figures 5, 6, and 8 - 16:
I don't think it is important to name the campaigns each time, it suffices to mention the locations (also in figure captions and text).
The subfigures are rather small, maybe you could move the legends to the top or bottom of the figure to allow more space for the subfigures?
Done, see new figures in the new section 5 and 6, in the answer of the major comment concerning length of section 5.

Caption line 1/2: Maybe better: ... for the different MCS reflectivity zones using the results from the four locations. (removing the second sentence)
I cannot see to where this comment is related to.

Figure 7: You say IWC in the caption but the figure label say CWC. Same in Figure 17.
Correction done.

Figure 14: The caption says "for M2 per for unity dimension.", the axis annotation says: "M2 [m-1], so not unity dimension. Please clarify.
The true unit is [m^{-1}]. Correction done

Figure 18: See comment about colours above.
A new figure with colourblind-friendly colours is made.

Table 2: The table is extremely hard to read, unfortunately! Maybe it could help to swap the 'with respect to median of' column with a 'radar reflectivity zone' column, and give the parameters in front of the temperature brackets.
Indeed, the table is complex to read. We do not understand the suggestion as there is no column "with respect to median of". However we suggest to shift this table in a last Appendices.

Tables in Appendix: I assume that the decimal point should actually be a point and not a comma - as in all your appendix tables?
Corrections done.

References

Field, P. R., Heymsfield, A. J., and A. Bansemer: Shattering and Particle Interarrival Times Measured by Optical Array Probes in Ice Clouds, Journal of Atmospheric and Oceanic Technology, 23, 1357-1371, 2006

Frey et al.: In situ measurements of tropical cloud properties in the West African Monsoon: upper tropospheric ice clouds, Mesoscale Convective System outflow, and subvisual cirrus, Atmos. Chem. Phys., 11, 5569-5590, 2011

Statistical Analysis of Ice Microphysical Properties in Tropical Mesoscale Convective Systems Derived from Cloud Radar and In-Situ Microphysical Observations

Emmanuel Fontaine[1,6*], Alfons Schwarzenboeck[1], Delphine Leroy[1], Julien Delanoë[2], Alain Protat[3], Fabien Dezitter[4], John Walter Strapp[5], Lyle Edward Lilie[5].

[1]Laboratoire de Météorologie Physique, UCA, CNRS, Aubière, France
[2]Laboratoire Atmosphère, Milieux et Observations Spatiales, UVSQ, Guyancourt, France
[3]Center for Australian Weather and Climate Research, Melbourne, Australia
[4]Airbus Helicopters, Toulouse, France
[5]Met Analytics, Toronto, Canada
[6*]now at Department of Atmospheric Sciences, National Taiwan University, Taipei, Taiwan

Correspondence to: E. Fontaine (emmanuel.r.j.fontaine@gmail.com)

Abstract. This study presents a statistical analysis of the properties of ice hydrometeors in tropical mesoscale convective systems observed during four different aircraft campaigns. Among the instruments on board the aircraft, we focus on the synergy of a 94GHz cloud radar and 2 optical array probes (OAP; measuring hydrometeor sizes from 10µm to about 1cm). For two campaigns, an accurate simultaneous measurement of the ice water content is available, while for the two others, ice water content is retrieved from the synergy of the radar reflectivity measurements and hydrometeor size and morphological retrievals from OAP probes. The statistics of ice hydrometeor properties is calculated as a function of radar reflectivity factor measurement percentiles and temperature. Hence, mesoscale convective systems (MCS) microphysical properties (ice water content, visible extinction, mass-size relationship coefficients, total concentrations and second and third moment of hydrometeors size distribution) are sorted in temperature (thus altitude) zones, and subsequently each individual campaign is analysed with respect to median microphysical properties of the global dataset (merging all 4 campaign datasets). The study demonstrates that ice water content (IWC), visible extinction, total crystal concentration, and second and third moments of hydrometeors size distributions are similar in all 4 type of MCS for IWC larger than 0.1g m^{-3}. Finally, two parameterizations are developed for deep convective systems. The first one concerns the calculation of the visible extinction as a function of temperature and ice water content. The second one concerns the calculation of hydrometeor size distributions as a function of ice water content and temperature that can be used in numerical weather prediction.

1 Introduction

Defining clouds and how they interact with the atmosphere is a major challenge in climate sciences and meteorology. Clouds play an important role in the evolution of the weather and climate on the Earth. They affect the dynamics and the thermodynamics of the troposphere, and impact the radiative transfer of energy in thermal and visible wavelengths by heating or cooling the atmosphere. In addition, clouds represent an important part of the hydrological cycle, due to evaporation and precipitation processes. Inversely, dynamic features such as the Madden Julian oscillation (MJO, perturbation of large scale circulation leading to an eastward propagation of organized convective activity) can also affect the development of deep convective clouds (Madden and Julian, 1994, 1971). Mesoscale Convective Systems (MCS) are complex clouds and are the result of specific synoptic conditions and mesoscale instabilities which lead to the development of cumulonimbus (Houze, 2004). The complexity of MCS is also relying on the dynamical, radiative, and precipitation characteristics which depend on the location in the evolving MCS (Houze, 2004). MCS can last several hours and can affect human societies in different ways. Indeed, MCS are often associated with hazardous weather events such as landslides, flash floods, aircraft incidents, and tornadoes, all which can cause loss of human lives.

Weather and climate models use rather simplified schemes to describe the ice hydrometeors properties. Parametrization disagreements due to larger uncertainties in the representation of ice properties in clouds (Li et al., 2007, 2005) lead to large variations in the quantification of ice cloud effects on climate evolution (Intergovernmental Panel on Climate Change Fourth Assessment Report). An accurate estimation of the spatiotemporal distribution of the Ice Water Content (IWC) is a key parameter for evaluating and improving numerical weather prediction (Stephens et al., 2002). Underlying hydrometeor growth processes in MCS vary in time (growing, maturing, decaying phase) but also in space, in other words horizontally (distance from active convective zone) and vertically (as function of temperature).

A number of studies (Gayet et al., (2012); Lawson et al., (2010) and Stith et al., (2014)), demonstrate the presence of different type of ice hydrometeors in evolving MCS. In the active convective area, super cooled droplets larger than 500µm until 3mm, were observed near -4°C and rimed ice hydrometeors about the same size below -11°C. Also at -47°C ~~large~~ rimed particles about 2-3mm from updraft regions coexisting with ice crystals about 100µm (pristine ice) were encountered. Near the convective zone of MCS (i.e fresh anvil) presence of pristine ice (about 100µm), aggregates of hexagonal plates (about 500µm to 1mm) and capped columns (about 500µm) has been reported (Lawson et al., 2010). In aged anvils, columns (~100µm), plates (~100µm), and small aggregates (about 200µm) are observed near -43°C while large aggregates about 2mm and more are found at lower altitudes (-36°C). Also in the cirrus part of MCS bullet-rosettes about 500µm and less (more common for in situ cirrus (Lawson et al., 2010)) and chain-like aggregates from 100µm to about 1mm are found (aggregates of small rimed droplets caused by electric fields: Gayet et al., 2012; Stith et al., 2014).

Commenté [EF1]: R1#5

With respect to ice particle density, Heymsfield et al., (2010) reported that ice particles seem to be denser near the convective part of MCS formed during the African Monsoon. Other studies have shown a variability of the mass-size relationship with temperature and related altitude (Fontaine et al., 2014; Schmitt and Heymsfield, 2010), which appears to be essentially linked to the variability of ice hydrometeor shapes related to different growth regimes (vapour diffusion, riming, aggregation).

Due to above mentioned spatiotemporal variations of MCS the different mean tendencies (hydrometeor concentration, ice water content, coefficients of mass-size relationship) reported in former studies can be partly linked to the chosen observation strategy of the MCS (i.e flight track in MCS) which of course is related to particular objectives of respective field projects (i.e. improvement of rain rate retrieval from satellite observations, icing condition at high altitude, comparison with ground radar observations, etc…).

Therefore the goal of this study is to investigate on the one hand the vertical variation of ice crystal properties in MCS (for example as a function of temperature) and on the other hand to study horizontal trends of ice microphysics at constant temperature levels. The latter will be accomplished by a composite analyses of microphysical properties and simultaneously measured radar reflectivity factor (*Z*). *Investigations on the impact of vertical velocity has been performed asides, however no significant tendencies were found to allow us to present* *our results as function of vertical velocity.* A frequency distribution of the profiles of the radar reflectivity factor throughout the MCS as a function of temperature allows to divide the microphysical in situ measurements into eight zones. For these height reflectivity zones microphysical properties are analysed and compared between the eight zones, but also intercompared between different locations and associated measurement campaigns where MCS were observed. Direct applications of this study are for example to improve retrievals of cloud properties from radar observations and also parameterization of ice properties in weather and climate models. Moreover, it can help identifying zones in MCS where numerical weather predictions fails in representing ice microphysics.

Commenté [EF2]: R1#1

Our statistical analysis is performed on cloud radar Doppler measurement and in-situ measurement. Cloud radar measurements include more than one million of data points of radar reflectivity factors and retrieved vertical velocities spanning from 170K to 273.15K (Temperature profiles from RASTA are calculating using re-analysis of ECMWF). And in-situ measurements include 55844 data points of 5 s duration in the temperature range from 215K to 273.15K. The following second section describes the utilized datasets and their derived parameters used in this study. *The third section presents the analysis of radar reflectivity factors (Z) which provides the ranges of Z to perform the intercomparison between the four types of MCS. Moreover, for each range of Z a statistical analysis of vertical velocity is presented to bind the vertical dynamic of MCS and ice microphysical properties. The section 4 present the methodology of intercomparison used in this study. And section 5, present the inter-comparison of the microphysical parameters as function of Z and T. The end of this section is dedicated to present shortly the results of the investigations performed about the impact of vertical velocity. The sixth section, provide the parameterization of visible extinction and the parameterization of ice hydrometeors distributions. The last section adds the discussion and conclusion.*

Commenté [EF3]: R1#8

Commenté [EF4]: R1#2

2 Data description

This study uses a data set where MCSs were observed in four different locations in the tropics and related to two different projects:

1. *Megha-Tropiques in Niamey, during July and August 2010: observation of continental MCS formed over the region of Niamey (Niger) during the West African Monsoon (Drigeard et al., 2015; Fontaine et al., 2014; Roca et al., 2015). These MCS developed over the continent. 7665 points of 5 seconds.*
2. *Megha-Tropiques in Maldives, during November and December 2011: observation of oceanic MCS developed over the southern part of the Maldives and related to the ITCZ (Inter Tropical Convergence Zone) in the Indian Ocean. (Fontaine et al., 2014; Martini et al., 2015; Roca et al., 2015). It includes MCS developed during the wet phase of MJO and two event with isolated convective systems developed during the dry phase of MJO. 3347 points of 5 seconds.*
3. *HAIC-HIWC in Darwin, from January to March 2014: observations of MCS formed over Darwin and the North-East cost of Australia during the North Australian Monsoon (Leroy et al., 2016; Protat et al., 2016; Strapp et al. 2016; Leroy et al. 2017, Fontaine et al. 2017). During this campaigns, MCS developed over the land, the ocean, and near the cost. 23265 points of 5 seconds.*
4. *HAIC-HIWC in Cayenne during May 2015: observations of MCS developed over the French Guyana during the peak of its raining season (Yost et al., 2018). Same as for Darwin, MCS developed over the land, the ocean, and near the cost. 21567 points of 5 seconds.*

Note that observations were performed in mature MCS. All four measurement campaigns were conducted with the French research aircraft Falcon-20 operated by SAFIRE (Service des Avions Francais Instrumentés pour la Recherche en Environnement). On board the Falcon 20 were mounted two optical array probes (OAP): the 2D-S (2D stereographic probe; Lawson et al., 2006) and PIP (Precipitation Imaging Probe; Baumgardner et al., 2011), the cloud radar RASTA operating at 94GHz (Protat et al., 2016; Delanoë et al., 2014). In addition, bulk IWC measurements *performed with the isokinetic evaporator probe (hereafter IKP-2 probe;* Strapp et al. 2016; Davison et al. 2010) were available for the HAIC-HIWC flight campaigns (Darwin and Cayenne).

Both OAP probes record black and white images of hydrometeors with a resolution of 10µm and 100µm (2D-S and PIP, respectively). They are used to derived the size of hydrometeors (Dmax [cm] in this study), their projected surface (S [cm2]), their concentrations as a function of their size (N(Dmax) [#/L/µm]). The sizes of hydrometeors span from 10 µm to 1.28 cm with Dmax calculated as a function of the projected surface of hydrometeors (taking the maximum of radius passing through its barycentre; see Figure 1 in Leroy et al., 2016).

During both HAIC-HIWC campaigns, the IKP-2 probe was used to measure total condensed water, composed exclusively of ice water content (IWC [g m-3]) and water vapour, then IWC were deduced using in-situ measurement of relative humidity. However, IWCs< 0.1g m-3 are not considered in this study, due to IKP-2 uncertainties particularly important for low IWC measurements (see Strapp et al. 2016a). For both Megha-Tropiques campaigns, IWC was retrieved using simulations of the reflectivity factor Z, thereby using the approximation of ice oblate spheroids (Fontaine et al., 2017; Fontaine et al., 2014). Results about accuracy of IWC retrieved from this method with regards to IKP-2 measurement are discussed in Fontaine et al., (2017).

The 94GHz RASTA radar measures Z and Doppler velocity Vd below and above the aircraft. RASTA has 6 antennas that allow measuring three non-collinear Doppler velocities, from which the 3 wind components (including the vertical air velocity) have been reconstructed (using the Protat and Zawadzki 1999 3D wind retrieval technique modified for the aircraft geometry).

Detailed description of data processing is documented in Leroy et al. (2016 and 2017), Protat et al. (2016), Strapp et al. (2016b), and Davison et al. (2016). These references give a processing description for both datasets of the HAIC-HIWC project. But, Megha-Tropiques datasets (Fontaine et al. (2014)) were reprocessed in order to undergo exactly the same version of processing tools for comparison reasons in this study.

Moreover, investigations have been performed to detect supercooled water using Rosemount icing detector (Baumgardner and Rodi 1989; Claffey et al. 1995; Cober et al. 2001) and Cloud Droplet Probe measurement. Few cases of super cooled water were detected and remove from the dataset (Leroy et al., 2016). Hence, the dataset used in this study is using exclusively data collected where only ice particles were measured. Also, retrieval of IWC for the Megha-Tropiques project were not performed in mixed phase conditions (more details in Fontaine et al., (2014) and (2017)).

3 Radar observations

3.1 Radar reflectivity factors

In this section distributions of radar reflectivity factors Z from nadir and zenith profiles are investigated for the 4 datasets. Figure 1 shows percentiles of Z as a function of T measured with RASTA during the 4 airborne

Commenté [EF5]: R2#1

Commenté [EF6]: R2#8

Commenté [EF7]: R1#6

Commenté [EF8]: R1#5

Commenté [EF9]: R1#7

Commenté [EF10]: R2#9

Commenté [EF11]: R1#9

Commenté [EF12]: R1#11

campaigns. The lines are colour coded as a function of the calculated percentiles (blue =1th, light blue = 10th, cyan =30th, green=50th, yellow=70th, orange=90th, and red=99th percentile). *The percentiles of Z are calculated for a merged dataset that include 11 flights for MT over Niamey, 11 flights for MT over Maldives, 19 flights for HAIC-HIWC over Darwin and 17 flights for HAIC-HIWC over Cayenne. Percentiles are not calculated as function of the number of profiles but by temperature ranges of 5K where only points with Z larger than -30dBZ are taken into account. Figure 1 shows that distributions of Z are not totally similar for all 4 airborne campaigns. MCS can expend over hundreds or thousands square kilometres, where size and repartition of their convective and stratiform areas can vary from one MCS to another. So the same sampling strategy in two different MCS would provide two different mean or median profiles of ice microphysics properties as function of T. But two different sampling strategy in the same MCS would have the same results. The idea of this study is to compare the properties of ice hydrometeors for different tropical MCS locations, thereby rendering comparable different MCS systems (as a function of temperature), through the analysis of the frequency distribution of profiles of Z dividing all MCS into eight zones. This strategy aims to reduce the impact of the different flight patterns and objectives for sampling MCS during each airborne campaigns used in this study.*

Commenté [EF13]: R2#10

Note that Z at 94 GHz is linked to the ice water content (Fontaine et al., 2014; Protat et al., 2016), but also to the size distribution of ice hydrometeors, respective crystal sizes, and mean diameter (Delanoë et al., 2014).

Our motivation to choose the limits of Z ranges on what the statistic of ice hydrometeors properties holds in two facts. First, Figure 1 shows that the variability of Z at a given T is large and this variability of Z vary along the altitude. We can observe in Figure 1 that Z extend from about -20dBZ to 18 dBZ at 260K while it spread out from -10dBZ to 10 dBZ at 200K. So, this has to be considered if we want to sort our dataset as function of T and Z. So the limit of the Z range cannot be the same for each altitude has meeting ice hydrometeors linked to 15 dBZ or linked to -20dBZ at 200K is quiet impossible. The second fact holds on result on a former study. Indeed, Cetrone and Houze, (2009) used the profiling radar of TRMM satellite ((Tropical Rainfall Measuring Mission; Huffman et al., 2007) to demonstrate with frequency distributions of radar reflectivity Z as a function of height that higher Z occur more often in convective echoes of MCS (in West African Monsoon, Maritime Continent and Bay of Bengal) than in their stratiform echoes. This former study was performed with the 13GHz radar profiler on board TRMM satellite, which is more sensitive to the precipitating particles (large drops and large ice crystals). The radar used in our study is more sensitive to smaller size of hydrometeors, then it is more adapted to sort the properties of ice crystals presented in our study. Hence, this study presents ice microphysical properties in MCS as a function of temperature layers and also as a function of zones of reflectivity Z. In order to fix the limits of a limited number of Z levels, this study takes the percentiles of all merged campaigns datasets shown by the solid lines (all data) in Figure 1. This defines Z ranges as a function of height. Hereafter, these ranges will be called MCS reflectivity zones and numbered 1 to 8:

- *MCS reflectivity zone 1:* $Z < Z^{1th}$
- *MCS reflectivity zone 2 :* $Z \in [Z(T)^{1th}; Z(T)^{10th}[$
- *MCS reflectivity zone 3 :* $Z \in [Z(T)^{10th}; Z(T)^{30th}[$
- *MCS reflectivity zone 4 :* $Z \in [Z(T)^{30th}; Z(T)^{50th}[$
- *MCS reflectivity zone 5 :* $Z \in [Z(T)^{50th}; Z(T)^{70th}[$
- *MCS reflectivity zone 6 :* $Z \in [Z(T)^{70th}; Z(T)^{90th}[$

- *MCS reflectivity zone 7 :* $Z \in [Z(T)^{90th}\,; Z(T)^{99th}[$
- *MCS reflectivity zone 8 :* $Z \geq Z(T)^{99th}$

Commenté [EF14]: R2#2

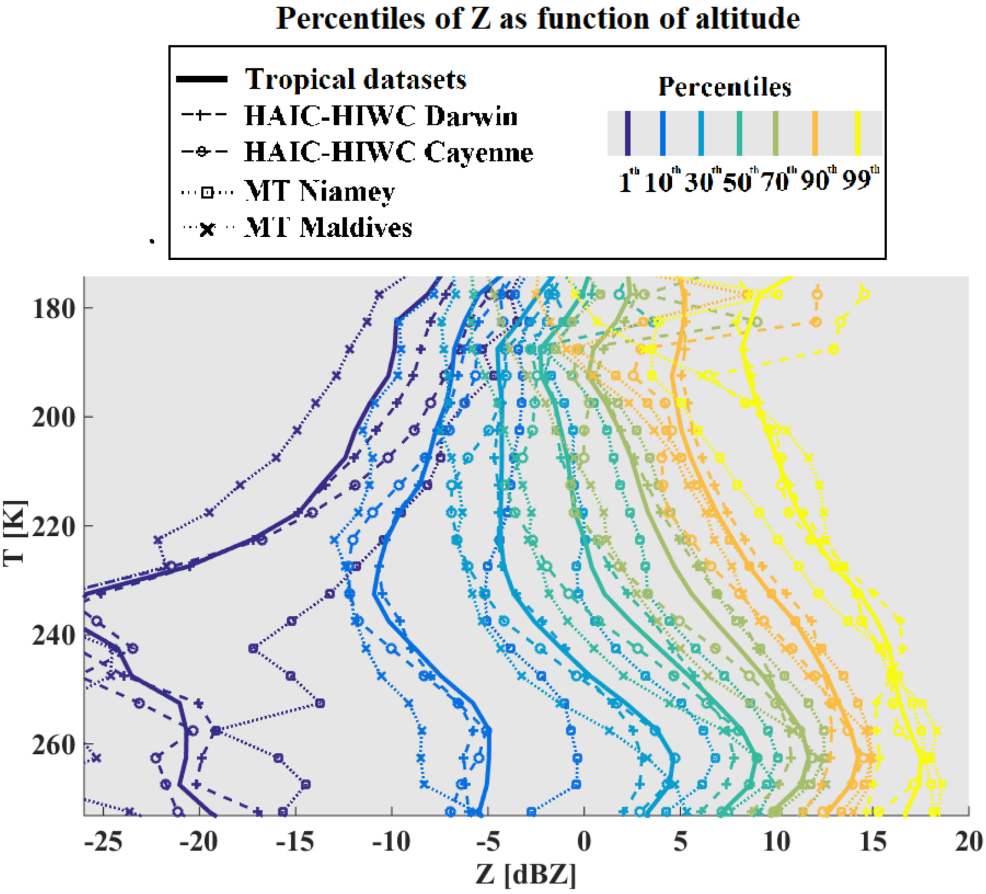

Figure 2: Median reflectivity factor *Z* and percentiles of radar reflectivity factors in dBZ on *x*-axis, as a function of temperature on *y*-axis.

Figure 2 shows an example of the method to store data as a function of T and MCS reflectivity zones. In Figure 2(a), we can see original processed *Z* profiles for the flight 13 of HAIC-HIWC of the Darwin experiment. In Figure 2(b), eight colours representing the above defined MCS reflectivity zones. This method is applied for all datasets thereby using all radar reflectivity profiles (*Z* from Nadir and Zenith direction).

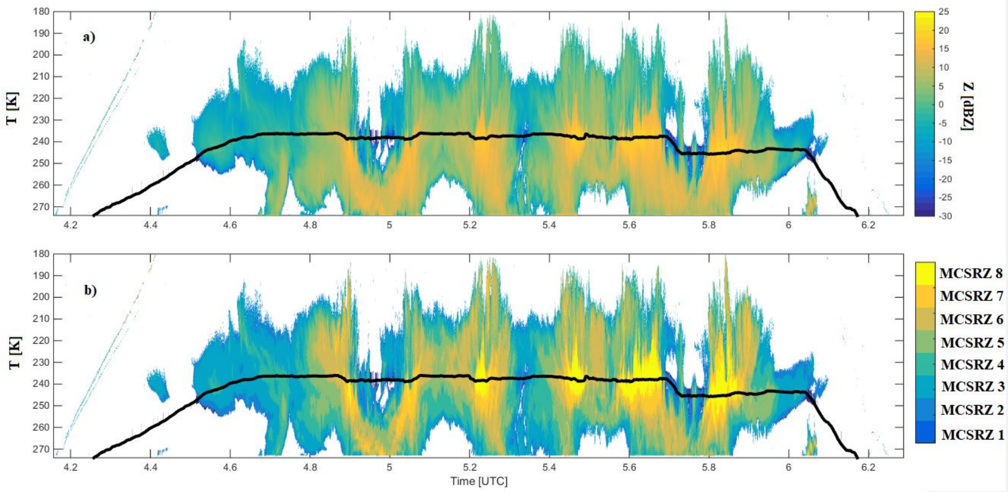

Figure 3: a) Time series of cloud radar profiles of flight 13 of HAI-HIWC at Darwin. Z color coded in dBZ and plotted as a function of the temperature (y-axis). b) Similar to a) with Z classified according to altitude dependent Z percentile ranges.

3.2 Retrieved vertical velocity in MCS reflectivity zones

This section investigates links between retrieved vertical velocity and MCS reflectivity zones. We assume that Vz (V_d) = w_{ret} + Vt, where Vt is the terminal velocity of hydrometeors (Delanoë et al., 2007, 2014) and w_{ret} the vertical wind speed. In a first order, our study investigates variability of bulk microphysical properties of the icy part of MCS as function of temperature range and Z range (i.e. MCS reflectivity zones). As no clear tendencies have been found as function of vertical velocities, we decide to investigate the probability to observe significant vertical movement in each range of Z (or MCS reflectivity zones). In other words, we investigate if there is any relationship between MCS reflectivity zones and vertical dynamic of MCS. We assume that convective part of MCS are associated with pronounced updraft and downdraft and that stratiform part of MCS have non-pronounced vertical velocity (w≈0m.s-1) (see Figure 16 from Houze 2004).

Figure 3 shows median updraft ($w_{ret}>0$) and downdraft ($w_{ret}<0$) in each MCS reflectivity zones (MCSRZ 2 to MCSRZ 8 from the top line to the bottom line respectively) and for each airborne campaign (Cayenne, Darwin, Maldives Island and Niamey, from left column to right column respectively). Black lines represent median updraft and downdraft for each respective airborne campaigns, while grey lines are median (solid line), 25th and 75th percentiles (dashed lines) and 10th and 90th percentiles (dotted lines) for the merged dataset. Black lines and grey lines are calculated using RASTA vertical profiles. The red stars are median downdraft and updraft when we use only vertical velocity measured by the aircraft (w; in-situ measurement).

We can observe a symmetry between updraft and downdraft in all MCS reflectivity zones for each campaigns, meaning that at a given altitude, absolute magnitude of downdraft is about the magnitude of updraft for median, 25th, 75th,10th and 90th calculated percentiles. For RASTA measurement, we can see that median updraft ($w_{ret}>0m.s^{-1}$) and median downdraft ($w_{ret}<0m.s^{-1}$) for each airborne campaigns agree well with median updraft and downdraft *for the merged dataset in all MCS reflectivity zones. Except for Maldives observations where median w_{ret} are smaller for T < 255K. Also, median in-situ w tend to be a bit smaller than median w_{ret}, except for updraft in Maldives above the bright band; $w \approx 2.5 m.s^{-1}$ versus wret $\approx 1 m.s^{-1}$.*

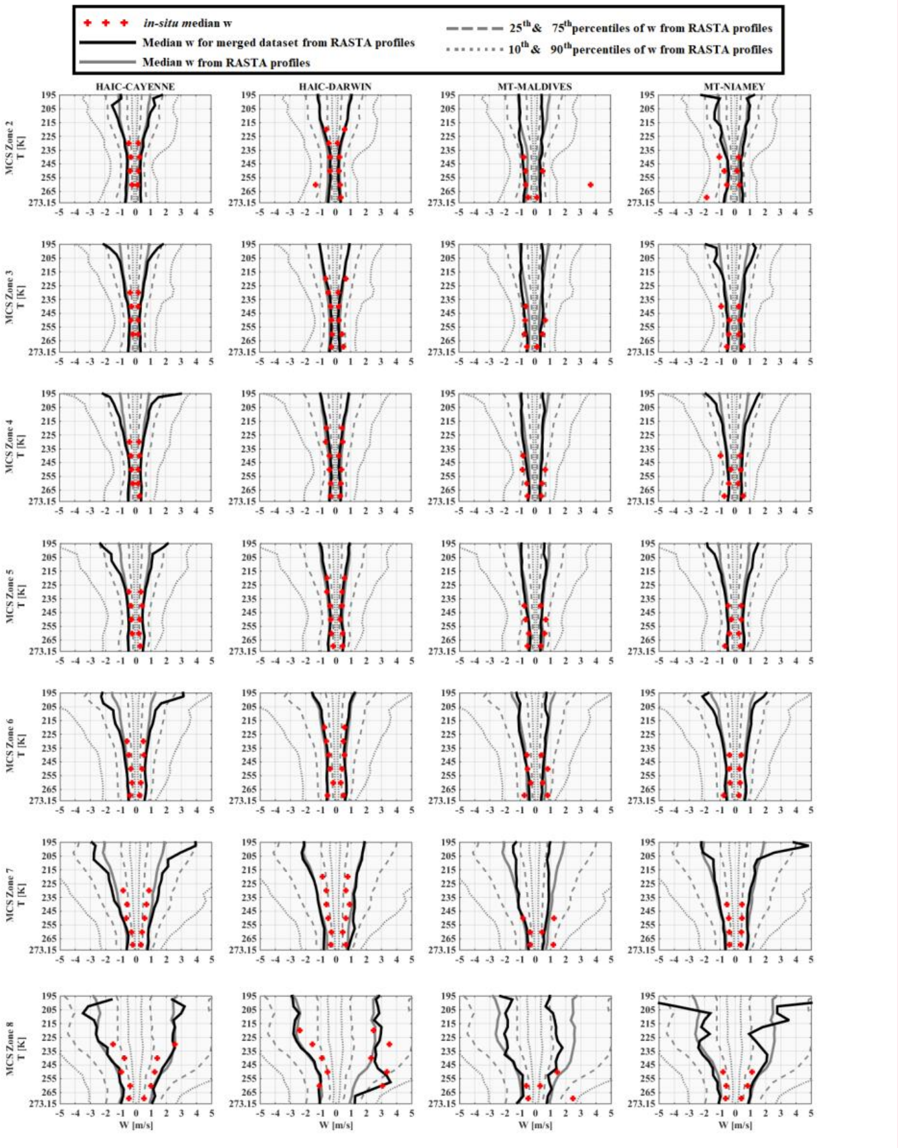

Figure 3: from the top line to the bottom line vertical velocities for MCS reflectivity zone 2 to MCS reflectivity zone 8.

In general the updraft and downdraft wind speeds increase with altitude and MCS reflectivity zones, where magnitudes of vertical velocity (negative and positive) are highest for MCS reflectivity zones 8. For all 4 datasets vertical wind speeds of MCS reflectivity zones 2-6 are smaller than 1m.s^{-1}.

To complete our study on vertical dynamic that could exist in each MCS reflectivity zones, we study the probability to observe vertical movement. We use a threshold for vertical velocity to distinguish between discernible vertical movement and nearly not.

We take roughly a value of 1m/s to be the threshold to detect vertical movement, such -1m/s < w < 1m/s there is no noticeable vertical movement neither upward nor downward. The decision of taking a threshold of 1m/s for updraft and downdraft, is motivated by the fact that we have to take into account the measurement uncertainty (less than 0.25-0.5m.s-1). Moreover, knowing that variance of vertical turbulences are about 1.5 m^2/s^2 (Large Eddy Simulations at 50 m resolution; personal communication with Dr. R. Didier). The fact that median wret for the merged dataset in MCS reflectivity zones 2 to 6 are smaller than 1m.s-1 consolidate our decision to take a threshold of 1m.s^{-1}.

Then, knowing T and Z, a probability to observe $| w_{ret} | \geq 1m\ s^{-1}$ is calculated as a function of MCS reflectivity zones and temperature. Colored solid lines in Figure 4 are probabilities calculated from RASTA measurement and dashed lines with stars are probabilities calculated with vertical velocity measured at the aircraft level (in-situ measurement). Both type of probabilities are different in each MCS zones and probabilities made with in-situ measurement are smaller than these calculated with RASTA retrievals; except in MCS reflectivity zones 8 in Darwin where they are similar. Hence, we know from the point of view of vertical velocity that the in-situ dataset is not representative to the observations from RASTA retrievals: different probability to observe vertical velocity with magnitude larger than 1m/s (updraft and downdraft).

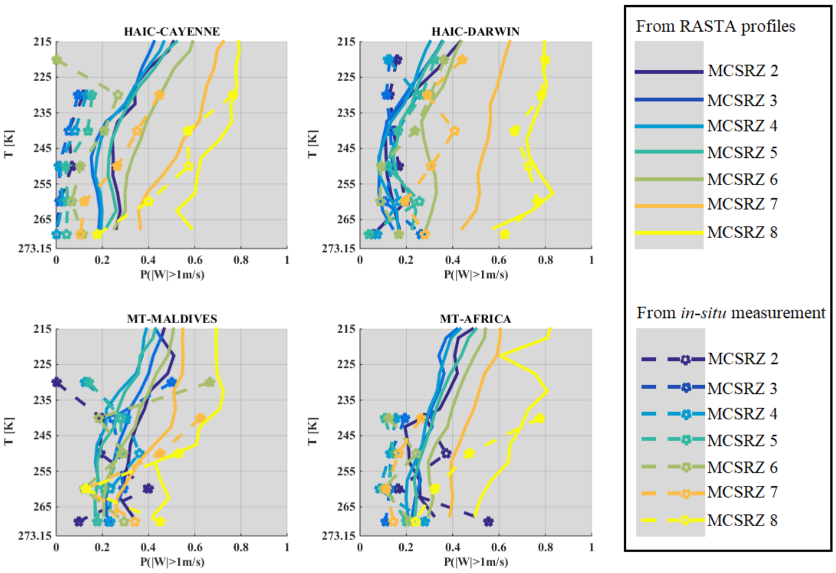

Figure 4: Probability to observe vertical velocity with absolute magnitude larger than 1m/s in each MCS reflectivity zone (MCSRZ; color scale) for measurement from the radar Doppler RASTA in solid lines and in dashed lines with stars marker for in-situ measurement.

In Figure 4 we show that probabilities to observe $| w_{ret} | \geq 1m\ s^{-1}$ are highest for MCS reflectivity zones 8 then 7 and 6, meaning that these MCS reflectivity zones tend to be more impacted by vertical movement (convective areas of MCS), than it is the case for other MCS reflectivity zones. Also, these probabilities generally increase with altitude for all airborne campaigns. Which meet the conclusions from Figure 3. Generally, in MCS reflectivity zones 5, 4, 3, and 2, the probabilities $P(|w_{ret} \geq 1|)$ as a function of T are close to each other with a decreasing trend as reflectivity decreases, except for the Maldives campaign. Statistically, MCS reflectivity zones 8 and 7 represent for all 4 datasets the most convective part of observed MCS and the lower reflectivity zones the stratiform part with significantly lower vertical wind speeds.

As a conclusion, at a constant altitude largest Z tend to be related with largest probabilities to observe vertical movement (downward or upward). In other words, MCS reflectivity zones 7 and 8 are good candidates to represent observations in the convective area of MCS or closer to the most convective part of MCS.

Commenté [EF15]: R1#3

4 Method of intercomparison

This study compares and discusses a series of ice cloud properties, such as IWC, visible extinction, α and β coefficients of the dynamically retrieved m(D) power law, large crystal proxy of PSDs, crystal number concentrations N, PSD 2nd and 3rd moments (M_2 and M_3, respectively), and the ratio of IWC/M_2. The above mentioned ice hydrometeor properties in all 4 MCS locations will be investigated as a function of T and MCS reflectivity zones (range of Z given by percentiles of Z as a function of T) which have been introduced in section 3. In the subsequent section 5 a series of figures presenting results for above mentioned ice cloud properties (parameter X) will be presented in a uniform format. In all these Figures (5, 7, 9, 11, 13, 15, 17, 21, 23, 25) we show the median values of *X*, averaging MCS data from the 4 merged dataset (with 25th and 75th percentiles represented by whiskers), as a function of T and MCS reflectivity zones. The grey band shows 25th and 75th percentiles of the parameter for the entire merged dataset thereby merging data from all MCS reflectivity zones. 25th, median, and 75th percentiles of all parameters presented in the figures for the merged dataset are given in Annexe C, in order to allow comparison with other datasets and evaluation of numerical weather prediction models. If the range of variability of this median of parameter *X* in MCS reflectivity zone ***i*** defined by its 25th and 75th percentiles, does not overlap with corresponding ranges of variability of *X* defined by the 25th and 75th percentiles of MCS reflectivity zones ***i***-1 and ***i***+1, respectively, this makes the median (4 tropical campaigns) of *X* a candidate for *X* parametrization as a function of MCS reflectivity zone and T.

Then, in all these Figures (6, 8, 10, 12, 14, 16, 18, 22, 24, 26) we calculate the median relative difference in percent (hereafter MRD-*X*) for all 4 individual MCS datasets (Cayenne (a), Darwin (b) , Maldives (c), and Niamey (d)) with respect to the median of *X* as a function of MCS reflectivity zone and *T*.

In order to take into account the uncertainties in all type of measurements, uncertainties (hereafter noted U(X)/X) represented by grey bands on Figure showing MRD-X) for each parameter X were taken from Baumgardner et al. (2017). When the MRD-*X* is larger than *U(X)/X*, this means that there is a significant difference between the median of the studied parameter for the tropical dataset and the respective *X* of the selected individual MCS dataset. For the case that MRD-*X* is smaller than or equal to *U(X)/X*, the median of *X* of the tropical dataset, under the condition that the median (4 tropical campaigns) of *X* is distinguishable between neighboring MCS reflectivity zones, can be utilized for the respective type of MCS. Hence, if the latter case is true for all 4 MCS locations, then the median (4 tropical campaigns) of *X* is suitable to represent all 4 types (=location) of observed MCS.

Commenté [EF16]: R2#11

Note that in all figures discussed in this section, the temperature of in-situ observations will be on the y axis and the color coded MCS reflectivity zones correspond to RASTA reflectivity statistics as a function of temperature. Measured/calculated parameters *X* are sorted into MCS reflectivity zones according to Z derived at flight level simultaneously to measured/calculated *X* parameter.

The comparison of ice hydrometeors' properties of the 4 MCS locations investigated in this study, will mainly focus on the question, if MRD-*X* (for individual MCS reflectivity zones) is larger or smaller than *U(X)/X*, also depending on MCS locations.

For each parameters presented in this study, either for the merged dataset or the campaigns individually (for calculation of MRD-X), the calculation are performed with the same conditions. The samples in each conditions (T bins and Z bins; Z bins vary as function of altitude, i.e. MCS reflectivity zones) have the same size for all parameters. Indeed, data points are selected if they meet the temperature and radar reflectivity criteria, but also the total concentration has to be positive (for Dmax >50µm); mixed phased conditions being excluded. So, the size of the samples (i.e. number of data points in each ranges of T and of Z) for NT, NT_{50}, NT_{500}, IWC, visible extinction, mass-size relationship coefficient, and max(D_{max}) are equal.

Commenté [EF17]: R1#14

Note that median X are calculated for a range of 10 K (except for the range [265K; 276.15K]), as MRD-X. However, for a temperature range and a MCS reflectivity zones MRD-X is deduced from a set of points that does not have the same in-situ temperature. So, relative difference are calculated using interpolated median of X as function of T (dashed colored lines in Figures 5, 7, 9, 11, 13, 15, 17, 21, 23, 25) for each MCS reflectivity zones. Then, MRD-X is deduced from this set of relative differences.

5 In-situ Observations in tropical MCS: HAIC-HIWC and Megha-Tropiques projects

Commenté [EF18]: R2#4

5.1 Ice water content

This section discuss about IWC measured during HAIC-HIWC project and the IWC retrieved for the Megha-Tropiques project. IWC from the four dataset were merged to calculate the main statistic (merged dataset). Figure 5 shows median IWC for the merged dataset as a function of T and as function of MCS reflectivity zones (colored lines). Solely, the graphical representation is limited to medians of IWC for MCS reflectivity zones 4 to 8. Indeed, IWC in MCS reflectivity zones 2 and 3 are linked to IWC smaller than 0.1 g m^{-3}, where IWC data are subject to less confidence. Globally, 30% of the data observed in 4 tropical MCS have an IWC lower than 0.1g m^{-3}, and the lower limit of MCS reflectivity zone 4 is defined with the 30th percentiles of Z. The figure reveals an IWC increases with increasing MCS reflectivity zone for a given range of temperature. IWC median values differ clearly as a function of the MCS reflectivity zone, and this for the entire range of temperatures, with only a few exceptions above the freezing level (T $\in$ [265 K; 273 K[), between MCS reflectivity zones 4 and 5, and MCS reflectivity zones 7 and 8, respectively, with small overlap in IWC ranges. In MCS reflectivity zones 4 to 7, median IWC increase with increasing T between 215 K and 260 K (where IWC has its maximum) and then slightly decrease as T further increases towards 273K. In MCS reflectivity zone 8 IWC behaves rather similar with a maximum IWC already reached at 250 K.

Commenté [EF19]: R1#10

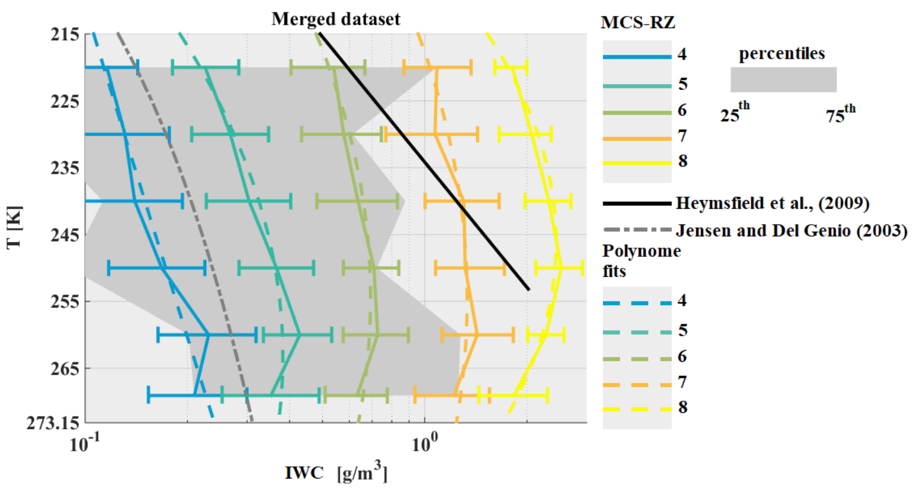

***Figure 5:** Median of IWC in [g/m^3] on x-axis, as a function of temperature in [K] on y-axis for different MCS reflectivity zones. Results for the merged dataset including both MT and both HAIC-HIWC datasets. The grey band represents 25th and 75th percentiles of merged dataset. Extremity of error bar show 25th and 75th percentiles of IWC in each MCS-RZ.*

Figure 6 shows MRD-IWC for the four different campaigns. It is necessary that we recall that median IWC as function of T and MCS reflectivity zones are calculated using a merged dataset where there are IWC from direct measurement and retrieved IWC from Z and PSD (Fontaine et al., 2017). Then, there is two different uncertainties *to consider to evaluate the MRD-IWC in each campaigns. Firstly, for Darwin and Cayenne campaigns the IWC were measured with IKP-2 probe (direct measurement) with an uncertainty on measured IWC increasing with temperature (~5% at 220K and ~20% at 273.15 K; Strapp et al., 2016). Secondly, for Niamey and Maldives IWC were retrieved using the method described by Fontaine et al., (2017) (indirect measurement) with an uncertainty with regards to the IKP estimated by about ±32%. Hence, in Figure 6-a) and Figure 6-b) the grey band area show the uncertainty of the IKP-2 probe that was used for Cayenne and Darwin campaigns. While in Figure 6-c) and Figure 6-d) the grey band area describe the uncertainty on the retrieval method for IWC that was used for datasets of Niamey and Maldives.*

Note that confidence in direct bulk IWC measurements from the IKP-2 is significantly higher than in indirect IWC calculations from the retrieval method (Fontaine et al., 2017).

Commenté [EF20]: R1#12

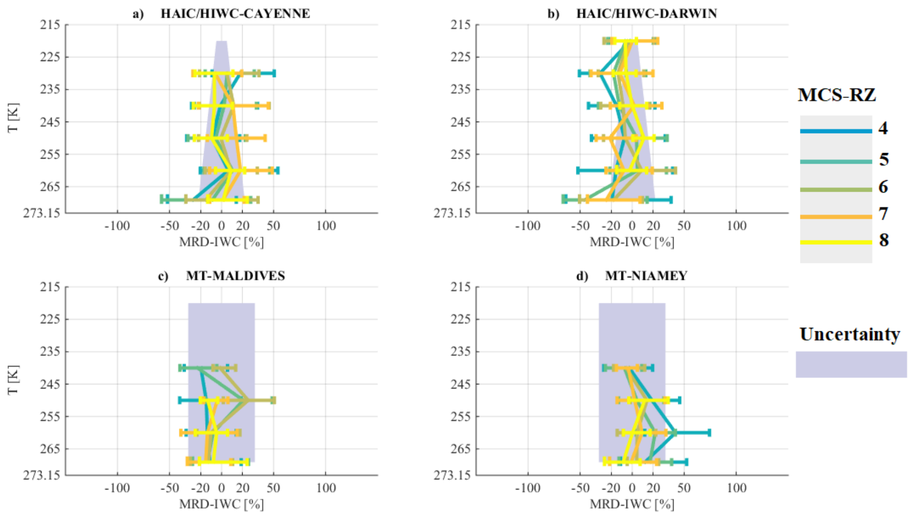

Figure 6: Median relative difference (MRD) of IWC during a) HAIC-HIWC in Cayenne, b) HAIC-HIWC in Darwin, c) Megha-Tropiques Maldives Islands and d) Megha-Tropiques in Niamey, with respect to median of IWC for the Tropical dataset on x-axis as a function of temperature in [K] on y-axis. The grey bands represent the uncertainties of the IWC measurement in b) and c), and the median deviation between measurement and the IWC retrieval method (Fontaine et al. 2016) in d) and e). Lines are colored as a function of the MCS reflectivity zones where in-situ measurement were performed, dashed colored lines are corresponding to the polynomial fit. Extremity of error bar show 25th and 75th percentiles of IWC relative error in each MCS reflectivity zone.

In addition, Figure 6(a), (b), (c), and (d) show MRD-IWC for all MCS reflectivity zones as a function of T. For all 4 tropical MCS, MRD-IWC in MCS reflectivity zones 4 to 8 are distributed around 0 and are in general less than 30-40% (25th to 75th percentiles). Measured IWC in MCS reflectivity zone 8 are in particular good agreement with the median IWC for all 4 tropical datasets, except maybe for high altitude MT-Niamey data. Uncertainty U(IWC)/IWC for IKP-2 measurements (Darwin and Cayenne) especially at high altitude (about 5%) is smaller than the expected deviation MRD-IWC. For mid and lower altitudes, MRD-IWC for Darwin and Cayenne particularly for zones 5 and 8 are of the order of corresponding U(IWC)/IWC. Concerning, MCS over Niamey and the Maldives Island, MRD-IWC (25th to 75th percentiles) in general do not exceed corresponding U(IWC)/IWC.

For comparison purposes with former studies, two IWC-T relationships from literature are added in Figure 5(a). Jensen and Del Genio (2003) suggested an IWC-T relationship in order to account for the limited sensitivity of the precipitation radar aboard the TRMM satellite, not allowing for small ice crystals at the top of convective clouds' anvils to be observed. They used radar reflectivity factors of a 35GHz radar based on Manus Island (North-East of Australia; 2.058°S, 147.425°E), thereby calculating IWC from an IWC-Z relationship (IWC=0.5(0.5.$Z^{0.36}$); Jensen et al., 2002). The resulting IWC-T relationship given by Jensen and Del Genio (2003) is reported by a dashed-dotted grey line, which fits between 75th percentiles of merged median IWC of MCS reflectivity zone 4 and 25th percentile of MCS reflectivity zones 5. We recall that IWC, as a function of T, in MCS reflectivity zones 4 and 5 are related to Z between 30th-50th and 50th-70th percentiles, respectively. We may notice that the IWC-T relationship from Jensen and Del Genio (2003) is different and smaller than the median IWC (4 tropical campaigns). Hence, IWC-T relationship from Jensen and Del Genio (2003) is more adapted to stratiform part of MCS where convective movement occurs less often.*

Moreover, Heymsfield et al., (2009) established an IWC-T relationship based on 7 fields campaigns (black line in Figure 5. They focused their study on maritime updrafts in tropical atmosphere for a temperature range T $\in$ [213.15K; 253.15K]. Their suggested IWC tend to be in the range of IWC of MCS reflectivity zones 6-8 with IWC increasing with T. We already showed in section 3.2 that MCS reflectivity zones 7 and 8 have higher probabilities to be convective (updraft regions with higher magnitudes of vertical velocity), as compared to other MCS reflectivity zones. Therefore, Heymsfield et al., (2009) IWC parametrizations for maritime updrafts are not inconsistent with data from this study.

Overall, this section demonstrates that variation of IWC with the temperature is similar in all type of MCSs for corresponding ranges of radar reflectivity factors. Hence, we assume that IWC-Z-T relationships developed in Protat et al., (2016) is usable for all types of MCS in the Tropics, at least for IWC larger than 0.1g m^{-3}.

5.2 Visible extinction

Figure 7 shows visible extinction coefficients (σ) calculated from OAP 2D images (approximation of large particles; Van de Hulst, 1981):

$$\sigma = 2 \cdot \sum_{15\mu m}^{12845\mu m} N(D_{max}) \cdot S(D_{max}) \cdot \Delta D_{max} \qquad [m^{-1}] \tag{1}$$

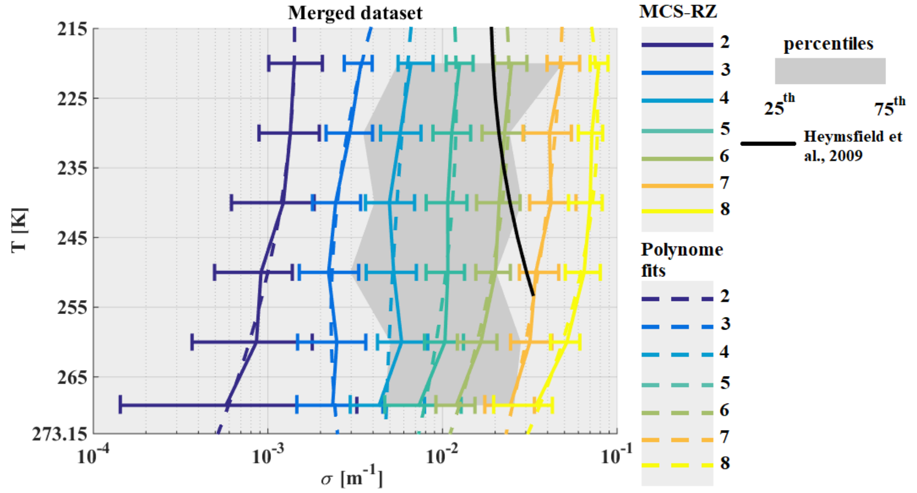

Figure 7: Same as Figure 5 but for visible extinction σ given on x-axis in m⁻¹.

In Figure 7, median σ (4 tropical campaigns) increase with MCS reflectivity zone as expected, and also increase with altitude (decrease with T), with larger gradients for T ∈ [245; 273.15] than for T ∈ [215K; 245K].

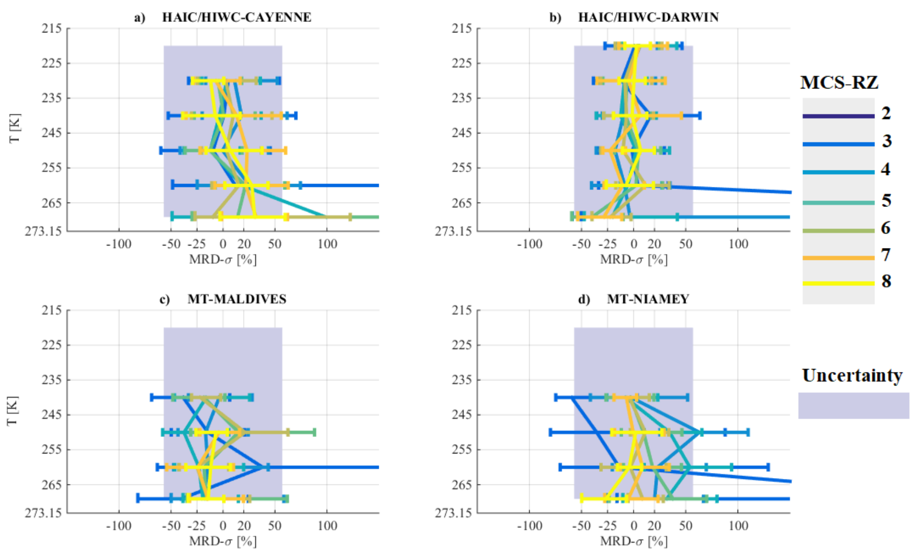

Figure 8: Same as Figure 6 but for visible extinction MRD-σ.

The uncertainty (U(σ)/σ) (grey band in Figure 8(a) to Figure 8(d) is calculated as follows:

$$\frac{U(\sigma)}{\sigma} = \sqrt{2 \cdot \frac{U(D)}{D}^2 + \frac{U(N)}{N}^2}$$
$$= \pm 57\% \qquad (2)$$

With $\frac{U(D)}{D} = \pm 20\%$*, taking into account the uncertainty in the calculation of the size of hydrometeors and* $\frac{U(N)}{N} = \pm 50\%$ *for the uncertainty on the calculation of the concentration of hydrometeors from optical array probes (Baumgardner et al., 2017). Above uncertainties are those for particles larger than 100 µm. Note, that if we took uncertainties for particles smaller than 100µm (with (U(D))/D=±50% and (U(N))/N=±100%) the uncertainty on the calculation of σ would increase to ± 122%. The reason why we do not take into account uncertainty of smaller particle is due to that these particles contribute little to the visible extinction (2% in the range [235K; 273.15] and 10% in the range [215K; 225K].*

Commenté [EF21]: R1#13

For all 4 types of tropical MCS, MRD-σ shown in Figure 8(a), 8(b), 8(c), and Figure 8(d) are in general smaller or equal to $\pm\frac{U(\sigma)}{\sigma}$*. Hence, visible extinction in tropical MCS tend to be similar for all types of MCS observed in the same range of T and MCS reflectivity zone. Also MRD-σ trends are very comparable to above discussed MRD-IWC trends.*

Furthermore, a σ–T relationship from Heymsfield et al. (2009) (black line) is added in Figure 7, which is calculated, as a function of T, as the sum of the total area of particles larger than 50µm plus the total area of particles smaller than 50µm multiplied with a factor of 2 in order to satisfy Eq. (1) and to compare with results of this study. We conclude that σ–T estimation presented in Heymsfield et al. (2009) for maritime convective clouds is rather comparable to median σ calculations (merged dataset) in MCS reflectivity zones 6 to 7 corresponding to higher reflectivity zones, and thus statistically to zones with some remaining convective strength.

5.3 Concentration of ice hydrometeors

Subsequently are presented observed total concentrations for the merged datasets integrating particle sizes beyond 55µm ($N_T(D_{max} > 55\mu m)$*; hereafter* $N_{T,55}$*):*

$$N_T(D_{max} > 50\mu m) = \sum_{Dmax=55}^{Dmax=12845} N(D_{max}) \cdot \Delta D_{max} \qquad [L^{-1}] \qquad (3)$$

Median of $N_{T,55}$ *as a function of T and MCS reflectivity zones are shown in Figure 9 as well as MRD-*$N_{T,55}$ *for the 4 tropical MCS locations in Figure 10 (a), 10(b), 10(c), and 10(d). We observe an increase of median* $N_{T,55}$ *with altitude for all MCS reflectivity zones. Also* $N_{T,55}$ *increases with MCS reflectivity zones for a given T, with highest* $N_{T,55}$ *in MCS reflectivity zone 8. The range of variability for* $N_{T,55}$ *reveals significant overlap of 25*th *and 75*th *percentiles of neighboring MCS reflectivity zones.*

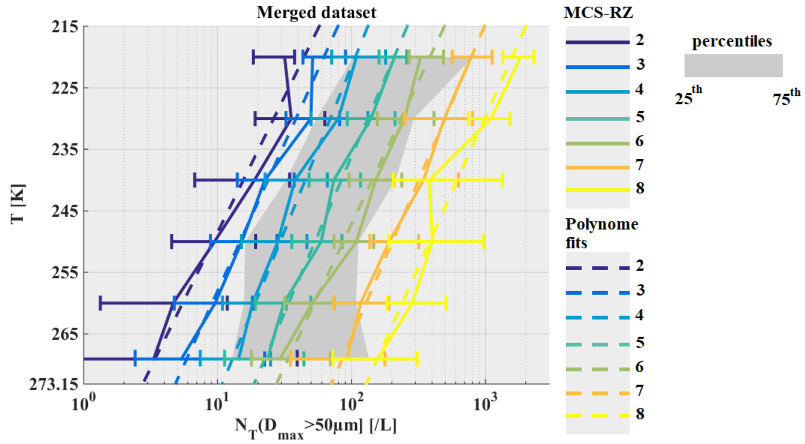

Figure 9: Same as Figure 5, but for total concentrations integrated beyond D_{max}=55µm in [L^{-1}].

Figure 10 show MRD-NT_{55} where measurement uncertainty on concentrations are assumed ±100% (Baumgardner et al., 2017). MRD- $N_{T,55}$ in 4 different tropical MCS locations, particularly for higher MCS reflectivity zones are of the order and even larger (75th percentile MRD-$N_{T,55}$) than the measurement uncertainty. Even if the limit of concentrations of ice hydrometeors are not well defined between neighboring MCS reflectivity zones (Figure 9). These concentrations tend to be similar for a given range of T and Z for the four different MCS locations.

A similar investigation is performed for total concentrations integrating beyond 15 µm (NT). Since major conclusion are similar to these given for NT_{55}, figures for NT are shown in Appendices A. Globally, median of $N_{T,55}$ for the merged dataset are smaller by about one order of magnitude with respect to the median of N_T for the same MCS reflectivity zone. And NT over Maldives tend to be larger than median NT for the merged dataset. It shows that for a given range of T and Z, we can observe very different concentrations of very small particles (about 15µm to 55µm) over the 4 different MCS locations (especially for Maldives: oceanic MCS) with a factor of 10 even larger. But when looking total concentrations beyond 55µm, the differences between the 4 locations mitigate, in order that for the 4 locations MRD-NT_{55} are about to be similar or smaller than measurement uncertainty of ice hydrometeors concentrations.

Commenté [EF22]: Authors correction for last review before submission: clarification

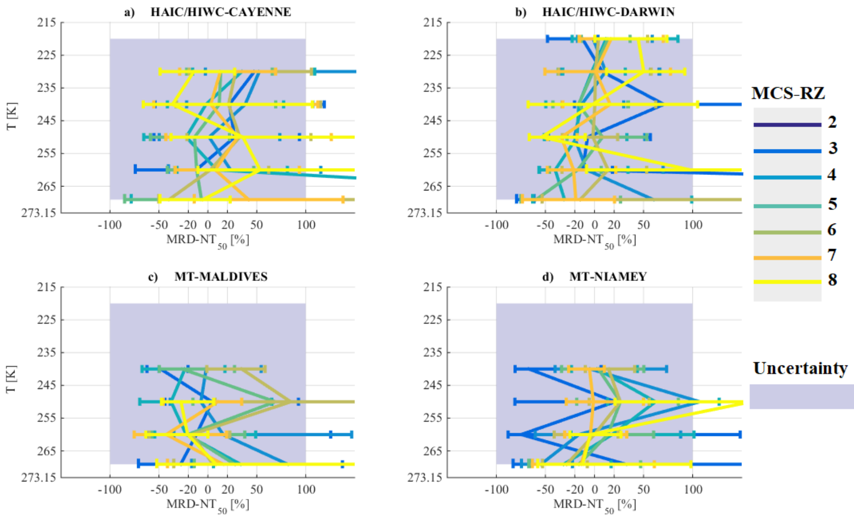

Figure 10: Same as Figure 6, but for MRD-NT$_{50}$.

Concerning concentration of larger hydrometeors, Figure 11 shows concentrations of hydrometeors when PSD are integrated beyond 500µm (hereafter $N_{T,500}$; eq. (4)), where the uncertainty on their measurement is estimated as about ±50% for hydrometeors larger than 100µm (Baumgardner et al., 2017).

$$N_T(D_{max} > 500\mu m) = \sum_{Dmax=505}^{Dmax=12845} N(D_{max}) \cdot \Delta D_{max} \quad [L^{-1}] \tag{4}$$

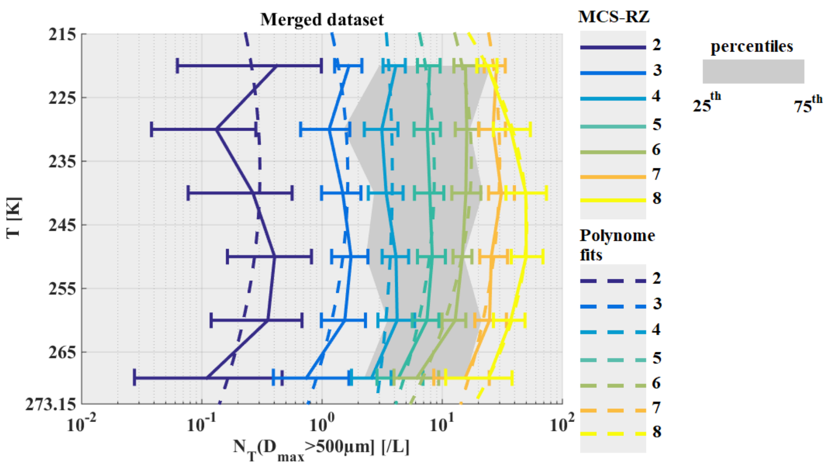

Figure 11: Same as Figure 5, but for concentrations of hydrometeors integrated beyond D_{max} =500µm in [L^{-1}].

In Figure 11 median $N_{T,500}$ are presented as a function of T and MCS reflectivity zone. The curves of median $N_{T,500}$ are different from curves of median N_T and $N_{T,55}$. Indeed, particularly for higher MCS reflectivity zones and in lower altitude levels (T ∊ [250K; 273.15K]), $N_{T,500}$ tends to increase with altitude, reaches a maximum value around T ∊ [235K; 250K], and then rather decreases for T ∊ [215K; 235K]. The range of variability for $N_{T,500}$ reveals a rather small overlap, if any, of 25th and 75th percentiles of neighboring MCS reflectivity zones 8, 7, and may be 6, mainly at coldest T ∊ [215K; 225K]. No overlap for MCS reflectivity zones 2-5 and concentration of ice hydrometeors beyond 500µm are rather constant from 215K to 265K for observations in MCS reflectivity zones 3 to 5.

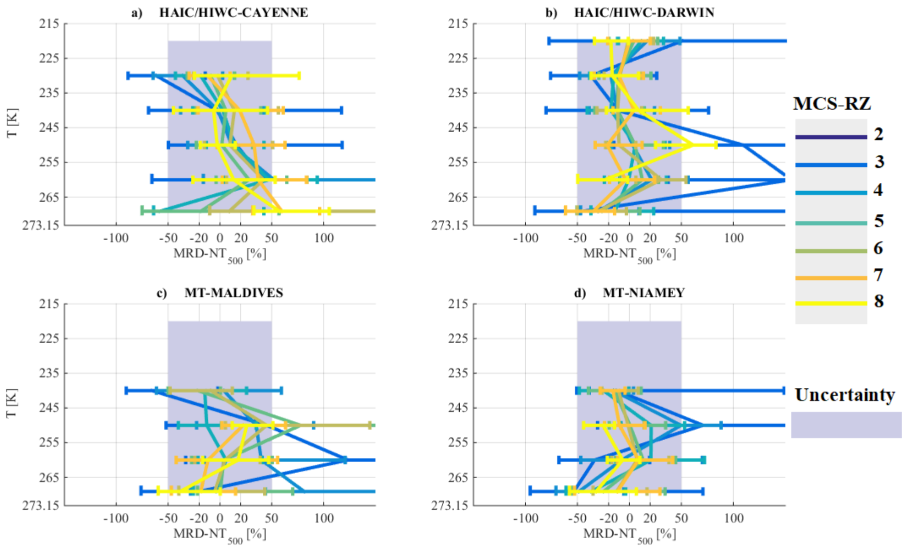

Figure 12: Same as Figure 6, but for MRD-NT_{500}.

Figure 12 (a), 12(b), 12(c), and 12(d) reveal that MRD-$N_{T,500}$ in higher MCS reflectivity zones are considerably smaller or roughly equal to the measurement uncertainty for large hydrometeors. Some smaller exc eptions are noticeable where MRD-$N_{T,500}$ are larger than the measurement uncertainty for very low altitudes at T ∊ [265K; 273.15K[, namely Cayenne in MCS reflectivity zones 7 and 8, and Darwin in MCS reflectivity zone 8. Note, that in general MRD-$N_{T,\,500}$ have smaller 75th percentiles (from Figure 10 (b), 10(c), 10(d), and 10(e)) compared to respective MRD-$N_{T,55}$ and MRD-N_T, showing that variability in each MCS reflectivity zone for hydrometeors larger than 500µm is smaller than the variability of concentrations which include smaller ($N_{T,55}$) and smallest (N_T) hydrometeors. This finding is clearly related to the uncertainty estimation given by (Baumgardner et al., 2017)) that small hydrometeors (D_{max}< 100µm) have a larger estimated uncertainty of 100% (due to shattering, very small sample volume), compared to the uncertainty of only 50% for larger hydrometeors (D_{max}>100µm). Hence, it is not surprising that variability around a median value is larger for N_T and $N_{T,55}$ than for $N_{T,500}$. It is important to resume here that not just MRD-$N_{T,500}$ is smaller than the uncertainty of 50%, but also that MRD-$N_{T,500}$ is tremendously smaller than MRD-$N_{T,55}$ and MRD-N_T. Even though we have to keep in mind that we'll never have *sufficient statistics in flight data, due to sampling bias of flight trajectories and variability of microphysics from one system to another. Indeed, Leroy et al., (2017) demonstrated that median mass diameter MMD_{eq} generally decrease with T and increasing IWC for the dataset of HAIC-HIWC over Darwin. However, for two flights performed in the same MCS, Leroy et al., (2017) showed that high IWC were linked to large MMD_{eq}, where MMD_{eq} tends to increase with IWC. This demonstrates that comparable high IWC can be observed for two different microphysical conditions (short-lived typical oceanic MCS versus long lasting tropical storm in one and the same dataset).*

We observe that total concentrations starting from 15µm can be different between MCS locations as a function of T and Z, especially in oceanic MCS over Maldives Islands in the more stratiform part of these MCSs where measured concentrations can reach 10 times the median concentrations observed globally for merged tropical dataset. Also MCS over Niamey show larger concentrations near the convective part of MCS. However, concentrations of ice hydrometeors beyond 55µm tend to be more similar as function of T and Z, even if the limits between each MCS reflectivity zones are not well defined.

Commenté [EF23]: R2#14

Between 4 MCS locations, differences of aerosol loads and available ice nuclei might exist. Despite those possible differences, ice crystal formation mechanisms may be primarily controlled by dynamics, thermodynamics and particularly by secondary ice production rather than primary nucleation; (Field et al., 2016; Phillips et al., 2018; Yano and Phillips, 2011) that regulate the concentrations of hydrometeors beyond ~55µm making these concentrations quiet rather similar for different MCS locations.

5.4 Coefficients of mass-size relationship

The relationship between mass and size of ice crystals is complex. Usually in field experiments the mass of individual crystals is not measured, instead bulk IWC is measured which is the integrated mass of an ice crystal population per sample volume to be linked to PSDs of ice hydrometeors. Yet IWC is not always measured or with low accuracy. Due to the complex shape of ice hydrometeors, various assumptions allow to estimate the mass of ice crystals for a given size. Indeed, many habits of ice crystals can be observed in clouds, primarily as a function of temperature and ice saturation (Magono and Lee, 1966; Pruppacher et al., 1998). Also hydrometeors of different habits can be observed at the same time (Bailey and Hallett, 2009). Locatelli and Hobbs (1974) and Mitchell (1996) suggested mass-size relationships represented as power laws with $m = \alpha \cdot D^{\beta}$ *for different precipitating crystal habits. Coefficients* α *and* β *vary as a function of the ice crystals habit. Further studies performed calculations of mean mass-size relationships (also using power law approximations) retrieved from simultaneous measurements of particle images combined with bulk ice water content measurements (Brown and Francis, 1995; Cotton et al., 2013; Heymsfield et al., 2010). Schmitt and Heymsfield (2010), Fontaine et al (2014), Leroy et al. (2016) showed that mass-size relationship coefficients* α *and* β *vary as a function of temperature. In the latter studies, coefficient* β *is calculated from OAP images, and then* α *is retrieved either also from processed images or constrained with integral measured IWC or radar reflectivity factor Z. Recently, Coutris et al (2017) retrieved masses of hydrometeors by an inverse method using direct measurement of PSD and IWC. In this latter study, the mass of ice crystals is retrieved without any assumption on the type of function linking mass and size of ice hydrometeors.*

This study uses the power law assumption to constrain the mass of ice hydrometeors. Thereby, the β exponent of the mass-size power law relationship is calculated (eq. 7) as presented in Leroy et al (2016) for hydrometeors defined by D_{max} dimension:

$$\beta = 1.71 \cdot f_s - 0.62 \cdot f_p \qquad (5)$$

Here f_p is the exponent of the perimeter-size power law relationship (Duroure et al. 1994) with $P(D_{max}) = e_p \cdot D_{max}^{f_p}$ $[cm]$ and f_s is the exponent of the 2D image area-size relationship (Mitchell, 1996) with $S(D_{max}) = e_s \cdot D_{max}^{f_s}$ $[cm^2]$. These two relationships are calculated using Images from 2D-S and PIP. Hence, β is a proxy parameter that describe the global (all over the size range of hydrometeors from 50µm to 1.2cm) variability of the shape of the recorded hydrometeors during the sampling process (Leroy et al., 2016; Fontaine et al., 2014). Figure 13 shows the variability of β as a function of temperature and MCS reflectivity zones for the merged dataset. For a given MCS reflectivity zone, β increases with increasing temperature. Also for a given temperature, β increases with MCS reflectivity zone, although MCS reflectivity zones 4, 5, 6, 7, and 8 share a range of common values for β, making it more uncertain to predict with a good accuracy using a parametrization as function of IWC and T.

Commenté [EF24]: R1#15

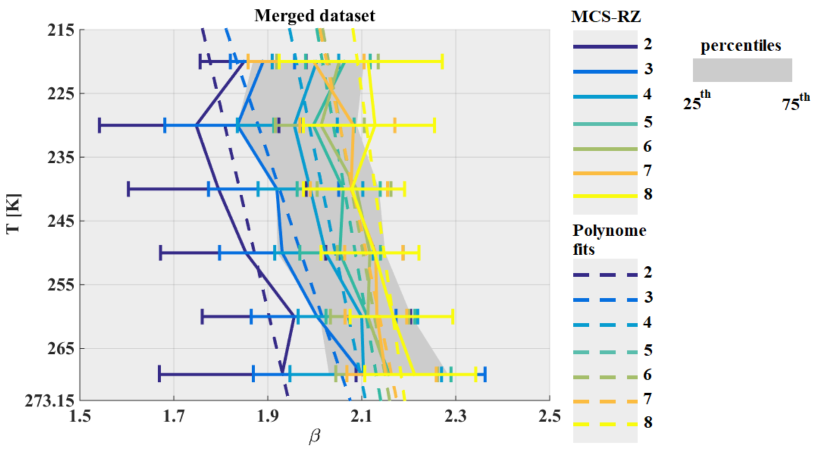

Figure 13: As Figure 5, but for exponent β of mass-size relationships for used ice hydrometeor size definition D_{max}.

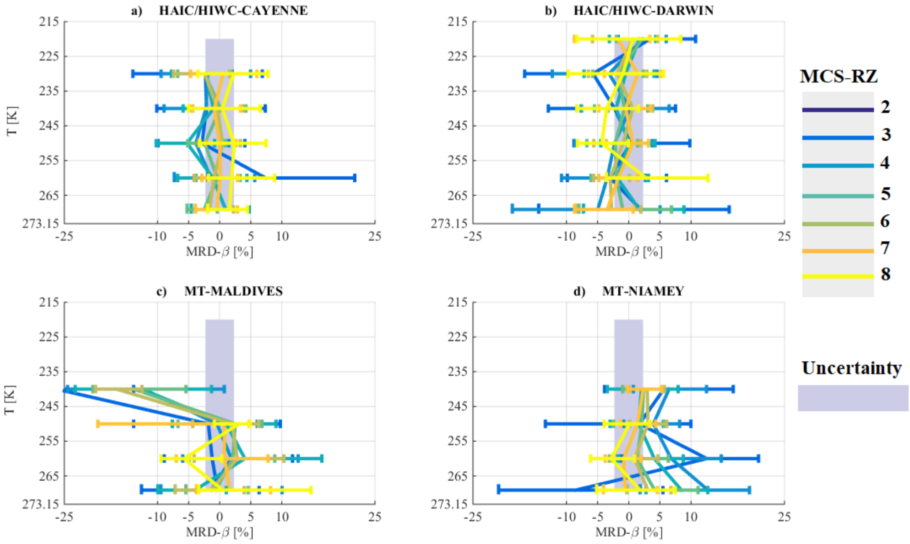

Figure 14: As Figure 6, but for exponent MRD-β.

In order to estimate the uncertainty on the calculation of β (grey band in Figure 14 (a), (b), (c), and (d), results from (Leroy et al., 2016) have been used, with U(β)/β=±2.3%. However, if we had calculated the uncertainty on retrieved β from the uncertainty on the measurement of the size and concentration of hydrometeors from OAP images, the uncertainty would have been by about 44%. Considering the small range of variability for β (1 to 3), the uncertainty given by Leroy et al., (2016) allow to highlight some differences overall ice particle habit. In general, MRD-β in MCS reflectivity zones 8 and 7 tend to be in the range of U(β)/β assuming that β are similar for all observed MCS in the four campaigns for the conditions described by MCS reflectivity zones 7 and 8.

However, in MCS reflectivity zones 2 to 6 MRD-β are more scattered around U(β)/β with sometimes larger MRD-β than uncertainty of β. Especially for MCS over Maldives and Niamey. Over Maldives at higher altitudes β tend to be smaller compared to the median β calculated for the merged dataset. While, MCS over Niamey tend to have β larger than median β calculated for the merged dataset.

Overall, the predictability of β coefficients as a function of T and MCS reflectivity zone remains challenging. We are aware of the fact that the power-law approximation has certain limits, trying to impose one single β to an entire crystal population composed of smaller (dominated by pristine ice) and larger crystals (more aggregation, also riming).

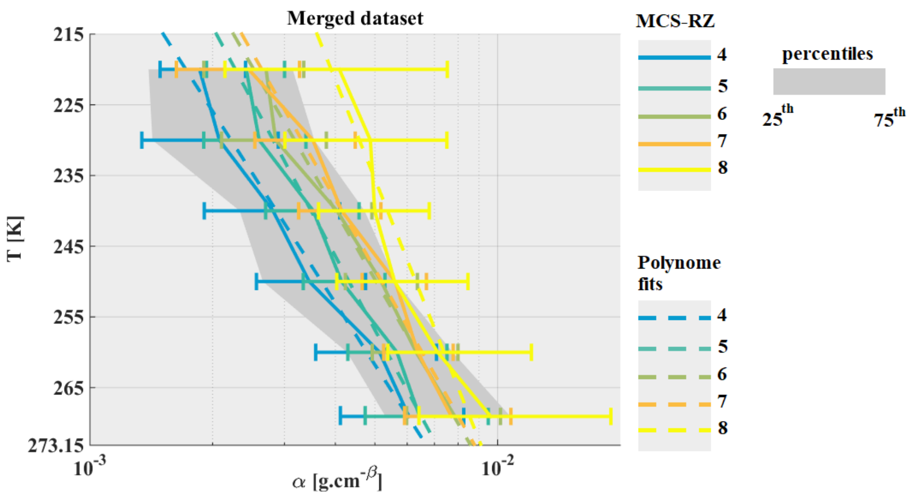

Figure 15: Same as Figure 5, but for α of mass-size relationships for used ice hydrometeor size definition D_{max}.

For HAIC-HIWC data, coefficients α are retrieved, while matching measured IWC from IKP-2 with calculated IWC thereby integrating PSD times m(D) power law relationship. For Maldives and Niamey datasets, coefficients α are retrieved from T-matrix simulations of the reflectivity factor (Fontaine et al., 2017).

For both situation, α calculation is solely constrained by the fact that the mass of ice crystals remains smaller or equal than the mass of an ice sphere with the same diameter D_{max}:

$$\alpha = \frac{IWC}{\sum_{15}^{12845} N(D_{max}) \cdot D_{max}^{\beta} \cdot \Delta D_{max}} \quad | \quad \alpha \cdot D_{max}^{\beta} \leq 0.917 \cdot \frac{\pi}{6} \cdot D_{max}^{3} \quad [g.cm^{-\beta}]. \qquad (6)$$

For the uncertainty calculation of α we take the maximum value of β which is 3:

$$\frac{U(\alpha)}{\alpha} = \sqrt{\left(\frac{U(IWC)}{IWC}\right)^2 + 3 \cdot \left(\frac{U(D)}{D}\right)^2 \left(\frac{U(N)}{N}\right)^2} \qquad (7)$$

Figure 15 shows median α coefficients as a function of T and MCS reflectivity zone. As it has been already stated in previous studies, α is strongly linked to the variability of β (Fontaine et al., 2014; Heymsfield et al., 2010). Figure 15 compared to Figure 13 confirms that results for α have similar trends as those discussed for β. α vary from 5.10^{-4} (in MCS reflectivity zone 2) to ≈2.10^{-2} (in MCS reflectivity zone 8). In general, α increases as a function of T for a given MCS reflectivity zone and also increases as a function of MCS reflectivity zone (and associated IWC) for a given T level. As already stated for the median exponent β in Figure 13, median α in MCS reflectivity zones 4, 5, 6, 7 and 8 are more or less overlapping.

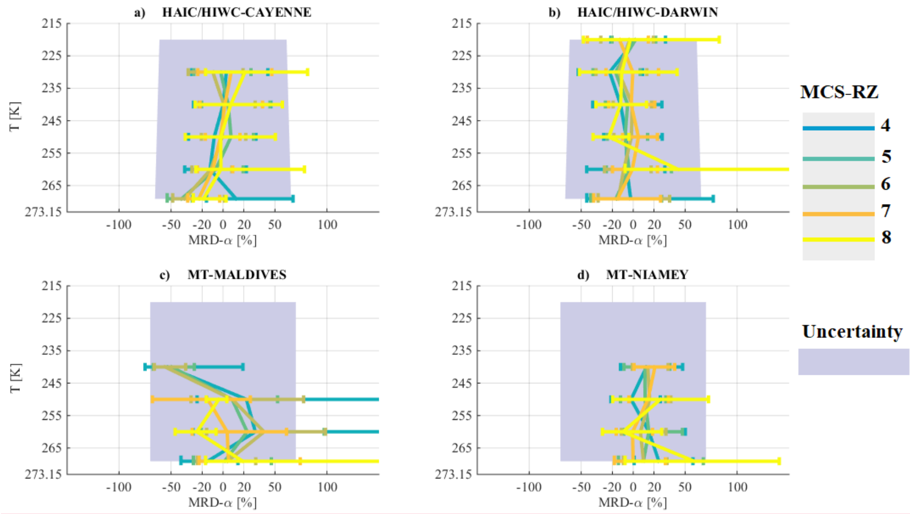

Figure 16: As Figure 6, but for exponent MRD-α.

From Figure 16(a) and Figure 16(b) we can note that even with a good accuracy of the measured IWC (from IKP-2; U(IWC)/IWC ≈ ±5% for the typical IWC values observed in HAIC-HIWC at 210K), the uncertainty of α, is rather large which is mainly due to uncertainties in OAP size and concentration measurements. Taking into account the large uncertainty on the retrieved α, we find that MRD-α for all 4 merged datasets for MCS reflectivity zones 4, 5, 6, 7, and 8 are smaller than U(α)/α. For data from Niamey (Figure 16 (d)), α tend to be larger than median α for the merged dataset (MRD-α not centered on 0, but shifted to positive values).

In previous sections, this study documented similar IWC values and visible extinction coefficients for a given range of Z and T and a clear increase of IWC and visible extinction coefficient from MCS reflectivity zones 4 to 8. The increase of α and β with MCS reflectivity zones is not as much clearly visible, whereas at least α seems to increase with temperature in different MCS reflectivity zones). Moreover, we cannot ignore that α and β tend to be larger in MCS reflectivity zone 8 than in MCS reflectivity zone 4, especially at higher altitude. But, the increase of IWC and visible extinction with MCS reflectivity zone Z is not linked to an increase of the mass-size coefficients. This conclusion takes into account the variability of the mass-size coefficients shown by 25 and 75 percentiles. Furthermore, ice hydrometeors habits describe with β in MCS reflectivity zone 4, 5 and 6 are different in MCS over Maldives and MCS over Niamey compared to MCS over Darwin and Cayenne (smaller β over Maldives and larger β over Niamey).

Because visible extinction (hence projected surface) and IWC are similar for the same range of T and Z in all types of MCS, but the shapes of crystals might be different from one to another MCS location. We assume that ratio of projected surface vs IWC is similar. In other words the density of ice per surface unity (or by pixels of projected surface) is similar as function of T and Z in all types of MCS even if there might be a possibility that the habit or the shape can be different (pure oceanic MCS vs pure continental MCS). Note that these assumptions are established for IWC larger than 0.1g.m^{-3}.

Commenté [EF25]: R1#16

5.5 Largest ice hydrometeors

Figure 17 investigates the variability of the size of the largest ice hydrometeors in the PSD (hereafter max(D_{max}) as defined in Fontaine et al (2017)). Figure 17 reveals globally for all MCS reflectivity zones that the median of max(D_{max}) increases with T, with larger hydrometeors at cloud base compared to cloud top, particularly in the stratiform cloud part, where PSD are mainly impacted by a combination of aggregation and sedimentation. At higher levels for T ∊ [215K; 245K[largest median of max(D_{max}) are observed in the most convective MCS reflectivity zone 8, followed by zones 7, 6, and 5, where sedimentation becomes more and more active. Below the 250K level, largest max(D_{max}) can be observed in MCS reflectivity zones 6 and 7 (still significant sedimentation source from above), followed by 5 (increasing depletion of large crystals) and 8 (more convective or at least transition zone from convective to stratiform cloud part). Smallest max(D_{max}) are observed in MCS reflectivity zones 2 and 3.

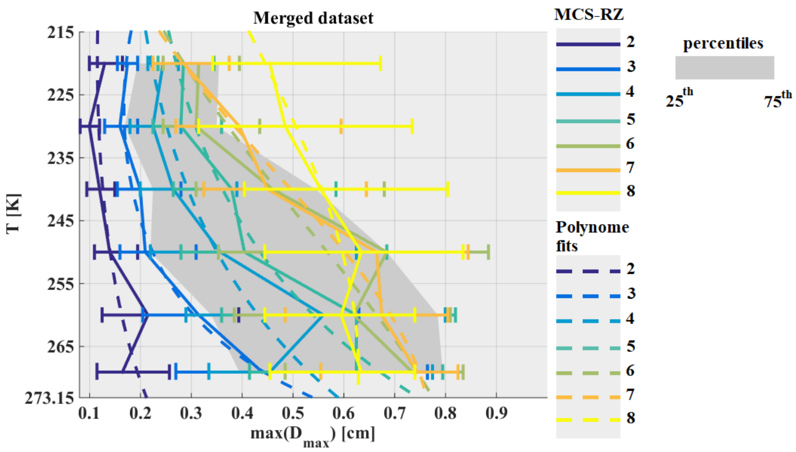

Figure 17: As Figure 5, but for maximum size of hydrometeors max(D_{max}) in PSD in [cm].

MRD-max(D_{max}) shown in Figure 18(a), 18(b), 18(c), and 18(d) are a bit larger than the measurement uncertainty estimated with ±20% ((Baumgardner et al., 2017). Cayenne, Darwin, and Niamey data are centered around the median max(D_{max}) of the merged dataset in MCS reflectivity zone 8 for all type of MCSs, in MCSs reflectivity zone 7 for MCS over Darwin, Cayenne and Niamey. MCSs over Cayenne and Darwin tend to have similar max(D_{max}) in other MCS reflectivity zones. Maldives dataset shows mainly negative MRD-max(D_{max}) values, indicating that max(D_{max}) for the Maldives Island data are generally smaller than those of the other three tropical datasets. Also MCS over Niamey show larger max(D_{max}) in MCS reflectivity zones 2 to 4, illustrating that snow aggregates can reach larger sizes during the West African monsoon than in other MCS locations. It confirms conclusions from Frey et al., (2011) and Cetrone and Houze (2009), who suggest that there are larger ice hydrometeors in MCS over continent than MCS over maritime regions.

Commenté [EF26]: R2#5

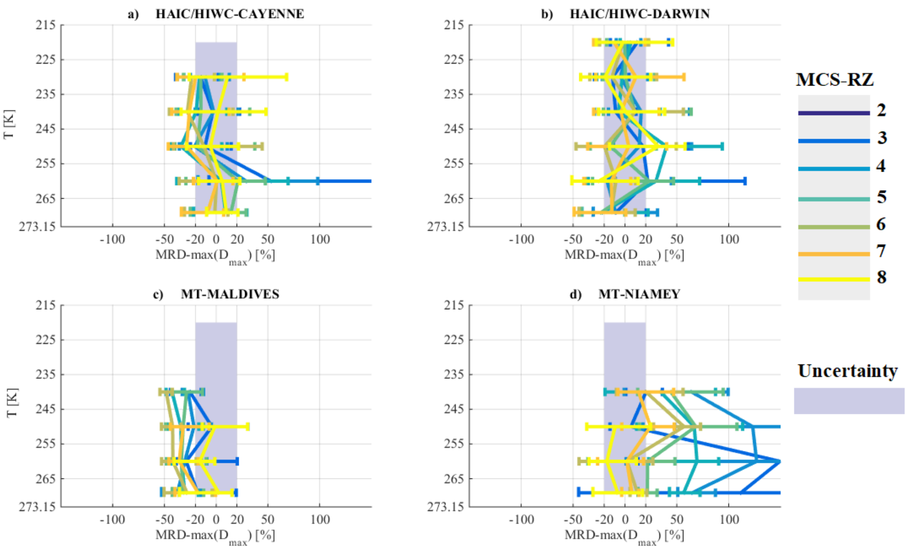

Figure 18: As Figure 6, but for maximum size of hydrometeors max(D_{max})

In this section, it is shown that in the stratiform part of MCS, largest hydrometeors are larger in MCSs over Niamey than in other types of MCS, and tend to be smaller in MCS over Maldives Islands. Mainly, large crystals (Dmax > 1mm) are agglomerates of pristine ice crystals, for which the growth process is leaded by aggregations (by sedimentation) instead of vapour diffusion. There is a possibility that largest hydrometeors are large pristine ice. Indeed, some large pristine ice (large dendrites) were found in the dataset (especially over Maldives see Figure 1 in Fontaine et al., 2014). However, their size do not exceed 3 to 4 mm. Hence, aggregation efficiency is different from one MCS type of MCS to another, this could explain the differences of mass-size coefficient β, as it is calculated on the slope in a log-log scale of mean perimeter and mean surface as a function of median diameter in each size bin. Because, large hydrometeors have a non-negligible impact on the slope (i.e. fp and fs, see Eq. (5)).

5.6 note on the impact of vertical movement on ice microphysic

This section discussed about the results of an investigation performed about the impact of vertical velocity on ice microphysical parameters presented earlier in this section 5. Aside the statistic performed on the merged dataset where vertical velocity are not considered, similar statistics were calculated for three sub-datasets such: i) w <-1m/s , (ii) -1m/s < w < 1m/s and (iii) w>1m/s. Then, median relative difference for the three conditions and for each parameters presented in this section 5 were calculated and compared to the median relative difference when no distinction is performed as function of vertical velocity. Firstly, we noticed that MRD-X for the merged dataset and MRD-X for the second condition (i.e. 1m/s < w < 1m/s) are similar (MRD-X: X being used to replace IWC, σ, NT, NT_{50}, NT_{500}, β, α, max(Dmax)). Secondly, differences of MRD-X in updraft and in downdraft with regards to MRD-X for merged dataset and no vertical movement are visible. But most of the times these differences are of the order of or smaller than measurement uncertainties (U(X)/X). Hence, the impact of vertical velocity (>0m.s-1

Commenté [EF27]: R1#17

Commenté [EF28]: Author's correction before last submission *or <0m.s-1) is not significant on ice microphysic parameters presented in section 5; except for IWC, NT and NT_{50}. Figures for these last parameters are presented in Appendices B.*

Appendices B shows shows when updraft have an impact on IWC NT and NT_{50} for a given range of temperature and MCS reflectivity zones. Figure B1 shows MRD-IWC, Figure B2 shows MRD-NT and Figure B3 shows MRD-NT50. For the others parameters impact of updraft are uncommon.

Commenté [EF29]: Author's correction before last submission

It appears that updraft tends to impact mainly concentrations of small hydrometeors and IWC for some type of MCS and some MCS reflectivity zones. So for NT (Figure B2), we observe larger NT for updraft in MCS observed over Cayenne, Maldives and Niamey. For Cayenne, it appears in MCS reflectivity zone 5 and 6 for temperatures between 245K and 265 K with NT 2 to 3 times larger than NT for merged dataset. For MCS over Maldives, median NT are 5 times to 20 times larger than NT when there is no noticeable vertical movement in MCS reflectivity zones 6, 7 and 8. Finally, for MCS over Niamey, we observe larger NT in updraft than NT for the merged dataset in MCS reflectivity zones 6 for T around 240 K and in MCS reflectivity zones 8 above the bright band. We have similar conclusions for NT_{50} (Figure B3), except that ratios between NT_{50} in updraft and NT_{50} when no updraft is smaller than the ratio between NT in updraft and NT when no updraft.

IWC are impacted by updraft, only for MCS over Cayenne, in MCS reflectivity zone 4, 5, 6 and 7. IWC in updraft tend to be larger about +50% than IWC when no updraft, except in MCS reflectivity zones 5 where IWC are about 2 times larger in updraft than IWC when no updraft.

This investigation on the impact of updraft and downdraft on ice microphysics, shows that updraft may have an impact on concentrations of small hydrometeors and IWC. However, updraft does not impact all type of MCS in the same way. So, there will need to perform deeper investigations on updraft impact.

Despites some noticeable impact of updraft on ice microphysic for our datasets, there is no significant (recurrence trough all types of MCS or as function of T or Z) results to assess them for the merged dataset. So, parameterizations provided in the next section are not as functions of vertical velocity.

Commenté [EF30]: R1#4

6. Parameterizations as function of IWC and T

Commenté [EF31]: R2#4

6.1 visible extinction

Since we concluded from Figure 7 and Figure 8 that visible extinction σ and IWC in tropical MCS tend to be similar for all MCS locations in the same range of T and for corresponding MCS reflectivity zones 4 to 8. Moreover, Figure 19 shows that there is a linear relationship between log(σ) and log(IWC). And log(σ) decrease with temperature increasing at constant log(IWC). Then, we performed a surface fitting using input coefficients log(IWC) and T to fit log(sigma) to deduce a parametrization of σ (Eq. (8)) as a function of IWC and T. This parameterization is limited for deep convective cloud (merged dataset) and data with IWC > 0.1g m^{-3}:

$$\sigma = exp(-0.0194587 \cdot T + 0.9134019 \cdot ln(IWC) + 1.2423609) \quad [m^{-1}] \quad (8)$$

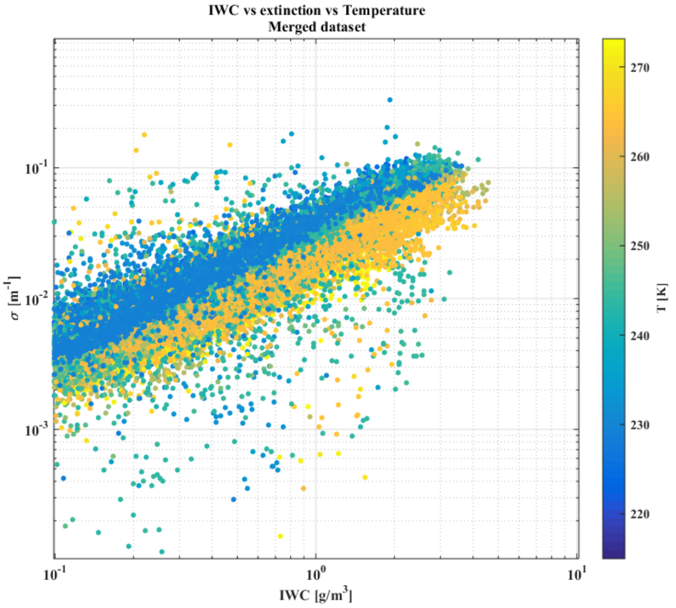

Figure 19: visible extinction in [m^{-1}] on y-axis as function of IWC in [kg.m^{-3}] on x axis and as function of T in [K] indicated by the color scale. Scatter plot using the merged dataset (4 campaigns).

Commenté [EF32]: R2#12

An evaluation of this parametrization is presented in Figure 20, where black lines in Figure 20-a) to Figure 20-d) represent median relative errors of σ (with 25th and 75th percentiles represented by whiskers) for the merged dataset predicted with Eq. (8), with respect to retrieved σ from OAP images from Eq. (1). In addition, median relative errors of σ for individual MCS datasets over Darwin, Cayenne, Maldives Islands, and Niamey with respect to σ calculations (Eq. (8)) are shown in Figure 20(a), Figure 20(b), Figure 20 (c), and Figure 20(d), respectively. The uncertainty ± $\frac{U(\sigma)}{\sigma}$ is given with the grey band. All relative errors (25th - 75th percentiles) tend to be smaller than ± $\frac{U(\sigma)}{\sigma}$, with median relative errors that are smaller than ±25% of σ uncertainty calculated from Eq. (2). In general, Eq. (8) seems to produce smallest relative errors of σ for Niamey and Darwin datasets (especially for IWC<2g m^{-3}).

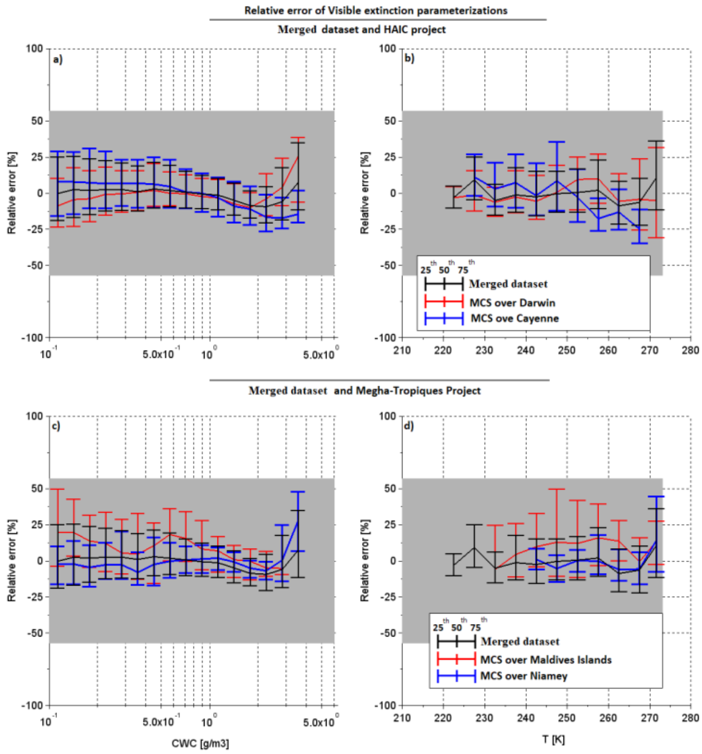

Figure 20: Relative errors of predicted visible extinction Eq. (8) with respect to measured visible extinction for a), b), c), and d. Relative errors as a function of IWC in a) and c) and as a function of T in b) and d). Black lines in 4 sub figures represent the relative errors when calculated for the merged dataset. In a) and b) red lines show median relative error for MCS over Darwin, and blue line for MCS over Cayenne. In c) and d) red line represent median relative errors for MCS over Maldives Islands and blue lines for MCS over Niamey. Bottom of error bar shows 25th percentiles of relative errors and 75th percentiles are given by top of error bar.

Noteworthy, optically thick clouds are responsible of large errors in retrieved cloud water path and condensed water concentration profiles retrieved from satellite imageries (Smith, 2014; Yost et al., 2010). Parameterizations, such as presented here, could help to improve retrieval methods on cloud water path but more investigations on the benefit of such parameterizations are needed, which is beyond the scope of this study.

6.2 Parameterization of ice hydrometeors distributions

6.2.1 Observations of PSD moment

Moments of PSD are convenient for numerical weather prediction to model microphysics of hydrometeor populations, since knowing the PSD n^{th} order moment allows to roughly describe cloud processes and their hydrometeors properties. Commonly, PSD of ice hydrometeors are modeled with Gamma distributions (Heymsfield et al., 2013; McFarquhar et al., 2007). The calculation of the n^{th} order moment is defined in Eq. (9) for PSD obtained from measurements of hydrometeors images, for example with OAP (optical array probes):

$$M_n = \sum_{D_{max}=55\mu m}^{D_{max}=1,2cm} N(D_{max}) \cdot D_{max}^n \cdot \Delta D_{max} \qquad [m^{n-3}] \tag{9}$$

The uncertainty of the n^{th} (n=2 and 3 in our study) moment is:

$$\frac{U(M_n)}{M_n} = \sqrt{n \cdot \frac{U(D)}{D}^2 + \frac{U(N)}{N}^2} \tag{10}$$

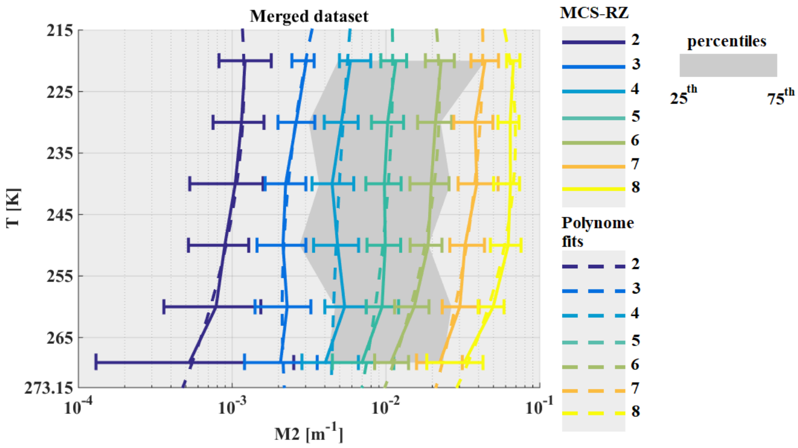

Figure 21: Same as Figure 5, but for M_2 per meter.

Figure 21 shows median second moment M_2 as a function of T for all MCS reflectivity zones for the merged global tropical dataset. Median M_2 slightly decrease with temperature for all individual MCS reflectivity zones, and distinctly increase with MCS reflectivity zone for a given T. The range of variability of median M_2 shows mainly negligible overlap, if any, of 25th and 75th percentiles of neighboring MCS reflectivity zones with the exception between MCS reflectivity zones 8 and 7 at low altitude ($T \in$[265; 273.15[).

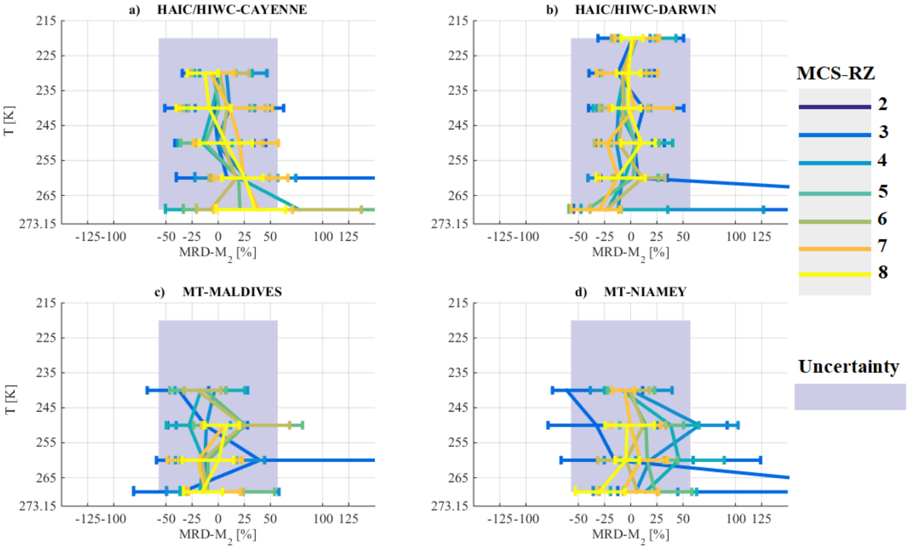

Figure 22: Same as Figure 6, but for MRD-M$_2$.

All 4 tropical MCS (Figure 22 (a), (b), (c), and (d)) show good agreement with the medians of M_2 in MCS reflectivity zones 3 to 8, with MRD-M_2 significantly smaller than $U(M_2)/M_2$. Few minor exceptions can be found for MCS over Cayenne (Figure 22 (b)) and Darwin (Figure 22 (c)) in the temperature range [265K; 273.15[. Also MCS over Niamey (Figure 22 (e)) show a larger MRD-M_2 in MCS reflectivity zones 2 and 3 for $T \in$ [265K; 273.15K[and $T \in$ [245K; 255K[, respectively.

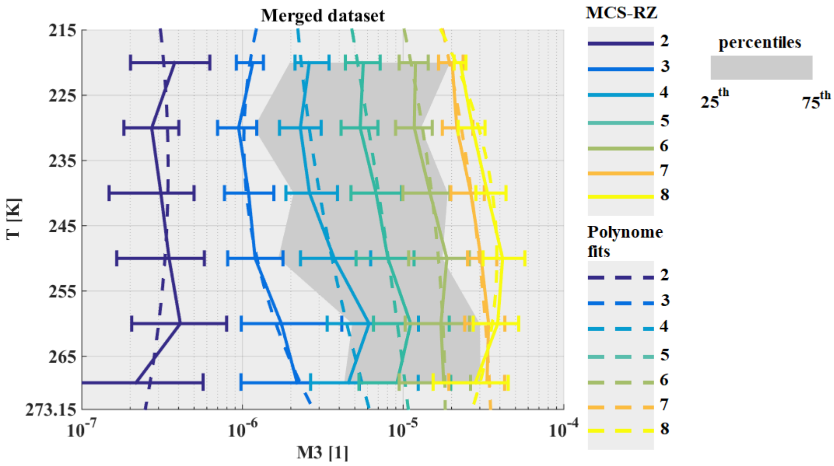

Figure 23: Same as Figure 5, but for the M_3 for unity dimension.

Figure 23 presents median third moment M_3 for merged dataset as a function of T and for different MCS reflectivity zones. Median M_3 in highest MCS reflectivity zones 8, 7, and to some extent zone 6 resemble the corresponding curves of median IWC (Figure 5), with a maximum value for median M_3 for $T \in$ [245K; 260K[. We also note a clear increase of median M_3 with MCS reflectivity zone from 2 to 8. The range of variability for M_3 reveals no overlap of 25th and 75th percentiles of neighboring MCS reflectivity zones 2-7, solely zone 7 overlaps with zone 8 for all temperatures. Third moment of MCS over Cayenne, Darwin and Maldives Islands in MCS reflectivity zones 2 to 8, shows MRD-M_3 smaller than $U(M_3)/M_3$, with few minor exceptions basically in the range of $T \in$ [265K; 273.15K[. MCS over Niamey tend to have MRD-M_3 that are sometimes larger than $U(M_3)/M_3$. Indeed, M_3 for MCS over Niamey tend to be larger in MCS reflectivity zones 5 and 2 in the range of $T \in$ [265K; 273.15K[, and in MCS reflectivity zone 4 for T larger than 255K as well as in MCS reflectivity zone 3 for T larger than 245K.

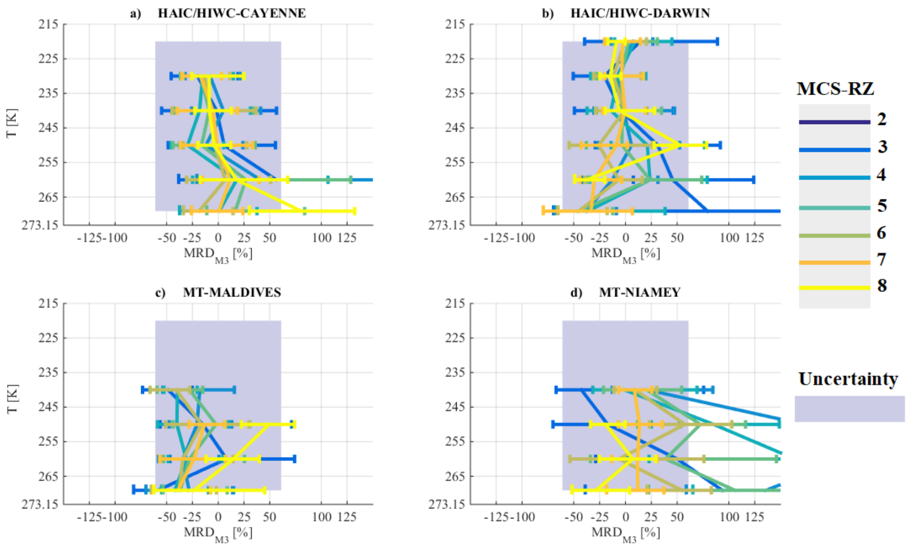

Figure 24: Same as Figure 6, but for the M_3.

Overall, this section illustrates that second and third moments of PSD are similar as a function of T and Z for all MCS locations of the underlying dataset. However, there are exceptions in MCS reflectivity zones 2, 3 and 4 in MCS over Niamey where larger third moments are calculated compared to those deduced for the merged global tropical dataset. Despite those exceptions, the next section explores the possibility to parameterize the second and third PSD moments as a function of IWC and temperature.

6.2.2 Parameterizations of M_2 and M_3

This section presents parametrizations to predict the 2nd and 3rd moment of the PSD for the merged dataset as a function of T and IWC (for this section IWC in the equation are in [$kg.m^{-3}$]), including IWC data larger than 0.1g m^{-3}. Indeed some moments can be directly linked to bulk properties of hydrometeor populations. For example, *moment M_0 for ice and liquid hydrometeors is equal to the total number concentration (N_T), moments M_2 and M_3 for liquid particles are proportional to visible extinction and liquid water content. However, for ice hydrometeors the physical interpretation of moments M_2 and M_3 is less obvious since ice hydrometeors are not spherical particles. The results for α and β coefficients of the $m(D_{max})$ relationship presented in section 5.4, illustrate that β varies between 1.5 and 2.3. This means that IWC is proportional to PSD moments between $M_{1.5}$ and $M_{2.3}$. Also uncertainties on the retrieved β coefficients do not allow to assess the variability of β as a function of IWC and T. Former studies performed in different cloud environments report mean values of β around 2. For example, Leroy et al., (2016) found β=2.15 for HAIC-HIWC in Darwin, Cotton et al., (2013) suggested β=2.0, Heymsfield et al., (2010) suggested β=2.1, and Brown and Francis (1995) established β=1.9. We are also aware of the fact that findings of β also depend on the utilized size parameter (D_{max}, D_{eq}, etc…) of 2D images (Leroy et al., 2016). Hence, we apply β=2 as an approximation, also proposed by Field et al., (2007), to link the second moment of hydrometeor PSD with IWC (Eq. 11). Subsequently, the ratio IWC/M_2 is calculated and denoted A.*

$$M_2 = \frac{IWC}{A} \quad [m^{-1}] \tag{11}$$

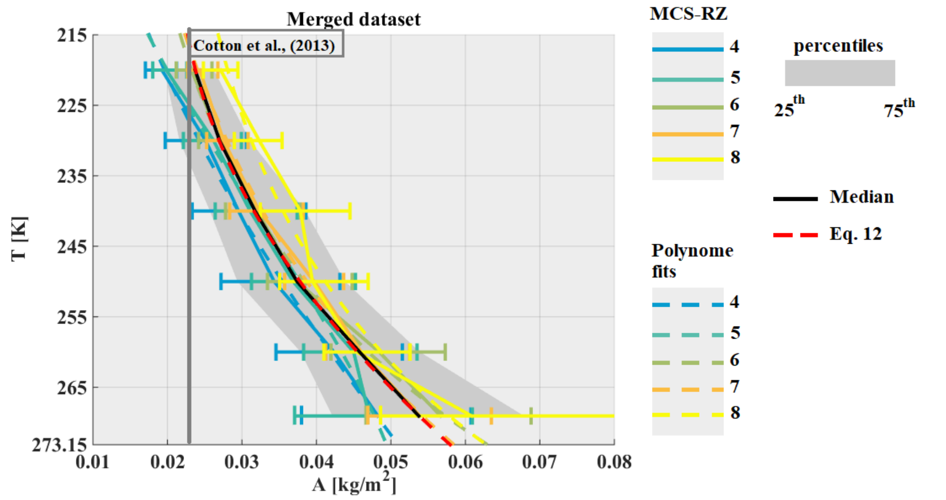

Figure 25: Same as Figure 5, but for the ratio A= IWC/M_2 in [kg m^{-2}].

Figure 25 shows retrieved median coefficients A for the merged dataset as a function of MCS reflectivity zones and T. Note that A is calculated in SI units (in Eq. (11) IWC is in kg.m^{-3}). The black solid line gives the median of A as a function of T, thereby merging all MCS reflectivity zones for the merged dataset with IWC > 0.1g m^{-3}. The grey band gives corresponding 25th and 75th percentiles of that median A. In addition, are calculated median A for all individual MCS reflectivity zones (on Figure 25) are solely illustrated median A for zones 4 to 8) for the merged dataset as a function of T. In general, median A calculated for individual MCS reflectivity zones 5, 6 and 7 are very similar to the median A when merging all MCS reflectivity zones (black solid line), whereas median A calculated for MCS reflectivity zone 4 tends to have smaller A values and median A calculated for MCS reflectivity *zone 8 have larger median A values than the overall median A (all MCS reflectivity zones merged) for comparable temperatures.*

However, when taking into account the variability in median A calculated for individual MCS reflectivi ty zones and associated 25th and 75th percentiles, we can state that median A generally increases with T, however it is not possible to assess that A increases with MCS reflectivity zones or IWC at constant temperature. As a comparison, we include the value of the pre-factor α (in SI unity) from Cotton et al. (2013) mass-size relationship (β=2.0, as is for second moment M_2, and α=0.0257). Clearly, α=0.0257 is not suited for deep convective systems as it represents ice crystals for T $\in$[215K; 225K[.

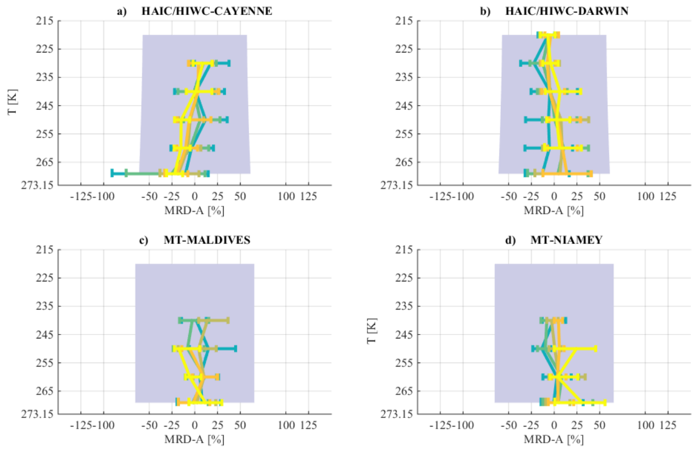

Figure 26: Same as Figure 6, but for the ratio MRD-A.

Figure 26 (a), 26(b), 26(c), and 26(d) illustrate that MRD-A are significantly smaller than U(A)/A, (same uncertainty than α: $U(\alpha)/\alpha$ = U(A)/A and median MRD results centered around 0%). Comparing results of A (Figure 26) with results presented for α (Figure 15, section 5.4) it is obvious in terms of variability and MRD in each type of MCS that A is better adapted to parametrize the PSD 2nd moment as a function of T. Eq. (12) fits the median of ratio A for the global tropical dataset (red dashed line, all MCS reflectivity zones merged), as a function of T in deep convective systems for IWC larger 0.1g m^{-3}:

$$A(T) = 0.0000075 \cdot T^2 - 0.0030598 \cdot T + 0.3334963 \qquad [kg.m^{-2}] \tag{12}$$

Hence, Field et al., (2007) proposed to retrieve the third moment M_3 as function of M_2 and T. These equations are recalled here with (in our case n=3):

$$M_n = M_2^{F(n)} \cdot D(n) \cdot exp(E(n) \cdot T_c) \tag{13}$$

T_C denotes temperature in °C and D(n), E(n) and F(n) are given by:

$$D(n) = exp(13.6 - 7.76 \cdot n + 0.479 \cdot n^2) \qquad (14)$$

$$E(n) = -0.0361 + 0.0151 \cdot n + 0.00149 \cdot n^2 \qquad (15)$$

$$F(n) = 0.807 + 0.00581 \cdot n + 0.0457 \cdot n^2 \qquad (16)$$

Figure 27 provides median relative errors (whiskers represent 25th and 75th percentiles) of parametrized moments M_2 (Figure 27 (a) and Figure 27 (b)) and M_3 (Figure 27 (c) and Figure 27 (d)) compared to respective moments calculated directly (Eq. (9) from PSD measurements (merged dataset). These relative errors are shown as a function of IWC (Figure 27(a) and Figure 27(c)) and as a function of T (Figure 27(b) and Figure 27(d)). Firstly, the red line shows median relative error of M_2 retrieved from Eq. (12) compared to M_2 derived from measured PSD (Eq. 9). In addition the grey band illustrates the uncertainty $U(M_2)/M_2$. Figure 27 (a) illustrates that below 2g m^{-3}, the median of this relative error is close to 0% with 25th and 75th percentiles significantly smaller than $U(M_2)/M_2$. However, for largest IWC beyond 2g m^{-3}, median relative errors are getting large (40% for 4g m^{-3} and 75% for 4.5g m^{-3}) and need to be corrected in order to reduce the bias between predicted M_2 and observed M_2. This is why Eq. (11) is modified with an expression shown in Eq. (17) in order to improve prediction of M_2 compared to measured M_2 (Eq. (10)) for highest IWC:

$$M_2 = \frac{IWC}{A(T)} \cdot exp\big(0.005853 \cdot exp(1025 \cdot IWC)\big) \qquad [m^{-1}] \qquad (17)$$

The effect of the expression added in Eq. (17) is illustrated by the blue line in Figure 27 (a) and Figure 27 (b), where median relative error of predicted M_2 are now closer to 0% also for large IWC. Note that in Figure 27 (b), median relative errors of the two above parametrizations (red and blue solid line) of M_2 are superposed as a function of T with a median relative error close to 0%. This means that the second part of equation (17) does not introduce any significant bias as a function of T, since the occurrence of IWC > 2g m^{-3} is smaller than 1% for the merged dataset.

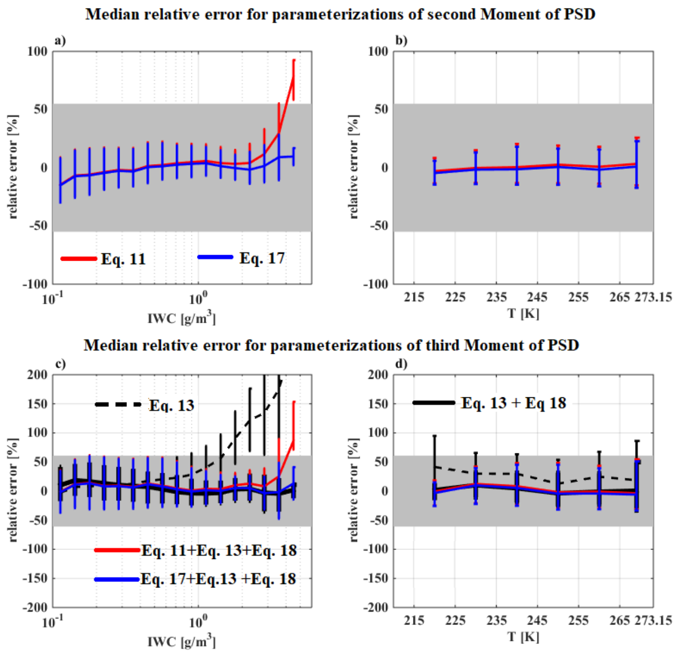

Figure 27: Relative error of parametrized M_2 and M_3 for merged dataset as a function of IWC in a) and c), and as a function of T in b) and d). Solid lines give median relative error and whiskers denote 25th and 75th percentiles of relative error. Grey bands shows measurement uncertainties for M_2 (55%; a) and b)) and M_3 (61%; c) and d)), respectively.

In Figure 27 (c) and Figure 27 (d)) are shown median relative error for parameterizations of the third moment, where the median relative error for all parameterization are calculated as function of measured M_3. First, we discuss the median relative error for parametrization of 3rd moment M_3 according to Field et al., (2007) (Eq. (13); black dashed lines) using the measured M_2. Then, we can see that the parameterization of Field et al., (2007) overestimate M_3 for IWC larger than 1g.m^{-3} and that overestimation of M_3 increase with IWC. Moreover, this overestimation of M_3 tend to decrease a bit as function of T.

To reduce this significant median relative error on measured M_3, particularly for large IWC in deep convective cloud systems, we provide a M_3 correction function for Eq. (13) as function of T and IWC:

$$M_3 = [-5.605 - 1.059 \cdot log(IWC) + 0.009536 \cdot T - 0.0418 \cdot log(IWC)^2 + 0.0007889 \cdot log(IWC) \cdot T] \cdot M_2^{F(3)} \cdot D(3) \cdot exp(E(3) \cdot T_c) \quad (18)$$

Then, three series of median relative error of M_3 where M_3 are computed with Eq. (19). First, Eq. (19) is used with measured M_2 (black solid lines) to show the efficiency of the correction applied as function of IWC and T and described in Eq. (19). Then, Eq. (19) is applied to M_2 calculated using Eq. (11) where there is no correction as *function of IWC to calculate M_2 (red solid lines). We observe that M3 are overestimated for IWC larger than 3g.m^{-3} and that there is no bias as function of T with median relative error close to 0%. Finally, Eq. (19) is used to compute M3 from M2 calculated with Eq. (17) when impact of large IWC is taken into account. We can see median relative error close to 0% for the third example of parameterization (i.e. Eq. (17) and Eq. (18)) with no bias as function of IWC and T.*

An identical investigation on median relative errors in the prediction of 2nd and 3rd moment as presented in Figure 27 has been investigated for individual MCS locations (figures not shown). For all type of tropical MCS, we observe that M_2 from Eq. (17) and M_3 from Eq. (18) tend to have smaller to equal median relative errors compared to the relative uncertainties $U(M_2)/M_2$ and $U(M_3)/M_3$, respectively. Beyond this general statement there are two noticeable observations. The first observation is that median relative errors of M_3 from Eq. (18) calculated either with M_2 from measurements (Eq. (9)) or from parametrized M_2 from Eq. (17) for MCS over Maldives Islands are close to $U(M_3)/M_3$ with 75th percentiles reaching 100% for IWC in the range [0.3; 0.6] g.m^{-3}. The second observation is that for MCS over Niamey, M_3 from Eq. (18) with M_2 from Eq. (9) or from Eq. (17) tend to overestimate respective moments calculated directly from PSD measurements by about 30 or 50%, respectively, in the area of higher IWC ([2; 3] g m^{-3}).

This section aims to produce parameterizations of the second and third moments of ice hydrometeor size distributions, which can be useful for the calculation of hydrometeor size distributions in numerical weather prediction using gamma distributions, but also (see the next section) for calculating rescaled ice hydrometeors size distributions (Field et al., 2007).

6.2.3 Rescaling of measured ice hydrometeors size distributions

From bulk properties as mixing ratio and total concentration in numerical weather prediction (NWP), ice hydrometeors size distributions (or PSD) properties can be derived from moment parameterization allowing simplified prediction of cloud microphysical processes such as precipitation. Usually, ice hydrometeors size distributions for hydrometeors are modeled by gamma distributions (Heymsfield et al., 2013; McFarquhar et al., 2007). Since the method of gamma distributions is relatively well documented, we focus this study on another type of PSD parameterization, which studies 'rescaled PSD' dealing with a 'mean diameter' defined by the ratio of the third moment over the second moment.

Commenté [EF33]: R2#15

In this section, we propose an update for the method proposed by Field et al., (2007) for deep convective cloud systems and IWC larger than 0.1g m^{-3}. For the entire dataset of this study we therefore apply the above method utilizing Eq. (19) and Eq. (20) to calculate function $\Phi_{2,3}(x)$ and x for individual measured PSD :

$$\Phi_{2,3}(x) = N(D_{max}) \cdot \frac{M_3^3}{M_2^4} \tag{19}$$

With x being the characteristic size:

$$x = D_{max} \cdot \frac{M_2}{M_3} = \frac{D_{max}}{L_{2,3}} \quad (20)$$

$\Phi_{2,3}(x)$ and x are dimensionless functions. Moreover, Field et al., (2007) deduced from their dataset, $\Phi_{2,3}(x)$ depending on cloud location; i.e. tropical troposphere or mid-latitude troposphere (here we focus on the equation established for the tropics):

$$Tropics: \Phi_{2,3}(x) = 152 \cdot exp(-12.4 \cdot x) + 3.28 \cdot x^{-0.78} \cdot exp(-1.94 \cdot x) \quad (21)$$

Hence, the variability of PSD in clouds, is not given by $\Phi_{2,3}(x)$, but by the variability of the 2nd and 3rd moments that allow retrieving functions x and $\Phi_{2,3}(x)$. Then, knowing x, $\Phi_{2,3}(x)$, M_2, and M_3 concentrations of ice hydrometeors can be parameterized such:

$$D_{max} = x \cdot \frac{M_3}{M_2} \quad (22)$$

and

$$N(D_{max}) = \Phi_{2,3}(x) \cdot \frac{M_2^4}{M_3^3} \quad (23)$$

Figure 28 shows the probability distribution function (PDF) of observed rescaled PSD in tropical MCS as a function of the x parameter. Thick black line represents $\Phi_{2,3}(x)$ from Field et al., (2007), thin dashed grey line represents median of $\Phi_{2,3}(x)$ for a given range of x, with whiskers showing 25th and 75th percentiles of $\Phi_{2,3}(x)$. The figure illustrates that Eq. (21) from Field et al., (2007) represents rather well $\Phi_{2,3}(x)$ as a function of x in highest PDF region (light yellow area) and fits well the median plot for $x \in [0.3; 6]$. However, Field et al., (2007) performed their study for diameter larger than 100µm while this study calculates rescaled PSD for D_{max} larger than 15µm for the underlying dataset. Thus, Eq. (21) does not fit median $\Phi_{2,3}(x)$ for x smaller than 0.3. Also for $x > 6$, Eq. (21) decreases too fast compared to the median of $\Phi_{2,3}(x)$ calculated for the global tropical dataset of this study, although Field et al., (2007) considered ice hydrometeors up to 2cm, whilst this study extrapolates PSD until 1.2845cm only (reconstruction of partial images to calculate particle size according to Korolev and Sussman 2000). A likely assumption to explain the differences for large $x > 6$ might be that the merged dataset of this study may have measured PSD with largest hydrometeors at a far higher frequency than this was the case for the dataset of Field et al., (2007).

Commenté [EF34]: R2#16

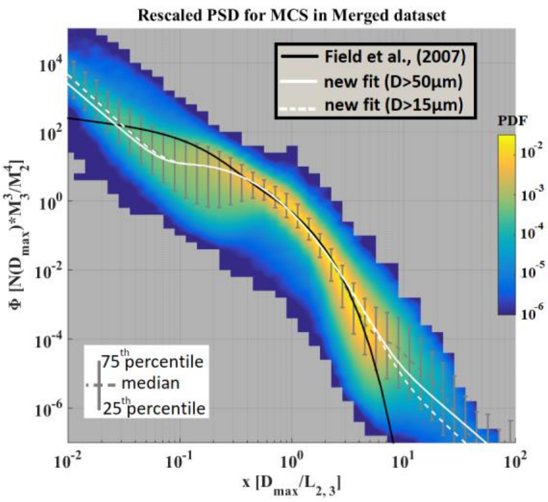

Figure 28: Probability distribution function of rescaled PSD ($\Phi_{2,3}$) on y axis as a function of hydrometeor characteristics size (x) on x axis, for the merged datasets. Black lines show fitted functions from Field et al., (2007), grey dotted lines show median rescaled PSD with error bar from 25th and 75th percentiles of rescaled PSD. Solid white line presents the new fitted function for the merged dataset for PSD beyond 55µm and dashed white line shows fitted function for PSD beyond 15µm (Eq. 24).

White lines (dashed and solid) show new fitted $\Phi_{2,3}(x)$ for the merged dataset of this study. The white dashed and solid lines can be represented by the following equation and aim to fit the median ($\Phi_{2,3}(x)$) of Figure 28 as a function of x:

$$Tropics\colon \Phi_{2,3}(x) = [exp(a_1)\cdot x^{a_2}] + \left[b_1 \cdot exp\left(-\frac{(ln(x)-b_2)^2}{b_3^2}\right)\right] \quad (24)$$

Where b1 = 9.484, b2 = -1.895 and b3 = 1.083. Note that dashed and solid white lines use different sets of coefficients a_1 and a_2 (Table 1). For white dashed line, a_1 and a_2 are calculated for D_{max} beyond 15µm, whereas for white solid line, a_1 and a_2 are calculated for D_{max} beyond 55µm. We can notice that the function for $D_{max} \geq$ 15µm produces higher $\Phi_{2,3}(x)$ as compared to the function fitted for $D_{max} \geq$55µm. In order to explain this difference, we recall that for MCSs over the Maldives Island concentrations of hydrometeors with $D_{max}\leq$55µm are higher compared to 3 other tropical MCS locations, which could affect the fitted coefficients a_1 and a_2 in the two different versions of $\Phi_{2,3}(x)$ calculations for the merged dataset. Another difference in small particle measurements could be a pure technical difference in small particle measurements (including shattering/out-of-focus/small sample volume artefacts) between 2D-S probe (this study) and 2D-C probe (Field et al. (2007) study).

Table 2 : Coefficients a1 and a2 for Eq. (24).

	a_1	a_2
Tropics: D_{max} >15µm	*-5.4114*	*-3.0026*

Tropics: $D_{max} > 55\mu m$	*-5.0032*	*-2.7822*

The parameterization developed in this study is performed on ice hydrometeors distributions defined as function of D_{max}. However, NWP usually assumes that ice hydrometeors are spherical. So, Appendices E explores the impact of assuming that ice hydrometeors are spherical in the context of this study, noting that volumes of ice hydrometeors recorded by OAP are not directly measured. This latter short study is performed supposing that the truth to define ice hydrometeors distribution might be around using D_{max} or spherical diameter. For both assumptions there is a need to perform sensitivity studies to assess which parameterization is more suited for NWP.

Commenté [EF35]: Author's adding. We think it is necessary to consider the assumptions use in NWP and to show what are the differences with the assumptions that are used in data analysis of in-situ measurement. Note: in NWP hydrometeors are spherical while for in-situ measurement hydrometeors are described as function of their maximum length through their 2D projection.

6 Discussion and conclusion

In this study we analyze in-situ aircraft observations of ice hydrometeor images and simultaneous cloud radar observations collected in tropical MCS in order to characterize the statistical properties of ice microphysics. The results are focused on the tropical MCS that include observations from: (i) the raining season over Cayenne (South America), (ii) the North-Australian monsoon over Darwin, (iii) deep convective systems over the Maldives Island in the ITCZ, and (iv) the West-African monsoon over Niamey.

The overall data analysis of ice hydrometeor properties has been performed as a function of temperature and the range of radar reflectivity factors measured at 94GHz. Therefore, all vertical profiles of aircraft onboard radar reflectivity measurements have been gathered and statistically analyzed in order to define delimited radar reflectivity zones, thereby reducing possible vertical bias due to the chosen flight track/altitude in the MCS systems. Hence, this study defines 8 MCS reflectivity zones that have been determined from radar reflectivity factor percentiles (1^{st} 10^{th} 30^{th} 50^{th} 70^{th} 90^{th} and 99^{th}) as a function of temperature, thereby merging all vertical reflectivity profiles of the entire merged dataset used for this study. Analysis of the retrieved vertical wind speeds in each MCS reflectivity zone reveals that the probability to observe a magnitude of vertical winds larger than $1 m.s^{-1}$ are similar in MCS reflectivity zones 1 to 5, but then strongly increase from MCS reflectivity zone 6 to 8. Generally, these probabilities increase with decreasing temperature for all MCS reflectivity zones. Also, the simple magnitude of vertical wind speeds is larger in MCS reflectivity zones 7 and 8, while in MCS reflectivity zones 1 to 6 the magnitude is rather small and similar, however the magnitude is a function of T. Our investigation do not allow to link directly MCS reflectivity zones and the stage of life cycle of *(i.e. Formation, maturation, decaying). The analysis of geostationary satellites data would be more suited for this topic (Fiolleau and Roca 2013). Then, studying the distribution of MCS reflectivity zones as function of life cycle of MCS and brightness temperature and/or visible reflectance could help to answer to this question*.

However, this study demonstrates that MCS reflectivity zones 7 and 8 exhibit highest probability to be related to the active convective zone and/or the most turbulent transition zone between the inaccessible part of the convective core and the stratiform part of MCS clouds, whereas MCS reflectivity zones 1 to 5 are rather associated with the so-called stratiform parts of MCS. MCS reflectivity zone 6 then represents the transition between stratiform and convective area of an MCS with a relatively small median magnitude of vertical winds, however with relatively high probability of vertical wind magnitudes beyond $1 m.s^{-1}$.

Commenté [EF36]: R2#3

Subsequently, the study compares microphysical properties (such as ice water content, extinction, concentrations, largest hydrometeor sizes, etc…) as a function of MCS reflectivity zone and temperature. The statistical analysis (median values, 25th and 75th percentiles) is performed for individual the MCS locations, whereas the merged dataset of the 4 tropical MCS locations serves as a reference. Relative differences of median microphysical properties in one MCS location compared to respective median properties of the reference dataset were quantified. Also uncertainties for all type of microphysical measurements and retrieved cloud parameters were calculated from Baumgardner et al. (2017).

Within the range of uncertainties, we showed that the variability of IWC, σ, $N_{T,50}$, $N_{T,500}$, M_2 and M_3 as a function of temperature and specific MCS reflectivity zones tends to be similar: For example, for IWC these conclusions apply for MCS reflectivity zones 4 to 8. MCS data from Niamey flight campaign (compared to the three other tropical MCS locations) reveal more exceptions when compared with median parameters calculated for the global tropical dataset, with a trend of larger 3rd PSD moments and larger hydrometeor sizes in the stratiform area of MCS. Assuming that largest hydrometeors ($max(D_{max})$) can be considered as a proxy for the aggregation process efficiency,findings of this study reveal that *aggregation process efficiency is higher for MCS over land than over islands and higher over islands close to large land masses than over islands in the middle of an ocean. It seems to confirm the results of Frey et al., (2011) and Cetrone and Houze (2009).*

Commenté [EF37]: R2#17

From the tropical dataset a parametrization of visible extinction is developed as a function of temperature and IWC (Eq. 8). This model allows retrieving σ from OAP measurements with an accuracy smaller than the measurement uncertainty of σ ($U(\sigma)/\sigma$ = 57%; Eq. (2)) for all four types of tropical MCS. Eq. (8) reveals best accuracy to represent directly calculated σ in MCS over Darwin and Niamey.

Also in this study the relationship between mass and size of ice hydrometeors ($m=\alpha.D^{\beta}$) is formulated with a classical power law approximation. A basic finding is that the variability of retrieved β throughout all MCS reflectivity zones is too large compared to its uncertainty. This would mean for example that varying β parameterization in NWP is not worthy to do. Indeed, NWP schemes are used to describe ice microphysics with PSD moments (here M_2 and M_3). Setting β=2 for the mass-size relationship allows to link IWC to the second moment directly as stated in Field et al., (2007).

Defining A as the ratio IWC/M_2, this study illustrates that A increases with temperature. Also A in MCS reflectivity zones 5, 6 and 7 are similar to the median A calculated for the entire dataset (Figure 16(a)). In MCS reflectivity zone 4 (smaller zones were not considered), A tends to be smaller in MCS reflectivity zones 4 and in MCS reflectivity zone 8, A tends to be larger than the median of A for the global tropical dataset. However, MCS reflectivity zones 4 and 8 share a wide range of variability with MCS reflectivity zones 5, 6 and 7. Hence, we use the variability of A as a function of temperature (parametrization in Eq. (13)) to predict the 2nd PSD moment in tropical and mid-latitude MCS. Whereas Eq. (12) retrieves M_2 in all type of MCS with a good accuracy, a correction is needed for high IWC (Eq. 17).

Hence, in this study the model of PSD moments presented by Field et al., (2007), has been considerably modified for PSD in deep convective cloud systems in order to predict the 3rd moment (M_3) from the known 2nd moment (M_2), IWC, and temperature T. This new parametrization of M_3 for deep convective cloud systems and IWC larger than 0.1 g m^{-3} is given by Eq. (12), Eq. (17), Eq. (18) and Eq. (24). The prediction of M_2 (Eq. 17) is more accurate than the prediction of M_3 (Eq. 18), when compared with M_2 and M_3 directly calculated from the measured PSD. Indeed, the predicted M_2 have median relative errors in the range [-25%; 25%] (corresponds to 25th and 75th percentiles of relative error of M_2) with an uncertainty of measured M_2 of about 55%. The predicted M_3 have median relative errors in the range [-40%; 55%] (which corresponds to 25th and 75th percentiles of relative error of M_3) with an uncertainty of measured M_3 of 61%.

Furthermore, we applied on the 4 tropical datasets the method of Field et al., (2007) of PSD rescaling with 2nd and 3rd moments of the measured PSD.

Field et al., (2007) gave for their dataset a parametrized function $\Phi_{2,3}$ that models rescaled PSD in the tropics as a function of the mean diameter (ratio between the 3rd moment and the 2nd moment of the PSD). The calculated rescaled PSD for the 4 tropical datasets are in good agreement with $\Phi_{2,3}$ parametrization given by Field et al., (2007) from diameters between 0.3-6 times the mean diameter (dimensionless characteristic size *x*). Below, 0.3 times the mean diameter, $\Phi_{2,3}$ of Field et al., (2007) tend to overestimate the rescaled PSD and finally underestimate them again below 0.03 times the mean diameter. These differences can be explained because of different diameter threshold to calculate the rescaled PSD. In our study, we calculate rescaled PSD starting at 15µm (or 55µm; see table 1 and Eq. (25)) while Field et al., (2007) used PSD only beyond 100µm. Also for large mean diameters we note significant differences between the rescaled PSD for the dataset of this study and $\Phi_{2,3}$ parametrization from Field et al., (2007). Indeed, for diameters larger than 6 times the mean diameter, $\Phi_{2,3}$ of Field et al., (2007) decreases rapidly and therefore underestimates the rescaled PSD by about 1 order of magnitude at diameters equal to 10 times the mean diameter. We do not think that these differences are due to the difference in the cut-off diameter of PSD (last available diameter for PSD) which has been 20000µm in Field et al., (2007) against 12845µm in this study. Field et al., (2007) used PSD of ice hydrometeors measured in anvils and cirrus clouds while the entire dataset for this study has been gathered closest to MCS stratiform and convective zones of deep convective systems.

This latter fact more likely explains differences between the rescaled PSD of this study and parametrized $\Phi_{2,3}$ from Field et al., (2007). Probably, the underlying dataset for this study contains more large hydrometeors in non-negligible concentrations, and related increased statistics on large hydrometeor concentrations.

The parametrization based on tropical PSD data beyond 15µm seems to degrade parametrization results for largest diameters (rescaled concentrations beyond parametrization). We suspect that this is due to very high concentrations of small hydrometeors in the range 15-55µm in MCS over Maldives Islands, which would finally suggest to recommend parametrization for tropical MCS solely based on PSD beyond 50µm, in order to retrieve ice properties in deep convective clouds that could serve in NWP.

To conclude on the parameterization of ice hydrometeors distribution. We performed an update of the computation of PSD as function of IWC and T performed by Field et al., 2007 for tropical convective clouds (see Eq. (11), Eq. (17) and Eq. (18)). This parameterization was used in the microphysical scheme based on (Wilson and Ballard, 1999) used in the configuration of the Met Office Global Atmosphere version 6.1 (Walters et al., 2017). Which was the version of the Unified Model used operationally by the Met Office for global weather and climate prediction. More precisely, the ice-snow concentrations was computed with the moment parameterization developed by (Field et al., 2007) and the mass-diameter relationship from Cotton et al., (2013). Here, we suggest *to use the new parameterization developed in our study for ice-snow concentrations when IWC are larger than 0.1 g.m^{-3}. Otherwise, we suggest to keep either the original version of Field et al., (2007) parameterization with the Cotton et al., (2013) mass size relationship. Or use the original version of Field et al., (2007) parameterization with A as function of temperature which would be a fit of the 25th percentile of A in MCS reflectivity zone 4 (see Table C12 in Appendices C).*

Commenté [EF38]: R2#6

We showed that IWC tend to be similar as function of temperature and MCS reflectivity zone, suggesting that IWC-Z-T relationship developed by Protat et al., (2016) would be available for IWC larger than 0.1g.m-3 in tropical MCS. In other words there is a confident relationship between IWC, Z and T in tropical MCS. Then, for the evaluation of NWP, we suggest to define the MCS reflectivity zones using the 25th percentiles of IWC as the lower limit of each MCS reflectivity zones (see Table C2 in Appendices C). Hence, for each MCS reflectivity zone visible extinction, hydrometeors concentrations (NT_{50}, NT_{500}, M_2 and M_3), reflectivity factors at 94GHz and vertical velocities from NWP can be compared with the findings of this study (see Table in Appendices C). This methodology should help to identify where NWP fails to represent the links between different parameters and IWC. Indeed, study the spatiotemporal variability of IWC in MCS is a complex topic. It needs a time reference and a space reference. For MCS, the time reference can be its life cycle, but there are MCS that have a more complex life cycle than others (merging of MCS, a new growing stage after a decaying stage). Concerning the space reference, there is a common view which is to observe the MCS from its most active area; its convective part. There are two difficulties to take into account here. First, there are very few direct measurement of cloud microphysic in the very convective area of MCS. Second, MCS can be the aggregation of many convective cells that can be well or not well organized (Houze 2004). Moreover, we saw that large IWC tend to be more associated to vertical movement than lower IWC, but it is not always true.

To test NWP of extreme weather events such MCS, we suggest using the statistic performed in this study, by testing the different conditions of others microphysical parameters observed for a given IWC and temperature.

Commenté [EF39]: R2#7

Finally, several findings from this study suggest more investigations on the variability on the relationship between projected surface and mass of ice hydrometeors encountered in underlying observations. Indeed, we find that ice “density” is similar as a function of *T* and *Z* reflectivity ranges in all 4 MCS locations. Hence, this is referring to the possibility to investigate a surface-mass relationship in MCS that should be a function of *T* and *Z*. Estimating that aerosol loads and corresponding CCN and IN properties may be more or less different in these four locations (continental aerosol over Africa with a strong influence of dust from Sahara, more cleaner troposphere over the Indian ocean, merging of continental and oceanic influences), we stipulate the need of investigating secondary ice production processes, that seem to regulate the concentrations of ice hydrometeors beyond 55µm.

Author contribution

Emmanuel Fontaine, Julien Delanoë, Alfons Schwarzenboëck and Alain Protat for conceptualized this study. John Walter Strapp, Lyle Edward Lilie, Emmanuel Fontaine, Delphine Leroy, Julien Delanoë and Alain Protat for data curation of this study. John Walter Strapp, Lyle Edward Lilie, Delphine Leroy, Julien Delanoë and Emmanuel Fontaine to perform the formal analysis. Alain Protat and Fabien Dezitter for funding acquisition for campaign observations. Alfons Schwarzenboëck, Lyle Edward Lilie, John Walter Strapp, Alain Protat Delphine Leroy, Julien Delanoë and Emmanuel Fontaine for investigations performed in this study. Lyle Edward Lilie, Delphine Leroy, Julien Delanoë and Emmanuel Fontaine for developing methodology used in this study. John Walter Strapp, Fabien Dezitter and Alfons Schwarzenboëck for the project administration. Alfons Schwarzenboëck, John Walter Strapp and Julien Delanoë for providing resources. Lyle Edward Lilie, Delphine Leroy and Emmanuel Fontaine for the development of software used in this study. Alfons Schwarzenboëck for the supervision of this study. Emmanuel Fontaine to provide visualization.

Emmanuel Fontaine for writing original draft. Alfons Schwarzenboëck, Alain Protat, John Walter Strapp, Fabien Dezitter and Julien Delanoë for writing review and editing.

Data availability

The HAIC-HIWC dataset that has been used within this study is shared within the European and North American HAIC/HIWC community for analysis and completion of aircraft industry/rulemaking and science objectives. A data sharing protocol has to be agreed upon and signed by all the parties. This means that post-processed data will be available to public not before January 2021. Therefore we cannot reply positively to demands TS5 and TS11, since rulemaking is actually ongoing within FAA and EASA aviation safety agencies, thereby processing the HAIC/HIWC data set. Concerning the dataset for the campaigns of observations of the Megha-Tropiques project: optical array probes data are available by contacting Alfons Schwarzenboëck and radar data are available by contacting Julien Delanoë.

Acknowledgements

The authors are grateful to Centre National d'Etude Spatiale (CNES) for funding the aircraft measurement campaigns within the Megha-Tropiques project. The data were collected using instruments from the French Airborne Measurement Platform, a facility partially funded by CNRS/INSU and CNES. The research leading to these results (HAIC-HIWC project) has received funding from (i) the European Union's Seventh Framework Program in research, technological development and demonstration under grant agreement no. ACP2-GA-2012-314314, (ii) the European Aviation Safety Agency (EASA) Research Program under service contract no. EASA.2013.FC27, and (iii) the Federal Aviation Administration (FAA), Aviation Research Division, and Aviation Weather Division, under agreement CON-I-1301 with the Centre National de la Recherche Scientifique. Funding to support flight project was also provided by the NASA Aviation Safety Program, the Boeing Co., and Transport Canada. Additional support was also provided by Airbus SAS Operations, Science Engineering Associates, the Bureau of Meteorology, Environment Canada, the National Research Council of Canada, and the universities of Utah and Illinois. The authors thank the SAFIRE facility for the scientific airborne operations. SAFIRE (http://www.safire.fr) is a joint facility of CNRS, Météo-France, and CNES dedicated to flying research aircraft.

References

Bailey, M.P., Hallett, J.: A Comprehensive Habit Diagram for Atmospheric Ice Crystals: Confirmation from the Laboratory, AIRS II, and Other Field Studies. J. Atmos. Sci. 66, 2888–2899. https://doi.org/10.1175/2009JAS2883.1, 2009.

Baumgardner, D., Abel, S.J., Axisa, D., Cotton, R., Crosier, J., Field, P., Gurganus, C., Heymsfield, A., Korolev, A., Krämer, M., Lawson, P., McFarquhar, G., Ulanowski, Z., Um, J.: Cloud Ice Properties: In Situ Measurement

Challenges. Meteorological Monographs 58, 9.1-9.23. https://doi.org/10.1175/AMSMONOGRAPHS-D-16-0011.1, 2017.

Baumgardner, D., Brenguier, J.L., Bucholtz, A., Coe, H., DeMott, P., Garrett, T.J., Gayet, J.F., Hermann, M., Heymsfield, A., Korolev, A., Krämer, M., Petzold, A., Strapp, W., Pilewskie, P., Taylor, J., Twohy, C., Wendisch, M., Bachalo, W., Chuang, P.: Airborne instruments to measure atmospheric aerosol particles, clouds and radiation: A cook's tour of mature and emerging technology. Atmospheric Research 102, 10–29. http://dx.doi.org/10.1016/j.atmosres.2011.06.021, 2011.

Baumgardner, D. and Rodi, A.: Laboratory and Wind Tunnel Evaluations of the Rosemount Icing Detector, J. Atmos. Oceanic Technol., 6(6), 971–979, doi:10.1175/1520-0426(1989)006<0971:LAWTEO>2.0.CO;2, 1989.

Brown, P.R.A., Francis, P.N., 1995. Improved Measurements of the Ice Water Content in Cirrus Using a Total-Water Probe. Journal of Atmospheric and Oceanic Technology 12, 410–414. https://doi.org/10.1175/1520-0426(1995)012<0410:IMOTIW>2.0.CO;2, 1995.

Cetrone, J., Houze, R.A.: Anvil clouds of tropical mesoscale convective systems in monsoon regions. Quarterly Journal of the Royal Meteorological Society 135, 305–317. https://doi.org/10.1002/qj.389, 2009

Claffey, K. J., Jones, K. F. and Ryerson, C. C.: Use and calibration of Rosemount ice detectors for meteorological research, Atmospheric Research, 36(3), 277–286, doi:10.1016/0169-8095(94)00042-C, 1995.

Cober, S. G., Isaac, G. A. and Korolev, A. V.: Assessing the Rosemount Icing Detector with In Situ Measurements, J. Atmos. Oceanic Technol., 18(4), 515–528, doi:10.1175/1520-0426(2001)018<0515:ATRIDW>2.0.CO;2, 2001.

Cotton, R.J., Field, P.R., Ulanowski, Z., Kaye, P.H., Hirst, E., Greenaway, R.S., Crawford, I., Crosier, J., Dorsey, J.: The effective density of small ice particles obtained from in situ aircraft observations of mid-latitude cirrus. Q.J.R. Meteorol. Soc. 139, 1923–1934. https://doi.org/10.1002/qj.2058, 2013.

Coutris, P., Leroy, D., Fontaine, E., Schwarzenboeck, A.: An Inverse Problem approach for the retrieval of ice particle mass from in-situ measurements. J. Atmos. Oceanic Technol. https://doi.org/10.1175/JTECH-D-17-0013.1, 2017

Davison, C. R., Strapp, J. W., Lilie, L., Ratvasky, T. P., and Dumont, C.: Isokinetic TWC Evaporator Probe: Calculations and Systemic Error Analysis, 2016, 8th AIAA Atmospheric and Space Environments Conference, Washington, DC. AIAA-4060. http://dx.doi.org/10.2514/6.2016-4060, June 17, 2016.

Davison, C. R., Landreville, C., and MacLeod, J. D.: Initial Development and Testing of Isokinetic Probe to Measure Total Water Content During Ground and Airborne Testing," NRC, LTR-GTL-2010-0002, Ottawa, Mar. 2010.

Field, P.R., Wood, R., Brown, P.R.A., Kaye, P.H., Hirst, E., Greenaway, R., Smith, J.A.: Ice Particle Interarrival Times Measured with a Fast FSSP. J. Atmos. Oceanic Technol. 20, 249–261. https://doi.org/10.1175/1520-0426(2003)020<0249:IPITMW>2.0.CO;2, 2003.

Delanoë, J., Protat, A., Bouniol, D., Heymsfield, A., Bansemer, A., Brown, P.: The Characterization of Ice Cloud Properties from Doppler Radar Measurements. J. Appl. Meteor. Climatol. 46, 1682–1698. https://doi.org/10.1175/JAM2543.1, 2007.

Delanoë, J.M.E., Heymsfield, A.J., Protat, A., Bansemer, A., Hogan, R.J.: Normalized particle size distribution for remote sensing application. Journal of Geophysical Research: Atmospheres 119, 4204–4227. https://doi.org/10.1002/2013JD020700, 2014.

Delrieu, G., Nicol, J., Yates, E., Kirstetter, P.-E., Creutin, J.-D., Anquetin, S., Obled, C., Saulnier, G.-M., Ducrocq, V., Gaume, E., Payrastre, O., Andrieu, H., Ayral, P.-A., Bouvier, C., Neppel, L., Livet, M., Lang, M., du-Châtelet, J.P., Walpersdorf, A., Wobrock, W.: The Catastrophic Flash-Flood Event of 8–9 September 2002 in the Gard Region, France: A First Case Study for the Cévennes–Vivarais Mediterranean Hydrometeorological Observatory. J. Hydrometeor 6, 34–52. https://doi.org/10.1175/JHM-400.1, 2005.

Drigeard, E., Fontaine, E., Wobrock, W., Schwarzenböck, A., Duroure, C., Williams, E.R., Russell, B., Protat, A., Delanoë, J., Cazenave, F., Gosset, M.: A Comparison of Airborne In Situ Cloud Microphysical Measurement with Ground-Based C-Band Radar Observations in Deep Stratiform Regions of African Squall Lines. J. Appl. Meteor. Climatol. 54, 2461–2477. https://doi.org/10.1175/JAMC-D-14-0262.1, 2015.

Ducrocq, V., Braud, I., Davolio, S., Ferretti, R., Flamant, C., Jansa, A., Kalthoff, N., Richard, E., Taupier-Letage, I., Ayral, P.-A., Belamari, S., Berne, A., Borga, M., Boudevillain, B., Bock, O., Boichard, J.-L., Bouin, M.-N., Bousquet, O., Bouvier, C., Chiggiato, J., Cimini, D., Corsmeier, U., Coppola, L., Cocquerez, P., Defer, E., Delanoë, J., Di Girolamo, P., Doerenbecher, A., Drobinski, P., Dufournet, Y., Fourrié, N., Gourley, J.J., Labatut, L., Lambert, D., Le Coz, J., Marzano, F.S., Molinié, G., Montani, A., Nord, G., Nuret, M., Ramage, K., Rison, W., Roussot, O., Said, F., Schwarzenboeck, A., Testor, P., Van Baelen, J., Vincendon, B., Aran, M., Tamayo, J.: HyMeX-SOP1: The Field Campaign Dedicated to Heavy Precipitation and Flash Flooding in the Northwestern Mediterranean. Bull. Amer. Meteor. Soc. 95, 1083–1100. https://doi.org/10.1175/BAMS-D-12-00244.1, 2013.

Field, P.R., Lawson, R.P., Brown, P.R.A., Lloyd, G., Westbrook, C., Moisseev, D., Miltenberger, A., Nenes, A., Blyth, A., Choularton, T., Connolly, P., Buehl, J., Crosier, J., Cui, Z., Dearden, C., DeMott, P., Flossmann, A., Heymsfield, A., Huang, Y., Kalesse, H., Kanji, Z.A., Korolev, A., Kirchgaessner, A., Lasher-Trapp, S., Leisner, T., McFarquhar, G., Phillips, V., Stith, J., Sullivan, S.: Secondary Ice Production: Current State of the Science and Recommendations for the Future. Meteorological Monographs 58, 7.1-7.20. https://doi.org/10.1175/AMSMONOGRAPHS-D-16-0014.1, 2016.

Field, P. R., Heymsfield, A. J. and Bansemer, A.: Shattering and Particle Interarrival Times Measured by Optical Array Probes in Ice Clouds, J. Atmos. Oceanic Technol., 23(10), 1357–1371, doi:10.1175/JTECH1922.1, 2006.

Field, P.R., Wood, R., Brown, P.R.A., Kaye, P.H., Hirst, E., Greenaway, R., Smith, J.A.: Ice Particle Interarrival Times Measured with a Fast FSSP. J. Atmos. Oceanic Technol. 20, 249–261. https://doi.org/10.1175/1520-0426(2003)020<0249:IPITMW>2.0.CO;2, 2003.

Fiolleau, T., Roca, R.: An Algorithm for the Detection and Tracking of Tropical Mesoscale Convective Systems Using Infrared Images From Geostationary Satellite. Geoscience and Remote Sensing, IEEE Transactions on 51, 4302–4315. https://doi.org/10.1109/TGRS.2012.2227762, 2013.

Fontaine, E., Leroy, D., Schwarzenboeck, A., Delanoë, J., Protat, A., Dezitter, F., Grandin, A., Strapp, J.W., Lilie, L.E.: Evaluation of radar reflectivity factor simulations of ice crystal populations from in situ observations for the retrieval of condensed water content in tropical mesoscale convective systems. Atmos. Meas. Tech. 10, 2239–2252. https://doi.org/10.5194/amt-10-2239-2017, 2017.

Fontaine, E., Schwarzenboeck, A., Delanoë, J., Wobrock, W., Leroy, D., Dupuy, R., Gourbeyre, C., Protat, A.: Constraining mass diameter relations from hydrometeor images and cloud radar reflectivities in tropical continental and oceanic convective anvils. Atmospheric Chemistry and Physics 14, 11367–11392. https://doi.org/10.5194/acp-14-11367-2014, 2014.

Frey, W., Borrmann, S., Kunkel, D., Weigel, R., Reus, M. de, Schlager, H., Roiger, A., Voigt, C., Hoor, P., Curtius, J., Krämer, M., Schiller, C., Volk, C. M., Homan, C. D., Fierli, F., Donfrancesco, G. D., Ulanovsky, A., Ravegnani, F., Sitnikov, N. M., Viciani, S., D'Amato, F., Shur, G. N., Belyaev, G. V., Law, K. S. and Cairo, F.: In situ measurements of tropical cloud properties in the West African Monsoon: upper tropospheric ice clouds, Mesoscale Convective System outflow, and subvisual cirrus, Atmospheric Chemistry and Physics, 11(12), 5569–5590, doi:https://doi.org/10.5194/acp-11-5569-2011, 2011.

Gayet, J.-F., Mioche, G., Bugliaro, L., Protat, A., Minikin, A., Wirth, M., Dörnbrack, A., Shcherbakov, V., Mayer, B., Garnier, A., Gourbeyre, C.: On the observation of unusual high concentration of small chain-like aggregate ice crystals and large ice water contents near the top of a deep convective cloud during the CIRCLE-2 experiment. Atmos. Chem. Phys. 12, 727–744. https://doi.org/10.5194/acp-12-727-2012, 2012.

Heymsfield, A. J., Schmitt, C. and Bansemer, A.: Ice Cloud Particle Size Distributions and Pressure-Dependent Terminal Velocities from In Situ Observations at Temperatures from 0° to −86°C, J. Atmos. Sci., 70(12), 4123–4154, doi:10.1175/JAS-D-12-0124.1, 2013.

Heymsfield, A.J., Bansemer, A., Heymsfield, G., Fierro, A.O.: Microphysics of Maritime Tropical Convective Updrafts at Temperatures from −20° to −60°. Journal of the Atmospheric Sciences 66, 3530–3562. https://doi.org/10.1175/2009JAS3107.1, 2009.

Heymsfield, A.J., Schmitt, C., Bansemer, A., Twohy, C.H.: Improved Representation of Ice Particle Masses Based on Observations in Natural Clouds. Journal of the Atmospheric Sciences 67, 3303–3318. https://doi.org/10.1175/2010JAS3507.1, 2010.

Heymsfield, A.J., Schmitt, C., Bansemer, A., van Zadelhoff, G.-J., McGill, M.J., Twohy, C., Baumgardner, D.: Effective Radius of Ice Cloud Particle Populations Derived from Aircraft Probes. J. Atmos. Oceanic Technol. 23, 361–380. https://doi.org/10.1175/JTECH1857.1, 2006.

Hogan, R.J., Tian, L., Brown, P.R.A., Westbrook, C.D., Heymsfield, A.J., Eastment, J.D.: Radar Scattering from Ice Aggregates Using the Horizontally Aligned Oblate Spheroid Approximation. J. Appl. Meteor. Climatol. 51, 655–671. https://doi.org/10.1175/JAMC-D-11-074.1, 2011.

Houze, R.A.: Mesoscale convective systems. Reviews of Geophysics 42, n/a–n/a. https://doi.org/10.1029/2004RG000150, 2004.

Huffman, G.J., Bolvin, D.T., Nelkin, E.J., Wolff, D.B., Adler, R.F., Gu, G., Hong, Y., Bowman, K.P., Stocker, E.F.: The TRMM Multisatellite Precipitation Analysis (TMPA): Quasi-Global, Multiyear, Combined-Sensor Precipitation Estimates at Fine Scales. J. Hydrometeor 8, 38–55. https://doi.org/10.1175/JHM560.1, 2007.

Jensen, M.P., Ackerman, T.P., Sekelsky, S.M.: Radiative Impacts of Anvil Cloud during the Maritime Continent Thunderstorm Experiment. J. Appl. Meteor. 41, 473–487. https://doi.org/10.1175/1520-0450(2002)041<0473:RIOACD>2.0.CO;2, 2002.

Jensen, M.P., Del Genio, A.D.: Radiative and Microphysical Characteristics of Deep Convective Systems in the Tropical Western Pacific. Journal of Applied Meteorology 42, 1234–1254. https://doi.org/10.1175/1520-0450(2003)042<1234:RAMCOD>2.0.CO;2, 2003.

Korolev, A., Isaac, G.A.: Shattering during Sampling by OAPs and HVPS. Part I: Snow Particles. J. Atmos. Oceanic Technol. 22, 528–542. https://doi.org/10.1175/JTECH1720.1, 2005.

Korolev, A., Sussman, B.: A Technique for Habit Classification of Cloud Particles. Journal of Atmospheric and Oceanic Technology 17, 1048–1057. https://doi.org/10.1175/1520-0426(2000)017<1048:ATFHCO>2.0.CO;2, 2000.

Lawson, R.P., Jensen, E., Mitchell, D.L., Baker, B., Mo, Q., Pilson, B.: Microphysical and radiative properties of tropical clouds investigated in TC4 and NAMMA. Journal of Geophysical Research: Atmospheres 115, n/a–n/a. https://doi.org/10.1029/2009JD013017, 2010.

Lawson, R.P., O'Connor, D., Zmarzly, P., Weaver, K., Baker, B., Mo, Q., Jonsson, H.: The 2D-S (Stereo) Probe: Design and Preliminary Tests of a New Airborne, High-Speed, High-Resolution Particle Imaging Probe. J. Atmos. Oceanic Technol. 23, 1462–1477. https://doi.org/10.1175/JTECH1927.1, 2006.

Leroy, D., Fontaine, E., Schwarzenboeck, A., Strapp, J.W.: Ice Crystal Sizes in High Ice Water Content Clouds. Part 1: On the computation of Median Mass Diameter from in-situ measurements. Journal of Atmospheric and Oceanic Technology 0, null. https://doi.org/10.1175/JTECH-D-15-0151.1, 2016.

Leroy, D., Fontaine, E., Schwarzenboeck, A., Strapp, J. W., Korolev, A., McFarquhar, G., Dupuy, R., Gourbeyre, C., Lilie, L., Protat, A., Delanoe, J., Dezitter, F. and Grandin, A.: Ice Crystal Sizes in High Ice Water Content Clouds. Part II: Statistics of Mass Diameter Percentiles in Tropical Convection Observed during the HAIC/HIWC Project, Journal of Atmospheric and Oceanic Technology, 34(1), 117–136, doi:10.1175/JTECH-D-15-0246.1, 2017.

Li, J.-L., Jiang, J.H., Waliser, D.E., Tompkins, A.M.: Assessing consistency between EOS MLS and ECMWF analyzed and forecast estimates of cloud ice. Geophysical Research Letters 34, n/a–n/a. https://doi.org/10.1029/2006GL029022, 2007.

Li, J.-L., Waliser, D.E., Jiang, J.H., Wu, D.L., Read, W., Waters, J.W., Tompkins, A.M., Donner, L.J., Chern, J.-D., Tao, W.-K., Atlas, R., Gu, Y., Liou, K.N., Del Genio, A., Khairoutdinov, M., Gettelman, A.: Comparisons of EOS MLS cloud ice measurements with ECMWF analyses and GCM simulations: Initial results. Geophysical Research Letters 32, n/a–n/a. https://doi.org/10.1029/2005GL023788, 2005.

Locatelli, J.D., Hobbs, P.V.: Fall speeds and masses of solid precipitation particles. Journal of Geophysical Research 79, 2185–2197. https://doi.org/10.1029/JC079i015p02185, 1974.

Madden, R.A., Julian, P.R.: Observations of the 40–50-Day Tropical Oscillation—A Review. Mon. Wea. Rev. 122, 814–837. https://doi.org/10.1175/1520-0493(1994)122<0814:OOTDTO>2.0.CO;2, 1994.

Madden, R.A., Julian, P.R.: Detection of a 40–50 Day Oscillation in the Zonal Wind in the Tropical Pacific. J. Atmos. Sci. 28, 702–708. https://doi.org/10.1175/1520-0469(1971)028<0702:DOADOI>2.0.CO;2, 1971.

Magono, C., Lee, C., Woo.: Meteorological Classification of Natural Snow Crystals. Journal of the Faculty of Science, Hokkaido University 2(4): 321-335, 1966.

Martini, A., Viltard, N., Ellis, S.M., Fontaine, E.: Ice microphysics retrieval in the convective systems of the Indian Ocean during the CINDY–DYNAMO campaign. Atmospheric Research. http://dx.doi.org/10.1016/j.atmosres.2014.12.013, 2015. McFarquhar, G. M., Timlin, M. S., Rauber, R. M., Jewett, B. F., Grim, J. A. and Jorgensen, D. P.: Vertical Variability of Cloud Hydrometeors in the Stratiform Region of Mesoscale Convective Systems and Bow Echoes, Monthly Weather Review, 135(10), 3405–3428, doi:10.1175/MWR3444.1, 2007.

Mitchell, D.L.: Use of Mass- and Area-Dimensional Power Laws for Determining Precipitation Particle Terminal Velocities. J. Atmos. Sci. 53, 1710–1723. https://doi.org/10.1175/1520-0469(1996)053<1710:UOMAAD>2.0.CO;2, 1996.

Phillips, V.T.J., Patade, S., Gutierrez, J., Bansemer,: A. Secondary ice production by fragmentation of freezing drops: formulation and theory. J. Atmos. Sci. https://doi.org/10.1175/JAS-D-17-0190.1, 2018.

Protat, A., Zawadzki, I.: A Variational Method for Real-Time Retrieval of Three-Dimensional Wind Field from Multiple-Doppler Bistatic Radar Network Data. J. Atmos. Oceanic Technol. 16, 432–449. https://doi.org/10.1175/1520-0426(1999)016<0432:AVMFRT>2.0.CO;2, 1999.

Protat, A., Bouniol, D., Delanoë, J., O'Connor, E., May, P.T., Plana-Fattori, A., Hasson, A., Görsdorf, U., Heymsfield, A.J.: Assessment of Cloudsat Reflectivity Measurements and Ice Cloud Properties Using Ground-Based and Airborne Cloud Radar Observations. J. Atmos. Oceanic Technol. 26, 1717–1741. https://doi.org/10.1175/2009JTECHA1246.1, 2009.

Protat, A., Delanoë, J., Strapp, J.W., Fontaine, E., Leroy, D., Schwarzenboeck, A., Lilie, L., Davison, C., Dezitter, F., Grandin, A., Weber, M.: The Measured Relationship between Ice Water Content and Cloud Radar Reflectivity in Tropical Convective Clouds. Journal of Applied Meteorology and Climatology 55, 1707–1729. https://doi.org/10.1175/JAMC-D-15-0248.1

Pruppacher, H.R., Klett, J.D., Wang, P.K., 1998. Microphysics of Clouds and Precipitation. Aerosol Science and Technology 28, 381–382. https://doi.org/10.1080/02786829808965531, 2016.

Roca, R., Brogniez, H., Chambon, P., Chomette, O., Cloché, S., Gosset, M.E., Mahfouf, J., Raberanto, P., Viltard, N.: The Megha-Tropiques mission: a review after three years in orbit. Frontiers in Earth Science 3. https://doi.org/10.3389/feart.2015.00017, 2015.

Schmitt, C.G., Heymsfield, A.J.: The Dimensional Characteristics of Ice Crystal Aggregates from Fractal Geometry. Journal of the Atmospheric Sciences 67, 1605–1616. https://doi.org/10.1175/2009JAS3187.1, 2010.

Smith, W.L.: 4-D Cloud Properties from Passive Satellite Data and Applications to Resolve the Flight Icing Threat to Aircraft. University Of Wisconsin-Madison. Ph.D thesis, 179pp., 2014.

Stephens, G.L., Vane, D.G., Boain, R.J., Mace, G.G., Sassen, K., Wang, Z., Illingworth, A.J., O'Connor, E.J., Rossow, W.B., Durden, S.L., Miller, S.D., Austin, R.T., Benedetti, A., Mitrescu, C., CloudSat Science Team, T.: THE CLOUDSAT MISSION AND THE A-TRAIN. Bull. Amer. Meteor. Soc. 83, 1771–1790. https://doi.org/10.1175/BAMS-83-12-1771, 2002.

Stith, J.L., Avallone, L.M., Bansemer, A., Basarab, B., Dorsi, S.W., Fuchs, B., Lawson, R.P., Rogers, D.C., Rutledge, S., Toohey, D.W.: Ice particles in the upper anvil regions of midlatitude continental thunderstorms: the case for frozen-drop aggregates. Atmospheric Chemistry and Physics 14, 1973–1985. https://doi.org/10.5194/acp-14-1973-2014, 2014.

Strapp, J.W., Lilie, L.E., Ratvasky, T.P., Davison, C.R., and C. Dumont.: Isokinetic TWC Evaporator Probe: Development of the IKP2 and Performance Testing for the HAIC-HIWC Darwin 2014 and Cayenne Field Campaigns, 8th AIAA Atmospheric and Space Environments Conference, AIAA Aviation, AIAA 2016-4059. http://dx.doi.org/10.2514/6.2016-4059, 2016a.

Strapp, J. W., G. A. Isaac. A. Korolev, T. Ratvasky, R. Potts, P. May, A. Protat, P. Minnis, A. Ackerman, A. Fridlind, J. Haggerty, and J. Riley.: The High Ice Water Content (HIWC) Study of deep convective clouds: Science and technical plan. FAA Rep. DOT/FAA/TC-14/31, available at http://www.tc.faa.gov/its/worldpac/techrpt/tc14-31.pdf. 105 pp., 2016b

Strauss, C., Ricard, D., Lac, C. and Verrelle, A.: Evaluation of turbulence parametrizations in convective clouds and their environment based on a large-eddy simulation, Quarterly Journal of the Royal Meteorological Society, 0(0), doi:10.1002/qj.3614, n.d.

Yano, J.-I., Phillips, V.T.J.: Ice–Ice Collisions: An Ice Multiplication Process in Atmospheric Clouds. J. Atmos. Sci. 68, 322–333. https://doi.org/10.1175/2010JAS3607.1, 2011.

Van de Hulst, H.C.: Light scattering by small particles, 470 pp, Dover, Mineola, N.Y., 1981.

Yost, C.R., Bedka, K.M., Minnis, P., Nguyen, L., Strapp, J.W., Palikonda, R., Khlopenkov, K., Spangenberg, D., Smith Jr., W.L., Protat, A., Delanoe, J.: A prototype method for diagnosing high ice water content probability using satellite imager data. Atmos. Meas. Tech. 11, 1615–1637. https://doi.org/10.5194/amt-11-1615-2018, 2018.

Walters, D., Boutle, I., Brooks, M., Melvin, T., Stratton, R., Vosper, S., Wells, H., Williams, K., Wood, N., Allen, T., Bushell, A., Copsey, D., Earnshaw, P., Edwards, J., Gross, M., Hardiman, S., Harris, C., Heming, J., Klingaman, N., Levine, R., Manners, J., Martin, G., Milton, S., Mittermaier, M., Morcrette, C., Riddick, T., Roberts, M., Sanchez, C., Selwood, P., Stirling, A., Smith, C., Suri, D., Tennant, W., Vidale, P. L., Wilkinson, J., Willett, M., Woolnough, S. and Xavier, P.: The Met Office Unified Model Global Atmosphere 6.0/6.1 and JULES Global Land 6.0/6.1 configurations, Geoscientific Model Development, 10(4), 1487–1520, doi:https://doi.org/10.5194/gmd-10-1487-2017, 2017.

Wilson, D. R. and Ballard, S. P.: A microphysically based precipitation scheme for the UK meteorological office unified model, Quarterly Journal of the Royal Meteorological Society, 125(557), 1607–1636, doi:10.1002/qj.49712555707, 1999.

Yost, C.R., Minnis, P., Ayers, J.K., Spangenberg, D.A., Heymsfield, A.J., Bansemer, A., McGill, M.J., Hlavka, D.L.: Comparison of GOES-retrieved and in situ measurements of deep convective anvil cloud microphysical properties during the Tropical Composition, Cloud and Climate Coupling Experiment (TC4). Journal of Geophysical Research: Atmospheres 115, n/a–n/a. https://doi.org/10.1029/2009JD013313, 2010.

Appendices A: total concentrations since 15 microns

Figure A1 shows median total concentration (N_T) as a function of T and MCS reflectivity zone for the merged datasets where concentrations of ice hydrometeors are integrating beyond 15µm:

$$N_T = \sum_{Dmax=15}^{Dmax=12845} N(D_{max}) \cdot \Delta D_{max} \quad [L^{-1}] \qquad (A1)$$

Median N_T systematically increase with MCS reflectivity zone and altitude, however with significant overlap of 25th and 75th percentiles of neighboring MCS reflectivity zones. Measurement uncertainty on concentrations given for small hydrometeors is about ±100% (Baumgardner et al., 2017).

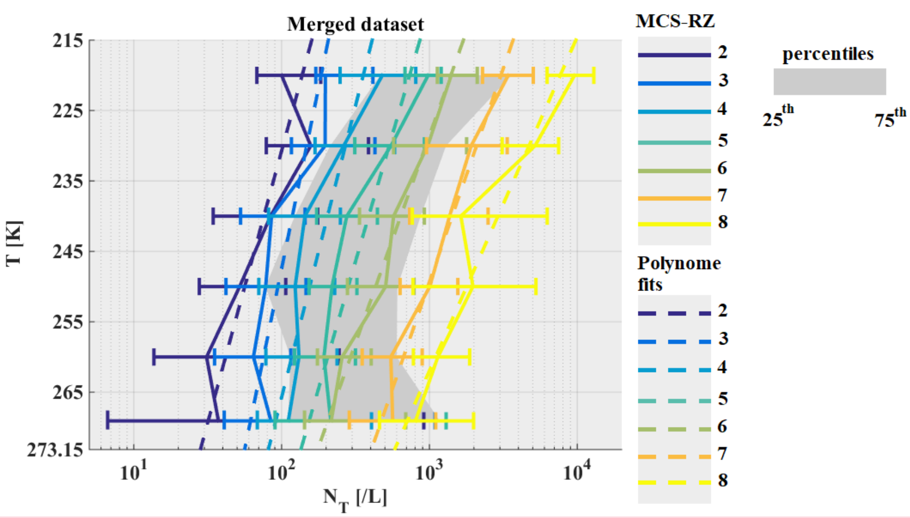

Figure A1: Same as Figure 5, but for concentrations of hydrometeors integrated beyond D_{max} =15µm in [L^{-1}].

Figure A2 (a-d) show MRD-N_T of MCS in the four different tropical locations. For MCS over Darwin and Cayenne, in all MCS reflectivity zones MRD-N_T are smaller than the measurement uncertainty, whereas for Niamey data this is the case only in MCS reflectivity zones 2, 5, 6 and 7. MCS over Maldives Islands yield significantly larger MRD-N_T than the measurement uncertainty, and those are primarily positive. Hence, MCS over Maldives Islands *have larger concentrations of hydrometeors for a same range of T and Z, than the three other types of tropical MCS. However, these larger concentrations observed do not concern zones where highest concentrations of hydrometeors were observed. For example, in MCS reflectivity zone 4 where MRD-*N_T *is reaching 1000%,* N_T *for the Maldives dataset are approximately 1000* L^{-1}*, which is similar to* N_T *observed in MCS reflectivity zones 7 and 8 for the same range of* $T \in [235K; 245K[$ *for the merged dataset. We recall that identical image data processing to remove shattering artefacts and to correct for out of focus images (Field et al., 2003; Korolev and Isaac, 2005; Leroy et al., 2016) have been applied for all 4 tropical datasets. Also the presence of super cooled droplets has been investigated (RICE, CDP probe), and few periods with super cooled water content have been removed for this study. Moreover, we showed in section 5.5 that MCSs over Maldives Islands tend to have smaller max(*D_{max}*) especially in MCS reflectivity zones 4, 5, 6 and 7 compared to the other MCS locations and that concentrations beyond 500µm in Maldives Islands observations are in the same range as the other types of MCS.*

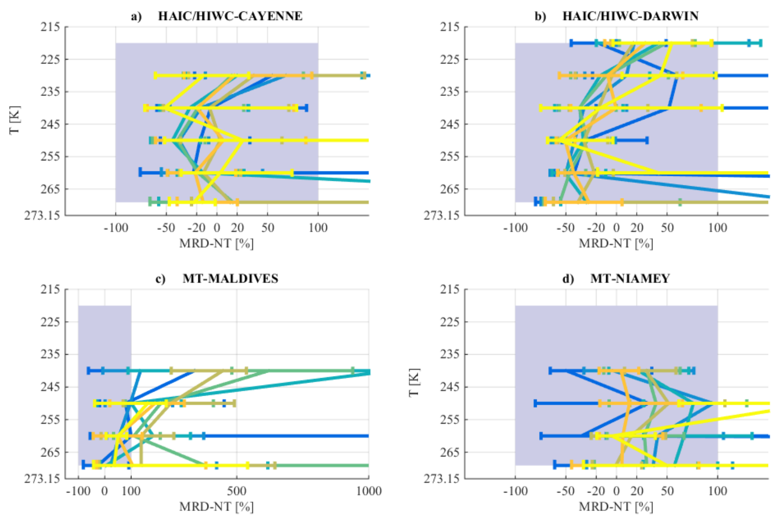

Figure A2: Same as Figure 6, but for MRD-NT.

Commenté [EF40]: R2#13

Appendices B: impact of updraft and downdraft on Median relative errors of IWC and total concentrations

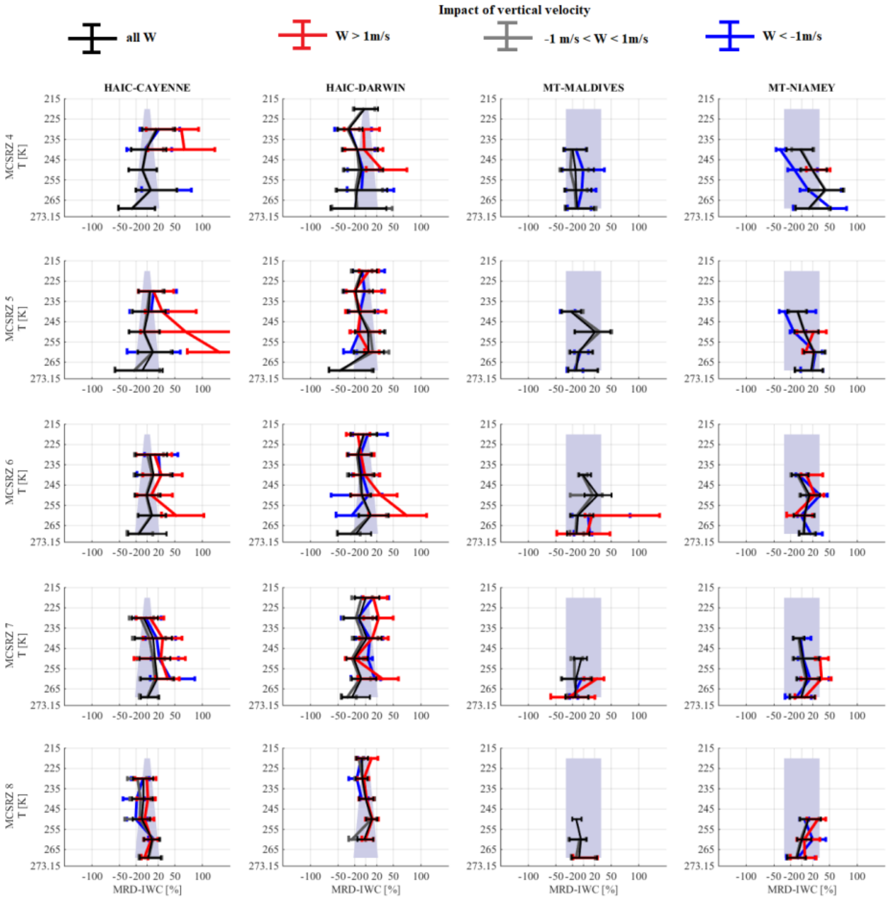

Figure B 1: Median relative difference of IWC (MRD-IWC) with regards to median IWC calculated for the merged dataset in each MCS reflectivity zone (Figure 5). Results are sorted as function of MCSRZ 4 (top line) to MCSRZ 8 bottom line. Blue lines represent MRD-IWC for vertical velocity smaller than -1m/s. Grey lines represent MRD-IWC for vertical velocity larger than -1m/s and smaller than 1m/s. Red lines represent MRD-IWC for vertical velocity larger 1m/s. The black lines represent MRD-IWC when there is no distinction as function of vertical velocity (same as in Figure 6-a, b, c, d).

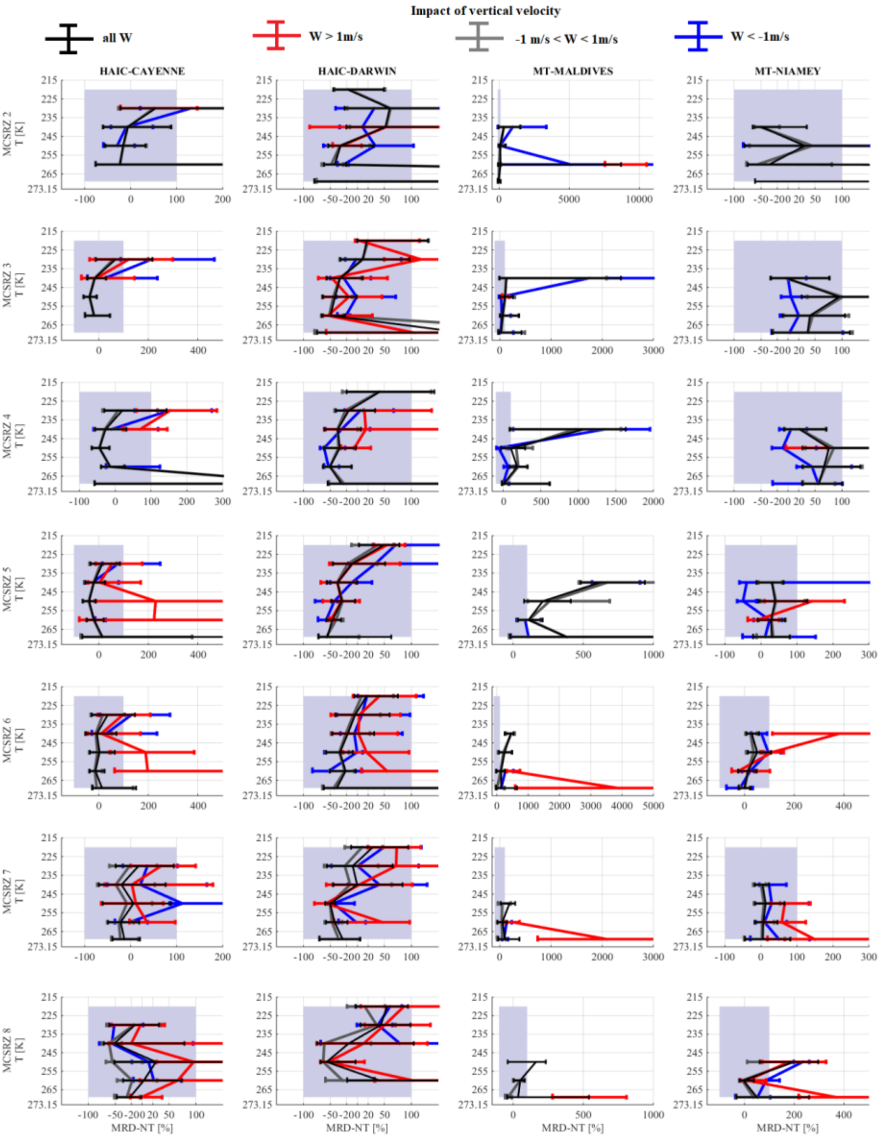

Figure B2: Median relative difference of total concentration of hydrometeors (MRD-NT) with regards to median total concentrations calculated for the merged dataset in each MCS reflectivity zone (Figure A1). Results are sorted as function of MCSRZ 2 (top line) to MCSRZ 8 bottom line. Blue lines represent MRD-NT for vertical velocity smaller than -1m/s. Grey lines represent MRD-NT for vertical velocity larger than -1m/s and smaller than 1m/s. Red lines represent MRD-NT for vertical velocity larger 1m/s. The black lines represent MRD-NT when there is no distinction as function of vertical velocity (same as in Figure A2-a, b, c, d).

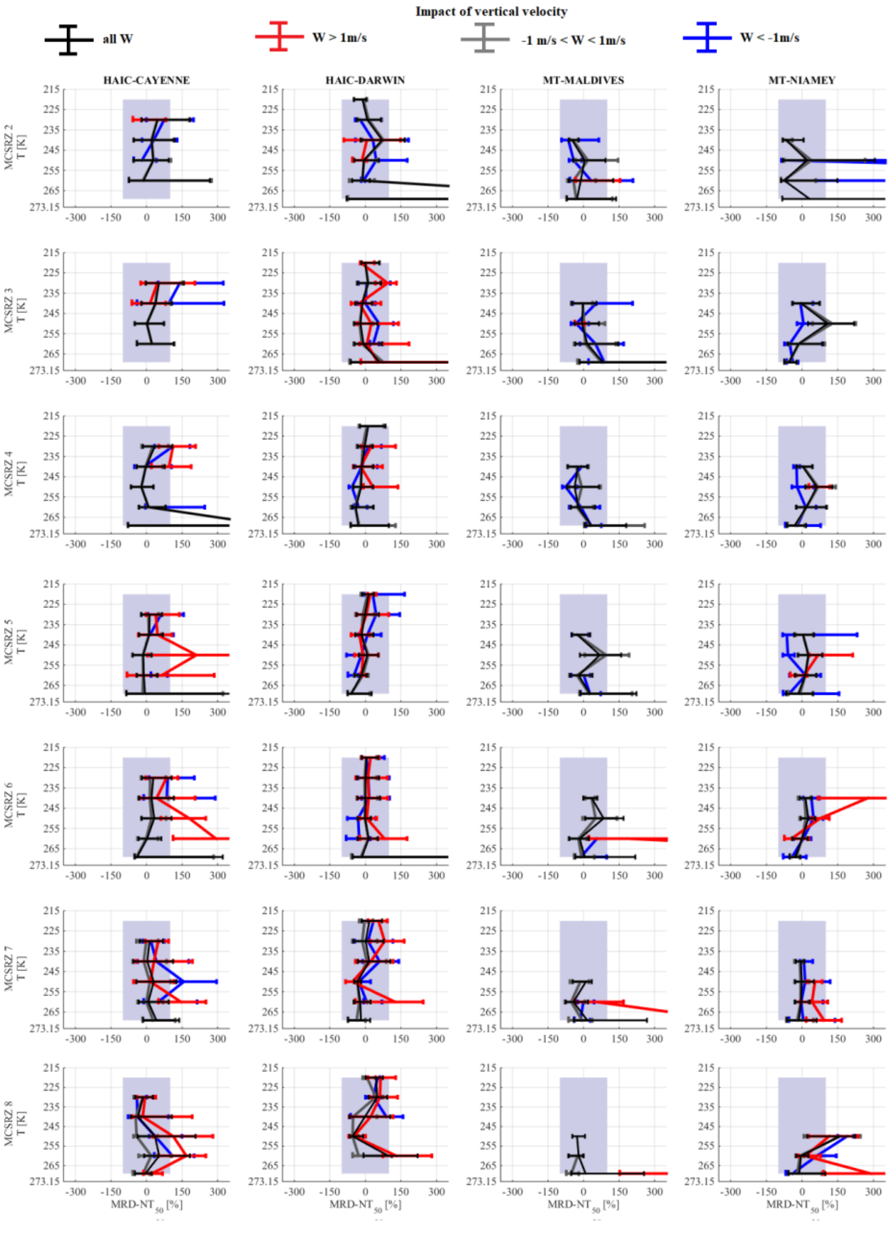

Figure B3: Median relative difference of concentration of hydrometeors summed over Dmax for Dmax larger than 50µm (MRD-NT$_{50}$) with regards to median total concentrations calculated for the merged dataset in each MCS reflectivity zone (Figure 9). Results are sorted as function of MCSRZ 2 (top line) to MCSRZ 8 bottom line. Blue lines represent MRD-NT$_{50}$ for vertical velocity smaller than -1m/s. Grey lines represent MRD-NT$_{50}$ for vertical velocity larger than -1m/s and smaller than 1m/s. Red lines represent

MRD-NT$_{50}$ for vertical velocity larger 1m/s. The black lines represent MRD-NT$_{50}$ when there is no distinction as function of vertical velocity (same as in Figure 10-a, b, c, d).

Appendices C: Tables.

Table C 1: Percentile of Radar reflectivity factors (Z) in [dBZ], shown in solid line in Figure 1.

T [K]	1rst [dBZ]	10th [dBZ]	30th [dBZ]	50th [dBZ]	70th [dBZ]	90th [dBZ]	99th [dBZ]
172.5	-7.00	-3.45	-0.96	0.90	2.83	5.32	11.70
177.5	-8.33	-5.14	-1.96	0.43	2.81	5.49	8.69
182.5	-9.44	-5.96	-3.01	-0.56	2.39	5.51	8.92
187.5	-9.93	-6.66	-4.07	-1.67	1.08	5.33	8.53
192.5	-10.15	-6.79	-4.14	-1.85	0.63	4.97	8.78
197.5	-11.08	-6.95	-3.80	-1.06	1.48	5.18	9.24
202.5	-12.08	-7.53	-3.87	-0.74	2.13	5.37	9.82
207.5	-13.25	-8.06	-4.00	-0.53	2.69	5.75	10.22
212.5	-16.88	-8.65	-4.11	-0.44	3.05	6.28	10.66
217.5	-26.79	-10.67	-4.54	-0.44	3.37	6.93	11.27
222.5	-30.13	-12.58	-5.21	-0.30	3.88	7.71	12.01
227.5	-28.30	-13.55	-5.17	0.06	4.61	8.60	12.94
232.5	-26.65	-13.08	-4.49	0.75	5.54	9.70	14.15
237.5	-26.54	-11.80	-3.26	2.11	6.76	10.92	15.08
242.5	-24.53	-10.27	-1.76	3.62	7.96	11.76	15.76
247.5	-23.78	-8.58	-0.20	5.16	9.13	12.51	15.98
252.5	-22.15	-6.76	1.64	6.58	10.14	13.17	16.37
257.5	-22.05	-5.97	3.18	7.89	11.09	13.78	16.86
262.5	-21.30	-5.83	4.01	8.59	11.44	14.11	17.43
267.5	-21.90	-5.65	3.89	8.26	11.03	13.72	17.34
272.5	-20.68	-5.77	2.88	6.86	9.57	12.60	16.66
277.5	-17.52	-4.84	2.73	6.25	8.90	12.07	16.42
282.5	-15.52	-6.62	-1.12	2.30	5.03	8.33	15.06
287.5	-14.40	-7.55	-2.90	0.40	3.18	7.88	38.13
292.5	-13.67	-7.94	-4.07	-1.37	1.04	4.55	10.49
297.5	-12.95	-7.52	-4.00	-1.18	2.90	27.11	42.87
302.5	-10.98	-4.72	0.81	8.39	14.21	29.74	44.98

Table C 2: Ice water content (IWC) in [g.m^{-3}] (Figure 5)

MCS RZ		**T [215;225[**	**T ∈ [225;235[**	**T∈ [235,245[**	**T∈ [245;255[**	**T∈ [255;265[**	**T ∈ [265;273,15[**
	25th	0.016	0.017	0.016	0.016	0.016	0.016
2	50th	**0.024**	**0.024**	**0.025**	**0.023**	**0.025**	**0.026**

	75th	0.029	0.034	0.042	0.033	0.041	0.063
3	25th	0.042	0.032	0.031	0.040	0.043	0.052
	50th	**0.053**	**0.052**	**0.054**	**0.062**	**0.070**	**0.098**
	75th	0.062	0.076	0.084	0.093	0.111	0.148
4	25th	0.081	0.082	0.090	0.112	0.149	0.136
	50th	**0.110**	**0.119**	**0.130**	**0.160**	**0.212**	**0.198**
	75th	0.138	0.163	0.180	0.216	0.298	0.284
5	25th	0.176	0.199	0.221	0.272	0.316	0.246
	50th	**0.220**	**0.261**	**0.295**	**0.351**	**0.413**	**0.342**
	75th	0.276	0.340	0.395	0.454	0.508	0.476
6	25th	0.402	0.430	0.476	0.561	0.556	0.479
	50th	**0.538**	**0.572**	**0.628**	**0.690**	**0.701**	**0.624**
	75th	0.662	0.742	0.822	0.818	0.863	0.762
7	25th	0.869	0.767	0.994	1.057	1.102	0.928
	50th	**1.083**	**1.069**	**1.294**	**1.295**	**1.402**	**1.204**
	75th	1.365	1.424	1.640	1.704	1.797	1.526
8	25th	1.604	1.644	1.951	2.116	2.009	1.443
	50th	**1.810**	**2.051**	**2.306**	**2.515**	**2.268**	**1.827**
	75th	1.998	2.352	2.690	2.907	2.555	2.282

Table C 3: visible extinction (σ) in [m^{-1}] (Figure 7).

MCS RZ		**T ∈[215;225[**	**T∈ [225;235[**	**T∈ [235,245[**	**T ∈ [245;255[**	**T∈ [255;265[**	**T [265;273,15[**
2	25th	0.00047	0.00071	0.00044	0.00045	0.00031	0.00013
	50th	**0.00097**	**0.00112**	**0.00102**	**0.00088**	**0.00078**	**0.00060**
	75th	0.00125	0.00172	0.00169	0.00128	0.00184	0.00413
3	25th	0.00253	0.00188	0.00166	0.00140	0.00135	0.00118
	50th	**0.00321**	**0.00262**	**0.00225**	**0.00205**	**0.00226**	**0.00217**
	75th	0.00363	0.00352	0.00316	0.00310	0.00337	0.00453
4	25th	0.00521	0.00400	0.00342	0.00355	0.00400	0.00284
	50th	**0.00616**	**0.00529**	**0.00466**	**0.00500**	**0.00542**	**0.00410**

	75th	0.00803	0.00697	0.00640	0.00685	0.00769	0.00762
5	25th	0.00978	0.00855	0.00785	0.00765	0.00749	0.00457
	50th	**0.01237**	**0.01101**	**0.01042**	**0.01030**	**0.00997**	**0.00693**
	75th	0.01484	0.01413	0.01348	0.01292	0.01281	0.01223
6	25th	0.01972	0.01674	0.01550	0.01512	0.01169	0.00900
	50th	**0.02478**	**0.02256**	**0.02088**	**0.01969**	**0.01596**	**0.01173**
	75th	0.03040	0.02904	0.02745	0.02387	0.01995	0.01515
7	25th	0.03969	0.02892	0.03133	0.02726	0.02393	0.01722
	50th	**0.04893**	**0.04083**	**0.04149**	**0.03386**	**0.03103**	**0.02404**
	75th	0.06096	0.05435	0.05773	0.04571	0.04127	0.03271
8	25th	0.06965	0.05976	0.05243	0.05033	0.04139	0.01991
	50th	**0.07865**	**0.07116**	**0.06944**	**0.06461**	**0.05125**	**0.03443**
	75th	0.08871	0.08247	0.08206	0.07942	0.06088	0.04287

Table C 4: Total concentration beyond 15µm (N_T) in [L^{-1}] (Figure A1).

MCS RZ		**T ∈[215;225[**	**T∈ [225;235[**	**T∈ [235,245[**	**T∈ [245;255[**	**T∈ [255;265[**	**T [265;273,15[**
2	25th	3.65E+01	7.73E+01	3.12E+01	2.51E+01	1.25E+01	6.01E+00
	50th	**7.41E+01**	**1.53E+02**	**8.32E+01**	**5.03E+01**	**3.11E+01**	**4.26E+01**
	75th	1.58E+02	3.62E+02	1.73E+02	1.20E+02	6.54E+02	2.14E+03
3	25th	1.67E+02	1.11E+02	5.11E+01	3.99E+01	3.24E+01	3.58E+01
	50th	**1.91E+02**	**1.92E+02**	**8.26E+01**	**7.46E+01**	**5.95E+01**	**7.92E+01**
	75th	3.79E+02	4.22E+02	1.42E+02	1.36E+02	1.10E+02	7.41E+02
4	25th	2.20E+02	1.56E+02	7.86E+01	6.92E+01	7.37E+01	6.47E+01
	50th	**4.65E+02**	**2.42E+02**	**1.34E+02**	**1.22E+02**	**1.23E+02**	**1.06E+02**
	75th	7.04E+02	5.41E+02	2.33E+02	2.27E+02	2.22E+02	4.02E+02
5	25th	6.63E+02	3.07E+02	1.70E+02	1.44E+02	1.19E+02	8.88E+01
	50th	**9.67E+02**	**5.45E+02**	**2.72E+02**	**2.10E+02**	**1.87E+02**	**2.14E+02**
	75th	1.17E+03	9.25E+02	4.39E+02	3.14E+02	3.11E+02	1.37E+03
6	25th	1.13E+03	5.70E+02	3.32E+02	2.73E+02	1.71E+02	1.38E+02
	50th	**1.40E+03**	**9.66E+02**	**5.64E+02**	**4.74E+02**	**2.51E+02**	**2.15E+02**

	75th	2.10E+03	1.77E+03	9.09E+02	7.59E+02	3.93E+02	6.93E+02
	25th	2.28E+03	9.57E+02	7.26E+02	6.30E+02	3.37E+02	2.70E+02
7	**50th**	**3.40E+03**	**1.91E+03**	**1.35E+03**	**9.98E+02**	**5.37E+02**	**5.58E+02**
	75th	5.05E+03	3.35E+03	2.45E+03	1.53E+03	8.78E+02	1.10E+03
	25th	6.26E+03	3.08E+03	7.64E+02	7.81E+02	7.63E+02	4.61E+02
8	**50th**	**9.55E+03**	**5.13E+03**	**1.68E+03**	**1.96E+03**	**1.13E+03**	**8.05E+02**
	75th	1.28E+04	7.37E+03	6.09E+03	5.20E+03	1.82E+03	1.99E+03

Table C 5: Total concentration since 50µm (*$N_{T\,50}$*) in [L^{-1}] (Figure 9).

MCS RZ		**T ∈[215;225[**	**T∈ [225;235[**	**T∈ [235,245[**	**T∈ [245;255[**	**T∈ [255;265[**	**T [265;273,15[**
	25th	8.65E+00	1.72E+01	5.24E+00	3.98E+00	1.18E+00	7.57E-01
2	**50th**	**2.13E+01**	**3.21E+01**	**1.68E+01**	**9.13E+00**	**4.49E+00**	**3.32E+00**
	75th	3.99E+01	5.77E+01	3.26E+01	1.90E+01	1.21E+01	4.28E+01
	25th	4.16E+01	3.05E+01	1.35E+01	8.50E+00	4.42E+00	2.18E+00
3	**50th**	**4.75E+01**	**4.70E+01**	**2.19E+01**	**1.39E+01**	**8.82E+00**	**4.79E+00**
	75th	8.35E+01	7.79E+01	3.68E+01	2.60E+01	1.74E+01	2.07E+01
	25th	6.38E+01	4.66E+01	2.15E+01	1.47E+01	1.02E+01	7.28E+00
4	**50th**	**1.05E+02**	**7.25E+01**	**3.56E+01**	**2.78E+01**	**1.72E+01**	**1.38E+01**
	75th	1.64E+02	1.23E+02	6.21E+01	4.49E+01	3.03E+01	2.46E+01
	25th	1.57E+02	9.14E+01	4.70E+01	3.33E+01	1.83E+01	1.11E+01
5	**50th**	**2.06E+02**	**1.39E+02**	**7.26E+01**	**5.66E+01**	**3.03E+01**	**2.30E+01**
	75th	2.49E+02	2.10E+02	1.14E+02	8.17E+01	4.78E+01	4.39E+01
	25th	2.68E+02	1.55E+02	9.50E+01	7.22E+01	3.00E+01	1.78E+01
6	**50th**	**3.28E+02**	**2.47E+02**	**1.50E+02**	**1.06E+02**	**4.91E+01**	**2.86E+01**
	75th	4.84E+02	4.12E+02	2.34E+02	1.45E+02	7.25E+01	6.47E+01
	25th	5.65E+02	2.49E+02	2.07E+02	1.36E+02	7.20E+01	3.35E+01
7	**50th**	**7.83E+02**	**4.92E+02**	**3.41E+02**	**1.90E+02**	**1.13E+02**	**9.02E+01**
	75th	1.12E+03	8.00E+02	6.20E+02	3.08E+02	1.84E+02	1.74E+02
8	25th	1.34E+03	7.26E+02	2.06E+02	1.90E+02	1.82E+02	7.29E+01

	50th	**1.82E+03**	**1.09E+03**	**3.86E+02**	**4.01E+02**	**2.83E+02**	**1.57E+02**
	75th	2.30E+03	1.51E+03	1.31E+03	9.29E+02	4.95E+02	3.10E+02

Table C 6: Total concentration since 500µm (*$N_{T\,500}$*) in [L^{-1}] (Figure 11).

MCS RZ		**T ∈[215;225[**	**T∈ [225;235[**	**T∈ [235,245[**	**T∈ [245;255[**	**T∈ [255;265[**	**T∈ [265;273,15[**
	25th	0.00E+00	1.96E-02	4.08E-02	1.33E-01	8.31E-02	1.68E-02
2	**50th**	**5.20E-02**	**7.23E-02**	**1.73E-01**	**3.41E-01**	**2.86E-01**	**8.60E-02**
	75th	2.05E-01	1.88E-01	4.13E-01	7.27E-01	6.52E-01	3.37E-01
	25th	1.12E+00	4.23E-01	8.37E-01	1.09E+00	8.64E-01	3.57E-01
3	**50th**	**1.57E+00**	**8.68E-01**	**1.33E+00**	**1.61E+00**	**1.40E+00**	**6.67E-01**
	75th	2.03E+00	1.43E+00	1.91E+00	2.22E+00	2.07E+00	1.29E+00
	25th	2.77E+00	1.92E+00	2.26E+00	2.96E+00	2.73E+00	1.67E+00
4	**50th**	**3.77E+00**	**2.73E+00**	**3.15E+00**	**3.95E+00**	**3.91E+00**	**2.40E+00**
	75th	4.54E+00	3.84E+00	4.40E+00	5.06E+00	5.51E+00	3.52E+00
	25th	5.61E+00	5.55E+00	5.71E+00	5.83E+00	5.29E+00	2.82E+00
5	**50th**	**7.78E+00**	**7.26E+00**	**7.68E+00**	**7.78E+00**	**7.19E+00**	**4.15E+00**
	75th	9.34E+00	9.48E+00	1.01E+01	1.02E+01	8.98E+00	6.60E+00
	25th	1.25E+01	1.27E+01	1.19E+01	1.21E+01	9.61E+00	3.83E+00
6	**50th**	**1.55E+01**	**1.60E+01**	**1.56E+01**	**1.45E+01**	**1.24E+01**	**6.07E+00**
	75th	1.97E+01	2.02E+01	2.06E+01	1.74E+01	1.53E+01	9.17E+00
	25th	2.26E+01	2.00E+01	2.41E+01	2.01E+01	1.83E+01	8.29E+00
7	**50th**	**2.83E+01**	**2.65E+01**	**3.08E+01**	**2.52E+01**	**2.42E+01**	**1.54E+01**
	75th	3.34E+01	3.35E+01	3.96E+01	3.44E+01	3.35E+01	2.40E+01
	25th	1.95E+01	2.69E+01	3.35E+01	3.71E+01	2.67E+01	1.06E+01
8	**50th**	**2.38E+01**	**3.75E+01**	**4.89E+01**	**4.99E+01**	**3.73E+01**	**2.43E+01**
	75th	2.85E+01	5.23E+01	7.29E+01	6.87E+01	4.86E+01	3.80E+01

Table C 7: pre-factor α of mass size relationship in [g cm$^{-\beta}$] (Figure 15).

MCS RZ		T ∈[215;225[	T∈ [225;235[	T∈ [235,245[	T∈ [245;255[	T∈ [255;265[	T [265;273,15[
2	25th	0.00095	0.00042	0.00053	0.00086	0.00152	0.00114
	50th	**0.00269**	**0.00099**	**0.00128**	**0.00172**	**0.00341**	**0.00322**
	75th	0.00574	0.00276	0.00320	0.00312	0.00876	0.00809
3	25th	0.00092	0.00059	0.00099	0.00149	0.00190	0.00319
	50th	**0.00126**	**0.00115**	**0.00181**	**0.00241**	**0.00341**	**0.00687**
	75th	0.00154	0.00197	0.00299	0.00379	0.00630	0.01077
4	25th	0.00142	0.00126	0.00184	0.00250	0.00343	0.00385
	50th	**0.00180**	**0.00198**	**0.00274**	**0.00340**	**0.00505**	**0.00592**
	75th	0.00235	0.00282	0.00404	0.00470	0.00711	0.00826
5	25th	0.00195	0.00188	0.00267	0.00333	0.00422	0.00481
	50th	**0.00241**	**0.00258**	**0.00351**	**0.00414**	**0.00562**	**0.00658**
	75th	0.00300	0.00336	0.00455	0.00529	0.00742	0.00950
6	25th	0.00189	0.00210	0.00324	0.00419	0.00486	0.00595
	50th	**0.00271**	**0.00285**	**0.00403**	**0.00513**	**0.00625**	**0.00782**
	75th	0.00334	0.00380	0.00492	0.00638	0.00793	0.01014
7	25th	0.00163	0.00253	0.00325	0.00466	0.00527	0.00594
	50th	**0.00245**	**0.00351**	**0.00415**	**0.00560**	**0.00637**	**0.00774**
	75th	0.00326	0.00447	0.00517	0.00668	0.00776	0.01077
8	25th	0.00214	0.00302	0.00363	0.00405	0.00538	0.00637
	50th	**0.00418**	**0.00485**	**0.00496**	**0.00558**	**0.00712**	**0.00953**
	75th	0.00748	0.00750	0.00679	0.00819	0.01173	0.01886

Table C 8: exponent of mass-size relationship β [no dimension] (Figure 13).

MCS RZ		T ∈[215;225[	T∈ [225;235[	T∈ [235,245[	T∈ [245;255[	T∈ [255;265[	T [265;273,15[
2	25th	1.67	1.54	1.58	1.66	1.74	1.66
	50th	**1.86**	**1.76**	**1.78**	**1.85**	**1.95**	**1.93**

	75th	2.07	1.96	1.99	2.02	2.21	2.08
3	25th	1.80	1.65	1.75	1.79	1.86	1.86
	50th	**1.88**	**1.82**	**1.91**	**1.92**	**2.00**	**2.08**
	75th	1.95	1.96	2.04	2.05	2.17	2.35
4	25th	1.90	1.82	1.87	1.91	1.96	1.94
	50th	**1.98**	**1.94**	**1.99**	**2.02**	**2.10**	**2.10**
	75th	2.03	2.04	2.10	2.12	2.22	2.26
5	25th	1.99	1.91	1.96	1.97	2.02	2.05
	50th	**2.07**	**2.00**	**2.06**	**2.05**	**2.11**	**2.16**
	75th	2.12	2.08	2.14	2.14	2.21	2.29
6	25th	1.91	1.92	2.01	2.04	2.03	2.04
	50th	**2.06**	**2.01**	**2.09**	**2.11**	**2.11**	**2.16**
	75th	2.14	2.11	2.16	2.19	2.20	2.26
7	25th	1.86	1.97	1.99	2.06	2.06	2.07
	50th	**2.00**	**2.08**	**2.08**	**2.13**	**2.13**	**2.15**
	75th	2.10	2.17	2.16	2.19	2.19	2.26
8	25th	1.93	1.98	1.97	2.01	2.07	2.10
	50th	**2.11**	**2.13**	**2.08**	**2.13**	**2.16**	**2.21**
	75th	2.27	2.25	2.19	2.22	2.29	2.34

Table C 9: ***max(D_{max})*** **in [cm] (Figure 17).**

MCS RZ		**T ∈[215;225[**	**T∈ [225;235[**	**T∈ [235,245[**	**T∈ [245;255[**	**T∈ [255;265[**	**T [265;273,15[**
2	25th	0.048	0.061	0.090	0.105	0.125	0.105
	50th	**0.090**	**0.095**	**0.110**	**0.140**	**0.195**	**0.165**
	75th	0.120	0.115	0.140	0.195	0.361	0.255
3	25th	0.155	0.120	0.145	0.155	0.205	0.245
	50th	**0.175**	**0.145**	**0.190**	**0.205**	**0.310**	**0.435**
	75th	0.195	0.180	0.265	0.295	0.620	0.762
4	25th	0.205	0.170	0.195	0.215	0.280	0.332
	50th	**0.235**	**0.212**	**0.260**	**0.347**	**0.525**	**0.445**

	75th	0.265	0.270	0.380	0.615	0.790	0.775
5	25th	0.235	0.225	0.265	0.280	0.350	0.415
	50th	**0.280**	**0.280**	**0.375**	**0.405**	**0.625**	**0.615**
	75th	0.340	0.355	0.575	0.685	0.820	0.795
6	25th	0.245	0.245	0.310	0.335	0.385	0.475
	50th	**0.315**	**0.310**	**0.460**	**0.665**	**0.625**	**0.735**
	75th	0.395	0.435	0.680	0.880	0.810	0.838
7	25th	0.225	0.270	0.325	0.445	0.480	0.557
	50th	**0.285**	**0.397**	**0.452**	**0.675**	**0.675**	**0.745**
	75th	0.375	0.595	0.645	0.846	0.810	0.825
8	25th	0.335	0.315	0.395	0.445	0.445	0.455
	50th	**0.455**	**0.480**	**0.555**	**0.632**	**0.595**	**0.635**
	75th	0.665	0.730	0.790	0.825	0.740	0.745

Table C 10: Second Moment of PSD (*M_2*) [m^{-1}] (Figure 21).

MCS RZ		T∈ [215;225[	T∈ [225;235[	T∈ [235,245[	T∈ [245;255[	T∈ [255;265[	T ∈ [265;273,15[
2	25th	4.33E-04	5.99E-04	3.90E-04	4.41E-04	3.03E-04	1.22E-04
	50th	**8.04E-04**	**9.32E-04**	**8.67E-04**	**8.18E-04**	**7.10E-04**	**5.50E-04**
	75th	9.78E-04	1.37E-03	1.42E-03	1.20E-03	1.57E-03	2.62E-03
3	25th	2.26E-03	1.71E-03	1.50E-03	1.36E-03	1.26E-03	1.01E-03
	50th	**2.85E-03**	**2.32E-03**	**2.03E-03**	**1.98E-03**	**2.07E-03**	**1.83E-03**
	75th	3.21E-03	3.08E-03	2.80E-03	2.80E-03	3.01E-03	3.50E-03
4	25th	4.59E-03	3.60E-03	3.10E-03	3.30E-03	3.70E-03	2.71E-03
	50th	**5.43E-03**	**4.73E-03**	**4.17E-03**	**4.60E-03**	**4.99E-03**	**3.72E-03**
	75th	6.99E-03	6.10E-03	5.69E-03	6.38E-03	6.91E-03	6.39E-03
5	25th	8.78E-03	7.82E-03	7.20E-03	7.11E-03	7.07E-03	4.43E-03
	50th	**1.13E-02**	**9.99E-03**	**9.56E-03**	**9.55E-03**	**9.19E-03**	**6.49E-03**
	75th	1.34E-02	1.27E-02	1.23E-02	1.21E-02	1.17E-02	1.07E-02
6	25th	1.79E-02	1.60E-02	1.42E-02	1.40E-02	1.10E-02	8.29E-03
	50th	**2.28E-02**	**2.09E-02**	**1.95E-02**	**1.83E-02**	**1.48E-02**	**1.06E-02**

	75th	2.77E-02	2.66E-02	2.53E-02	2.25E-02	1.85E-02	1.38E-02
7	25th	3.57E-02	2.75E-02	2.93E-02	2.57E-02	2.27E-02	1.53E-02
	50th	**4.41E-02**	**3.79E-02**	**3.86E-02**	**3.22E-02**	**2.96E-02**	**2.21E-02**
	75th	5.39E-02	4.94E-02	5.29E-02	4.31E-02	3.95E-02	3.11E-02
8	25th	6.02E-02	5.30E-02	4.92E-02	4.77E-02	3.96E-02	1.85E-02
	50th	**6.73E-02**	**6.39E-02**	**6.39E-02**	**6.21E-02**	**4.95E-02**	**3.23E-02**
	75th	7.41E-02	7.30E-02	7.36E-02	7.53E-02	5.84E-02	4.27E-02

Table C 11: Third moment of PSD (M_3) in [1] (Figure 23).

MCS RZ		**T ∈[215;225[**	**T∈ [225;235[**	**T∈ [235,245[**	**T∈ [245;255[**	**T∈ [255;265[**	**T ∈ [265;273,15[**
2	25th	1.29E-07	1.30E-07	1.07E-07	1.43E-07	1.68E-07	5.16E-08
	50th	**1.78E-07**	**2.09E-07**	**2.29E-07**	**2.98E-07**	**3.83E-07**	**1.92E-07**
	75th	2.12E-07	2.98E-07	4.00E-07	5.38E-07	6.36E-07	5.66E-07
3	25th	7.85E-07	5.40E-07	6.75E-07	7.36E-07	8.89E-07	7.74E-07
	50th	**1.06E-06**	**8.08E-07**	**9.69E-07**	**1.11E-06**	**1.56E-06**	**1.92E-06**
	75th	1.27E-06	1.08E-06	1.43E-06	1.67E-06	3.59E-06	5.23E-06
4	25th	1.85E-06	1.47E-06	1.75E-06	2.15E-06	3.08E-06	2.52E-06
	50th	**2.44E-06**	**1.99E-06**	**2.43E-06**	**3.57E-06**	**5.71E-06**	**3.98E-06**
	75th	3.08E-06	2.80E-06	3.61E-06	5.99E-06	1.13E-05	1.12E-05
5	25th	4.13E-06	3.92E-06	4.59E-06	4.80E-06	5.95E-06	5.13E-06
	50th	**5.55E-06**	**5.20E-06**	**6.64E-06**	**7.83E-06**	**1.08E-05**	**8.69E-06**
	75th	7.08E-06	6.84E-06	9.57E-06	1.13E-05	1.93E-05	1.93E-05
6	25th	9.42E-06	8.92E-06	9.88E-06	9.93E-06	9.93E-06	8.90E-06
	50th	**1.19E-05**	**1.17E-05**	**1.45E-05**	**1.77E-05**	**1.66E-05**	**1.75E-05**
	75th	1.43E-05	1.51E-05	1.93E-05	2.50E-05	2.54E-05	2.62E-05
7	25th	1.66E-05	1.75E-05	1.98E-05	2.51E-05	2.37E-05	1.91E-05
	50th	**2.02E-05**	**2.16E-05**	**2.63E-05**	**3.05E-05**	**3.35E-05**	**3.28E-05**
	75th	2.36E-05	2.71E-05	3.20E-05	3.82E-05	4.24E-05	4.25E-05
8	25th	2.07E-05	2.20E-05	2.80E-05	3.13E-05	2.74E-05	1.54E-05

	50th	**2.27E-05**	**2.69E-05**	**3.29E-05**	**4.16E-05**	**3.89E-05**	**2.84E-05**
	75th	2.45E-05	3.21E-05	4.30E-05	5.76E-05	5.22E-05	4.57E-05

Table C 12: coefficient *A* in [kg m^{-2}] (Figure 25).

MCS RZ		**T ∈[215;225[**	**T∈ [225;235[**	**T∈ [235,245[**	**T∈ [245;255[**	**T∈ [255;265[**	**T ∈ [265;273,15[**
	25th	0.021	0.018	0.018	0.019	0.017	0.019
2	**50th**	**0.031**	**0.025**	**0.032**	**0.031**	**0.041**	**0.048**
	75th	0.042	0.038	0.064	0.054	0.085	0.163
	25th	0.017	0.016	0.018	0.024	0.025	0.029
3	**50th**	**0.018**	**0.023**	**0.026**	**0.032**	**0.037**	**0.052**
	75th	0.020	0.030	0.036	0.041	0.051	0.071
	25th	0.017	0.019	0.023	0.027	0.034	0.037
4	**50th**	**0.020**	**0.025**	**0.029**	**0.034**	**0.042**	**0.048**
	75th	0.021	0.031	0.038	0.043	0.051	0.061
	25th	0.018	0.022	0.026	0.031	0.038	0.038
5	**50th**	**0.020**	**0.026**	**0.031**	**0.037**	**0.045**	**0.047**
	75th	0.023	0.030	0.037	0.045	0.053	0.061
	25th	0.021	0.024	0.028	0.033	0.042	0.047
6	**50th**	**0.023**	**0.027**	**0.032**	**0.037**	**0.048**	**0.057**
	75th	0.026	0.031	0.038	0.045	0.057	0.069
	25th	0.023	0.025	0.028	0.036	0.041	0.047
7	**50th**	**0.024**	**0.028**	**0.032**	**0.040**	**0.046**	**0.054**
	75th	0.027	0.031	0.038	0.044	0.053	0.064
	25th	0.025	0.029	0.032	0.035	0.041	0.048
8	**50th**	**0.027**	**0.032**	**0.038**	**0.039**	**0.045**	**0.060**
	75th	0.030	0.035	0.045	0.047	0.053	0.080

Appendices D: summary of inter-comparison of ice microphysical properties in MCS.

Table D1 summarizes qualitatively the findings for IWC, visible extinction (σ), total concentrations ($N_{T,50}$ for D_{max}>50µm; $N_{T,500}$ for D_{max}>500µm), 2nd moment (M_2) and 3rd moment (M_3) of hydrometeor PSD, and largest hydrometeors sizes (*max*(D_{max})). It highlights the main tendencies of microphysical parameters in each types of MCS with regards to the median calculation performed for the merged dataset, such: ≅ for similar values, + for larger values and – for smaller values than merged dataset. Also, it points out the exceptions noting their location as function of the temperature range and the MCS reflectivity zones.

Commenté [EF41]: Author's correction

Table D1: Evaluation of parameter X (X for IWC, σ, $N_{T,55}$, $N_{T,500}$, , M_2, M_3 and *max*(D_{max})) , for each type of tropical MCS (Darwin, Cayenne, Maldives Islands, Niamey) with respect to the global tropical dataset thereby comparing median values in corresponding MCS reflectivity zones. Two sub-columns for each type of MCS: The first column gives an evaluation of the main trend: ≅ if MRD-X is comparable to the uncertainty range, + if MRD-X is larger than the uncertainty range, - for smaller values. In the second sub-column are reported the number of exceptions with respect to the main trend (first column) with: Z(Y)≅ or Z(Y)+ or Z(Y)-. Z number stands for a particular MCS reflectivity zone (with Z= 2, 3, 4, 5, 6, 7, 8) , Y number represents a particular T range (with Y=1 for T ∈ [265K; 273.15K[, Y=2 for T ∈ [255K, 265K[, Y=3 for T ∈ [245K; 255K[, Y=4 for T ∈ [235K; 245K[, Y=5 for T ∈ [225K; 235K[, and Y=6 for T ∈ [215K; 225K[).

With respect to median of	MCS over Darwin		MCS over Cayenne		Maldives Islands MCS		Niamey's MCS	
IWC	≅	4(6)+, 5(1)-	≅	4(1,5)-, 5(5)-	≅		≅	4(2)+
σ	≅	5(1)+	≅	8(1)-	≅		≅	2(4)-
$N_{T,55}$	≅	4(1)+	≅	3(1)+	≅		≅	8(3)+, 3(3)+
$N_{T,500}$	≅	8(1)+, 7(1)+	≅	8(3)+, 8(1)-	≅	7(4)+, 3(1)+	≅	8(1)-
M_2	≅	4(1)+, 5(1)+	≅	8(1)-, 2(1)+	≅		≅	4(6), 2(6)+
M_3	≅	8(1)+	≅	8(1)+, 2(1)+	≅		≅	2(1)+, 3(1,2,3)+ 4(1,2)+ 5(1)+
max(D_{max})	≅	2(2)+, 7(3,4)-	≅	6(3)-, 8(2)-, 8(3)+	-	8≅	+	6(1,2) ≅, 7 ≅, 8 ≅

Appendices E: rescaled PSD parameterization for spherical equivalent diameter

Models for NWP usually use the assumption that ice hydrometeors are spherical. However, our study presents results using maximum diameter (D_{max}). There is a possibility that the last definition might not be adapted for NWP. We propose to explore the impact on the proposed parameterizations of PSD calculated in the main text when assuming the volume of spherical hydrometeors. First, we need to compute the volume of the hydrometeors from the in-situ measurement. Hence, we assume that hydrometeors are oblate spheroids. It is possible from the images recorded by the OAP to deduced D_{max} and the width (width: length perpendicular to D_{max}). With this assumptions it is possible to calculate the volume of such oblate spheroids ($V(D_{max}) = 0.25*\pi*width(D_{max})*D_{max}^2$). Then, we calculate the equivalent spherical diameter for the volume computed for this spheroid (D_{sp} =

(6*V(Dmax)/ π)^{1/3}). For each bin of D_{max} there is a calculation of the mean width from all its particles and for every 5 seconds period. Then, second and third moment (M_{2Dsp} and M_{3Dsp}, respectively) of PSD can be calculated replacing D_{max} in Eq. (9) with D_{sp} (Eq. E1).

$$M_n = \sum_{D_{max}=55\mu m}^{D_{max}=1,2cm} N(D_{sp}) \cdot D_{sp}^n \cdot \Delta D_{sp} \qquad [m^{n-3}] \qquad (E1)$$

Because, it is calculated on measured PSD, $N(D_{sp}) = N(D_{max})$ and $\Delta D_{sp} = \Delta D_{max}$. The results for second moment of PSD are presented in Figure E1 and Figure E2, respectively. Where Figure E1 shows M_{2Dsp} and Figure E2 shows MRD-M_{2Dsp} both as function of MCS reflectivity zones and temperature. Same for M_{3Dsp} and MRD-M_{3Dsp} presented in Figure E3 and Figure E4 respectively. For the second moment of PSD as function of Dsp results are similar than for second moment for PSD as function of D_{max}, except that for a given MCS reflectivity zones M_{2Dsp} are about 30% smaller than M_2 from D_{max}. We obtain the same conclusion for the third moment, but M_{3Dsp} are about 40% to 50% smaller than M_3 from D_{max}. Moreover, MRD-M_{2Dsp} and MRD-M_{3Dsp} are similar to MRD-M_2 and MRD-M_3 from D_{max}.

As second and third moment from PSD as function of Dsp are smaller than second moment from PSD as function of D_{max}, Eq. (12) and Eq. (18) need to be updated such (Figure E5 and Figure E6):

$$A(T) = 1.656 \cdot 10^{-5} \cdot T^2 - 0.0070224 \cdot T + 0.7780590 \qquad [kg.m^{-2}] \qquad (E2)$$

Hence, Eq. (E2) is used in Eq. (17) to calculate the second moment of PSD as functions of D_{sp}. Then, Eq. (E3) is used instead of Eq. (18) to calculated third moment of PSD as function of D_{sp}.

$$M_3 = [-3.066 - 0.6124 \cdot log(IWC) + 0.004251 \cdot T - 0.02495 \cdot log(IWC)^2 + 0.0002413 \cdot log(IWC) \cdot T] \cdot M_2^{F(3)} \cdot D(3) \cdot exp(E(3) \cdot T_c) \qquad (E3)$$

Figure E7 shows efficiency of the updated parameterization for second and third of PSD as function of D_{sp}. Figure E7 and Figure 27 are similar, demonstrating that the parameterization for PSD as function of D_{sp} is as accurate as the one for PSD as function of D_{max}. Moreover, Figure E8 shows that the function $\Phi_{2,3}(x)$ (Eq. 19, Eq. 20 and Eq. 24) is also valid to describe PSD as function of equivalent spherical diameter.

This appendices explores the consequences of using PSD as function of equivalent spherical diameter (as PSD are usually described in NWP) on the parameterization of ice hydrometeors size distribution in MCS developed in the main part of this study. On the four equations that describe this parameterization, only two equations need to be updated with new coefficients: Eq. (12) becomes Eq. (E2) and Eq. (18) becomes Eq. (E3). While Eq. (17) and Eq. (24) are applicable to both types of PSD whether PSD are as function of D_{max} or as function of D_{sp}.

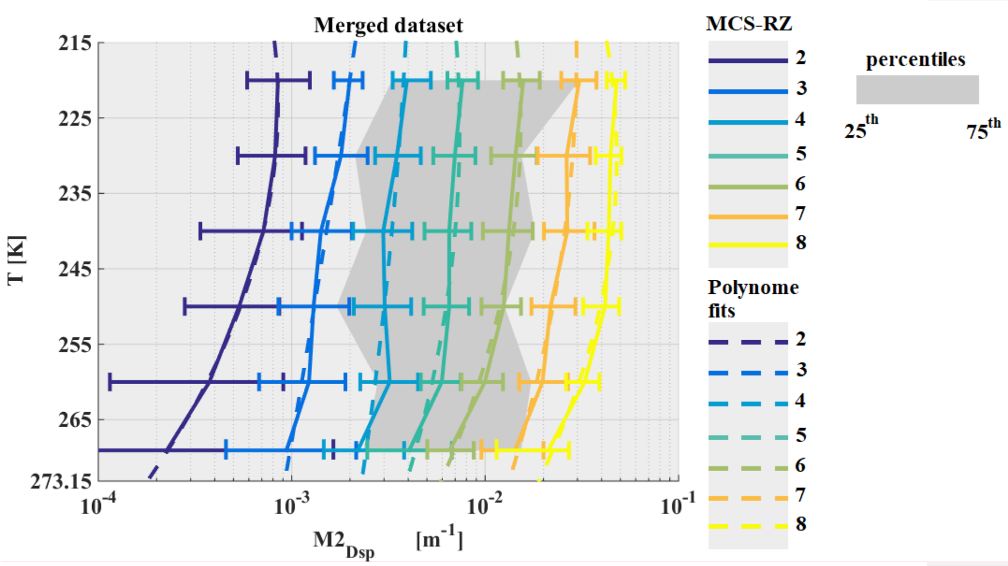

Figure E 1: ***Same as Figure 5, but for M_2 per meter, where PSD are used as function of equivalent spherical diameter***

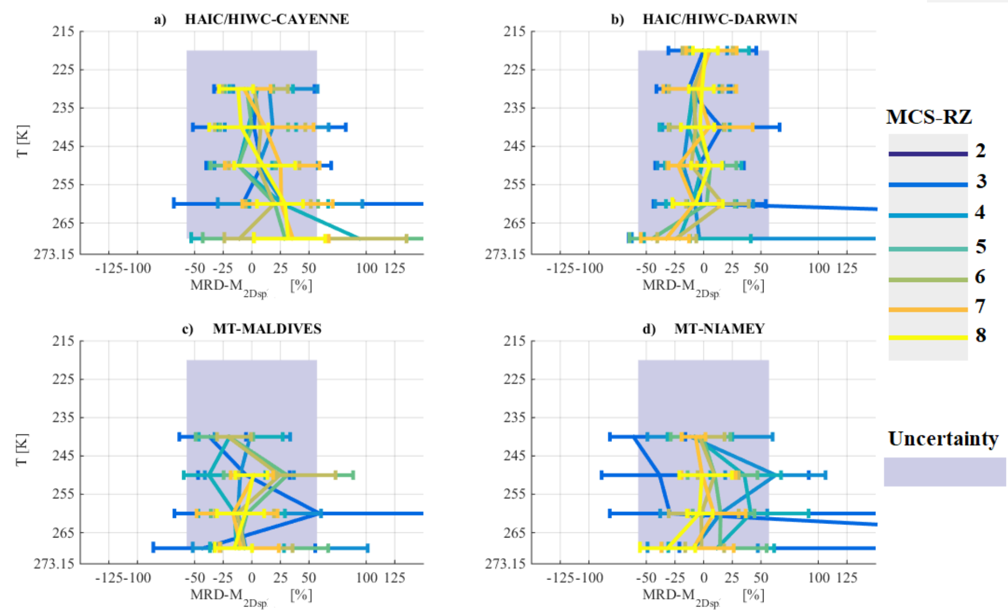

Figure E 2: ***Same as Figure 6, but for MRD-M_2, where PSD are used as function of equivalent spherical diameter.***

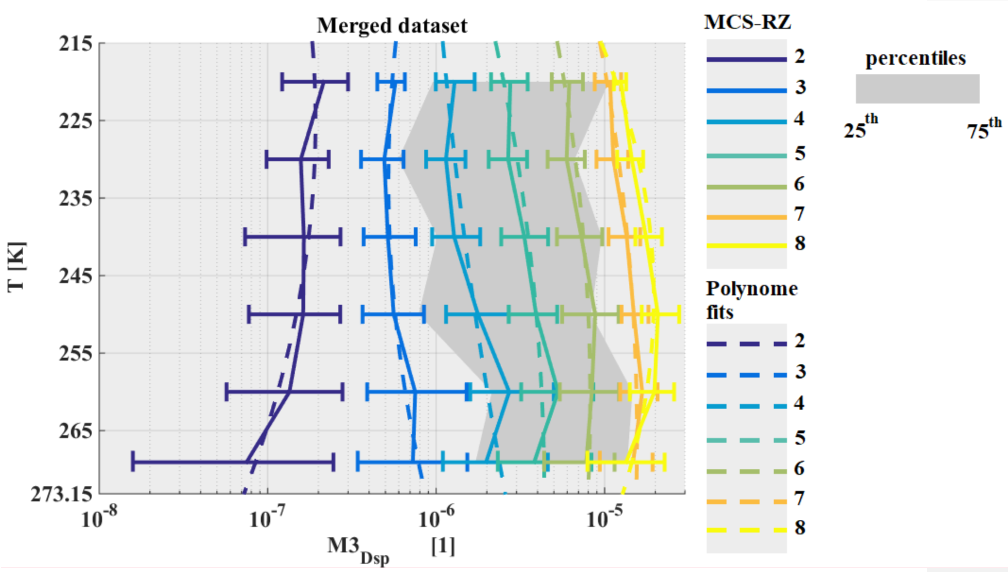

Figure E 3: *Same as Figure 5, but for M_3 per meter, where PSD are used as function of equivalent spherical diameter.*

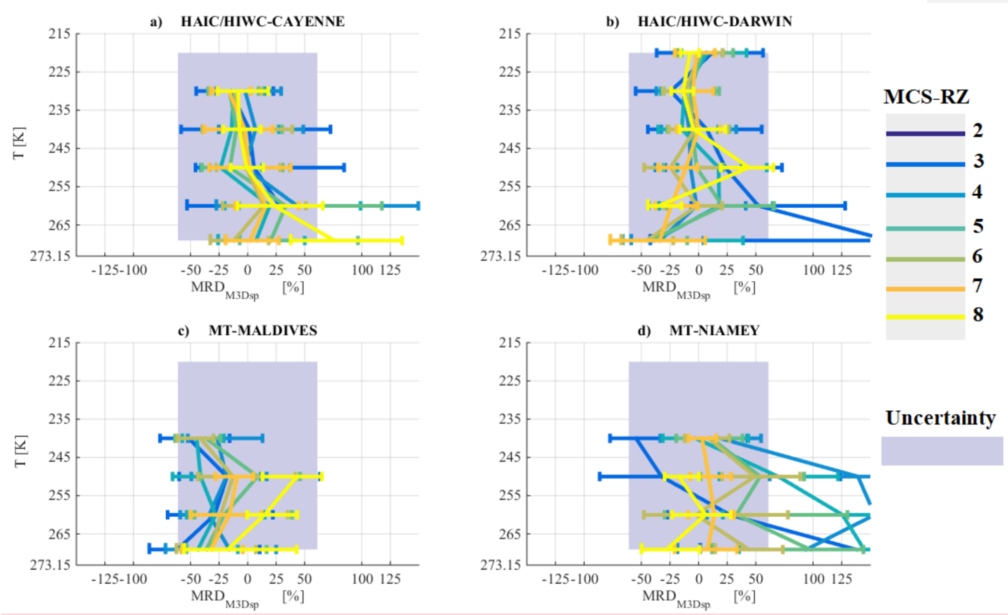

Figure E 4: *Same as Figure 6, but for MRD-M_3, where PSD are used as function of equivalent spherical diameter.*

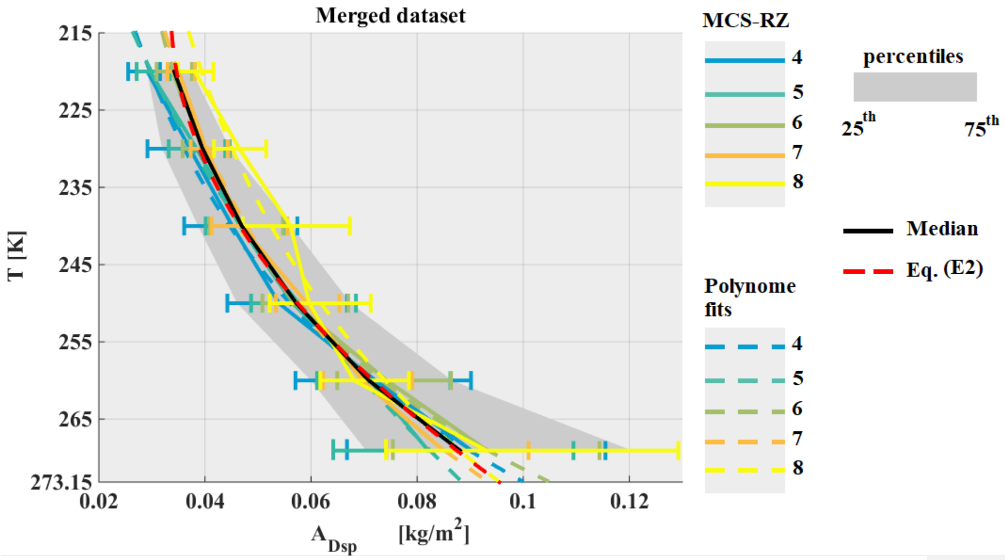

Figure E 5: *Same as Figure 5, but for the ratio A= IWC/M_2 in [kg m^{-2}], where PSD are used as function of equivalent spherical diameter.*

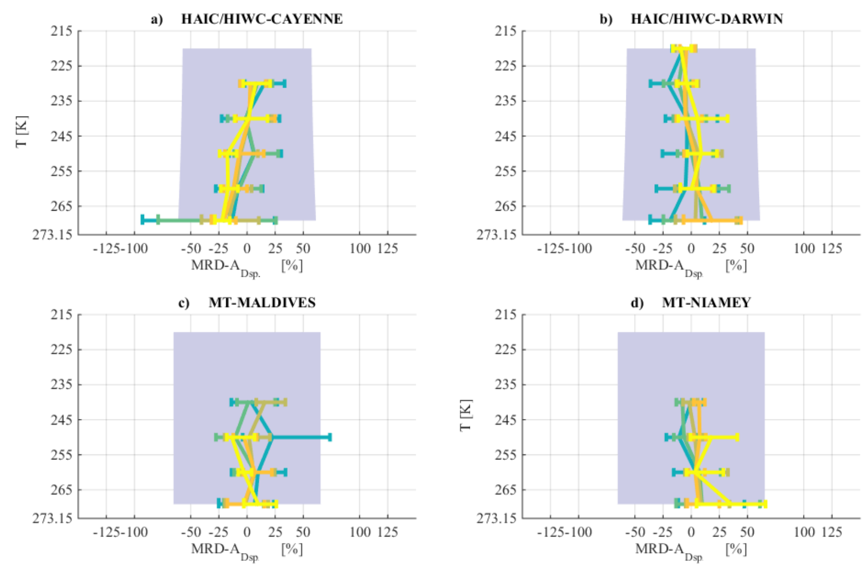

Figure E 6: *Same as Figure 6, but for the ratio MRD-A, where PSD are used as function of equivalent spherical diameter.*

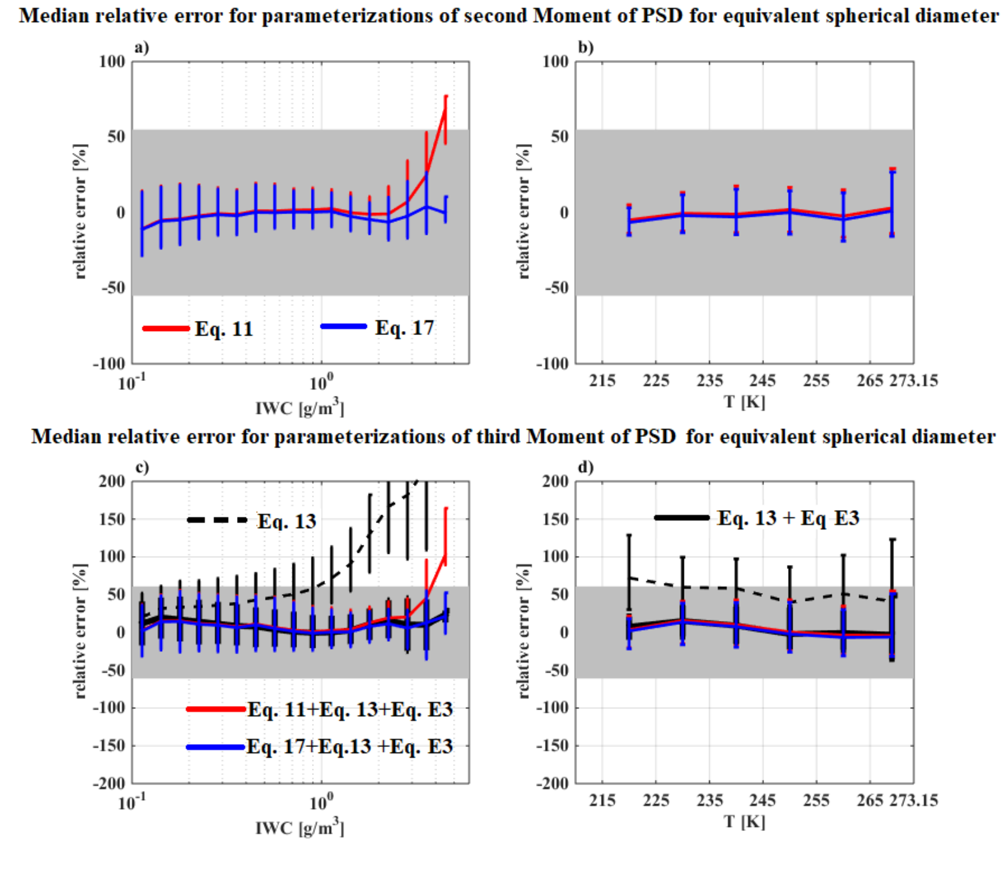

Figure E 7: ***Relative error of parametrized M_2 and M_3 for merged dataset as a function of IWC in a) and c), and as a function of T in b) and d). Solid lines give median relative error and whiskers denote 25th and 75th percentiles of relative error. Grey bands shows measurement uncertainties for M_2 (55%; a) and b)) and M_3 (61%; c) and d)), respectively. For PSD as function of equivalent spherical diameter.***

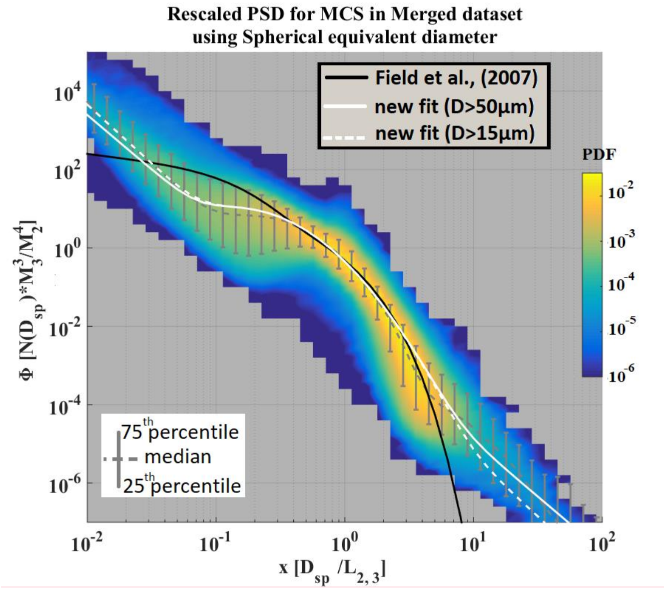

Figure E 8: ***Probability distribution function of rescaled PSD ($\Phi_{2,3}$) on y axis as a function of hydrometeor characteristics size (x) on x axis, for the merged datasets. Black lines show fitted functions from Field et al., (2007), grey dotted lines show median rescaled PSD with error bar from 25th and 75th percentiles of rescaled PSD. Solid white line presents the new fitted function for the merged dataset for PSD beyond 55µm and dashed white line shows fitted function for PSD beyond 15µm (Eq. 24). When PSD are calculated as function of equivalent spherical diameter.***

Commenté [EF42]: Author's adding. We think it is necessary to consider the assumptions use in NWP and to show what are the differences with the assumptions that are used in data analysis of in-situ measurement. Note: in NWP hydrometeors are spherical while for in-situ measurement hydrometeors are described as function of their maximum length through their 2D projection.